Pervasive Motion Tracking and Physiological Monitoring

Thesis for the Degree of Doctor of Philosophy

Richard Woodward

The Imperial College of Science, Technology and Medicine
Department of Mechanical Engineering

Academic advisors:
Ravi Vaidyanathan[1] & Sandra Shefelbine[2]

[1]Department of Mechanical Engineering
Faculty of Engineering
Imperial College London
UK

[2]Department of Mechanical
and Industrial Engineering
Northeastern University
USA

September, 2015

Examiners

Professor Frédéric Marin
Department of Biomechanics and Bioengineering, Université de Technologie de Compiègne, France
Doctor Jonathan Jeffers
Department of Mechanical Engineering, Imperial College London, England

Declaration of Originality

I, Richard Woodward, declare that all work presented in this thesis is of my own, except where indicated and referenced accordingly.

Copyright Declaration

The copyright of this thesis rests with the author and is made available under a Creative Commons Attribution Non-Commercial No Derivatives licence. Researchers are free to copy, distribute or transmit the thesis on the condition that they attribute it, that they do not use it for commercial purposes and that they do not alter, transform or build upon it. For any reuse or redistribution, researchers must make clear to others the licence terms of this work.

Acknowledgements

I would like to express my appreciation to my supervisors Doctor Ravi Vaidyanathan and Doctor Sandra Shefelbine for all their support, encouragement, and enthusiasm as I have pursued this research. I was very lucky to have two experienced academics, who have entirely different strategies and thought processes, guide me in completion of this PhD. I have been given a number of fantastic opportunities and experiences over the past four years and for that I am extremely grateful.

Many of the applications presented in this thesis were made possible by the hard work and input from several individuals. These include Doctor Niamh Nowlan, for your supervision and knowledge in the foetal monitoring research; Adina Draghici, for your incredible effort in the SCI rowing application; Doctor Daniel Katz, for your clinical input and work in the Anaesthetic monitoring study; and Alex Wolf and all the EIS team in the force analysis study.

Thank you to Professor Alison McGregor and Professor Etienne Burdet for use of their laboratories and facilities. As well as their incredibly helpful post-doctoral researchers: Thomas Burton, Enrica Papi, Lynsey Duffell, and Michael Mace.

Thank you to all the subjects and participants in this research. Without your time, effort, and feedback, this research would not be possible. I am grateful to the James Dyson Foundation for believing in this work and financially supporting throughout.

Finally, to my family, mum, dad, Nick, and Bethany, thank you for your love and support throughout, and to my friends, who have kept morale high.

Abstract

This thesis presents a new system of monitoring human motion and muscle activity concurrently, in pervasive and uncontrolled environments, for prolonged periods of time. Current technologies such as optical based motion tracking and electromyography (EMG) are considered the gold standard, but have limited use outside of a controlled laboratory environment. Restraints on collection durations, due to temporary sensors, as well as a limited collection space in which monitoring is capable, results in a constrained system which is not suitable for prolonged observation.

Using a custom made inertial measurement unit (IMU) and mechanomyography (MMG) sensor, information from both motion and muscle activity was combined, in order to better understand human activity by allowing prolonged collection in unrestricted environments. IMU and MMG measurements have been compared to standard optical tracking and EMG measurements, demonstrating the viability of this technology in a clinical setting and particularly in the natural environment.

This novel sensor is lightweight, inexpensive, low power, wireless, easy to use, gives results comparable to standard laboratory techniques, and is able to monitor motion and muscle activity over long periods of time. This work shows a strong agreement with the current literature on MMG response to increments of force, and a greater sensitivity to muscular fatigue detection when compared against EMG, all through pervasive studies. Using machine learning and pattern recognition methods, gait analysis and detection of progressive change over time was achieved in typical and atypical conditions, over prolonged periods. Finally, this work has shown applicable use in prosthesis control and gesture switching. Outside of muscle monitoring, alternative uses have been established, with preliminary results showing a suitable use in foetal monitoring.

This work establishes a novel method of human motion and muscle monitoring which produces a suitably high accuracy when compared against the gold standard, however, without the limitations which confine the wearer to a finite space or limited duration time. The studies presented here introduce a number of areas in which prolonged and pervasive collection can expand this field, while producing complementary results against laboratory based technology.

Keywords: Mechanomyography, Inertial Measurement Unit, pervasive

Contents

List of Figures xiii

List of Tables xv

1 Introduction 1
- 1.1 Aims and Objectives . . . 3
- 1.2 Structure of Thesis . . . 4
- 1.3 Summary . . . 5

2 Background 7
- 2.1 Introduction . . . 8
- 2.2 Motion Tracking . . . 8
  - 2.2.1 Optical . . . 10
  - 2.2.2 Mechanical . . . 12
  - 2.2.3 Magnetic . . . 12
  - 2.2.4 Inertial Measurement Unit . . . 13
    - 2.2.4.1 Altitude and Heading Reference Systems . . . 14
  - 2.2.5 Other Motion Tracking Methods . . . 15
  - 2.2.6 Technology Requirements and Feasibility . . . 16
  - 2.2.7 Data Processing . . . 17
    - 2.2.7.1 Classification . . . 18
  - 2.2.8 Conclusion . . . 19
- 2.3 Muscle Monitoring . . . 20
  - 2.3.1 Contraction Types . . . 21
  - 2.3.2 Electromyography . . . 21
  - 2.3.3 Mechanomyography . . . 23
  - 2.3.4 Fatigue and Cross Talk . . . 25
  - 2.3.5 Applications . . . 25
  - 2.3.6 Conclusion . . . 27
- 2.4 Motion and Muscle Fusion . . . 28
- 2.5 Chapter Summary . . . 29

3 Design 31
- 3.1 Introduction . . . 32
- 3.2 Identification of Needs . . . 32
- 3.3 Inertial Measurement Unit . . . 33
  - 3.3.1 Core Functionality . . . 33
  - 3.3.2 Inertial and Pressure Sensors . . . 34
  - 3.3.3 Auxiliary Port . . . 34
  - 3.3.4 Battery Life and Storage/Transmission Capabilities . . . 35

3.3.5 Manufacturing . . . 35
3.3.6 Firmware . . . 35
3.3.7 Summary . . . 36
3.4 Acoustic Sensor . . . 36
3.4.1 Construction . . . 38
3.4.2 Manufacturing . . . 38
3.4.3 Summary . . . 39
3.5 Force Gauge . . . 39
3.6 Iteration and Improvement of Technology . . . 40
3.6.1 Sensor Integration and Wearable Aspects . . . 40
3.6.2 Stakeholder Feedback on Design . . . 41
3.7 Software . . . 43
3.8 Chapter Summary . . . 44

4 Validation **47**
4.1 Introduction . . . 48
4.2 Validation of Frequency Sensitivity . . . 48
4.3 Validation of Muscle Contraction Data . . . 48
4.4 Validation of Motion Data . . . 50
4.5 Chapter Summary . . . 56

5 Physiological, Clinical, and Fatigue Studies **59**
5.1 Introduction . . . 60
5.2 Force Analysis . . . 60
5.2.1 Research Question and Hypothesis . . . 62
5.2.2 Method . . . 62
5.2.3 Results . . . 64
5.2.4 Discussion and Conclusion . . . 64
5.3 Isometric Fatigue Monitoring with Typical Subjects . . . 67
5.3.1 Research Question and Hypothesis . . . 68
5.3.2 Method . . . 68
5.3.2.1 Changes Post Fatigue . . . 70
5.3.2.2 Changes During Fatigue . . . 72
5.3.3 Results . . . 73
5.3.4 Discussion . . . 74
5.3.4.1 Sustained Fatigue Analysis of Results . . . 75
5.3.4.2 Pre and Post Fatigue Analysis of Results . . . 76
5.3.5 Conclusion . . . 77
5.4 Isotonic Fatigue Monitoring with Spinal Cord Injury Subjects . . . 77
5.4.1 Research Question and Hypothesis . . . 78
5.4.2 Method . . . 79
5.4.2.1 Data Processing . . . 81

5.4.3 Results and Discussion . . . 81
5.4.3.1 Foot Force Verses MMG Amplitude . . . 82
5.4.3.2 Stroke Length Verses Gyroscope Frequency . . . 83
5.4.4 Conclusion . . . 85
5.5 Clinical Application of Anaesthetic Monitoring . . . 86
5.5.1 Research Question and Hypothesis . . . 87
5.5.2 Method . . . 88
5.5.3 Results . . . 89
5.5.4 Discussion . . . 90
5.5.5 Conclusion . . . 91
5.6 Chapter Summary . . . 93

6 Gait Analysis and Activity Monitoring 95
6.1 Introduction . . . 96
6.2 Activity Classification in Typical Gait . . . 96
6.2.1 Research Question and Hypothesis . . . 97
6.2.2 Method . . . 97
6.2.2.1 Signal Processing . . . 98
6.2.3 Results . . . 102
6.2.4 Discussion and Conclusion . . . 103
6.3 Progressive Changes in the Gastrocnemius . . . 105
6.3.1 Research Question and Hypothesis . . . 106
6.3.2 Method . . . 106
6.3.3 Results . . . 109
6.3.4 Discussion . . . 109
6.3.4.1 Comparison of Typical and Atypical Results . . . 110
6.3.5 Conclusion . . . 112
6.4 Asymmetric Differences in the Rectus Femoris . . . 113
6.4.1 Research Question and Hypothesis . . . 113
6.4.2 Method . . . 114
6.4.2.1 Signal Processing . . . 115
6.4.3 Results and Discussion . . . 117
6.4.3.1 Typical Analysis of Results . . . 119
6.4.3.2 Atypical Analysis of Results . . . 119
6.4.3.3 Comparison of Typical and Atypical Results . . . 120
6.4.4 Conclusion . . . 121
6.5 Chapter Summary . . . 122

7 Human Machine Interfaces 123
7.1 Introduction . . . 124
7.2 Prosthesis Control and Gesture Switching . . . 124
7.2.1 Research Question and Hypothesis . . . 125

7.2.2 Method . . . 125
7.2.2.1 System Calibration . . . 129
7.2.3 Results . . . 132
7.2.4 Discussion and Conclusion . . . 132
7.3 Chapter Summary . . . 137

8 Discussion **139**
8.1 Introduction . . . 140
8.2 Summary of Contributions . . . 140
8.3 Limitations . . . 141
8.4 Future Work . . . 142

9 Conclusion **143**
9.1 Final Comments . . . 144

Bibliography **145**

A Appendix: Non-Muscular Acoustic Application **163**
A.1 Introduction . . . 164
A.2 Foetal Activity and Pregnancy Monitoring . . . 164
A.2.1 Research Question and Hypothesis . . . 166
A.2.2 Method . . . 166
A.2.2.1 Data Pre-Processing . . . 167
A.2.2.2 Foetal Peaks and Push Button Detection . . . 168
A.2.2.3 Validation . . . 168
A.2.2.4 Algorithm . . . 169
A.2.3 Results and Discussion . . . 169
A.2.4 Conclusion . . . 170
A.3 Summary . . . 172

B Appendix: Mechanomyography Muscles of Interest **173**
B.1 MMG use in Literature . . . 175

C Appendix: Technical Design and Drawings **175**
C.1 MMG Technical Drawings . . . 176
C.2 Aktiv Case Technical Drawings . . . 180
C.3 Battery Case Technical Drawings . . . 183
C.4 MMG Circuit Diagrams . . . 186
C.5 Aktiv Circuit Diagrams . . . 187
C.6 Aktiv BOM List . . . 191
C.7 Aktiv-P Circuit Diagrams . . . 191
C.8 Aktiv-P BOM List . . . 195
C.9 Force Gauge Circuit Diagrams . . . 195

List of Figures

2.1 Current motion and muscle monitoring methods . . . 9
2.2 Pervasive motion and muscle monitoring methods . . . 9
2.3 Representation of relative positioning . . . 10
2.4 Representation of absolute positioning . . . 10
2.5 Image of the Gypsy 7 Torso Mechanical Capture System . . . 13
2.6 Two foot position tracking with an IMU . . . 16
2.7 Description of different muscle contractions . . . 22
2.8 EMG verses MMG with increasing MVC . . . 24

3.1 Image of the Aktiv IMU . . . 34
3.2 Packet form for each data type . . . 37
3.3 Posatskiy *et al* MMG sensor . . . 38
3.4 Woodward *et al* MMG sensor . . . 39
3.5 Acoustic sensor microphone board . . . 40
3.6 Image of force gauge developed to determine MMG contact pressure . . . 41
3.7 Iteration change of acoustic sensor . . . 42
3.8 Iteration of the IMU/battery cases . . . 43
3.9 Screenshot of data converter program . . . 45
3.10 Screenshot of real-time clock update program . . . 45

4.1 Acoustic sensor testing apparatus . . . 49
4.2 Acoustic sensor frequency response . . . 49
4.3 Isometric validation setup . . . 50
4.4 Isometric validation EMG and MMG results . . . 51
4.5 Sensor set up for optical validation . . . 52
4.6 MMG signal denoising process . . . 54
4.7 Comparison of EMG and MMG during gait . . . 56

5.1 Image of a medical dynamometer . . . 61
5.2 Force analysis study sensor setup . . . 63
5.3 MMG amplitude and frequency change during DCER study . . . 65
5.4 Repetition time duration, acceleration, and velocity change during DCER study 66
5.5 Sensor configuration isometric fatigue study . . . 70
5.6 Fatigue study stages one and three . . . 71
5.7 Fatigue study stage two . . . 71
5.8 Block diagram of fatigue study sensor setup . . . 71
5.9 Example of squat detection for stages one and three of the fatigue study . . . 72
5.10 Example of peak detection using accelerometer data from stage two of the fatigue trial . . . 73
5.11 MMG and EMG RMS results comparing pre and post-fatigue . . . 74

5.12 MMG and EMG MPF results comparing pre and post-fatigue 75
5.13 RMS and MPF changes during fatiguing action 76
5.14 Sensor attachment method and subject operation of the Concept2 ergometer 80
5.15 Stages of rowing and muscle contraction 80
5.16 Raw gyroscope and MMG data obtained and processed from the rowing application 82
5.17 Foot force and MMG RMS changes during rowing task for both AB and SCI subject groups 84
5.18 Stroke length and gyroscope MPF changes during rowing task for both AB and SCI subject groups 85
5.19 Device developed for anaesthetic application 89
5.20 Raw results with TOF twitch estimation in pre-NMBA muscle 91
5.21 FFT response in pre-NMBA muscle 92

6.1 Algorithm flow chart of raw data classification into activity 101
6.2 Raw gyroscopic data used in classification of activities 103
6.3 Amputee subject donning sensors 107
6.4 Example of stride segmentation from lower leg gyroscopic data 108
6.5 Results for progressive changes in the gastrocnemius between typical and atypical gait 111
6.6 Strap used in quadriceps monitoring study 115
6.7 Typical subject donning sensors for quadriceps monitoring study 116
6.8 Example of stride segmentation from upper leg gyroscopic data 117
6.9 Gyroscope and MMG results for quadriceps monitoring study 118

7.1 Gesture control test environment 126
7.2 Sensor configuration for prosthesis control 126
7.3 Visual of the grips used in prosthesis control 128
7.4 Stages of prosthesis control 129
7.5 Flow chart showing the gesture switching method used for prosthesis control 129
7.6 Interface between human and prosthetic hand 130
7.7 Flow diagram of the MATLAB process for prosthesis manipulation 131
7.8 Screenshot of the software developed for the HMI application 133
7.9 Results showing HMI methods without donning time taken into consideration 135
7.10 Results showing HMI methods with donning time taken into consideration . . 136

A.1 Image of a medical ultrasound scanner 165
A.2 Image of the band used in the foetal monitoring study 168
A.3 Pregnancy monitoring data from a subject in third trimester pregnancy . . . 170
A.4 Image of the Aktiv-P IMU 171
A.5 First prototype of the improved pregnancy monitor 171

C.1 MMG microphone schematic 186

List of Tables

2.1 Motion technology pros and cons . . . 20
2.2 Muscle monitoring technology pros and cons . . . 28

3.1 Aktiv attributes . . . 37

4.1 RMSE results for motion validation . . . 53
4.2 Stages of human gait . . . 55

5.1 Estimated MVC % for each subject at 20 and 80 kg . . . 63
5.2 Percentage results of RMS and MPF post-fatigue . . . 75
5.3 Results comparing foot force against MMG RMS for both AB and SCI subject groups . . . 83
5.4 Results comparing stroke length against Gyroscope MPF for both AB and SCI subject groups . . . 83
5.5 Baseline TOF results in pre-NMBA muscle . . . 92

6.1 Human activity classification results . . . 103
6.2 Results for motion and muscle activity change over time . . . 110
6.3 Results for motion and muscle differences between right and left leg . . . 120
6.4 *t*-test results of gyroscope and MMG between subjects in quadriceps monitoring study . . . 121

7.1 HMI average test duration and donning results . . . 134
7.2 Results of paired *t*-test in HMI application . . . 134

A.1 Results for pregnancy monitoring study . . . 170

B.1 Use of MMG in literature and muscles of interest . . . 174

C.1 MMG sensor BOM list . . . 186
C.2 Aktiv (Mark I) BOM list . . . 190
C.3 Aktiv-P (Mark I) BOM list . . . 194
C.4 Force gauge BOM list . . . 196

1

Introduction

Contents

1.1 Aims and Objectives 3
1.2 Structure of Thesis 4
1.3 Summary 5

Human motion and physical activity monitoring are thriving fields in both academia and clinical studies, and are used in diagnosis of disease, monitoring therapy, rehabilitation training, and sports technique analysis[1–3]. However, rarely is human motion recorded outside of the clinical or laboratory environment. Movement and muscular activity are common measurements in motion analysis and are separately used to characterise the patient's abilities. Patient activity monitored continuously, outside of a laboratory, would allow for improved diagnoses of disease, the ability to track rehabilitation progress, or the opportunity to provide remote therapy. While extensive work has been performed in the realm of human motion tracking, the majority of studies have concentrated on collection within a controlled environment, such as a gait laboratory.

It is common practice to concurrently monitor both motion and muscle activity in gait laboratories and clinics, in order to better understand conditions. However, controlled environments have their limitations, including the confinement to an observation room or laboratory, limitations in collection time, and other disadvantages such as cost of technology and constrained mobility.

These hindrances can result in short collection sessions, which can miss long lasting conditions or progressive changes in conditions over time. Furthermore, subjects are constantly aware of their actions during highly controlled observation, and are likely performing at their best, which may hide underlying problems seen when moving naturally.

These limitations, as well as time consuming processes involving the application of markers and electrodes associated with current motion and muscle monitoring technologies, indicates a gap in the field where an unobtrusive, wearable device, capable of logging data from both human motion and muscle activity, for an extended length of time, has broad potential use.

Existing devices often require external power or computational sources, such as a laptop or handheld computer, due to processing or power requirements. Past literature in motion and gait analysis have recognised that real-time operation, wireless properties, and portability, as major deficiencies that must be addressed for a clinically viable system[4,5].

Furthermore, past literature has identified multiple failures in sensor development in this area, which do not conform to patient or clinicians standards resulting in redundant systems which the relevant parties are not interested in working with[6]. Bergmann and McGregor reviewed 843 papers in body-worn sensors and recognised that only eleven were deemed suitable for clinical inclusion, due to the wearable devices failing to satisfy the stakeholders requirements.

Current methodology relies on electromyography (EMG) signals for muscular contraction information, which require single-use electrodes, electrical conductive gel, and often shaving and abrasion of the skin. Due to the lack of long term and pervasive EMG collection, current

literature only details data collected from short periods of time and for a limited range of subject motion within the confinements of a laboratory.

Mechanomyography (MMG) offers an alternative method to monitoring muscle activity. Low frequency vibrations emitted by skeletal muscle are produced during contraction and represent the mechanical activity of muscle generated by lateral oscillation of muscle fibres[7]. Benefits over EMG include MMG's ease of application, a higher signal to noise ratio (SNR), multiple uses for a single sensor, and elimination of the need to shave and apply conductive gel[8,9].

Motion analysis is often achieved using optical based methods, which rely on cameras and reflective markers on the moving object. In recent years, this has also been accomplished with smaller, embedded systems, like inertial measurement units (IMU) and global positioning devices, however, optical systems vastly dominate the motion monitoring community due to its accuracy and establishment in the field.

Although muscle monitoring alone has been collected over prolonged periods of time[10,11], this work is the first of its kind combining MMG with human inertial data. Muscle and motion collection outside of a laboratory has received limited attention in literature, however, all applications have utilised EMG, which has narrowed their collection time and ability of pervasive use[12,13].

1.1 Aims and Objectives

The work presented here demonstrates the potential of pervasive motion and muscle activity monitoring, in the context of rehabilitation monitoring, prosthetic control, and general human activity. To achieve this a custom IMU is introduced, consisting of a gyroscope, accelerometer, magnetometer, and barometer, and MMG muscle sensing technology using pressure based sensors. This work also introduces a structure of sensor development from the onset, creating a design that incorporates the requirements of all stakeholders. The objectives of this work were to:

1. Design and develop a system capable of collecting motion and muscle activity for use in an uncontrolled pervasive environment, and validate the system against the current gold standard in motion and muscle monitoring.
2. Understand the relationship of MMG signal amplitude and frequency, against voluntary and involuntary muscular force and fatigue in pervasive environments, and compare against the current literature.
3. Integrate this technology into a clinical environment, with system design targeted towards the use of medical professionals, in order to demonstrate full stakeholder inclusion by abiding to their needs in a device.

4. Monitor human muscle and gait activity in an uncontrolled environment, and classify a variety of commonly performed activities using unsupervised learning methods.
5. Recognise and track change in muscular and gait performance over a prolonged period of time in typical and atypical subjects, in the natural environment.
6. Understand lower extremity symmetric differences in muscular and gait performance in unilateral gait conditions.
7. Apply motion and muscle information to control and change grips in upper body prosthetics to alleviate user interaction.

1.2 Structure of Thesis

This thesis is structured into nine chapters, with a summary of the remaining eight chapters below.

Chapter 2 - Background Detailed literature review and background. This chapter introduces the concepts and collection methods of motion and muscle monitoring, and discusses the current limitations and gaps in the field.

Chapter 3 - Design This chapter details the research performed in selection of suitable devices and sensors in order to achieve the aims and objectives listed above. Sensor development, based on feedback from stakeholders involved in the process, was detailed and discussed. Other technology used and developed throughout this work is also detailed here.

Chapter 4 - Validation The technology developed is tested and validated against the gold standard of motion tracking and muscle monitoring techniques. Results, accuracy, and suitability in human applications are discussed.

Chapter 5 - Physiological, Clinical, and Fatigue Studies Application to semi-controlled studies in order to obtain clinical-level observations of muscular signal response to changes in force and fatigue, albeit, in a non-clinical, uncontrolled environment.

Chapter 6 - Gait Analysis and Activity Monitoring Through full adoption of uncontrolled methods and environments, this chapter looks at the monitoring and classification of human activity, using unsupervised algorithms, as well as the tracking of muscular and gait change over prolonged periods of time. Furthermore, this chapter investigates bilateral gait differences in individuals with unilateral conditions.

Chapter 7 - Human Machine Interfaces Utilising the link between human-computer interaction and user needs in assistive technology, this chapter introduces a fusion between muscle contraction and upper limb movement, with advanced prosthesis control and gesture switching achieved.

Chapter 8 - Discussion Analysis and reflection of what was unique, novel, and successful about this research. Furthermore, limitations and future work are established, as well as reiteration of the aims and objectives listed above.

Chapter 9 - Conclusion A summary and conclusion of this work.

1.3 Summary

The objective of this research is to combine pervasively collected motion and muscle data, and synergise their attributes to give a more comprehensive understanding of human activity in scenarios either impractical or inaccessible in a controlled laboratory environment.

2

Background

Contents

2.1 Introduction **8**
2.2 Motion Tracking **8**
2.3 Muscle Monitoring **20**
2.4 Motion and Muscle Fusion **28**
2.5 Chapter Summary **29**

2.1 Introduction

Human motion and muscle monitoring is a well established and useful method for identifying disorders, tracking rehabilitation, and studying human activity. However, most present methods are limited to use in controlled settings, such as laboratories and clinical environments. The current technologies used for both motion and muscle monitoring are highly accurate and provide a standardised result recognised across the field, however, they are not without their disadvantages, including size, cost, complexity, and limitations in both time and space in which they can be used. Furthermore, controlled studies impose restrictions on natural human performance with specific instructions of how to perform tasks or activities to be monitored, and a short time window of collection may miss vital information only seen through prolonged monitoring.

A device capable of pervasive and prolonged collection bridges the limitation seen in current methods. A concealable, lightweight, easy to use, and affordable device could be applied to numerous applications not possible within a controlled environment, such as everyday activities like travelling to work, sporting activities, or regular rehabilitation routines.

Such as device would provide useful information to the user, but also clinicians and those wishing to monitor the activities of the user. Physiotherapists could track completion of rehabilitation plans, monitor if they are performing the tasks correctly, or if they are performing them at all, completely remotely and without direct contact. Furthermore, such technology could track change over time, to determine how well the routine is improving the users condition.

Current methods requires time and effort to attach sensors and technology, often by qualified personnel, and can be quite bulky to wear (Fig. 2.1). However, by applying techniques used in the controlled environment, it is possible to get a more natural measurement of motion in the open environment (Fig. 2.2). In this thesis the close relationship between human motion and muscle contraction is further analysed, which can advance the understanding of human movement.

This chapter will review the current relevant techniques in human motion and muscle monitoring. Furthermore, the process taken in selection of suitable technology is presented while noting the practicality of each choice for uncontrolled monitoring.

2.2 Motion Tracking

There are two forms of motion in regards to the movement of objects; absolute and relative. Different motion tracking technologies use either relative (Fig. 2.3) or absolute (Fig. 2.4)



Figure 2.1: Current methods in motion and muscle monitoring use inconcealable technology and require numerous markers and electrodes to be attached, which takes both time and effort to apply. Image from the ARD Research Laboratory, with permission requested[14].



Figure 2.2: Alternative methods in motion and muscle monitoring, using lightweight and concealable sensors, could be applied to studies outside of the laboratory.

positioning, and an understanding of each is necessary in selection of a suitable system.

In motion tracking technologies, optical devices produce results in an absolute frame; tracking physical location of a body from one position to another in the coordinate system of the laboratory (ground coordinate system). However, other, non-optical motion tracking technology, such as accelerometers, output their data in a relative form; monitoring changes in regards to the frame of the device, in the coordinate system of the segment to which they are attached.

In order to monitor human motion there are several options currently available. Each with their pros and cons, but most often there is a compromise of portability against accuracy. The following describes four popular methods of motion tracking; optical, mechanical, magnetic, and inertial. These methods were selected due to properties deemed viable for this research

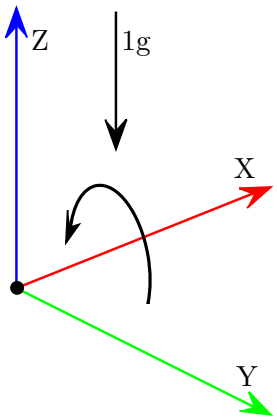


Figure 2.3: Relative positioning shows change relative to a reference frame. In regards to an accelerometer, the plane in which gravity (1g) is in can be monitored through rotation of the device.

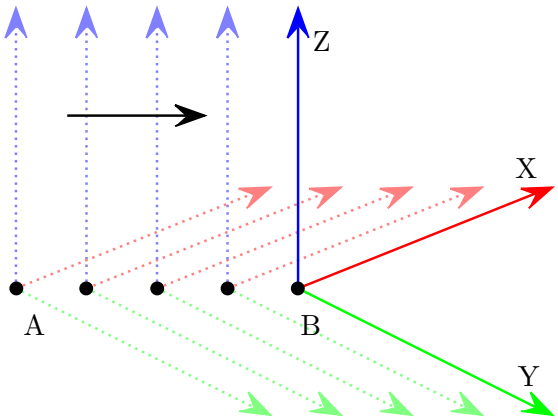


Figure 2.4: Absolute positioning shows change in a global frame. Movement in a physical space can be tracked, such as from point A to point B.

and their advantages and disadvantages are listed. Furthermore, some other motion tracking methods have been discussed and why they are not plausible for this work.

Data processing, sensor feasibility, and requirements are also discussed and used in selection of a suitable motion tracking device for this research.

2.2.1 Optical

Optical based tracking is repeatedly referred to as the 'gold standard' of motion tracking[15–17], due to its high positional accuracy and ability to monitor in three-dimensions. Optical based methods can be further divided into two subsections of active and passive systems.

Passive based methods use reflective markers which are placed on the moving object of interest to detect motion, accompanied by infrared cameras to detect positional changes of the markers in three-dimensions. In human applications the markers are generally placed directly on the skin of the subject atop of bony anatomical points to reduce movement artefacts (Fig. 2.1). The infrared cameras ignore clothing, skin, and other materials/objects which fall beneath a reflective threshold so that only the markers are detected. Even with thresholds in place this method is not perfect, as other reflective metals, mirrors, or direct sunlight on light-coloured objects can exceed said threshold resulting in anomalies. Vicon, a popular brand of passive based optical tracking systems, have been found to have a very high accuracy with some achieving accuracies as high as 63 μm positional error[18]. However, for optimal three-dimensional readings there must be a clear line of sight from each camera to marker which requires at least two cameras to have line of sight at all times. Optical systems typically have multiple cameras located within the collection medium for the best accuracy, although this becomes very expensive due to the cost of such a system which is in the hundreds of thousands[19].

Soft tissue artefacts (STA) are a large problem in applications where absolute movement is paramount. Many papers have analysed improvement methods to reduce these artefacts[20–23], with one review stating many factors can be taken to improve results as best as possible, however STA are still a very unknown area[24]. Models have been produced in order to characterise motion even with misplacement of markers and purposely included artefacts which have found to reduce error, however it was stated that the best practice is to spend additional time and effort in order to correctly place the markers in the first place[25].

Markers are attached to the skin using tapes or adhesives, however, some bands, straps, and Lycra suits are available with the markers pre-attached for quicker donning. Although straps and suits reduce the amount of time require to find correct points and attach markers they are not without their disadvantages with some introducing more motion artefacts than direct attachment to the skin[26].

Active based methods perform collection in the opposite way by placing multiple light emitting diodes (LED's) on the moving object which illuminate one at a time in order for cameras to detect positional change. Due to the active nature of these markers they do require their own power source, which means an additional requirement for each subject to carry during data collection.

Optical methods are a popular choice in literature for human motion tracking, with Vicon branded systems being largely used in this field. Optical systems produce absolute results with the individual reflective markers being tracked through space and time to a high accuracy, showing movement from a start to end point. However, optical systems have the disadvantage of reducing mobility and creating a constrained environment in which an object can move within. Other objects within the collection medium may result in an insufficient number of cameras having line of sight with a marker, which can produce dropped samples that require an offline estimation of where that marker is believed to be before being re-added to a data set. Objects such as flights of stairs have been found to hinder optical tracking methods which has led to alternative motion tracking options being pursued, such as inertial measurement units[27]. Optical based methods have been used together with force plates and electromyography in order to track human gait, including healthy subjects and atypical subjects with conditions such as cerebral palsy and amputation[1,28].

Other optical methods which do not require the use of markers include standard camera based tracking which rely on synchronised monocular grayscale images of a subject[29], Laplacian Eigenmaps[30], or tracking the contour of objects frame by frame[31]. Other commercial camera technologies such as the Microsoft Kinect, which combines regular camera technology with infrared to track in three-dimensions, has been found to give suitably high accuracy in object tracking when compared with Vicon, but without the limitations of portability and cost [32]. As with the marker based technologies the main limitation in optical based capture is the limited range of motion as subjects must stay within the confinements of the camera. These

methods also have a high computational load, especially when performing object tracking in real-time.

Despite a high level of accuracy, optical based methods are limiting for this work with their high cost and controlled collection space. Although possible, taking an optical system outside of a laboratory would be incredibly impractical, and collecting pervasive data by developing a portable system is nigh impossible. In clinical applications the length of time to apply the markers, the cost of the system, and size of the technology, is much less of a concern and can be accommodated, however, for home-use studies these disadvantages are less acceptable.

2.2.2 Mechanical

Mechanical systems consist of a device directly connected to the moving object of interest in order to monitor its movement. Typically this involves a mechanical frame connected to a transducer such as a potentiometer or rotary encoder which converts physical movement to a signal representing change in position. For human motion tracking this often involves an exoskeleton frame which is worn by the user, such as the Gypsy motion capture system developed by MetaMotion (Fig. 2.5)[33]. This device has the benefit of being able to collect very accurate readings from its mechanical potentiometers, along with the recording method being fairly simple; however, due to the required mechanical frame it can reduce degrees of freedom (DOF) by limiting the user's motion[34].

Subjects in home-use monitoring studies have voiced their concerns and dislike towards non-concealable device and those that restrict normal daily behaviour[6]. Although producing high results, a mechanical system would impose many limitations on practical data collection and it is believed subjects would not be willing to use it on a day-to-day basis.

2.2.3 Magnetic

Magnetic sensors determine movement of an object by analysing a change in a magnetic field. More specifically the most popular method uses a transmitter and receiver which contain tri-axis orthogonal coils that can detect a change in movement by the change in the magnetic field between them. Magnetic sensors are considerably cheaper than optical systems, however they have disadvantages including disturbances produced by ferrous metals and electrical devices in the collection mediums vicinity[35]. Magnetic sensors have an accuracy in the range of ~1.5 mm, which makes them less accurate than optical based systems but still possess a high accuracy[36]. This method can be worn more comfortably, thus not limiting movement as mechanical systems might, but do have a problem with external noise from outside sources.

Much like optical based methods, the need for a transmitter and receiver would limit the range of collection space a user could move within. Furthermore, the amount of ferrous metals in the home environment is abundant and trying to remove artefacts produced from these disturbances would be non-trivial.



Figure 2.5: Image of the Gypsy 7 Torso Mechanical Capture System, used with permission from MetaMotion[33].

2.2.4 Inertial Measurement Unit

Inertial measurement units (IMU's) are used abundantly in motion tracking literature, mostly due to their low latency, low cost, and portability[34]. Through a combination of microelectromechanical systems (MEMS) such as accelerometers, gyroscopes, and magnetometers, these devices are able to collect or transmit relative motion information based on results from these individual components or through a fusion of all of them using special algorithms (see Section 2.2.4.1). Individually, each component collects differing information from the environment. Accelerometers use a small mass within their circuitry to monitor changes in the Earth's gravitational field. By rotating the accelerometer gravity will move from one dynamic plane to another. Gyroscopes monitor angular momentum, usually measured in degrees per second. When a gyroscope is moved it determines the rate of change from one point to another, and through calculation is able to determine how many degrees it had moved, or would have moved, within one second. A magnetometer works on a similar principle to the magnetic sensors discussed above in that it can detect a change in orientation based on a change in the Earth's magnetic field on each dynamic plane. Much like other magnetic based sensors the magnetometer is also disrupted by ferrous metals and electrical fields.

IMU's are very often compared with optical tracking within literature due to its very high accuracy and its recognition as the gold standard in the motion tracking arena. IMU results have shown to be good in comparison to optical tracking with reported accuracies exceeding 90%[4,37,38]. The aim of most academics is to replicate the same accuracy of optical-based methods, but with the portability, freedom, and reduced cost, of IMU's. Research has found that body-mounted sensors can be very accurate, in the area of less than 7% RMS error in some cases[39]. Others found that inertial sensors in comparison to visual based gave a mean error of 2.27 cm without filtering, or 1.73 cm with a kinematic models filter[40–42].

The use of IMU's over optical systems have many advantages, such as cost and removing the limitation of being confined to a laboratory to collect data. However, some disadvantage of

IMU's include battery life, computation requirements, and data storage. Although these disadvantages were problematic in some earlier papers in this field, the technology has developed over time (as predicted by Moore's Law[43]) so that these are not as evident anymore.

2.2.4.1 Altitude and Heading Reference Systems

As previously mentioned, optical and IMU technologies output different motion information. Where optical technology produces positional (absolute) information of a moving object, IMU's can only produce relative information in their raw form. However, although the relative data cannot provide global information, it is possible to produce absolute positions through a combination of these sensors using an altitude and heading reference system (AHRS). An AHRS algorithm converts relative information from each component into a single absolute position by determining fixed global attributes. As Earth's gravity and magnetic poles do not change, the AHRS algorithm uses information from the accelerometer and magnetometer to determine a global start position. Through changes in rotation from the gyroscope, and further information from the accelerometer and magnetometer, the algorithm is able to calculate a change in absolute position over time, much like that from an optical motion tracking device.

Calculating absolute data from an IMU is beneficial, as having human positional data broadens the understanding of activity and health, however, AHRS algorithms are nontrivial and have many difficulties associated with them.

In order to estimate position from the accelerometer the accelerations must be integrated twice; once for velocity, and again for position. AHRS algorithms rely on this double integration of the combined sensor data which is not without its problems. The positional estimation can become increasingly inaccurate over time due to the quadratic growth of the accelerometer data which contains both sensor noise and calibration offsets. While some AHRS algorithms process just accelerometer and gyroscope data, many also include magnetometer data as well. The magnetometer is often excluded due to the additional inaccuracies it can introduce with local ferrous metals and electronic systems. However, in ideal situations the magnetometer can provide very useful additional information to the algorithm and can increase accuracy significantly[44].

Most popular AHRS systems use basic Kalman filters, a linear algorithm which estimates parameters from the sensor noise and calibration offsets errors mentioned above in order to optimise the process. However, others use the more advanced extended Kalman filter (EKF) or unscented Kalman filters, which are non-linear improvements on the Kalman filter, for more accurate results, with a trade-off of added complexity[45, 46]. These methods often return their rotation information in the form of Euler angles[47], however the use of quaternions have become a more preferred method due to their numerical stability and ease of use[48]. One major benefit of using quaternions over Euler angles or rotation matrices is their solution to

the gimbal lock problem; an issue where two of the three axes become parallel with each other, resulting in the rotation system falling into a 2D space as opposed to the original 3D space. Kalman filters are recursive processes and are computationally heavy, which some research has found are not fast enough to be used in various real-time situations[47]. Many have combined Kalman filters with other algorithms, such as Gauss-Newton methods (another optimising function), in order to reduce the complexity of a non-linear result from an EKF or unscented Kalman filters into a more manageable linear result[49]. Others have removed the need for Kalman filters altogether with methods such as gradient descent[50]. Some have opted to reduce complexity by performing their calculations offline or by removing components, such as the gyroscope, and have still obtained accurate results albeit movements must be slow[51].

IMU's have been used throughout literature for determining absolute position, but all experience the same drift and bias errors as mentioned above. Many have attempted to counteract these issues by using ground truths such as resetting errors at stationary periods[50], additional position data from global positioning satellites (GPS)[52], and fusion with optical based methods[53,54]. Fig. 2.6 shows an example of drift in a recreation of the foot tracking application documented in Madgwick *et al* with two feet[50]. Although individually each foot is tracking sufficiently due to a reset of drift during stationary periods, there is an exponential increase in drift between each foot, estimating that after a short walk of 3 m in a straight line the feet are close to 1 m apart.

Despite the issues presented here with calculation of absolute data from relative sensors, many applications do not require absolute information, and therefore these calculations are redundant. However, even in pervasive applications where absolute tracking is not needed, an AHRS algorithm will need to be implemented in order to validate results against optical methods, which do use absolute positioning, although this would be performed within a controlled environment and therefore the handling of noise and errors is much more manageable.

2.2.5 Other Motion Tracking Methods

Outside of the methods listed above there are many other motion tracking systems. The methods listed here were not deemed suitable for this work, either due to limited use or infeasibility in human application.

Navigation devices have been developed which combine vibrators, GPS modules, and LED's built into a belt to give tactile sense of direction when navigating to a location[55]. Although very suitable for navigation purposes this method has limited applications and was therefore not considered for this work.

Radio and microwave sensing are a popular method of navigation systems in aircrafts, however they have a very low resolution and are scarcely used in human applications[4,34].

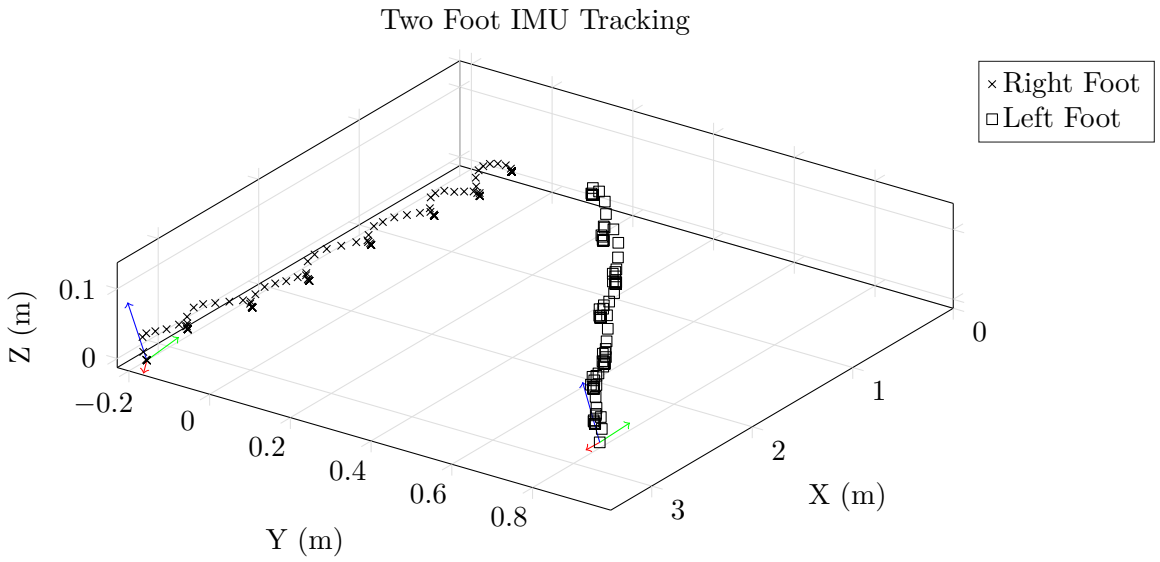


Figure 2.6: Example of two foot positional tracking with an IMU of a subject walking in a straight line, recreated as published by Madgwick *et al* with a single foot[50]. X and Z plane information track to a sufficient accuracy, however Y plane information is significantly off by estimating the two feet are ~1 m apart by the end of collection, even over a very short period where the subject walked 3 m.

Wearable technology, fitted into textiles, has been seen in human applications, due to their lightweight and ease of attachment. Despite this, their results have been found to lack accuracy, due to difficulties in calibration, however, this technology is still in the early days of development and improvements are expected[56].

2.2.6 Technology Requirements and Feasibility

This research has a number of applications which call for a certain set of requirements such as durability for use outside of a laboratory, sufficient battery life for prolonged use, and the technology being discrete enough for users to be comfortable wearing.

Prolonged data collection and use outside of a clinical environment has been found to contain more detailed results which may be missed during short collection sessions in a gait laboratory[57–60]. It has been recognised that certain factors have to be taken into account for successful extended collection outside of a laboratory including special consideration of long battery life to last several hours or days[61], small form factor so that the device does not become a burden to the wearer[62,63], and wireless capabilities for ease of use, transmission of data, and synchronicity between multiple sensors[64].

Some inertial systems have opted to remove the gyroscope due to its power consumption exceeding ten times more than that of an accelerometer[61], and have found ways to achieve sufficient data analysis without one[65,66]. However, others have mentioned the importance of the gyroscope, due to the non-trivial calculations of angular velocities in an accelerometer-only system[67,68]. The combination of sensors, predominantly accelerometers and gyroscopes, is

documented in many papers. Researchers have investigated the benefits of using accelerometers and gyroscopes on their own, and their influence on each other when combined. Attempts have been made to determine angles and angular velocity using just accelerometers, but results showed that with larger root mean square (RMS) values, accelerometers alone cannot produce accurate angular velocity readings[37]. Similar experiments using just gyroscopes have also been undertaken. Results show that integral drift was present, resulting in the need for discrete wavelet transforms to cancel out the error[15]. Combinations of inertial and visual sensors have been performed, resulting in each complementing each other[54].

While many studies developed their own technology for motion analysis, some have achieved the same results by using either commercially available IMU's[50,69], motion tracking suits[26], or inertial components available in mobile phones[70–72]. While using phones have their benefits, such as ease of acquirement and many subjects already owning the technology necessary, they have found to have disadvantages such as phone placement/orientation and disruption of the algorithm during normal phone use[71]. However, in applications such as phone security it has been found that unique walking styles are recognisable to an accuracy of 94.3%, allowing only the phone owner access to the device and removing the need for PIN or password[72].

Sensor feasibility is important when it comes to asking people to wear technology. If the device is uncomfortable, heavy, hinders mobility or range of motion, or requires too much input or human interaction to operate, the device will quickly become redundant as subjects and patients will not want to work with it. Furthermore, even with a reward incentive it has been found that this may not be enough for complete participation in studies[73]. In terms of medical applications where clinical personnel are involved, they too must be happy with how the device is operating and how the data is presented so that they can make sense of it. They also found that patients wanted the devices to be robust, light, and had a preference to non-visible sensors. It is evident from this statistic that inclusion of all stakeholders involved in the application process must be taken into consideration if the device is to be a success. If clinicians, engineers, patients, or carers (if applicable) are not happy with an aspect of the device or application then it is likely the project will not progress beyond prototyping stages.

2.2.7 Data Processing

Methods for processing the data vary depending on the application. These range from determining position and angles of joints and limbs, to classification of activities and abilities using simplistic or machine learning techniques.

Applications range from health monitoring and general activity analysis such as walking estimation, including cadence, stride length, and speed[40,63,66,68], to clinical applications such as detection, diagnosis, and monitoring of medical conditions such as cerebral palsy[69,74], and patellofemoral pain syndrome (PFPS)[75].

Generally, the processing requirements or computational load on a motion tracking system is governed by whether information is needed to be processed in real-time, as in immediately as data is collected, or offline (post data collection). In offline applications the only system requirement is the collection and storage of raw data, which can be dealt with at a later stage using a desktop/laptop computer where computational power is far greater and processing time and power consumption is less of a concern. Real-time processing, alternatively, requires the data to be handled as soon as it is received, which means the motion tracking device itself needs sufficient hardware to not only process the data fast enough (to keep up with the sampling rate), but also in an efficient way to minimise power consumption. Naturally, processing offline, where possible, is desirable as it considerably reduces the load on the system meaning less power consumption and longer battery life (if applicable) and less processing power required, however, in applications where a user needs a visual display, for example, a real-time implementation would be needed. Many pervasive motion studies do not require a constant stream of information to the wearer, and therefore offline processing is often suitable.

2.2.7.1 Classification

Classification, the process of extracting physiological or volitional activity from sensor signals, is critical for identification of activities, gestures, orientations, or movement in human application. Classification methods are very broad and can range from simplistic determination of static and dynamic activities (standing verses walking) to advanced techniques which implement machine learning and pattern recognition algorithms. Some simpler methods involve recognising which plane gravity is in on a tri-axis accelerometer in order to recognise standing, sitting, and lying[76,77], while others have used a single axis to determine the same information[78]. More technical approaches use methods such as wavelet transforms to monitor the elderly which pose a fall risk[15], hidden Markov models (HMM) to recognise activities such as eating and drinking[79], cadence estimation[68], and real-time classification[80], Bayes decision rule for motion detection[62], and principal component analysis (PCA) and Bayesian classification for gait analysis[70,74].

Alternatively, more in depth knowledge of human motion can be achieved by categorising multiple activities into separate events, such as walking, running, standing, and climbing stairs[80–82]. These methods often use supervised learning techniques where a training set is built by collecting data of known activities which are then used as templates for future data sets. Subsequent data sets are then compared against the training templates in order to determine activities which a set most closely resembles. Although accurate, this method may not be practical in situations where subject's activity strategies may change over time, such as during rehabilitation, as training sets will need to be recollected each time their strategy changes.

Unsupervised methods, however, do not require training sets as their method of classifying activities is done without prior collected data as a reference. Examples of unsupervised

learning in motion analysis include gait analysis and activity classification, much like those described above, however do not require training or retraining of data as recognised as a disadvantage to supervised methods[68,83].

Classification applications are equally as broad and include calculating angle and angular velocity of the upper body and leg during rise from a chair[37], analysis of the effects of age related sarcopenia[57], and body acceleration tracking of free-range animals[84]. Other applications intend to train subjects in activities, such as horseback riding[85], while others attempt to retrain in situations where an ability has been lost of hindered[75]. Kinematic models are used a lot in the field of biomechanics, and motion analysis has been used to build models to estimate forearm[40,42] and upper limb movements[41], characterise typical gait[26,39], and atypical gait[69].

2.2.8 Conclusion

In order to select a suitable motion tracking technology for pervasive applications a number of requirements need to be fulfilled, as seen below. Whereas some criteria needs to be minimised, such as power consumption and size, others need to be maximised, such as portability and accuracy.

To be minimised		To be maximised	
Power	Computational load and/or power consumption of the device.	**Accuracy**	Performance of the device.
Preparation	Time taken to prepare the device for use and/or calibration time.	**Portability**	Portability of the device and whether it can be moved.
Cost	Overall cost of the device including any consumable (if applicable).	**Access**	Accessibility to a user, such as any restrictions of use, or if it is commercially available.
Restriction	Restriction of movement or confined to an environment.	**Simplicity**	How simple the device is to use and operate.
Size	Size and weight of the device.	**Longevity**	Length of time the device can be used, such as battery life or other time dependant parameters.

Although many techniques and devices exist for motion tracking, it has been stated that there is no one device which can be used for every application[4,34]. Additionally, with as many technologies there are equally as many way to analyse and process the data, therefore a strong understanding of what is to be achieved with each human monitoring application is needed[86]. Conclusively, each technology was analysed for their applicability into human applications for pervasive use and their pros and cons can be seen in Table 2.1. Optical based methods, although arguably the most accurate, produced too many limitations including cost and confinement to a laboratory making it inaccessible in pervasive studies. Similarly,

Table 2.1: Different types of motion based technology and their pros and cons.

Technology	Pros	Cons
Optical (e.g. Vicon)	Gold Standard	Cost Not Portable
Magnetic	Accurate to high degree	Cost Susceptible to noise Limited portability
Mechanical	Portable Simple (in theory)	Cost Limited DOF Fragile
Inertial	Portable Cheap Light	Battery life

mechanical systems were ruled out due to the constraints the exoskeleton frame put on mobility and range of motion. Furthermore, mechanical systems are expensive and not discrete enough for use in public. Magnetic systems were disregarded as environmental disturbances would cause too many erroneous results in uncontrolled studies. Currently there is no optimal data collection, nor processing method, with a specific application to pervasive monitoring.

Optical based methods within a laboratory are an obvious choice, as parameters such as size, weight, concealment, or power consumption and not critical as they are in pervasive studies. Despite IMU's difficulty with absolute positioning, many pros were identified with cost, size, power consumption, and preparation time being low, whereas accuracy, accessibility, and simplicity of use are all high. Although absolute positional information would be beneficial, it was not seen as a necessity as the relative information from each of the IMU's components produce plenty of useful human motion information, therefore the difficulties in accurate absolute positions from inertial data are moot.

Due to these reasons, this research has chosen IMU's as the means of human motion collection. Being small, light, and easy to conceal makes IMU's optimal for subject use. Furthermore, the length of a single battery life is more than sufficient for prolonged use, and literature supports the use of IMU's in motion tracking applications[87].

2.3 Muscle Monitoring

Following motion analysis, muscle monitoring is of great interest to this work and is highly complementary to motion. Through fusion of motion and muscle information an additional understanding of human activity, which would be unobtainable with just one sensory type, is to be gained.

Muscle monitoring will broaden the understanding of human activity by introducing information such as muscle force, contraction change over time, and fatigue monitoring. When a muscle contracts there are two physiological phenomenon's happening; an electrical response, and a mechanical response. Two different muscle analysis technologies are detailed here, electromyography and mechanomyography, which respectively monitor the electrical and mechanical activity of a contraction. Benefits and downfalls will be listed and weighed in selection of a suitable muscle monitoring technology to be paired with human motion information.

Much like the selection of a suitable motion system, muscle monitoring systems need to be chosen for their pervasiveness abilities, unobtrusiveness to the user, and with specific applications in mind.

2.3.1 Contraction Types

In physiology there are three types of muscle contraction, two of which are of interest to this research, they include:

Isometric A contraction where muscle fibres contract, but there is no change in muscle length, nor movement in a joint. Also known as a static motion.

Isotonic A contraction where tension remains unchanged, however, the muscle length changes. Isotonic contractions can be further split into two types:

- **Concentric** Muscle shortens, while muscle tension increases.
- **Eccentric** Muscle lengthens, while muscle tension decreases.

The third type, isokinetic, is the opposite of isotonic in that tension changes during a movement where the speed remains unchanged. Isokinetic is not of great interest to this research as it rarely, if at all, appears in practical applications. Isokinetic contractions in exercise and training are controlled by a dynamometer; a machine that moves at a certain speed and varies its resistance to maintain that speed. Dynamometers are commonly used in literature to measure these contraction types, as well as monitor voluntary force output, and speed in non-static applications[88–90]. A visual representation of isometric and isotonic contractions can be seen in Fig. 2.7.

2.3.2 Electromyography

Electromyography (EMG) is a method of collecting skeletal muscle activity by means of monitoring the electrical response emitted from contracting muscle fibres.

Preparation of the skin and impedance requirements limit the length of time EMG can be used. A study which analysed both wet electrodes, which use electrical conductive gels to lower impedance, and dry electrodes, which do not require gels or adhesive for attachment, has been performed in order to determine longevity[92]. Despite finding suitable performance

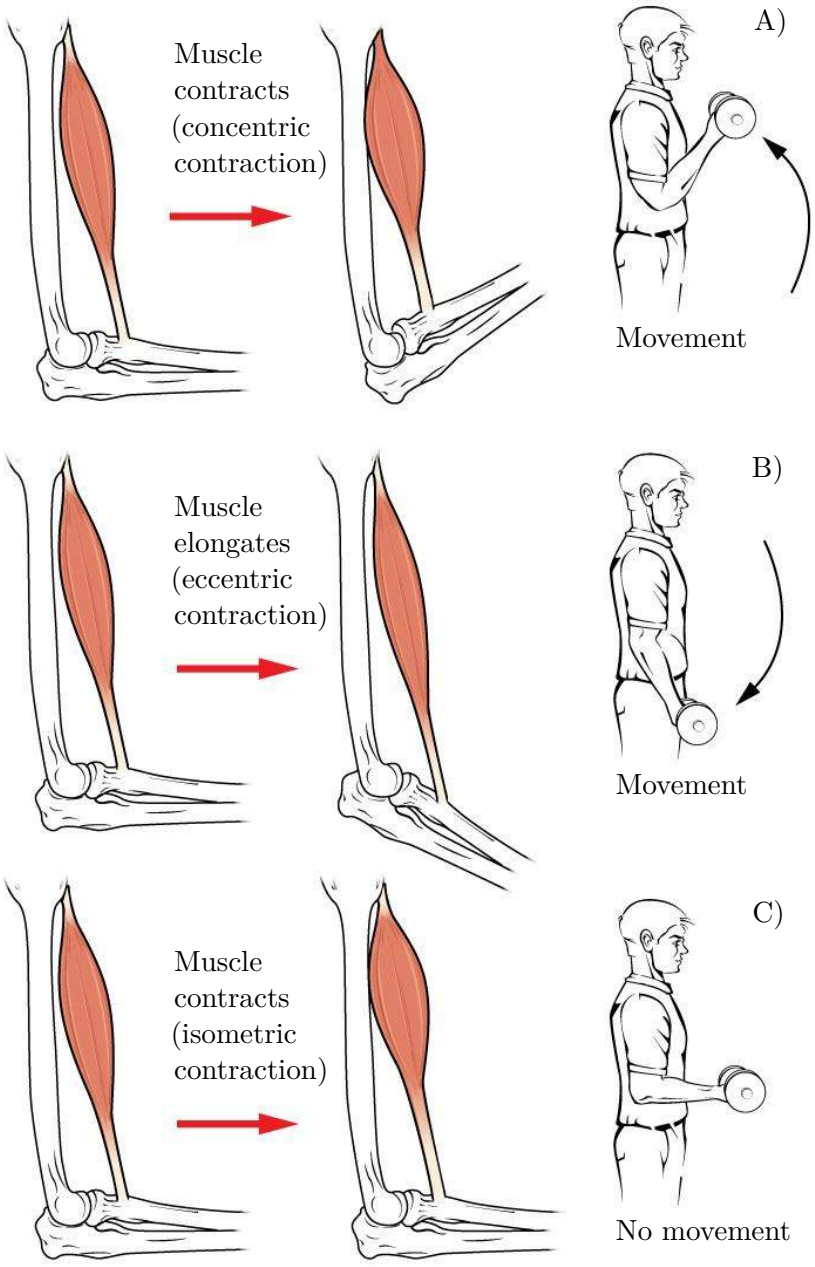


Figure 2.7: Image showing the different muscle contraction movements. Isotonic concentric (A), isotonic eccentric (B), and isometric (C). Reproduced under the creative commons licence CC BY 4.0[91].

from textile based sensors, which allows for a comfortable collection over a long period of time, all electrodes tested did see a change in impedance over time.

A great deal of literature is available on the signal processing aspects of EMG data, including classification of muscular activity[93], noise removal[94,95], and activity detection analysis[96]. In a review by Norali *et al* they found that multiple issues are present in EMG collection, including motion artefacts and signal instability, however, methods are presented in order to reduce these interferences such as amplification, filtering, and processing techniques[97].

The vast majority of EMG related research focuses on surface EMG, in which electrodes are

placed on the skin atop of a muscle of interest in order to monitor its activity [98]. Although a popular choice due to its non-invasive nature and ease of use, surface EMG is limited to superficial muscles. Another option is intramuscular EMG, which uses fine wire needles that are inserted into the muscle of interest[99]. These can monitor both deep and superficial muscles, however many countries have limited intramuscular EMG use to clinical personnel only, due to its invasive manner. Intramuscular methods also only give activity information of the immediate location of the needle tip, which limits the information of global muscle contraction especially for larger muscles.

Surface electrodes, which have a larger surface area to collect from, are further limited by skin impedance. This limitation can be reduced (but not completely removed) by means of preparing the skin before use. Shaving the area of hair, abrasing the skin with a rough pad in order to create a better surface for adhesion, and cleaning with an alcoholic wipe to remove oils and dirt, are all common steps in order to reduce impedance[98].

2.3.3 Mechanomyography

Mechanomyography is a low frequency vibration generated by lateral oscillations of muscle fibres, active muscle fibre twitches, and mechanical properties of contractions of skeletal muscle[7,9,100,101]. Mechanomyography has been referred to as many things over its development, such as sound myography (SMG), acoustic myography (AMG), and phonomyography (PMG), until mechanomyography (MMG) was fully adopted at the 1995 CIBA Foundation Symposium.

MMG signals change with varying strength contractions and its vibration is found to increase linearly depending on the tension, with the dominant frequency in the range of 25±2.5 Hz, and the majority of signal power below 50 Hz[102–105]. It has also been found that peak-to-peak acoustic amplitude increased with increasing temperature; likewise, increasing force up to 100% maximum voluntary contraction (MVC) increases acoustic amplitude[8]. However, forces over 80-90% have been found to lower or plateau the response[9,106,107]. Orizio *et al* stated that the MMG phenomenon derives from the summation of active muscle fibres twitches, but is only linear for low firing rates[100]. EMG does not share this response and its amplitude increases throughout all MVC, as seen in Fig. 2.8[108].

Muscles on opposite sides of the site of interest, for example the biceps and triceps brachii muscles, produced signals 180° out of sync with each other[106]. Furthermore, isometric torque production of the quadriceps has been found to increase as knee flexion increases[109].

MMG is often compared to EMG, which is considered the gold standard in muscle monitoring and is used abundantly in practice[7,8]. However, MMG is believed to be a suitable alternative and a good indicator of muscle activation when EMG is not feasible, for example in terms of chronicle implants and environments with electrical noise[110]. Sensor placement on the muscle has been found to be less important for MMG as opposed to EMG in that the signal

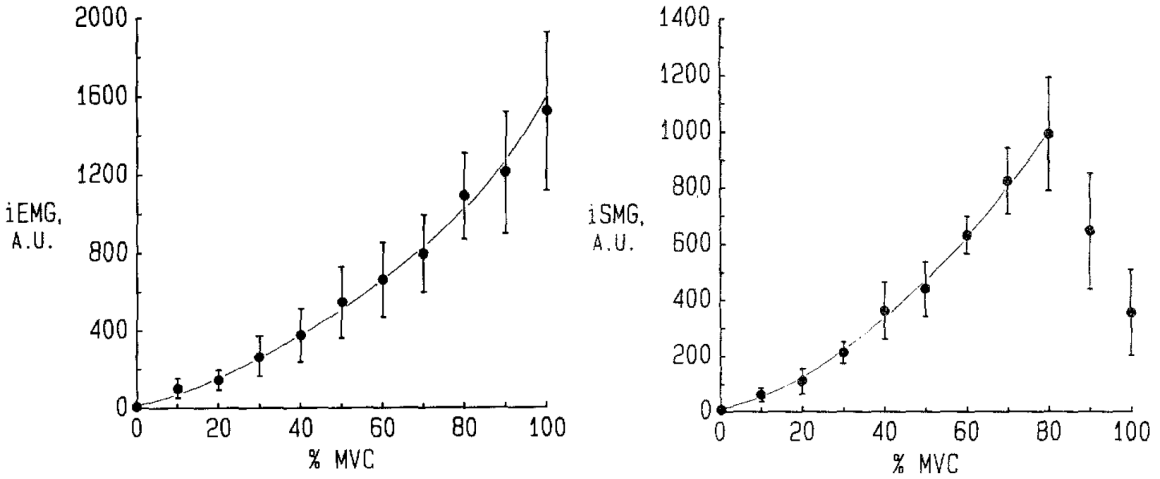


Figure 2.8: Comparison of mean integrated EMG and MMG (denoted here as soundmyography (SMG)) with increasing MVC. While EMG signal intensity increases throughout increasing voluntary muscle force, MMG declines above 80% MVC. Reproduced from Orizio *et al* 1989 with permission obtained through Springer Licensing[108].

response has been found to be sufficient when moved around on the body of a muscle[111]. MMG has been used to monitor a wide range of muscles which can be seen in Appendix B.

There are multiple means of collecting MMG information, most common methods include the use of accelerometers[100,110–122], microphones[7,101,123–130], hydrophones[106], piezoelectric elements[107–109,131,132], lasers distance sensors (LDS)[133], and near-infrared spectroscopy (NIRS)[123]. Unlike EMG, which can be bought as a complete technology, MMG is monitored using off-the-shelf components or custom made devices, due to no commercial products being available at this time.

Microphones are a very popular method of detecting MMG; however, almost as equally popular is the use of accelerometers to detect lateral extensions of muscles of interest. To determine the suitability of these methods, experiments have been performed such as comparing accelerometers with lasers, finding minimal difference between the two but with accelerometer being more suitable due to price, cost, and size[111].

Microphone performance has been compared with that of accelerometers also, finding that motion artefacts are far less apparent in microphones than accelerometers[134]. Other work in movement artefacts combined the two sensors of microphones and accelerometers to obtain more accurate results, finding that muscle activation results are far more accurate with the synergy of both technologies[135,136].

Methods to determine the best manufacturing of each technology has been performed, finding that in terms of microphone use and their housing the best sized chamber was 7 mm in diameter and 5 mm in height with a conical shape, which achieved an increase in gain of 6.79±1.06 dB/Hz against cylindrical shaped chambers[125]. Likewise, Silva *et al* found that microphones produced 6 dB more than accelerometers, albeit with a differing diameter of 13 mm and height of 2 mm which produced the highest SNR[126]. Accelerometers encased in

silicone have also been found to produce a better SNR than their non-encased counterpart, due to rejection of high frequency noise[118].

2.3.4 Fatigue and Cross Talk

Understanding when a muscle is fatiguing can be very beneficial in activity monitoring applications. If a user was to be alerted that their muscles were fatiguing this could reduce injury, provide information on the users physical limit, or allow for efficient muscle strength training techniques.

MMG can provide data to suggest when muscles are, or about to, fatigue. Although EMG methods can also produce information on fatigued muscle[137], both MMG and EMG show different attributes when muscle approaches and enters a fatigued state and reports have found MMG has a better result in predicting onset of fatigue[110].

Research has found that in a comparison between fresh and fatigued muscle, both EMG and MMG results show altered muscle unit responses shortly after a fatiguing exercise. However, after time to recover, changes in MMG's time and frequency domains are still present, contrary to EMG[131], with work stating that the effects of fatigue can last for hours[138]. Further work in MMG's time and frequency domains have found that after fatiguing isometric exercise the muscle unit activation strategy (MUAS) has substantial changes in comparison to fresh muscle, believed to be a result of impaired recruitment of fast, more fatigable muscle units[112].

MMG's median frequency (MF) of the power density spectra progressively decreases from the onset of a contraction, which is believed to be a result of circulatory and metabolic processes in the muscle (intramuscular mechanical pressure) that can be used to determine muscle fatigue before the sensation of fatigue becomes apparent[110,123]. Other work has found that MMG can be used to detect force changes when muscle is fatigued[7].

Cross talk is a problem where contraction information from neighbouring muscles influences the signal received on the muscle of interest. This problem is evident for both EMG and MMG techniques with suggestion that adjacent muscles could cause issues[104]. The understanding of cross talk is still unclear, however, studies have found that with proper precautions taken, such as sufficient distance between electrodes and sensors, that cross talk can be reduced, although not complete ruled out[109,139,140].

2.3.5 Applications

MMG has been used in a variety of applications, either in situations where EMG is infeasible, or accompanying EMG for more accurate results.

The vast majority of MMG literature looks at isometric muscle contractions, which minimises artefacts and other external noises which can be produced through motion. Dynamic

movements, which fall under isotonic contractions, have limited published MMG research, resulting in a gap in the field. However, in work where dynamic motion has been performed, often compared with isometric, results have shown that unique characteristics are seen in MMG signals between isometric and isotonic contractions, proving that MMG data can be obtained regardless of the type of motion[141,142]. Motion and skin artefacts are big limitations in accurate muscle monitoring, as they often obscure the contraction information, making interpretation difficult. EMG literature has less of a divide between isometric and isotonic contractions, as motion artefacts are less of an issue compared to MMG, however, they are still evident and precautions such as band-pass filtering are still applied.

EMG is used abundantly in biomechanics, gait analysis, muscular disorders, and human machine interfaces (HMI), as well as a vast array of applications, including monitoring of joint forces and stress in wall squats[143], cadence and muscle response during cycling[144], and prosthesis control[145].

Advanced prosthesis often use myoelectric sensors in order to control the limb. Research has been performed where the myoelectric electrodes (EMG) have been replaced with MMG[128], finding that MMG allows the use of soft sockets, removes the risk of wire breakage (due to the ability of distal recording), has the ability to classify between prosthesis gestures, and has the potential to detect and make use of weaker contractions, even finding MMG as a more accurate predictor of fatigue against EMG[105,136]. Furthermore, due to the similarities with EMG based prosthesis, patients are able to continue controlling the limb with little to no additional training with the MMG counterpart [146]. Comparison of prosthesis motion rejection was found to be very similar between EMG and MMG, however with a much better variation for sensor position with the MMG sensors[117]. Although MMG has many benefits over EMG, it has been noted that the best systems should use both sensor types as complementary to each other[147].

Gesture recognition, where specific actions are recognised and processed, has been achieved using MMG. A variety of classification methods have been used, including PCA and quadratic discrimination analysis (QDA)[113], continuous wavelet transforms (CWT)[148], and the use of stationary processes[149]. Results have been further improved with the inclusion of visual based systems resulting in an accuracy of 97.8% for two gestures[149]. Methods have also been improved with an increase in MMG sensors, finding that multiple sensors situated on the forearm produced a high accuracy[148,150].

Researchers and clinicians are interested in the diagnosis of medical conditions, specifically neuromuscular disabilities, by detecting the activation of muscles in subjects suffering from such conditions. Work has been performed with those suffering from Parkinson's, measuring differences in elbow agonists and antagonists[124]; sarcopenia, measuring the vastus lateralis during contractions of different intensities[115]; and spinal cord injury, evaluating the correlation between MMG and passive knee angular movement of the rectus femoris and vastus lateralis[116].

Other applications include the use of MMG for monitoring balance and posture[114], the integration of EMG into textiles, creating wearable power amplifiers[151], and control of orthotic devices[119]. MMG has been used as a HMI which allowed a binary input from the user while rejecting other sources such as speaking and humming[148], while other machine interfaces target low cost applications due to the expensive devices currently on the market[152].

Electrical stimulation is sometimes used for further evaluation of muscle and nerve function[9,100,112,138], but also in applications such as drug monitoring when muscles are under paralytic drugs, such as during surgery[122,153].

As with the selection of motion based technology, the type of muscle monitoring sensing needs to be selected based on its applicability to pervasive use. With this in mind important parameters such as ease of use, non-invasiveness, cost, ease of acquirement, and integration into motion collective methods are of the most importance. Table 2.2 shows a similar comparison of technologies to that used for selection of the motion technology. Using the same parameters previously listed, in which differing criteria needed to be minimised and maximised, MMG, surface EMG, and intramuscular EMG have been compared in order to select the most suitable technology for this work.

MMG has been found to be cheap, small, require little preparation, and has low power consumption. Likewise, it is easy to use, highly portable, and can be used for long periods of time due to being non-invasive and unaffected by changes in skin impedance such as during perspiration. The potential of MMG has been well recognised for some time, however, with no commercial device available, and a lack of proprietary sensors, the technology for MMG collection is immature and under developed. Furthermore, data analysis techniques for MMG signals, in particular for non-isometric contractions, are not well established.

2.3.6 Conclusion

Surface EMG, although accurate and the gold standard in muscle monitoring, lacks longevity of use for pervasive application, can be high in cost, and requires amplification and additional electronic components which can raise power needs and portability. Furthermore, intramuscular EMG is invasive and has a limited time in which it can be used. Access is minimal as only trained professionals can use the device, and although accurate, the information provided is only for a small area of muscle so is not practical in these studies. As with the use of optical systems in motion applications, the limitations of EMG listed here, such as how long it can be used, the amount of time it takes to apply the electrodes to the skin, and cost, are all less important in laboratory applications as they are in pervasive collection, and are therefore less of a concern.

From these results the technology chosen is MMG, due to viable use in pervasive applications, the ability to be used for prolonged periods of time, and ease of use with a well supported accuracy claim from current literature. Despite being susceptible to disturbances such as

Table 2.2: Different types of Muscle monitoring technology and their pros and cons.

Technology	Pros	Cons
Surface electromyography	Gold Standard Ease of use Non-invasive	Cost Limited Portability Long preparation time One use electrodes Limited use time
Intramuscular electromyography	Accurate results	Invasive Requires trained personnel to use Cost Limited use time
Mechanomyography	High accuracy Cost No preparation Ease of use Size and weight	Susceptible to noise Not as well established as EMG

noise and skin artefacts there are methods available to reduce such problems, including filtering techniques and using *a priori* knowledge by only looking at data collected at times of interest.

2.4 Motion and Muscle Fusion

Individually, muscle activity and motion tracking provide useful information which benefits many human monitoring applications. However, through combination of the two, a complementary additional understanding is achieved, which broadens the current gap in the field, as well as assists in the difficulties associated in pervasive studies. Inertial measurement units have been selected for monitoring motion and MMG for monitoring muscle activity. Individually they both meet necessary criteria such as being small, light, inexpensive, and easy to use, while still producing high results, allowing for unrestricted use in many environments, while not hindering movement or activity.

Fusion of these technologies, whereby motion and muscle activity is combined, has seen very limited use outside of a controlled environment, as recognised in the sparse relevant literature. However, collection of both motion and muscle activity is common in gait laboratories and clinical environments, with the likes of optical tracking and EMG being used for characterising gait disorders and other muscle/motion anomalies.

Some literature has looked at both motion and muscle activity using only IMU's[120,121]. Through filtering of the inertial data into low (motion) and high (muscle activity) frequencies, it was possible to obtain both data types without dedicated EMG or MMG sensors. However, in completely uncontrolled scenarios this method is questionable as noise and skin artefacts

could produce false positives for muscle contraction estimation. Furthermore, the sampling rate of the data is important, as although not required to be particularly high for motion information, due to fairly slow human movement speeds, the collection of muscle information requires a much higher sampling rate and therefore segmentation of inertial data could be troublesome with these two differing data types. Although MMG contractions are typically around the 25 Hz range, they have been found to be as low as 2 Hz, and therefore the splitting of motion and muscle information could result in the loss of particularly low frequency muscle information.

Research has been performed in using more accessible technology in clinical environments. Substituting an optical system for an IMU, posture and balance monitoring was achieved with additional information from EMG and a balance platform[13]. Although the hardware itself was not combined into a single package, the use of commercial technology meant a cheaper solution to current methods in gait laboratories. However, although cheaper and more portable, the use of this technology is not completely pervasive as it still required multiple pieces of individual technology to be applied to the subject, a controlled protocol of use, and the additional problems associated with wet electrode EMG, as stated before.

Further fusion of motion and muscle data has been demonstrated in a HMI application which combined both EMG and IMU technology to interact with a computer in lieu of a mouse[154]. Although accurate, the application seemed limited to just the computer HMI task, and the use of wet electrode EMG again limited the amount of time it could be used. However, fusion of both the IMU and EMG data allowed for specific hand gesture recognition to an accuracy of 88%, which displays the potential of motion and muscle fusion in further human applications. As with other literature in this field, the biggest limitation in pervasive studies is the lack of practicality in a single package device which can be easily donned and doffed, and the use of EMG which has impedance issues that can cause problems in prolonged applications.

More pervasive studies, of which technology is packaged in a single, wearable, form, has been observed in more uncontrolled environments, with IMU combined with EMG[12], and MMG sensors[155]. As longevity of EMG has been identified as limited, due to degrading electrode contact and change in skin impedance, MMG has been recognised as a more favourable alternative to EMG for prolonged use. Although only demonstrating intermittent collection over the course of a day, one paper has identified the need for an IMU and MMG device which can collect for continuous prolonged periods of time[155].

2.5 Chapter Summary

By means of combining human motion and muscle activity, this research intends to close the gap in current literature by fusing the two data sets in order to obtain additional, complementary information. The research presented in the following chapters describes

the development and implementation of a single-packaged, easy to use device, which can collect pervasive data for prolonged periods of time. The unique attributes of this work is the synergy of motion and muscle activity of humans in an uncontrolled and unrestricted environment, outside of a laboratory or clinical setting. Current research performed on external or home-use fusion of motion and muscle activity is particularly unexplored, of which this work will analyse.

3

Design

Contents

3.1 Introduction 32
3.2 Identification of Needs 32
3.3 Inertial Measurement Unit 33
3.4 Acoustic Sensor 36
3.5 Force Gauge 39
3.6 Iteration and Improvement of Technology 40
3.7 Software 43
3.8 Chapter Summary 44

3.1 Introduction

Having selected inertial measurement units and mechanomyography as the means of human motion and muscle monitoring technologies, a selection of devices was required. Currently, no commercial MMG sensor is available, and all literature either utilises current technology on the market, such as accelerometers or condenser microphones, or develop their own.

IMU's, on the other hand, are fairly common commercially, and are available in a number of packages such as complete devices, or system on a chip (SOC). Although IMU's are generally much cheaper than that of alternative technology, they do still vary in price, ranging from a high region of ~£1000 for xSens, a mid-range of ~£300 for x-IMU, and a low-range of ~£50 for a breakout board IMU. Furthermore, each of these technologies vary in functionality, with the cheapest option offering the least customisation and additional technology like data storage options or transmission methods such as Bluetooth or WiFi.

Despite a wide range of choice in terms of IMU's, each found had a limitation which could not be overcome. These include cost, limitations of functionality, but most commonly a lack of ability to collect MMG data alongside motion. Although most IMU's allow you to select and change various parameters like sampling rate and what data type to output, they are very often 'closed source' in that the firmware does not allow editing to suit a particular need. With the exception of the x-IMU, most other IMU's do not have an auxiliary port, which allows additional sensors to be collected alongside the inertial data. Being small, wearable, and light are all requirements of a device in this research, and therefore combining two technologies, such as a DAQ and an IMU, in order to collect both MMG and inertial data respectively, is impractical and creates another issue with data synchronisation.

Due to the limitations of current market IMU's, and the lack of commercial MMG sensors, it was decided that both devices will be custom made from the ground up. A fully integrated system was developed for concurrent motion and muscle collection.

3.2 Identification of Needs

Stakeholder inclusion is paramount in the successful design, development, and distribution of a device of this nature. Unsuccessfully meeting the needs of the user, poorly presented data, or lack of functionality, will result in a device which clinicians are not happy working with, and wearers are reluctant to use. Therefore, from the onset, this system has been designed and implemented with the stakeholders needs in mind. Specific requirements include:

Size and weight The device must be small enough for unobtrusive wearability, while light enough to be forgotten while worn.

Battery life Due to the prolonged monitoring this research is targeted towards, the system must have sufficient battery life to last at least a working day before recharging, with either enough storage or transmission capabilities to handle the data collected.

Simplicity The device must be easy to use and not confusing for the user. Operation must be obvious and non-complex.

Unrestrictive Through a low profile, non-obtrusive sensor mounting, and non-protruding wires, the system should be easily worn and unrestrictive in regular day-to-day activities.

Data presentation Other than hardware requirements, the software and data presentation must be in an easy to follow, easy to interpret way.

These requirements were used in initial design of both the IMU and MMG sensors developed here, as well as throughout the iterations and improvements made during this research.

3.3 Inertial Measurement Unit

In order to accurately and efficiently collect human movement in a number of different applications, inertial measurement units were selected as the technology of choice due to low cost, weight, processing abilities, and ease of use. The majority of other possible choices were not selected usually due to their high cost and lack of portability. The IMU developed, called the Aktiv (45x30x9 mm (LxWxH)), can be seen in Fig. 3.1.

3.3.1 Core Functionality

Processing, data collection, and power management was performed by means of a PIC microcontroller, produced and manufactured by Microchip. This integrated circuit (IC) samples data at 40 million instructions per second (MIPS) with a 16 bit architecture.

The IMU has an on-board power management circuit, which allows the charging of a lithium-ion (Li-ion) battery through a micro USB port. Charging times are between one and two hours with a 1000 mAh Li-ion battery (50x33x6 mm (LxWxH)), which is displayed to the user by a red LED that turns off when fully charged.

Turning the device on was performed using a switch that put the device initially in a ‘sleep mode’ where sensors, processing, and transmission are all disabled and the PIC is put into a low power state. Through a button press the IMU can be switched into ‘active mode’ where all sensors and processes are turned on and data is either transmitted (via Bluetooth or USB) or stored (on a micro SD card), depending on the desired function, which is set during initial programming of the device. These modes are easily distinguishable by the user with either a red (sleep) or green (active) LED being illuminated when in each respective mode.

An on-board crystal oscillator (32.768 kHz) is also present, which allows real-time clock and calendar functionality so that data stored on the micro SD card can be time stamped

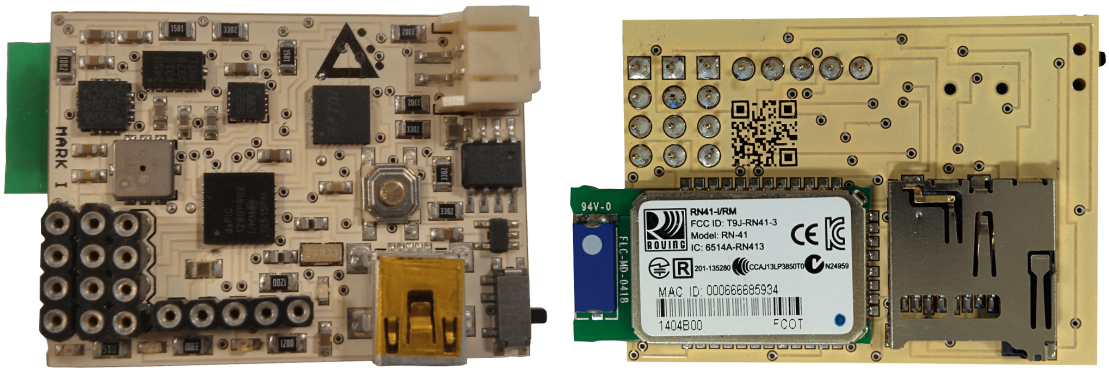


Figure 3.1: The Aktiv IMU without battery - front (left) and back (right). Image not to scale.

for assistance with offline processing. The oscillator has a high frequency tolerance of ±20 ppm (0.002%), which is used for very high accuracy in sampling rates for both inertial and additional sensors.

3.3.2 Inertial and Pressure Sensors

Inertial data was collected by means of an accelerometer, gyroscope, magnetometer, and a barometer. Communication between sensors and the microcontroller was achieved using I^2C at a bus speed of 400 kHz. Each component had its own maximum sampling rate, however, the inertial sensors combined had a maximum sampling rate of 128 Hz, which is more than sufficient for human motion collection[156]. The barometer had a much slower sampling rate of 1 Hz, however this too was sufficient for altitude changes in human applications when going up or down stairs or elevators.

3.3.3 Auxiliary Port

In order to collect MMG data simultaneously with the inertial and pressure data, a dedicated auxiliary port was implemented onto the board. This port, which allowed up to four additional sensors to be attached, could sample either analogue or digital devices, or could be used as a digital trigger for synchronisation needs.

Predominantly this port was used as an analogue input and had a variable range of sampling rates from 4 Hz to 1024 Hz at 10 bit analogue to digital (ADC) conversion. To reduce computational need, increase battery life, and reduce transmission bandwidth, it was possible to select only the necessary ports needed for a specific application, from one to four channels, or turned off completely if the auxiliary port was not needed. The ability to select the number of channels needed is an improvement over the x-IMU, which was only able to collect from all ports, or none at all.

3.3.4 Battery Life and Storage/Transmission Capabilities

Data is manipulated by means of one of three methods. A micro SD card, which can be inserted into the back of the device, can store and process data at a later date and supports card sizes up to 64 GB, which communicates with the microcontroller by SPI. Data can be processed in real-time by either USB transmission using the same USB port mentioned for charging above, or a class one Bluetooth module (v2.1), which can transmit the data wirelessly (both of which communicate with the microcontroller via UART). Bluetooth was selected over other wireless technologies due to its abundant use in other devices, such as personal computers and mobile phones, which allows for easier communication between devices. A blue LED indicates when the Bluetooth module is active and transmitting. Data is transmitted and stored in binary format to keep size very small. In order to convert the raw binary data into meaningful accelerations or rotations a post-processing program was written to quickly convert results and output them into a comma-separated file type (CSV), which is discussed in Section 3.7.

Through extensive testing with all channels of the auxiliary port turned on, and inertial, pressure, and auxiliary sensors sampled at their maximum rate of 128 Hz, 1024 Hz, and 1 Hz respectively, the Aktiv was capable of ~10 hours of battery life for all three data processing methods (USB, Bluetooth, or SD storage) mentioned above. Likewise, with the same sensors and sampling rates an SD card of 1 GB can store a little over 24 hours of data, whereas a 64 GB card could store 66 days.

3.3.5 Manufacturing

The Aktiv IMU was developed and tested using a solderless prototype circuit board (breadboard), which was built upon with each function listed above using through-hole components. Following completion of testing and development with the prototype board the first iteration (Aktiv Mark I) was manufactured. The circuit board is a two layer printed circuit board (PCB) and comprises of almost entirely surface mount components, which were hand assembled in the UK.

3.3.6 Firmware

The Aktiv IMU is programmed entirely in MPLAB with the XC16 compiler and is written predominantly in C, however, Assembly has been used in places where C was not feasible. All data is stored and transmitted in its raw binary form, meaning conversion to meaningful information is either performed offline, or in real-time on the receiving device.

Inertial data (accelerometer, gyroscope, and magnetometer), barometer, and auxiliary port data are separated into individual packets, each with a header byte preceding the data, and

two checksum bytes following the data. The checksum bytes are equal to the sum of the header and data bytes, which is calculated before transmission/storage. This checksum is recalculated on the receiving device or through offline processing and compared with the checksum value in each packet to determine successful transmission/storage of the data.

Fig. 3.2 shows the packet sizes and structure for each data type transmitted/stored. In order for the barometer to produce temperature and pressure data it requires a ground truth reading right when the device is turned on, which collect initial readings and configuration parameters. The auxiliary packets change size depending on how many channels are turned on. Just one channel will have a packet size of five bytes, whereas all four channels will have a packet size of 11 bytes.

3.3.7 Summary

As part of this research the IMU's developed here, had to satisfy several criteria to be successful in the applications to be performed. The device had to be used by a number of different personnel, including engineers, clinicians, and patients/subjects, therefore ease of use was an important factor when designing.

In order to collect muscle data alongside inertial information the device needs functionality to attach additional sensors with ease, while not impairing any other aspect of the device's ability.

Finally, sampling rates of each sensor type needs to be high enough for each application, which is generally above 40 Hz for inertial components[157], while also satisfying the Nyquist-Shannon sampling theorem. The devices main attributes can be seen in Table 3.1.

3.4 Acoustic Sensor

In order to monitor muscle MMG responses, an acoustic sensor was chosen due to its better SNR over accelerometers[126], low cost, ease of manufacturing, and better rejection of motion artefacts[125].

The sensor presented here is based on that developed by Posatskiy *et al* at the University of Toronto's Prism Lab, which relies on the detection of a pressure change within a sealed chamber[125,134]. The chamber is covered by a piece of Mylar, and a microphone (Knowles SPU1410) positioned at the opposite end of the chamber records the pressure change when the membrane is disturbed. Both the choice of microphone and Mylar used in this device were selected on their suitability in MMG collection, as discovered and documented by Posatskiy *et al*.

When the device is placed on the skin above a superficial muscle of interest, the sound produced during contraction propagates through the membrane and creates a pressure

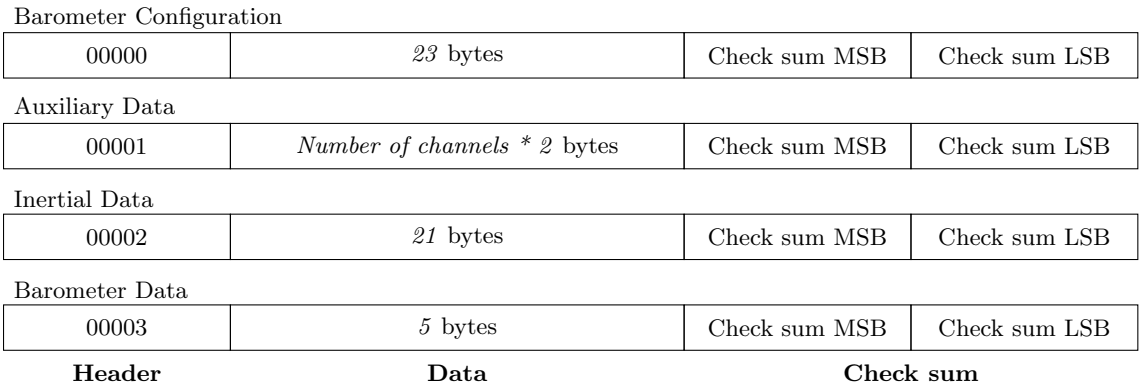


Figure 3.2: Packet form for each data type, which are identified using a unique header byte value. The two check sum bytes (most significant and least significant byte (MSB/LSB)) equal the sum of the header and data bytes of each packet.

Table 3.1: Key attributes of the Aktiv IMU.

Inertial sampling rate	128 Hz (max), 64 Hz (typical)
Auxiliary sampling rate	1024 Hz (max/typical)
Pressure sampling rate	1 Hz (max/typical)
PIC clock speed	80 MHz (max), 40 MHz (typical)
Battery life	10 Hours
Battery type and size	Lithium-ion, 1000 mAh (typical)
Charging time	Between 1 and 2 hours
Storage capabilities	~1 day (1 GB), ~66 days (64 GB)
Crystal oscillator clock	32.678 kHz (±20 ppm)
I^2C (inertial sensors)	400 kHz (fast mode)
SPI (micro SD card)	10 MHz
UART (USB and Bluetooth)	230400 bd
Number of auxiliary channels	4
User input	Switch (on/off), button (sleep/active mode)
Programming language(s)	C/Assembly
Notification LEDs	1x green (active mode), 2x red (sleep mode and charging), 1x blue (Bluetooth)

difference within the chamber. The lateral movement of fibres during a contraction produces a low frequency vibration, nominally around 25 Hz with the majority of signal power below 50 Hz, which is collected by the MMG sensor[7, 103, 104, 158]. Following the technical specifications discovered by Posatskiy *et al*, a chamber height and diameter of 5 mm and 7 mm respectively was used, which they report produces a maximum gain, reduces the frequency-response fluctuation, and reduces high-frequency distortions. Its conical shape increases signal gain by 6.79 dB/Hz[125]. Fig. 3.3 shows the Posatskiy *et al* design, whereas Fig. 3.4 shows the design presented as part of this work (21x9 mm (⌀xH)).

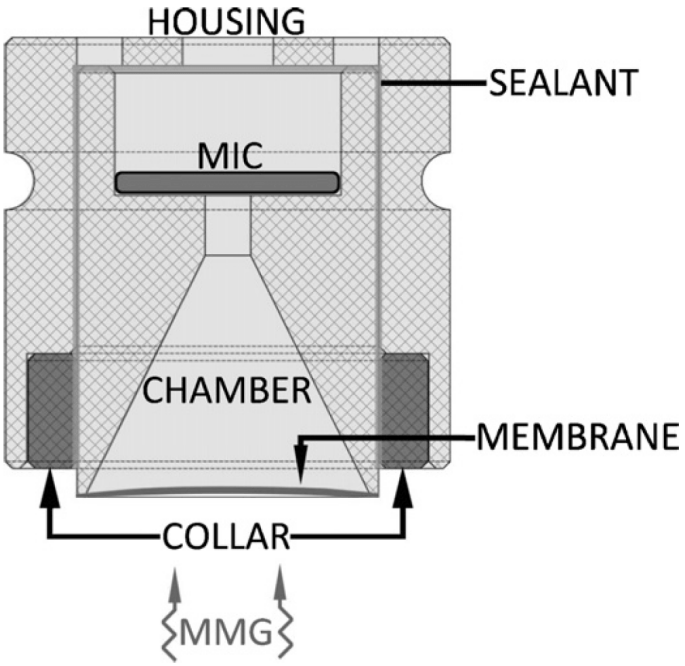


Figure 3.3: MMG sensor designed and presented by Posatskiy and Chau. Reproduced from Posatskiy *et al* 2012 with permission obtained through RightsLink[125]. Image not to scale.

3.4.1 Construction

The MMG sensor presented here consists of three parts:

Housing The housing is the core of the sensor, with a conical chamber at one end, and a microphone at the other. Sound propagates though the chamber to the microphone, which is mounted atop a circuit board. Silicone is inserted on top of the microphone to stop back propagation of sound and improve acoustic containment.

Sleeve The sleeve keeps the Mylar membrane taut when stretched across the bottom of the housing. This is achieved using friction compression, with no adhesives involved.

Clip The clip serves two purposes: to contain the sensor, and for attachment methods. The clip has a number of features to enhance the usability of the device, including a double level groove, which allows attachment to fabric, and small holes in the top to allow for sewing to clothing. Additional holes in the top of the clip allow for disassemble of the sensor, if repairs are required.

3.4.2 Manufacturing

The acoustic sensor was manufactured in two parts. The first is the sensor body, which is 3D printed using an Objet Eden 500v printer in VeroWhitePlus material (acrylic). The parts have an interference fit with a gap of 0.15 mm between each connecting part. This allows a tight fit, which keeps the membrane taut and removes the need of adhesives to keep parts together.

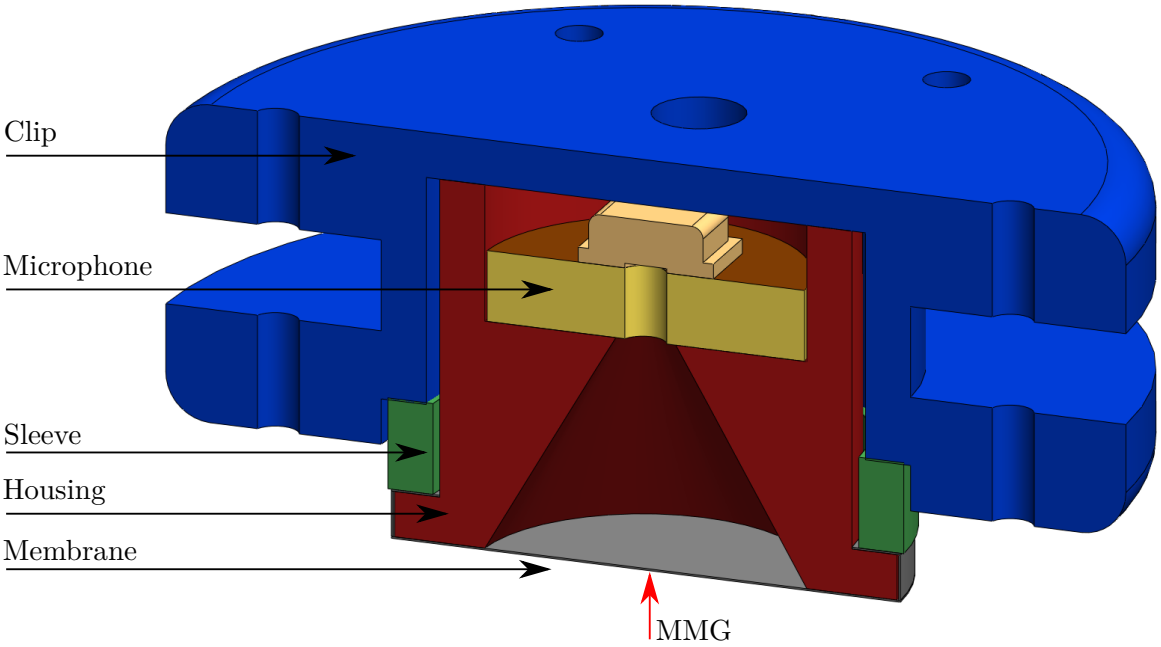


Figure 3.4: The MMG sensor designed and presented as part of this research. Image not to scale.

The second stage is the manufacturing of the microphone PCB boards. The boards are milled using a LPKF ProtoMat S63 manufacturing machine, and then the assembly of the single surface mount microphone to the board is achieved using by automated pick and place. Three wires are soldered to the board, by hand, which provide the power (positive and ground), and signal. Fig. 3.5 shows a constructed microphone board.

3.4.3 Summary

Although larger than a typical EMG electrode (~20x1.5 mm (⌀xH)) the MMG sensor described here has a sufficiently low profile, can be used multiple times, and does not hinder movement or range of motion.

The sensors are cheap to make (~£10), easy to attach to clothing or bands to be worn, and can be sampled by the Aktiv IMU developed.

3.5 Force Gauge

MMG sensors attachment to the skin can produce varying results when contact pressure differs. Although the range of contact pressure is quite broad, meaning a fairly minimal difference is seen within a degree of tightness to the skin/muscle of interest, some applications requires a much more sensitive analysis of muscle performance, which cannot be achieved through estimation of sensor contact pressure.



Figure 3.5: Acoustic sensor microphone PCB board design, with microphone and wires attached. Image not to scale.

Therefore, a device was developed to determine MMG sensor contact pressure when attached to the skin of a subject. The device, as seen in Fig. 3.6, consists of a force sensitive resistor (FSR), small circuitry including a microcontroller, and a liquid crystal display (LCD).

When a force is applied to the FSR the circuitry converts the change in resistance to a measurement in grams, which is then displayed on the LCD for the user. Optimal applying forces have been found to be below 200 g, which has been found to be high enough to avoiding relative movement of the sensor with respect to the muscle surface[104].

3.6 Iteration and Improvement of Technology

Unlike the development process of the IMU, which was finalised on one iteration, the acoustic sensor went through numerous versions. Changes from each version were usually minimal, such as an attempt to reduce height, size, or correct lose fitting parts from trial and error. However, more substantial changes include the substitution of single-core wire, which was vulnerable to breakage, to a multicore wire, which eliminated these problems, and various design changes, which reduced the size by 45%. Fig. 3.7 shows a comparison of some of the sensor iterations.

3.6.1 Sensor Integration and Wearable Aspects

Outside of hardware development, the technology had to be integrated into bands, straps, and clothing in order to be worn. This process involved many iterations, as feedback from the wearers of the technology often had improvement suggestions or practical information on what does, and does not, work in wearable technology such as this.

This work used a variety of attachment methods, including elasticated straps which wrapped around limbs of interest or compression sleeves often used in sports (as seen in Fig. 2.2). The MMG sensor attached with ease to these attachment methods, as a simple hole cut into the fabric allows for the sensor to be securely fastened and sewn in place. However, the IMU and battery are less accommodating to such attachment methods, as they have to be secured, protected, and still allow easy interaction for user operation.

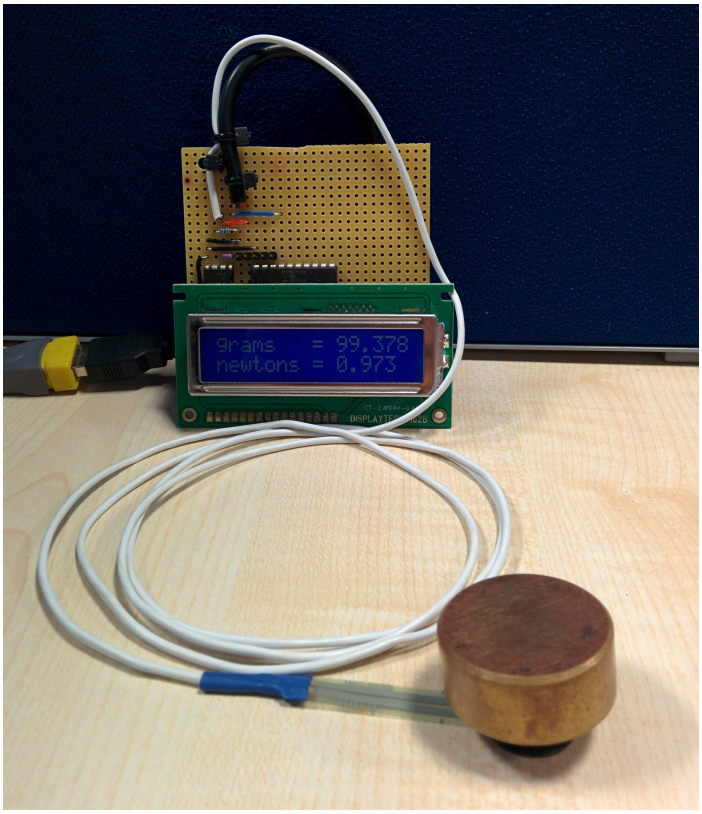


Figure 3.6: Force gauge used to determine MMG contact pressure on the skin. Image shows the FSR with a 100 g weight atop of it. The LCD is displaying a reading of 99.378 g; an accuracy of 99.4%. The device is powered by USB and is portable for use in a home environment.

In order to achieve successful IMU/battery attachment, cases were constructed which would allow easy integration into braces and clothing. The cases went through multiple iterations and designs, the first and last of which can be seen in Fig. 3.8. All versions were 3D printed using additive manufacturing methods.

3.6.2 Stakeholder Feedback on Design

Feedback from the stakeholders involved in this research, especially those wearing the technology, was very beneficial to the development and practicality of sensor attachment. Following the first iteration of the IMU/battery cases, of which were printed using a low-cost, layer based, 3D printer (RepRap), suggestions from the wearers led to the final versions of both the MMG sensor and IMU/battery cases, as well as improvements in attachment methods. These included:

Robustness Early iterations of the cases were made using low-cost printing methods, which resulted in a low quality construction that were prone to breaking.

Ease of use Although specific access points were implemented into the IMU cases in order to switch on the device, press the 'active/sleep' button, or plug in the USB cable for charging, the feedback from users suggested larger openings and better positions in order to access the IMU more easily.

Design The first version of cases had lids which sat on top of the IMU board, which had a tendency to fall out of place. The final case versions had a redesigned sliding lid which

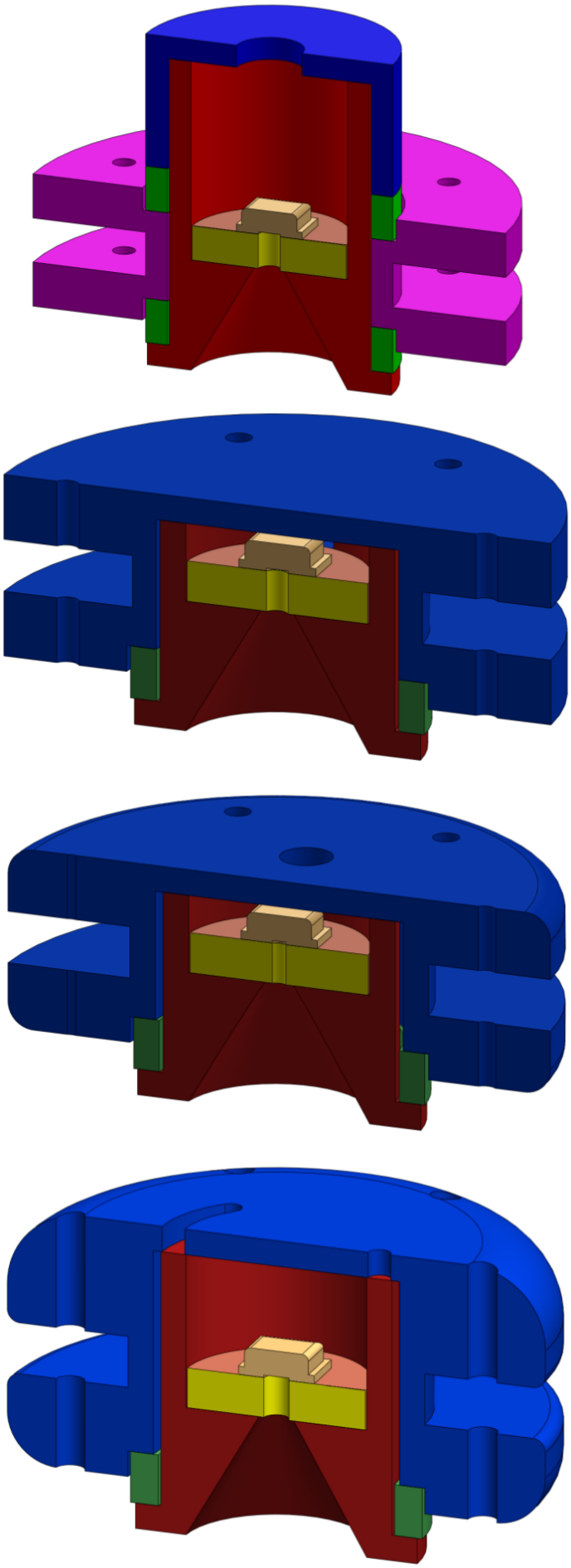


Figure 3.7: From top to bottom:

Version 4 - The cap (blue) allowed for easy repair and dismantlement, however, contained a lot of wasted space above the microphone board;

Version 7 - Removal of the cap resulted in a reduction in size by 45%, however with the sacrifice of dismantlement once assembled;

Version 8 - Allowed dismantlement by means of a number of 'push holes' on the top of the clip (blue), which allowed the housing (red) to be pushed out for membrane repairs. The edges were rounded in order to avoid catching on clothing;

Version 10 - The final version brought together all of the benefits of the previous versions, with rounded edges, 'push holes' for dismantlement, and additional space above the microphone for silicone to prevent sound back-propagation.

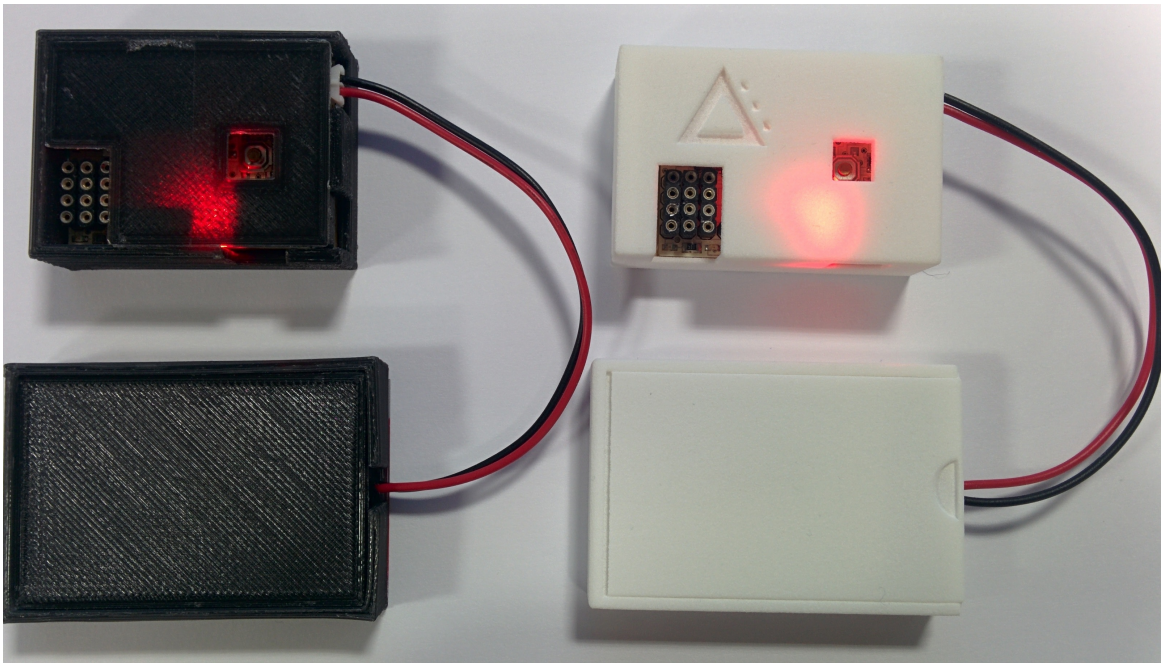


Figure 3.8: Iteration change of IMU/battery cases from the first version (left) to the last (right). The black case was printed using a RepRap 3D printer in PLA material and suffered from a weak structure and poor design. The white case is the result of constant stakeholder feedback and improvements, including a much stronger nylon material, better design both practically and aesthetically, and a lower profile for better concealment and wearability.

locked in place.

Profile Improvements were made to both IMU and MMG housing in order to round off edges and corners, lower profile, and change attachment locations (where applicable) in order to lower obtrusiveness.

3.7 Software

Data transmitted or stored from the IMU was saved in a binary format (BIN) and was converted to CSV files, which can be opened by Microsoft Excel or virtually any text editor. Each data type (inertial, barometer, and auxiliary) is written to separate CSV files for simplicity in processing and further storage. Online processing was also possible, using MATLAB and a Bluetooth connection. Data can be streamed from the IMU and displayed, in real-time, in a graphical form.

A standalone program was written, which could process individual files, or multiple files within a directory, and output their converted file types. Also written in C, this program had a minimalistic appearance and could convert a ten hour BIN file in under fifteen seconds. Fig. 3.9 shows a screenshot of the program in use. Another piece of software of a similar appearance was written to program the real-time on-board clock, which keeps track of the date and time that is written to each BIN file when created on the SD card. The program,

as seen in Fig. 3.10, connects to the IMU via Bluetooth or USB, and updates the on-board real-time calendar/clock to the current date and time.

3.8 Chapter Summary

An inertial measurement unit and a mechanomyography sensor were designed and developed for human motion and muscle activity monitoring, using feedback from stakeholders involved in the process. Furthermore, necessary software, manufacturing, and peripherals such as cases to house the IMU, and a force gauge to monitor MMG contact pressure, have been presented here.

The following chapters validate these sensors against other measurement techniques, and apply the technology to a range of applications. All schematics and technical drawings can be found in Appendix C for all the technology presented in this chapter.

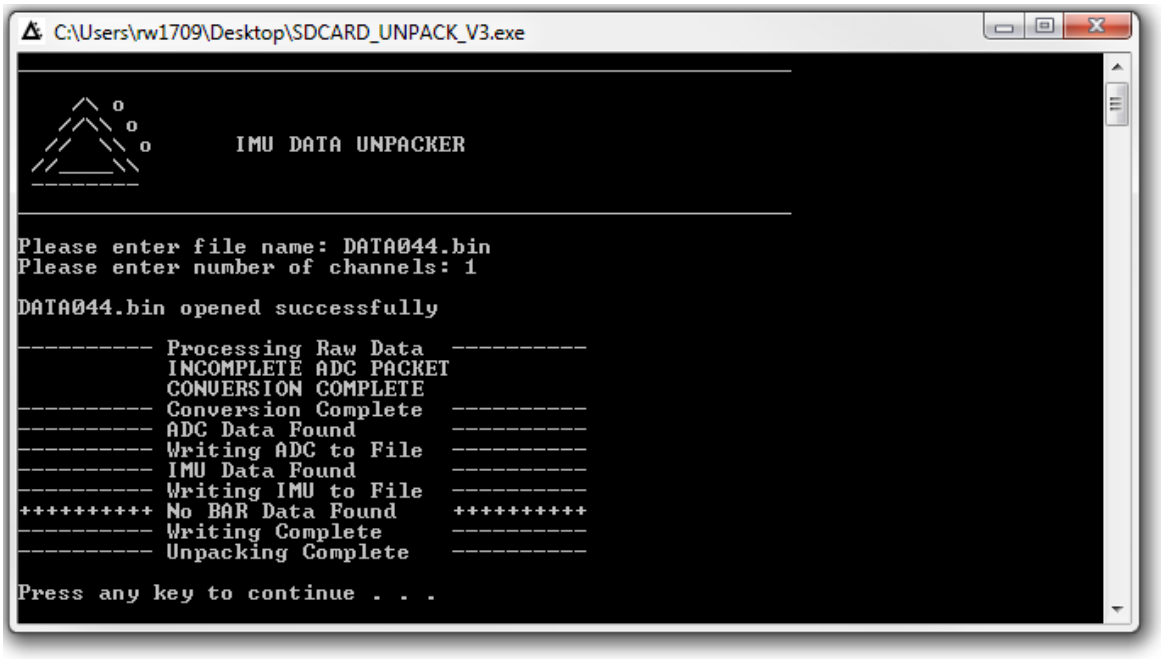


Figure 3.9: Screenshot of the data converter program that processes the binary data into usable sensor information. The number of channels entered indicates the number of auxiliary ports active is this data set. The 'incomplete ADC packet' message is a result of the IMU being stopped during an ADC packet being collected, and thus this packet was lost. In this example the barometer was disabled in order to show the programs recognition of a missing data type and the processing of the remaining data.

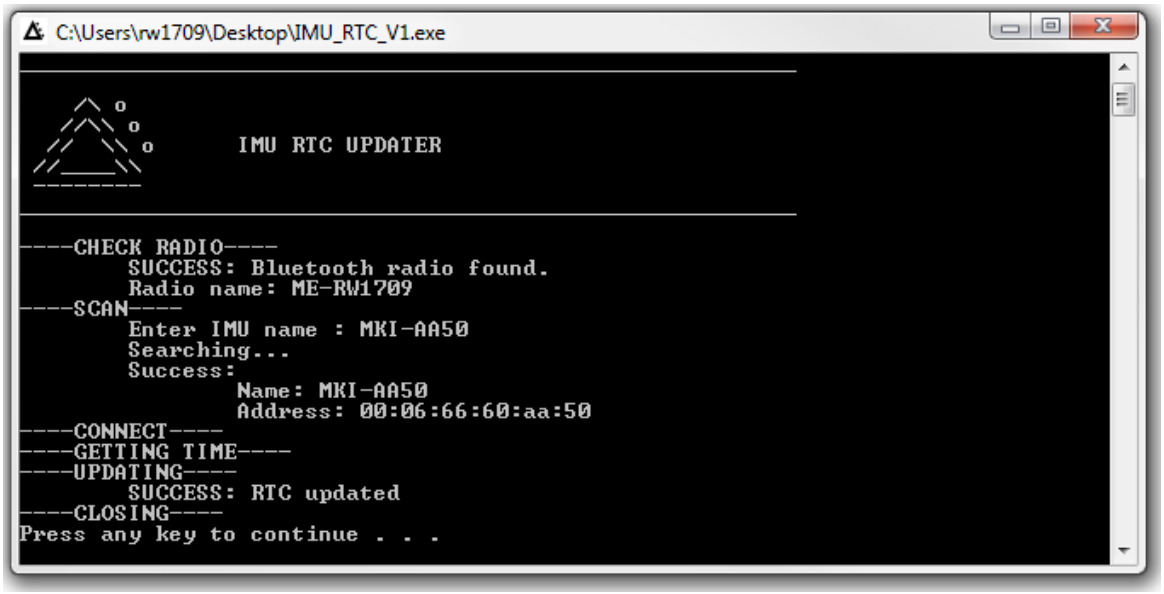


Figure 3.10: Screenshot of the real-time clock update program that changes the on-board clock to the current date and time. After connecting to the IMU via Bluetooth the date and time is taken from the computer used to run the program and sent to the IMU for updating.

4

Validation

Contents

4.1 Introduction 48
4.2 Validation of Frequency Sensitivity 48
4.3 Validation of Muscle Contraction Data 48
4.4 Validation of Motion Data 50
4.5 Chapter Summary 56

4.1 Introduction

In order to demonstrate the accuracy and usability of the technology present here, a number of tests and experiments were performed with the comparable gold standard technologies and controlled rigs with known responses.

All studies were approved by the Imperial College Research Ethics Committee (ICREC) and written consent was obtained from all subjects involved.

4.2 Validation of Frequency Sensitivity

To determine the ability of low frequency collection using the acoustic sensor, an apparatus was constructed to be used with a custom made vibration rig which oscillates at an accurate frequency. An acoustic sensor was sandwiched between a wooden base and a sheet of Plexiglas with the chamber pointing upwards. A plastic point was attached to the vibrating rig which tapped the Plexiglas on each oscillation (Fig. 4.1). The Plexiglas interface was used in order to protect the sensor membrane from being pierced by the plastic point and to create an additional medium for the sound to propagate through. The amplitude was set to a peak of 1 V and the frequencies were increased logarithmically from $10^{0.2}$ to $10^{2.4}$ with increments of 0.2. The vibration frequency was confirmed using a force gauge (Endevco Corp. model 2103-100) on top of the mass of the rig.

The accuracy of the sensor was determined by the difference of the fast Fourier transform (FFT) of the force gauge against the FFT of the acoustic sensor data. Data was collected from both the force gauge and acoustic sensor for ten seconds per frequency. The ten seconds were processed by FFT and the single frequency with the highest magnitude was compared between the force gauge and acoustics.

Results produced from the vibration rig were highly accurate with a mean error of 1.74% (STD 1.17) when the acoustics were compared against the outputted force gauge frequencies. The frequency sweep can be seen in Fig. 4.2 which shows a sufficiently high magnitude in the MMG range of interest between 1 and 100 Hz, and a particularly high magnitude between 10 and 50 Hz, further confirming this sensors usability in MMG applications.

4.3 Validation of Muscle Contraction Data

In order to determine the performance of the acoustic device in sensing isometric mechanomyogram contractions (MMG muscle activity with no motion), the acoustic sensor was compared against an EMG system used commonly in a clinical environment. Both EMG and acoustic

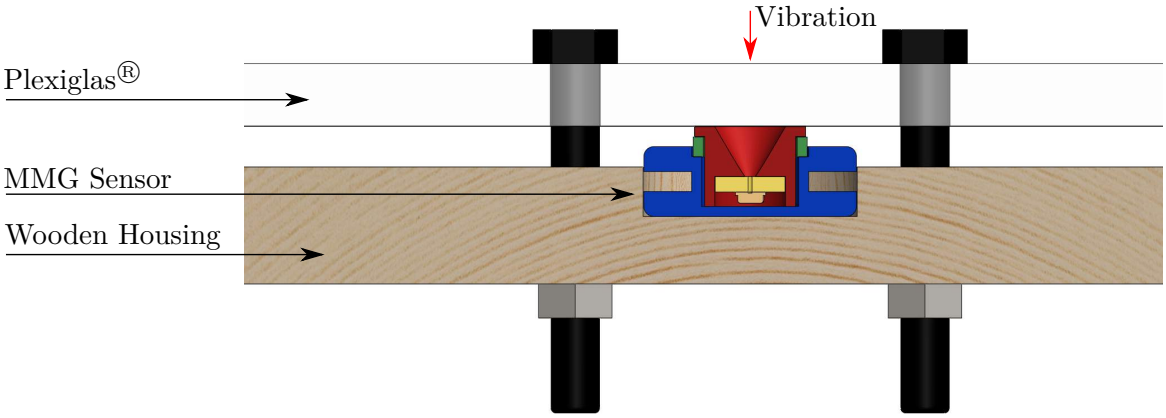


Figure 4.1: Cross section of apparatus used for validation of acoustic sensor frequency response.

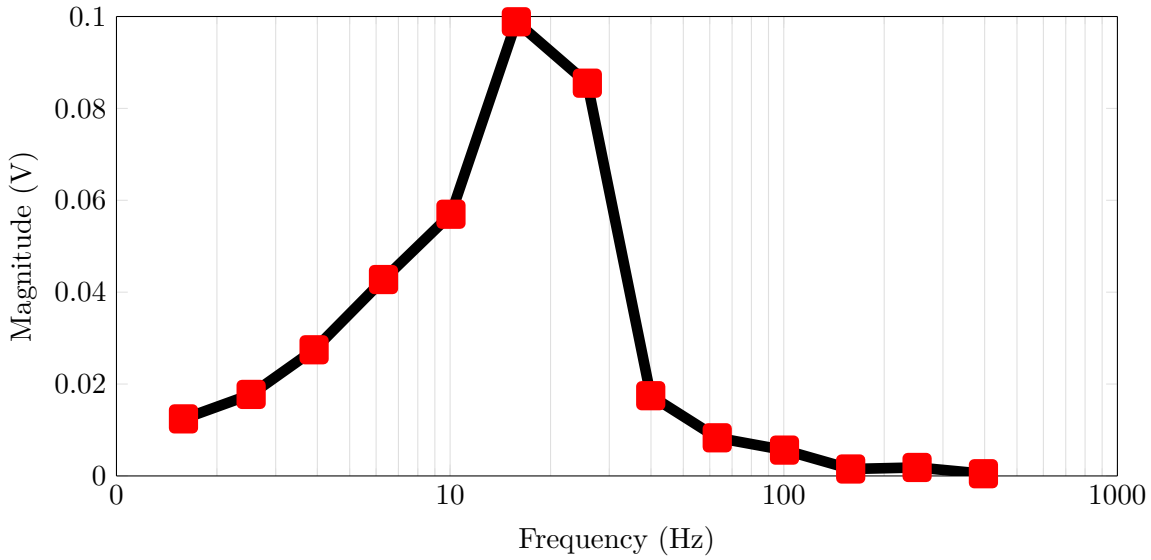


Figure 4.2: Frequency sweep of acoustic sensitivity response showing largest magnitude response in the 1 to 100 Hz range; MMG area of interest.

sensors were amplified using an ISO-DAM8A isolated biological amplifier (acoustic gain 10x, EMG gain 1000x) and were band-pass filtered between 10 Hz and 1 kHz. Both were sampled at 1 kHz using a CED Power1401 DAQ board.

Contractions were produced from extension of the wrist while monitoring the extensor carpi radialis longus on the subject's left arm. Interelectrode impedance for the EMG was kept below 2000 Ω by shaving and lightly abrasing the skin and the electrodes were placed on either side of the acoustic sensor, positioned in the centre belly of the muscle. The sensors were spaced 2.5 cm apart from each other, with 5 cm spacing between the two EMG electrodes. A reference EMG electrode was placed on the ulnar head on the opposing wrist.

One subject was asked to position their arm on an arm rest fixed to the table with their elbow at a 90° flexion and their palm flat on the rest (Fig. 4.3). A strap was used to keep the subject's forearm on the rest, with an additional strap covering the fingers. The subject was asked to perform an isometric contraction of 100% MVC by extending their

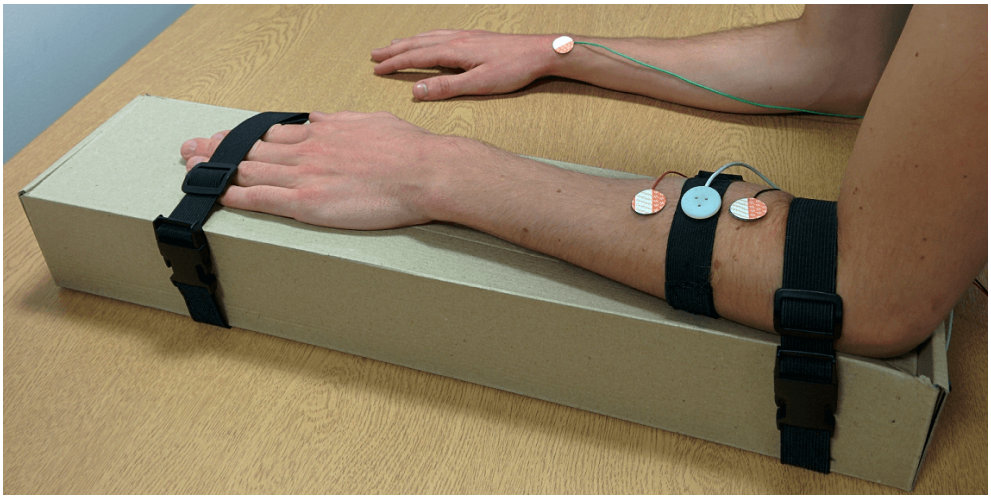


Figure 4.3: Setup for isometric contraction experiment. EMG electrodes can be seen on either side of the acoustic sensor on the subject's left extensor carpi radialis longus muscle. A ground EMG electrode can be seen on the ulnar head of the right wrist.

wrist and holding the contraction for approximately five seconds. This was repeated five times with a five second break in-between. Results seen in Fig. 4.4 show five repetitions of a sustained isometric contraction from both MMG (blue dashed) and EMG (red dot-dashed). By determining a baseline signal during muscle inactivity, an energy thresholding method was used to detect the onset and offset periods of each contraction. The results display a close onset of 41 ms, on average, however, MMG exhibits a later offset of 204 ms than EMG, which also means a longer hold signal was seen in MMG. MMG also displayed larger onset and offset peaks, therefore it is believed the later offset is due to motion artefacts generated by movement of the wrist.

4.4 Validation of Motion Data

To validate the sensor's ability to collect motion and muscle data concurrently, a ten camera Vicon system and a Myon EMG system were used at the same time as an Aktiv IMU and acoustic sensor in a local gait analysis laboratory. A single computer controlled the synchronisation of the optical system, EMG, IMU, and MMG technologies. Muscle activity from the gastrocnemius muscle and motion of the lower leg were recorded as the subject walked and climbed stairs in the laboratory. Two subjects, both male, were recruited in this study. Three tasks; walking, ascending stairs, and descending stairs, were performed for five trials of each. Out of the five trials for each task the four with fewest optical marker drops were taken and analysed.

Fig. 4.5 shows all devices attached to a calf sleeve. A triple-quiver marker was placed on top of the IMU which was tracked by the optical cameras, whereas the EMG and acoustic sensors were placed on the lateral head of the gastrocnemius. The optical system was sampled at

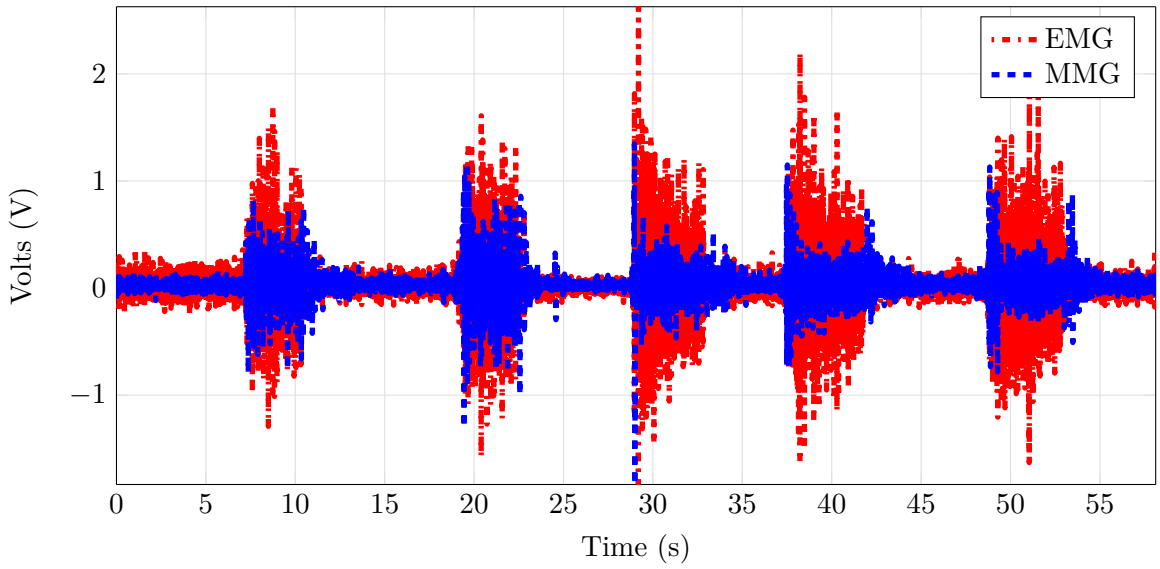


Figure 4.4: Isometric contractions from the extensor carpi radialis longus muscle with EMG (red dot-dashed) and MMG (blue dashed) response.

100 Hz, IMU at 50 Hz, and EMG and MMG at 1 kHz. Optical data was downsampled to 50 Hz in order to match the IMU sampling rate.

Optical results were output as positional data and a single X, Y, and Z coordinate was determined by finding the centre position of the triple-quiver marker set. All data was resized to include only motion within the centre of the laboratory and then smoothed using a moving average algorithm. The magnitude of the accelerations from the Aktiv was calculated using (4.1) where n is the current sample and N is the total number of samples collected; X, Y, and Z, represent each respective accelerometer plane.

$$Magnitude = \sum_{n=1}^{N} ({X_n}^2 + {Y_n}^2 + {Z_n}^2)^{0.5} \tag{4.1}$$

As mentioned in Chapter 2, the calculation of absolute position from IMU's can result in drift, due to the integration stages of conversion. Stationary periods were determined whenever the magnitude dropped below 66% of the maximum and were used as ground truths to correct results and remove such drift from the raw data. Using an AHRS algorithm developed by Madgwick *et al*, the IMU raw data was converted to quaternions that allowed the results to be aligned to the earths coordinate frame which determined the global accelerations[45,50,67]. Both the decision to use Madgwick's method, as well as the quaternion representation of rotations, were selected due to their low computational requirements and low complexity. Using the accelerations, the velocity was calculated through integration, and position through integration of velocity. As optical results are outputted as position they were converted in the opposite way to the IMU, by differentiating the position to get velocity, and differentiating velocity to get accelerations.



Figure 4.5: Calf brace containing optical, IMU, MMG, and EMG technologies. The optical reflective markers can be seen in a triple-quiver, attached to the IMU case. Both the IMU and its accompanying battery were within 3D printed cases situated on the lateral side of the leg. The white sensor located on the gastrocnemius is the MMG acoustic sensor, whereas the EMG electrodes were situated either side the MMG underneath the brace (not seen).

Following calculations of acceleration, velocity, and position of both optical and IMU data, each was high pass filtered using a 1st order Butterworth filter with a cut-off of 0.5 Hz. The accelerations, velocities, and positions of the optical and IMU data were compared using root mean square error (RMSE) differences to determine accuracy, whereas MMG and EMG data was analysed to determine onset and offset of signal response. The RMSE was determined by (4.2), where N is the total number of data samples, VD is the optical accelerations/velocity/position and ID is the same for the IMU. This value was converted into a percentage error for ease of analysis. All data was processed in MATLAB.

$$RMSE = \sqrt{\frac{1}{N}\sum_{n=1}^{N}|VD - ID|^2} \tag{4.2}$$

Analysis of the results produced from simultaneous optical and IMU validation showed a high accuracy across each plane and activity. Table 4.1 shows the results of three activities (walking, stair ascend, and stair descend), for all three of their planes (X, Y, and Z), and all three dynamic types (acceleration, velocity, and position).

These results show a high accuracy, however, from Table 4.1 it was evident that some tasks and motion planes have a better result than others. Expectably, the accelerations of each task were much better than that of the corresponding positions due to the drift errors produced during the integration stages in order to obtain position. Therefore, accuracy is expected to decline from acceleration to position of each task. Literature has shown poor results in regards to determining positional data from IMU's, due to the non-trivial elimination of error and drift. Although this research is more targeted to relative motion applications, as opposed to positional tracking, this information is necessary for validation.

Table 4.1: RMSE results of IMU compared to optical tracking in all three planes (X, Y, and Z) and all three dynamic types (acceleration, velocity, and position). Results of an accuracy above 85%, between 70% and 85%, and below 70% are coloured green, yellow, and red respectively.

	Average Percentage of Accuracy (%)								
	Acc X	Acc Y	Acc Z	Vel X	Vel Y	Vel Z	Pos X	Pos Y	Pos Z
Walking	91.30	90.83	83.11	93.94	91.88	93.99	89.53	81.81	67.82
Stairs Ascend	94.66	95.83	94.98	90.82	88.86	89.32	90.56	82.88	65.67
Stairs Descend	93.90	91.51	87.36	92.63	91.16	90.35	88.18	87.69	76.86

Due to the nature of the MMG collection using a microphone, the data is susceptible to motion and skin artefacts, along with oscillation noise caused during initial contact (heel strike) and initial swing (toe off) of gait. Although standard filtering methods can reduce artefacts to an extent, impact vibrations were found to contain frequencies which overlapped with MMG's signal of interest, which resulted in a signal with unrecognisable contraction periods. Therefore, the impact vibration artefacts were filtered from the MMG data using the IMU accelerometer data as a guide to where impacts occurred. The accelerometer data was normalised between one and zero and resampled to 1 kHz to match the MMG sampling rate. The MMG data was filtered using a band-pass Butterworth filter between 10 Hz and 100 Hz then divided by the accelerometer magnitude (4.3), where n is the current data point, NMA is the normalised magnitude of the accelerometer, and $MMGS$ is the smoothed MMG signal. Therefore, at time intervals with large magnitude accelerations (such as impact vibrations) the MMG data was significantly reduced. However, when accelerations were small, the MMG activity changed marginally. Analysis of gastrocnemius muscle activation during gait has recognised an onset contraction around 10% of the gait cycle (end of loading response), with a peak at 40% (mid terminal stance), and an offset at 50% (end of terminal stance), which is comparable to expected contraction periods[159]. This method works well because no muscle contractions are expected in the gastrocnemius at the impact points during gait. EMG data was filtered between 10 and 500 Hz.

$$MMGS_n = \frac{MMG_n}{NMA_n} \tag{4.3}$$

Fig. 4.6 shows gyroscopic data, accelerometer data with calculated magnitude, unprocessed (raw) MMG data, filtered MMG data, and filtered and processed MMG (top to bottom, respectively). It can be seen that in the unprocessed and filtered MMG plots it is difficult to determine contraction periods due the vibration artefacts (initial contact is highlighted with a red background). The processed MMG data has been filtered, smoothed, and motion and shock artefacts removed using the accelerometer filtering method described above. A comparison between the top plot (gyroscope data) and the bottom plot (processed MMG) show that the stance stages of gait, highlighted with a blue background, coincide with muscular contraction periods.

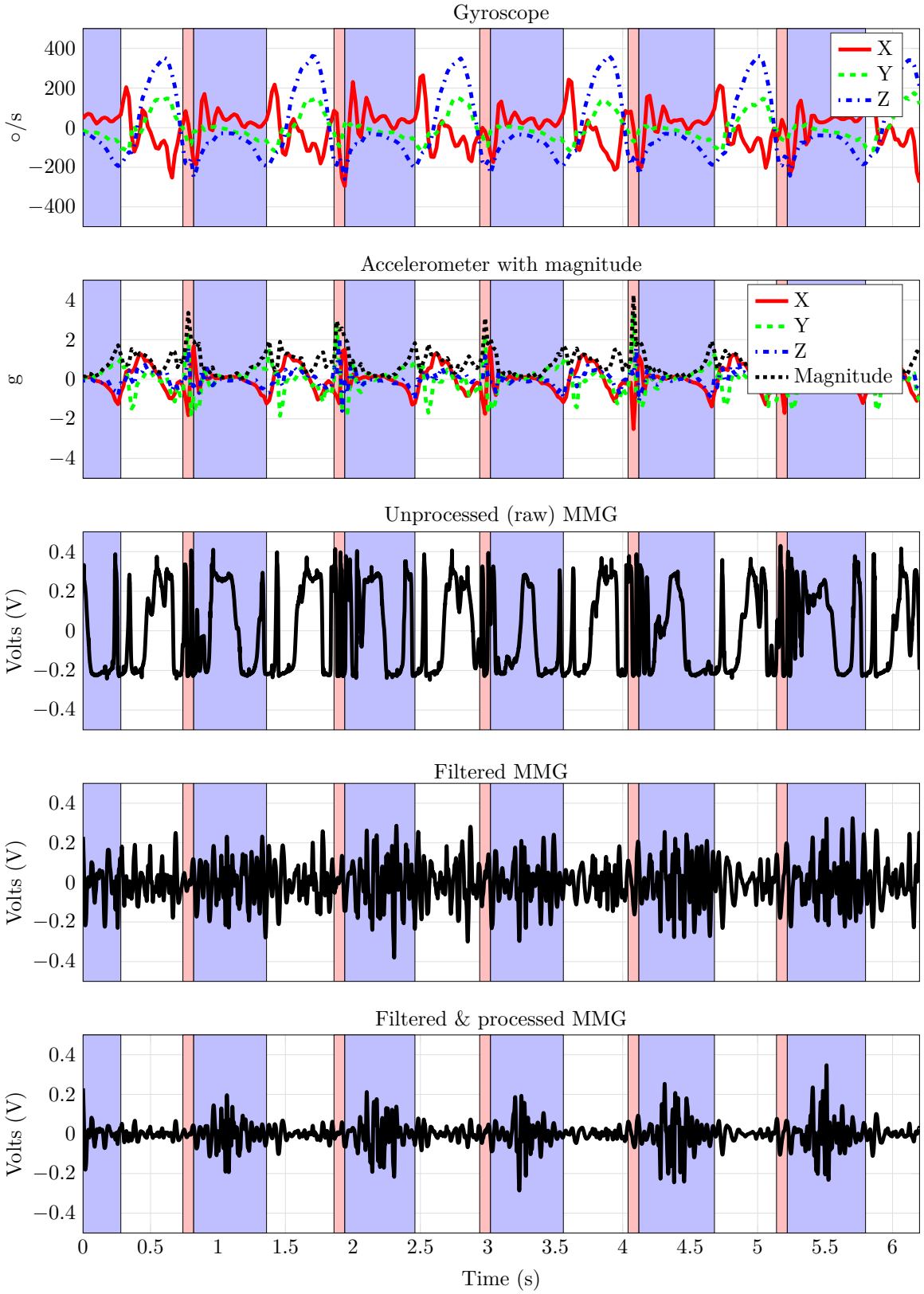


Figure 4.6: MMG signal denoising. From top to bottom: Gyroscopic data, accelerometer data with magnitude overlaid, unprocessed (raw) MMG data, filtered MMG data, and filtered and processed MMG data. Blue shaded backgrounds represent time periods of flat foot stance during gait, whereas red shaded backgrounds represent heel strike during gait.

Table 4.2: Stages of human gait detailing both period and phase information, including duration of each phase.

Period	Phase	Duration	Description
Stance	Initial Contact (IC)	0% to 2%	First instant of foot touching the floor, typically with the heel.
	Loading Response (LR)	2% to 12%	Body weight is transferred onto the forward limb.
	Mid Stance (MSt)	12% to 31%	Limb advances over the stationary foot. First part of single limb support.
	Terminal Stance (TSt)	31% to 50%	Heel rises and second part of single limb support is completed.
	Pre-Swing (PSw)	50% to 62%	Double limb support. Limb response to weight transfer and prepares for swing.
Swing	Initial Swing (ISw)	62% to 75%	Increased knee flexion and foot leaves the floor.
	Mid Swing (MSw)	75% to 87%	Limb advances through the swing phase.
	Terminal Swing (TSw)	87% to 100%	Limb advance is complete, limb positioned ready for initial contact.

One cycle of human gait can be broken down into several sections in order to better understand the process. One of the more detailed breakdowns is the Rancho Los Amigos (RLS) system which splits the cycle into two core periods; stance and swing, and then further breaks down each period into phases. Table 4.2 shows a breakdown of the gait cycle as denoted by the RLS system, with the estimated duration of each phase as presented by Perry and Burnfield[160].

The majority of muscular activity from the gastrocnemius is produced during plantar flexion of the ankle, thus a signal response is expected during the stance period of the gait cycle between mid stance and terminal stance phases[159]. Results from both EMG and MMG fell within the stage of gait as expected, however, MMG contraction duration exceeded that of EMG, and in most cases began before EMG contraction response. It is believed this is due to motion artefacts produced at the onset and offset of contraction, similar to that seen in the isometric validation data (Fig. 4.4). Although the denoise process reduces disturbances produced during high acceleration point of gait, large onset/offset peaks in MMG data will be minimised, but not completely removed. Fig. 4.7 shows one stride from a subject during the walking task. The blue background show the stance period during gait and it can be seen that both EMG and MMG responses were at their highest here. Furthermore, the gait cycle is presented above the gyroscopic data in order to describe muscle action throughout one stride.

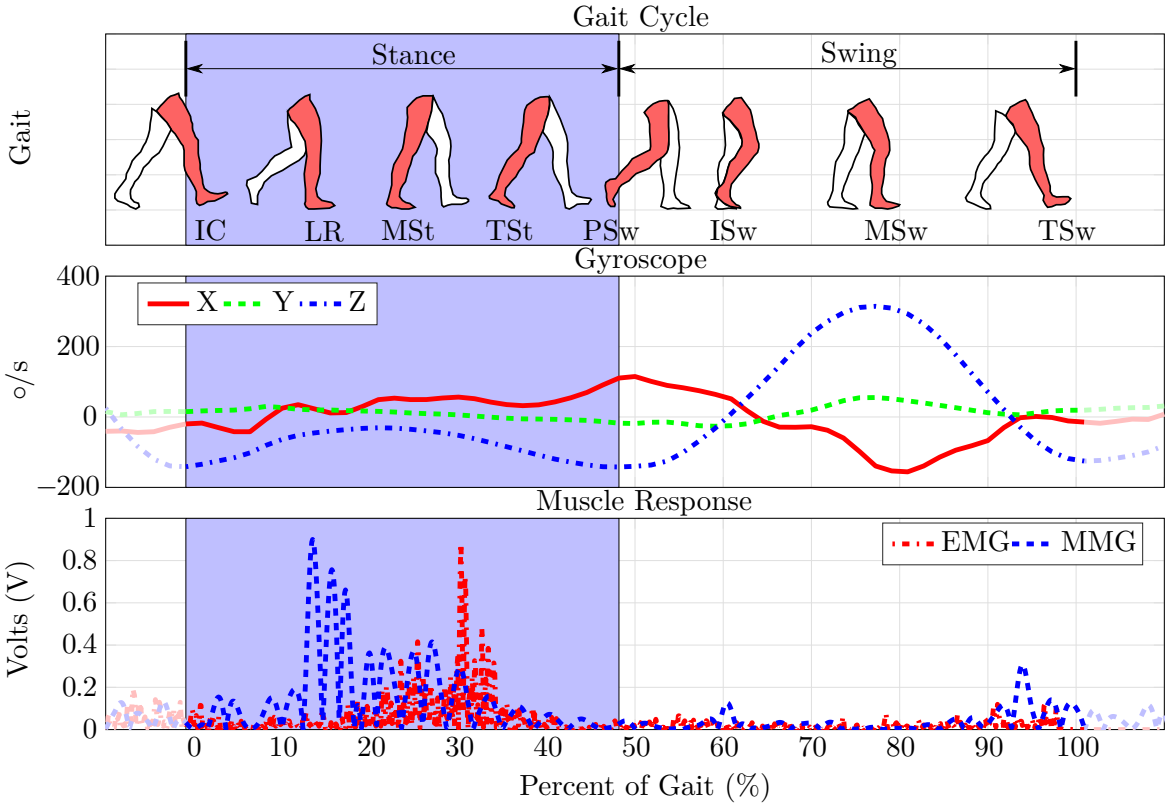


Figure 4.7: Analysis of motion and muscle response during one gait cycle. Top - Gait cycle. The stance phase consists of Initial Contact (IC), Loading Response (LR), Mid Stance (MSt), Terminal Stance (TSt), and Pre-Swing (PSw) whereas the swing phase consists of Initial Swing (ISw), Mid Swing (MSw), and Terminal Swing (TSw). Middle - Motion; Gyroscopic data. Swing phase is clearly shown, predominantly in the Z plane (blue dot-dashed). Bottom - Muscle response; EMG (red dot-dashed) and MMG (blue dashed). Both EMG and MMG contraction responses were detected within the stance period, starting during LR and lasting until TSt. The blue shaded background represent the stance phase during gait.

4.5 Chapter Summary

This chapter has validated both the developed acoustic sensor and the inertial measurement unit in a number of key areas for inclusion in human monitoring applications. In regards to the acoustic sensor, it has been determined that a range of frequencies, including those within the MMG range of interest, is not only possible but also exhibit a high enough signal magnitude for human application. Furthermore, when applied to both isometric and isotonic contractions in two controlled human experiments the results were comparable with that of EMG, the clinical gold standard.

Likewise, the work presented here displays a high accuracy of inertial data when compared with optical based methods, known for their incredibly high positional resolution. Although results were not as accurate in IMU positional estimation, they are still of a high calibre, however, are of little interest to the following applications. Position estimation from IMU's

is notoriously troublesome, and a lot of research has been performed in order to improve results, usually through fusion with other, non-inertial, technologies[161–163]. Acceleration and velocity results, on the other hand, were sufficiently high, especially in regards to planes with high motion.

It has been found that the developed IMU can compare sufficiently with the clinical standard, however, without the limitations of environmental collection space, cost, size, weight, and portability. When combined, both the acoustic sensor and IMU have been shown to work well in a concurrent arrangement, as well as fusing both technologies in order to filter gait data, as seen in Fig. 4.6.

These results suggest that pervasive collection of motion and muscle activity is possible, and the following chapters further validate and demonstrate the usability of this technology in a number of applications.

5

Physiological, Clinical, and Fatigue Studies

Contents

5.1 Introduction **60**
5.2 Force Analysis **60**
5.3 Isometric Fatigue Monitoring with Typical Subjects **67**
5.4 Isotonic Fatigue Monitoring with Spinal Cord Injury Subjects . . . **77**
5.5 Clinical Application of Anaesthetic Monitoring **86**
5.6 Chapter Summary **93**

5.1 Introduction

Understanding fundamental muscle performance during physical exertion is vital in diagnosis of muscular disorders, strength training, and rehabilitation. Monitoring muscle activity, such as contraction intensity and fibre firing rates, can assist in characterising change over time, and prevent injury when exertion is pushed too far.

This chapter introduces physiological and clinical applications in which the developed IMU and MMG sensors were applied to changes in muscle condition, through increases in voluntary and involuntary force, and fatigue. These studies further validate the developed sensors against the clinical gold standard of physiological monitoring, including EMG for muscle observation, and dynamometers for human voluntary force estimation. Furthermore, this work has confirmed that such monitoring can be performed outside of a controlled environment, and with inexpensive technology.

The first three studies present pervasive monitoring methods using MMG as a muscle monitoring technology, and IMU's to monitor movement and repetition of activities. The final application presents this technology to a clinical study in order to demonstrate the sensor's usability in controlled environments, as well as uncontrolled.

5.2 Force Analysis

Monitoring how muscles cope during physically demanding tasks is vital in gaining an insight into human performance and recognising the mechanisms behind force generation. While this is studied abundantly in hospitals and laboratories, the same monitoring in a natural environment has yet to be realised.

Technology in which motion and muscle activity can be collected and analysed in an uncontrolled setting could benefit those required to undergo rehabilitation or strength training regimes, which currently requires them to attend a clinic or hospital where trained professionals can monitor their activity.

While muscle activity is monitored by EMG or MMG, muscular force is usually determined using technology such as force gauges or dynamometers (Fig. 5.1) which produce a quantitative measure of muscle strength when a user applies a maximum force against a resistive system. This maximum force is used as their 100% maximum voluntary contraction (MVC).

Literature has shown a strong correlation between an increase in voluntary force and an increase in signal amplitude, for both EMG and MMG[108,164–166]. However, where EMG measures of muscle activity typically shows a linear or curvilinear increase in amplitude from minimal to maximum voluntary force[167], the relationship between MMG signal and



Figure 5.1: Image of a medical dynamometer used in calculation of MVC, as well as allowing isometric, isotonic, and isokinetic contractions to be performed. MVC's are calculated by strapping the limb of interest to a fixed arm attached to the system and having the user apply a maximum force against the arm. After a set number of repeated trials the average force value is taken as the 100% MVC value. Lower percentage MVC's are calculated by dividing the average force value. Image taken at the Nick Davey Laboratory within the Human Performance group at Charing Cross Hospital with permission.

muscle force is less clear with some reporting a curvilinear (quadratic or cubic) response throughout[166], a linear or curvilinear response up to 75/80% MVC followed by a decline up to 100% MVC[108,165], and an 'S-shape' response from low to mid MVC's, a stabilisation, and then a further increase up to 100% MVC[164].

MMG frequency parameters also show a complex relationship, with reports of a stable response from 10% to 20% MVC, followed by a linear increase from 20% to 80% MVC, and a sharp increase from 80% to 100% MVC[158], however, EMG has been found to produce a similar non-linear response in frequency with an increase in force[168].

Despite a lack of agreement in MMG literature, recent studies have reported that the response can differ between subjects, muscles, and muscle actions performed[90,169]. Furthermore, it has been suggested that the sensitivity and non-linear responses seen in MMG amplitude and frequency relationships contains more information on motor control strategies when compared with EMG[108,158].

The majority of MMG force studies focus on isometric contraction, however, there have been studies on MMG amplitude and frequency responses during dynamic constant external resistance (DCER) tasks[170–172]. DCER studies monitor contractions in which external resistance does not change (such as free weights), while joint flexion and extension occurs during eccentric and concentric movements. Results reported show a linear increase in signal amplitude from concentric and eccentric DCER muscle actions from the biceps brachii during an increase in lifting weight[170,171]. Frequency response, on the other hand, shows a curvilinear increase response, with a decline at higher loads above 80% MVC[172].

5.2.1 Research Question and Hypothesis

The aims of this study were, firstly, to determine the relationships of MMG amplitude and frequency with voluntary force during a DCER test. The second aim was to measure muscle and motion information outside of a controlled environment. It was hypothesized that MMG would be able to detect changes in activity, comparable with EMG. Furthermore, it was hypothesized that inertial changes would be recognised as exertion increased through an increase in weight.

Six weight lifters (all male) were recruited through the English Institute of Sport (EIS) to perform a barbell bench press while movement of their upper arm was tracked using an IMU, and muscular activity from their biceps brachii was monitored using MMG. This research was approved by the Imperial College Research Ethics Committee (ICREC) and written consent was obtained from the subject involved.

5.2.2 Method

All subjects recruited were experienced weight lifters and trainers for the EIS. The biceps brachii of the right arm was located, and the MMG sensor positioned, on a line between the medial acromion and the fossa cubit, 33% from the fossa cubit[173]. The IMU was attached to a stretchy band which wrapped around the arm, with the sensor placed on the lateral side (Fig. 5.2).

All subjects knew their maximum bench press (one-rep max (1RM)) weight prior to testing, which was used as their 100% MVC and subsequent MVC percentages were calculated from this value. Weight was increased from 20 kg (just the weight bar) to 80 kg with 10 kg intervals. 80 kg was selected as the maximum as it resulted in approximately 80% MVC for all subjects involved. Estimated MVC's for each subject at the minimum and maximum weight can be seen in Table 5.1.

Each subject was asked to start with both hands on the weight bar before performing five repetitions of bringing the bar down to the chest and back up with arms straight. On the fifth repetition the bar was put back on the rack. Each subject had three minutes of recovery time between trials. Inertial data was sampled at 50 Hz, whereas MMG was sampled at 1 kHz. Data was transmitted via Bluetooth to a laptop where it was stored for offline processing.

MMG data was filtered between 10-100 Hz using a 3^{rd} order Butterworth filter, whereas inertial data was smoothed but not filtered. Each subject had different strengths and therefore their MVC's varied for each weight. MMG data was scaled and normalised against their calculated MVC to remove a bias between subjects.

Repetitions were detected from the accelerometer data, recognising and isolating peaks from the movement. This study only analysed the concentric portion of the motion, so as to



Figure 5.2: Image of a subject in preparation of a bench press. MMG and IMU sensors can be seen on the right upper arm.

Table 5.1: Estimated MVC % for each subject at 20 and 80 kg, based on their maximum bench press (1RM)

		Subject							
		A	**B**	**C**	**D**	**E**	**F**	**Mean**	**STD**
Estimated	20 kg	19	14	25	18	22	18	19.3	3.8
MVC (%)	80 kg	76	55	100	73	89	73	78.6	15.4

monitor the generated force from the biceps brachii during the task. From the isolated segments of each repetition, the MMG amplitude (RMS) and mean power frequency (MPF) were determined and an average was calculated for each weight and subject. RMS and MPF equations can be seen in (5.1) and (5.2) respectively, where n is the current sample, N is the total number of samples, M is the highest harmonic considered (499 Hz; just below the Nyquist frequency at a sampling rate of 1 kHz ($0.5f_s$)), f is frequency, and P is power.

$$RMS = \sqrt{\frac{1}{N}\sum_{n=1}^{N}|MMG_n|^2} \tag{5.1}$$

$$MPF = \frac{\sum_{n=1}^{M} f_n P_n}{\sum_{n=1}^{M} P_n} \tag{5.2}$$

Inertial data was further analysed in order to characterise changes in movement. First, the average time duration for each weight trial was calculated from mean elapsed time taken

to complete each repetition. Secondly, acceleration and velocity were calculated using the AHRS algorithm presented by Madgwick *et al*[50], which has been used in other studies in this report, including the validation against optical tracking (Chapter 4).

Linear regression analysis was performed on the MMG RMS, MMG MPF, time duration, acceleration, and velocity results, against force. Pearson's correlation coefficients (r) were calculated as well as the P values to determine significance of signal change over force. Furthermore, linear slope gradients (b), and percentage change from starting to finishing force levels (20 and 80 kg weights, respectively) were also calculated.

5.2.3 Results

MMG RMS ($r = 0.92$, $b = 7.62$ mV.kg^{-1}, $P < 0.01$) and MPF ($r = 0.92$, $b = 0.21$ Hz.kg^{-1}, $P < 0.01$) both show a significant positive linear relationship with increasing weight (Fig. 5.3). MMG RMS was 19% higher between highest and lowest force levels, with a range of 0.26 V to 0.3 V. MMG MPF saw a 31% increase between highest and lowest force levels, with a range of 4.7 Hz to 6.2 Hz.

Motion results also had a strong linear relationship with increasing weight, however, acceleration (r = -0.92, b = -0.3 m/s/s.kg^{-1}, $P < 0.01$) and velocity (r = -0.76, b = -0.05 m/s.kg^{-1}, $P < 0.01$) showed a significant negative trend, whereas time duration ($r = 0.82$, $b = 0.09$ s.kg^{-1}, $P < 0.05$) was significantly positive (Fig. 5.4). Time duration saw a change of 68% with a range between 0.82 s to 1.4 s, whereas acceleration and velocity saw a change of -62% and -28% and a range of 3.39 m/s/s to 1.31 m/s/s and 1.24 m/s to 0.9 m/s, respectively.

5.2.4 Discussion and Conclusion

Results correspond with that found in past literature, with a significant ($P < 0.01$) correlation in MMG amplitude and frequency as force was increased. Other than velocity, which showed a strong linear correlation ($0.6 < r < 0.79$), time duration and acceleration showed a very strong ($0.8 < r < 1.0$) linear correlation, when using the suggested guide for interpreting the absolute value of r[174]. All motion results were also found to have a significant change over force increase.

As stated above, literature tends to agree in that MMG amplitude increases with force, however, relationships often differ from study to study ('S-shape', linear, or curvilinear). Furthermore, studies generally report a change in response above 75% or 80%, usually a decline or plateau in response. It has been reported that beyond 80% MVC the active muscle units discharge rate, and the muscular stiffness, both limit the pressure waves generated by the dimensional changes of the active fibres, resulting in a decline in amplitude[108]. Results presented here show no decline throughout the increase in force, however, as seen in Table 5.1, the average MVC at 80 kg was below 80%, which could explain why no change was seen. It

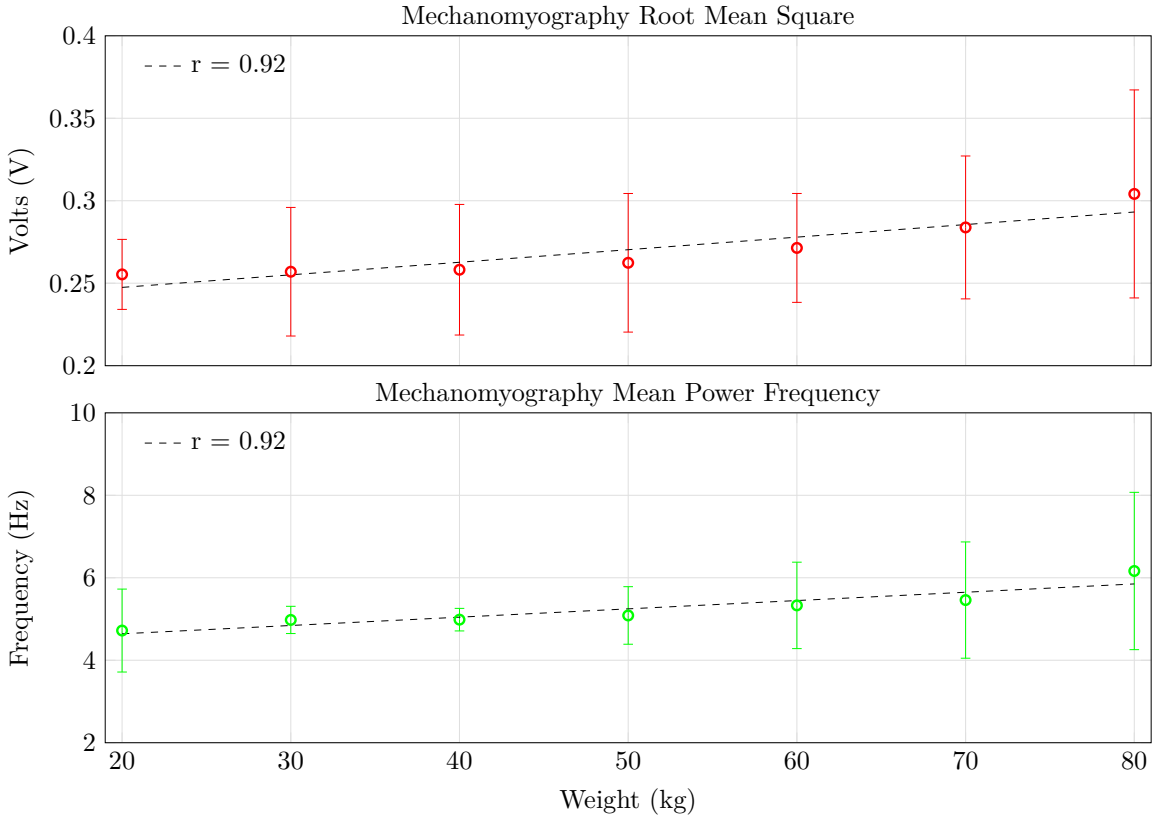


Figure 5.3: Figure presenting MMG RMS (top) and MMG MPF (bottom) against change in weight (kg). Linear regression lines (black dashed) are also presented with their corresponding Pearson's correlation coefficient values showing a significant positive linear relationship for both RMS and MPF results.

was hypothesized that continuing to 100% MVC for each of the subjects would produce a decline in amplitude response.

Frequency change showed a significant steady linear increase in frequency from 4.7 Hz up to a maximum of 6.2 Hz. Standard deviation in the frequency domain increased as weight increased (Fig. 5.3). This was believed to be due to differing strength abilities in the subjects, with some being able to handle the heavier weights better than others, resulting in an increasing variance as weight increased.

Motion results showed a decline in acceleration and velocity while time difference increased as exertion increased. Force generation from a muscle is functional to its velocity; as velocity decreases, force increases. MMG amplitude was seen to increases with the additional exertion required from heavier weight, which explains the decline seen in velocity, and in turn the accelerations due to its coupling with velocity.

Unique attributes of this study have shown that it was possible to monitor changes in muscle activity and motion in a pervasive setting, with inexpensive, non-confining or restrictive, and quick to don and doff sensors. While muscle results suggest a suitable accuracy in monitoring changes in force, motion information was necessary in segregation of repetitions

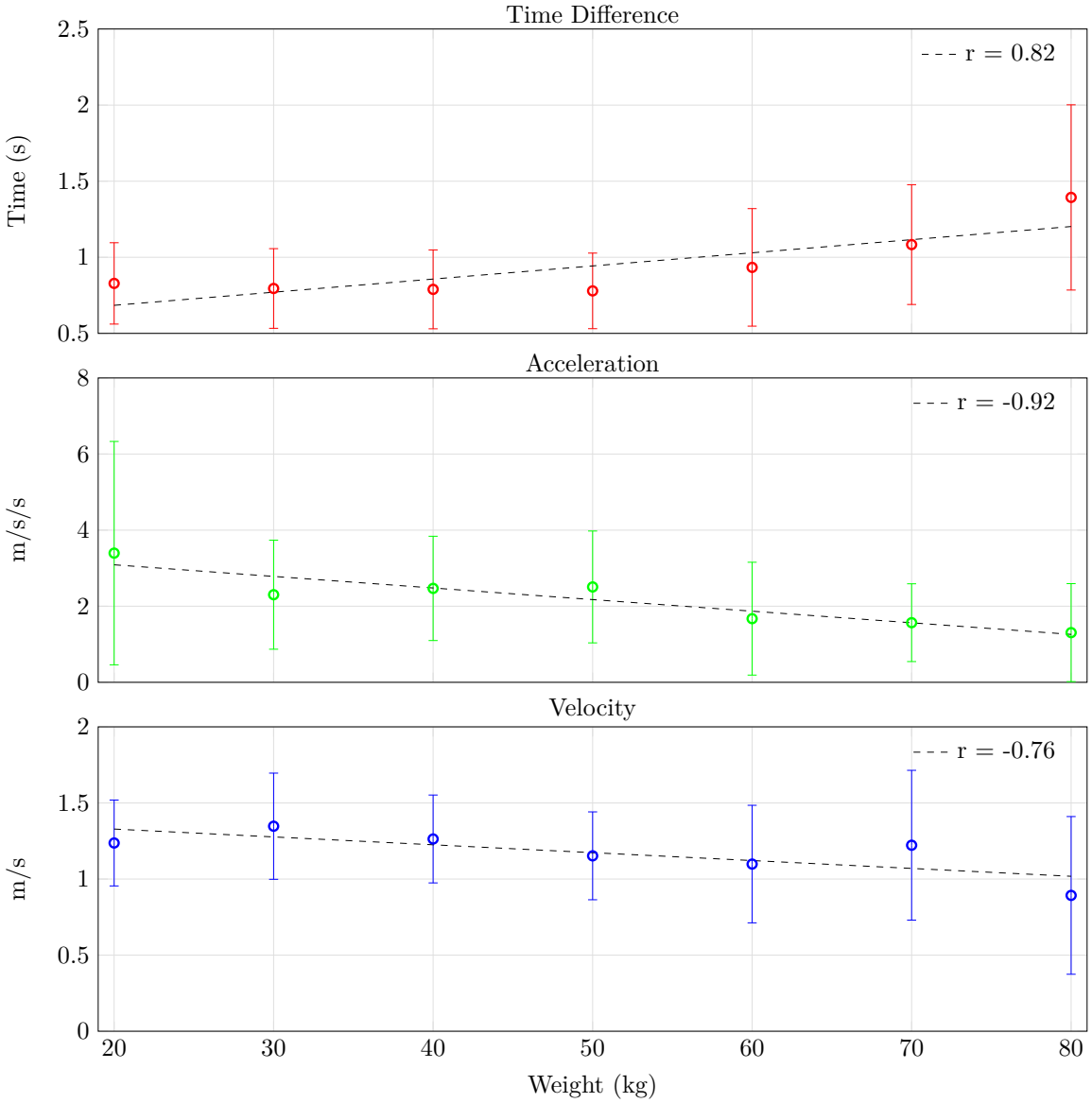


Figure 5.4: Figure presenting time duration (top), acceleration (middle), and velocity (bottom) against change in weight (kg). Linear regression lines (black dashed) are also presented with their corresponding Pearson's correlation coefficient values showing a significant positive linear relationship for time duration, and a significant negative linear relationship for acceleration and velocity.

as well as isolation of the concentric contraction periods of each repetition which were used for analysis.

The results presented here confirm that MMG amplitude and frequency components have a strong correlation to increases in force, while inertial results have shown that velocity and acceleration decrease as the exertion of a task increases. It has been confirmed that combination of IMU and MMG sensors could be used in an external setting for rehabilitation programmes. However, there are limitations in this study, including precautions to be taken to reduce motion and other artefacts, and the need to estimate MVC based on individual maximum bench press. Nonetheless, this device has potential to monitor long-term exertion

and activity, which could be used to analyse strength improvement over time, without the need for regular observation from clinical personnel.

5.3 Isometric Fatigue Monitoring with Typical Subjects

Following from amplitude and frequency components of MMG signal with changes of voluntary force, it is of great interest to understand how the signal changes with the introduction of muscle fatigue. Understanding muscle characteristics during, or prior, to fatigue has a number of applications which complement the findings shown in the previous study. First, understanding when a muscle has fatigued, and in turn when the muscle returns to a nominal state, can assist in physical training and muscle conditioning. Secondly, recognising muscle changes before onset of fatigue can act as an indicator to exert less, thereby avoiding fatigue before it happens.

Fatigue is well documented for both EMG and MMG based studies with both phenomenon's producing complementary results when compared. However, MMG signal amplitude and frequency response differ throughout literature, and it has been found this depends largely on the muscle being examined and the fatiguing protocol used[175]. This is similar to the findings of MMG and force relations detailed previously.

Many studies have concluded that EMG amplitude increases, while EMG frequency decreases, during a sustained isometric fatiguing activity, regardless of MVC intensity[110,131,176]. MMG, however, has a more complex relationship, with results suggesting an increase in MMG amplitude in low intensities (~5-50% MVC)[110,176–181], stable in medium intensities (~50-75% MVC)[8,176,181,182], and a decrease in high intensities (~75-100% MVC)[131,176,180,181,183], during a sustained isometric fatiguing activity. Equivalent responses from MMG frequency components are less complex, with literature stating the MPF declines or fluctuates throughout differences in MVC intensities[88,110,131,176,177,179–181,183,184]. Although variations are found in amplitude and frequency components in fatiguing studies, literature continues to agree on a strong correlation of MMG amplitude against voluntary force[7,8,185].

A number of papers have analysed changes in MMG and EMG responses before and after a fatiguing activity, finding that both MMG and EMG amplitudes are greater and MMG and EMG frequencies are lower, on average, post-fatigue at low (10%)[177,186], and medium (70%) intensities[187]. Furthermore, one study monitored EMG and MMG amplitude and frequency components before and after a sustained isometric activity as the subject's supported their own body weight[123]. While MMG and EMG amplitudes were seen to be greater post-fatigue, EMG MPF was lower, whereas no change was seen in MMG MPF.

A number of studies have looked at the level of voluntary contraction verses knee flexion in the quadriceps and hamstring muscles during unloaded squats. The rectus femoris has been found to contract at 49% MVC between 60°-90° (eccentric), and 32% MVC between

90°-60° (concentric), when compared against a 100% MVC reference[188]. Another study has reported similar results with a 40% MVC at 60° knee flexion for the rectus femoris during a held isometric squat[189].

5.3.1 Research Question and Hypothesis

The study presented here uses a wall squat fatigue test to determine the effects of fatigue on the MMG signal. Similar to Yoshitake *et al*, who used body weight as opposed to a known MVC to induce fatigue, this study implements an unloaded squatting task while monitoring the rectus femoris muscle. The majority of fatiguing studies have used force gauges or dynamometers, similar to that seen in other muscle physiological studies, which require training to use, are expensive, and are large in size. This study measures muscle activity pre, during, and post-fatigue, using lightweight and portable sensors, of which are easy to use and can be applied in a variety of environments.

This experimental protocol will confirm two key understandings of muscle activity during fatiguing activities; change during a fatiguing activity, and changes post-fatigue. Using an inertial measurement unit to monitor movement and determine repetitions/contraction time periods, and concurrent collection of EMG and MMG, this study produces complementary results to the current literature, while demonstrating the use of more pervasive technology. It was hypothesized that MMG could identify fatigue, both during a fatiguing activity, and post-fatigue after an elapsed time.

Five able bodied subjects, one female and four male, were recruited for this study. This research was approved by the Imperial College Research Ethics Committee (ICREC) and written consent was obtained from the subject involved.

5.3.2 Method

Subjects were asked not to perform any strenuous activities at least two days before the experiment. This study has analysed contraction data from the rectus femoris while the subjects perform a squatting activity to fatigue. Unlike the previous study, which was performed in a pervasive environment which restricted the use of EMG, this study was performed within a more controlled setting, and therefore both MMG and EMG are collected concurrently with motion information from an IMU. The rectus femoris was chosen as the muscle of interest due to an ease in accessing and locating, as well as being commonly used in other muscle based squatting studies[190–192].

Prior to the study, each subject had their rectus femoris located on their right leg with the EMG and MMG electrodes placed at 50% on a line between the anterior spina iliaca superior and the superior part of the patella[173]. MMG was placed at the 50% point, with EMG on either side of the MMG, following the hip/knee line, with 5 cm spacing between them (2.5 cm between EMG and MMG). The EMG reference electrode was placed on the anterior

spina iliaca superior (right side). The IMU was placed on the lateral side of the right leg, parallel with the hip/knee line. The EMG electrode areas were shaved and abrased before adhesive attachment. The MMG sensor was attached to a stretchy band which the IMU was also attached to (Fig. 5.5).

The study was split into three stages. Subjects performed unloaded squats to determine the muscle performance before fatigue (stage one), fatigued their muscles with a wall squat (stage two), and then performed unloaded squats once more to determine muscle performance post-fatigue (stage three). The stages are described in detailed below.

Stage One Each subject was asked to perform five two-legged unloaded squats, where the squat was held for five seconds, with a five second pause between each. Feet were spaced in line with the shoulders. Hands were placed on the hips and subjects were asked to squat to a 75° knee flexion and 90° hip flexion. Actual knee flexion was estimated using inertial information, however, hip flexion was not monitored in this study (Fig. 5.6).

Stage Two Following stage one, subjects were immediately asked to perform the second task of a two-legged wall squat. This consisted of the subject squatting with their back against a wall, with their knees at a 75° flexion, hip flexion at 90°. Again, actual knee flexion was estimated using inertial information. Feet were again in line with the shoulders, with the hands placed flat against the wall. The subject was asked to remain in this position for as long as possible, with the quadriceps quickly fatiguing. Once they could no longer withhold the position they were asked to stand up from the wall and sit on a chair provided (Fig. 5.7).

Stage Three In order to recognise long lasting muscle fatigue, each subject was given a ten minute recovery period at this point before stage three began. Stage three was the same as stage one, with five two-legged squats performed to the same knee and hip flexion angles as before (Fig. 5.6).

Subjects were instructed in the correct squatting method prior to testing, with knee and hip flexion angles estimated.

The EMG system used was a g.tec g.BSamp biological amplifier with a g.tec g.GAMMAbox electrode driver. The amplified EMG signal had a maximum output of 10 V, therefore its voltage was dropped using a passive voltage divider so that it would not damage the IMU (maximum voltage input of 3.3 V), and was then sampled at 1 kHz using channel one of the IMU's auxiliary port. Likewise, the MMG sensor was attached to channel two of the IMU's auxiliary port and was also sampled at 1 kHz. MMG was not amplified. The inertial components (gyroscope, accelerometer, and magnetometer) of the IMU were sampled at 50 Hz. All data was transmitted to a laptop via Bluetooth where it was stored using MATLAB. A block diagram of the system configuration can be seen in Fig. 5.8.

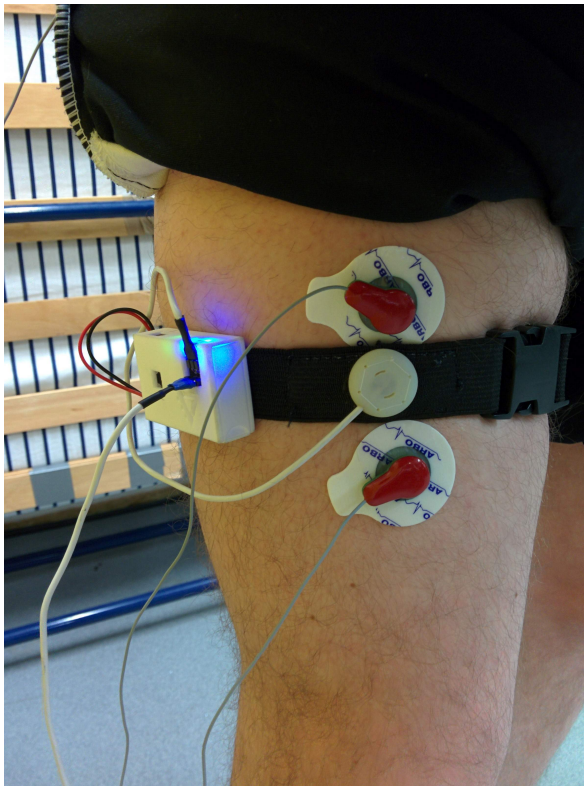


Figure 5.5: Sensor configuration for fatiguing study with MMG and EMG electrodes positioned 50% between the anterior spina iliaca superior and the superior part of the patella, and the IMU parallel to the line on the lateral side of the leg.

In offline processing the MMG data was filtered between 10-100 Hz, whereas EMG was filtered between 10-500 Hz, using a 3rd order Butterworth filter. IMU data was smoothed using a moving average but not filtered. All data processing was performed in MATLAB.

Estimation of knee flexion was achieved by zeroing off the accelerometer data when standing, in order to get a resting gravitational reading perpendicular with the horizontal plane. The knee flexion angle was calculated using (5.3), where $ACCX$ is the acceleration from the X plane measured in g's, multiplied by 90° to convert to degrees.

Although accurate in estimation of the thigh orientated in relation to gravity, this calculation does not take into account ankle flexion, and therefore assessment of knee flexion was only approximated. Both EMG and MMG data were scaled and normalised against the calculated flexion angle to minimise bias between subjects.

$$angle(^\circ) = ACCX * 90^\circ \tag{5.3}$$

5.3.2.1 Changes Post Fatigue

Stages one (pre-fatigue) and three (post-fatigue) were processed by first identifying data windows containing each of the five squat repetitions. The eccentric, isometric, and concentric contraction periods from each squat were isolated and analysed using the accelerometer data in the X plane; the axis in parallel with knee flexion movement. Data windows containing squats were extracted at points where the X plane accelerometer data exceeded a 10% increase



Figure 5.6: Stage one and three - Five two-legged squats held for five seconds, with a five second pause between. Hands on hips, feet shoulder width apart. Squat angle performed to a knee flexion of 75°.

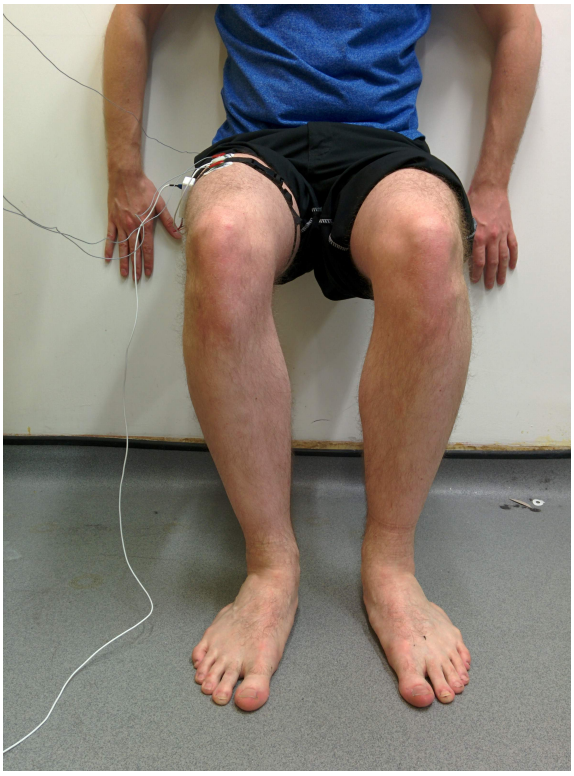


Figure 5.7: Stage two - Two-legged wall squat held for as long as possible. Hands flat against the wall with knee flexion at 75°. Feet shoulder width apart.

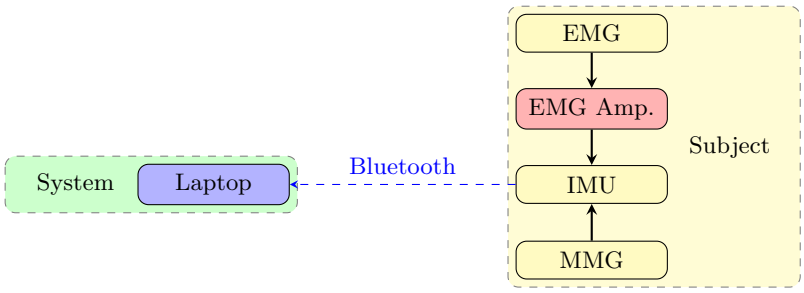


Figure 5.8: Block diagram showing the setup used to collect and transmit EMG, MMG, and IMU data from a subject. Data was transmitted to a laptop via Bluetooth where a MATLAB script collected and stored the data for offline processing.

and decrease in gradient from the stationary signal. Windows with a negative accelerometer gradient were taken as eccentric periods, whereas positive accelerometer gradients were taken as concentric periods. Isometric, or sustained periods, were determined as the data between the eccentric and concentric windows (Fig. 5.9).

Each contraction window (eccentric, isometric, and concentric) was resized into two seconds, one second either side of the centre of the window. This was to reduce movement artefacts and produce a uniform window size for processing. MMG and EMG were averaged between each of the five squats for each of the contraction windows, for both pre and post-fatigue

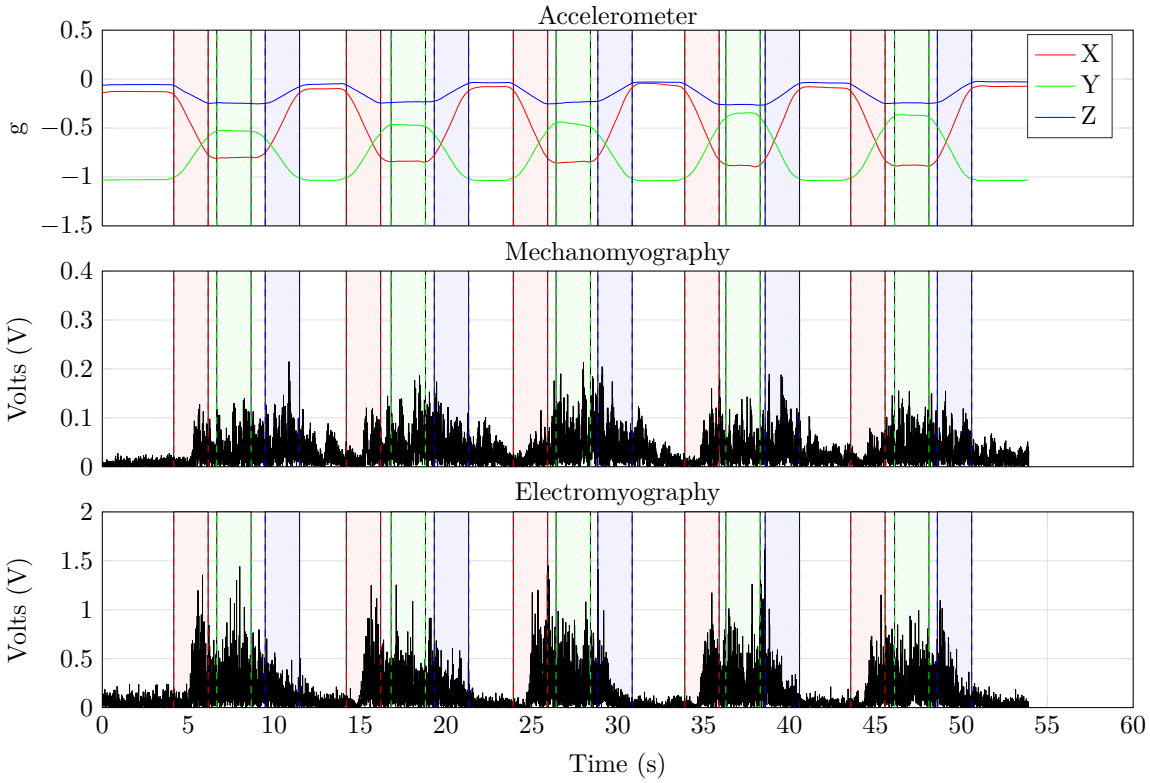


Figure 5.9: Example of peak detection using accelerometer data from stages one and three of the fatigue trial. Each repetition was detected and the start and stop points were segmented for eccentric (red), isometric (green), and concentric (blue) contractions.

data sets. This data was then grouped between subjects to obtain an average population result.

Mean amplitude (RMS) and frequency (MPF) were calculated for eccentric, isometric, and concentric contractions for both EMG and MMG, pre and post-fatigue. RMS and MPF were represented as a percentage change between pre and post-fatigue for each contraction type for EMG and MMG, and a paired t-test was used to determine significance of change.

5.3.2.2 Changes During Fatigue

Stage two (fatiguing action) isolated the single wall squat in the same way as stages one and three; by detecting changes in accelerometer gradient, however, this stage only processed and analysed the isometric period during the held contraction (Fig. 5.10). The first and last second of the isometric window were removed to reduce motion artefacts.

The isometric period was split into one second, non-overlapping windows, and each window had its RMS and MPF calculated, for both EMG and MMG data. Subject data was then grouped and the mean RMS and MPF was calculated.

Linear regression analysis was performed on the RMS and MPF change over time for both MMG and EMG, and Pearson's correlation coefficients (r) and statistical significance (P)

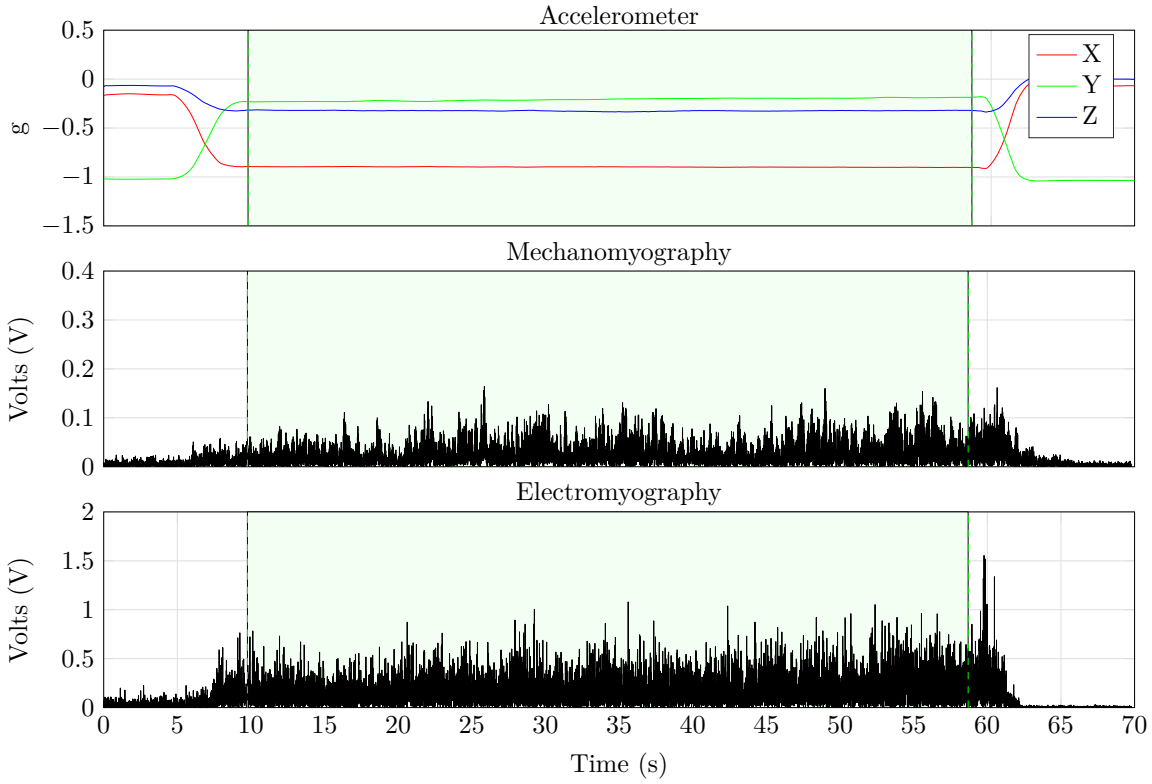


Figure 5.10: Example of peak detection using accelerometer data from stage two of the fatigue trial. Start and stop points were segmented for the held isometric contraction (green).

were calculated. Furthermore, linear slope gradients (b) and percentage change from fresh to fatigued muscle states were also determined.

5.3.3 Results

Comparisons between pre and post-fatigue saw an increase in RMS amplitude in all contraction types (eccentric, isometric, and concentric) for both MMG and EMG, with an average percentage increase of 24% and 8%, respectively (Table 5.2). However, only MMG RMS results were significantly different (Eccentric and Concentric; $P < 0.01$. Isometric; $P < 0.05$). Fig. 5.11 shows a comparative result of each contraction type for the RMS results, for both MMG and EMG, pre and post-fatiguing action.

Both MMG and EMG MPF saw a 1% decrease in percentage post-fatigue (Table 5.2). Neither MMG nor EMG were significantly different between pre and post-fatigue. Fig. 5.12 shows an equivalent comparative result for the MPF results, pre and post-fatiguing action.

MMG RMS ($r = 0.96$, $b = 0.33$ mV.%, $P < 0.01$) and EMG RMS ($r = 0.76$, $b = 2.25$ mV.%, $P < 0.01$) show a significant positive linear relationship against time during the muscle fatigue activity, with an RMS increase of 74% and 50% for MMG and EMG respectively. MMG MPF (r = -0.33, b = -0.02 Hz.%, $P < 0.05$) decreased 4% in frequency during fatigue, and resulted in a weak linear correlation against time, albeit still significant. EMG MPF (r

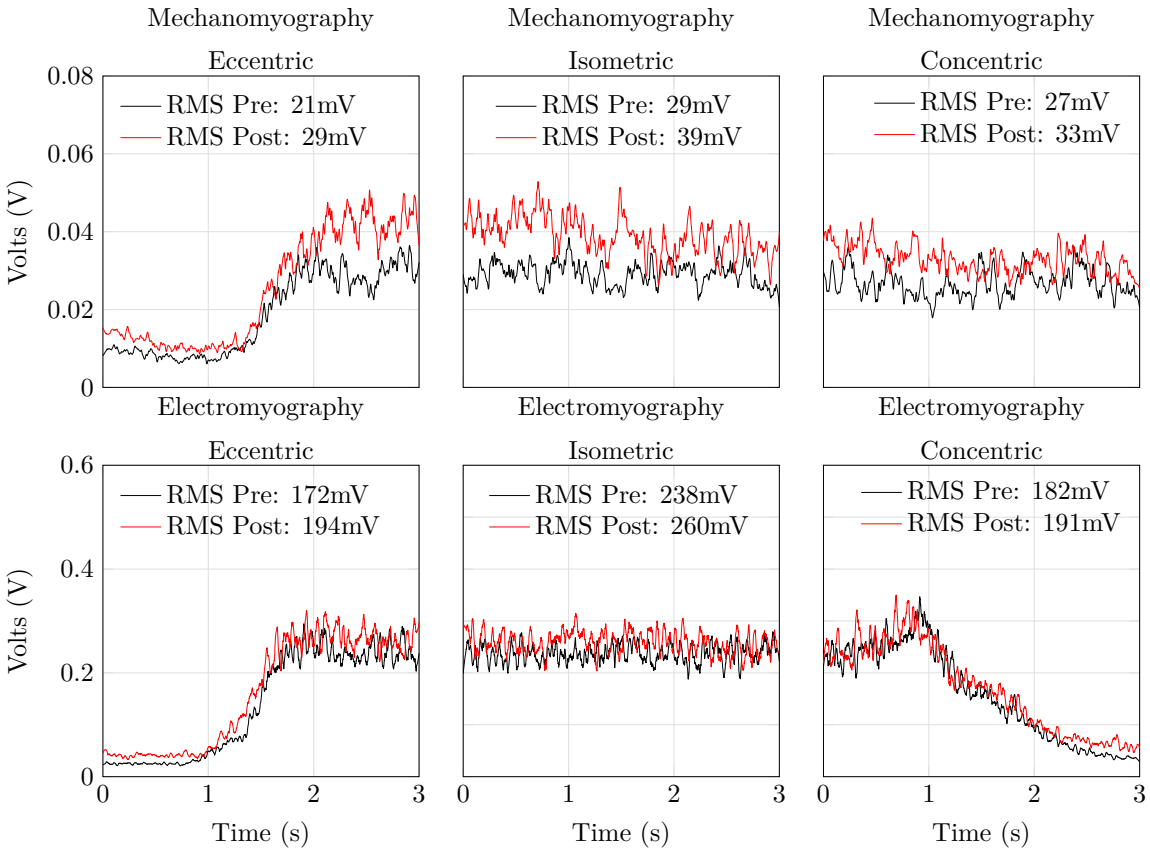


Figure 5.11: Comparison of pre (black) and post-fatigue (red) RMS results for MMG (top row) and EMG (bottom row). Data has been split into eccentric (left column), isometric (middle column), and concentric (right column) contractions.

= -0.56, b = -0.15 Hz.%, $P < 0.01$) declined significantly throughout fatigue with a moderate negative linear relationship and an 9% decrease on average. Fig. 5.13 shows the change in RMS and MPF for both MMG and EMG during the sustained fatiguing activity, represented as a percentage of average duration.

Average knee flexion angles across all subjects were estimated at 73° for both pre and post-fatigue, whereas a 70° knee flexion was calculated during the sustained fatiguing activity.

5.3.4 Discussion

This study recognised changes both during a fatiguing action, as well as in post-fatigue muscle activity. Through the combination of MMG and IMU technology squatting repetitions were identified and segmented into the three stages of contraction activity; eccentric, isometric, and concentric.

Literature detailed in the introduction of this study report between 32% and 49% MVC for the rectus femoris in unloaded squats between 60° and 90°, eccentric and concentric, respectively. Knee flexion angles for this study averaged between 70° to 73° across all stages,

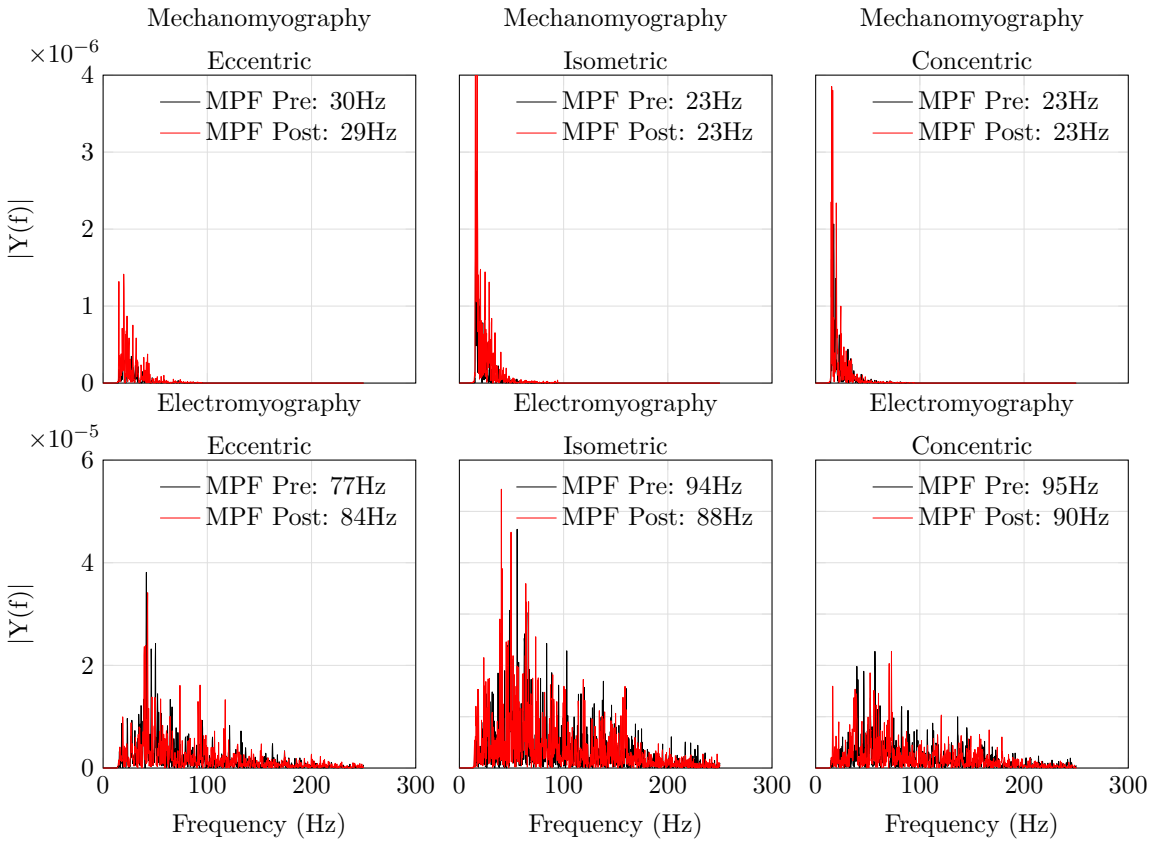


Figure 5.12: Comparison of pre (black) and post-fatigue (red) MPF results for MMG (top row) and EMG (bottom row). Data has been split into eccentric (left column), isometric (middle column), and concentric (right column) contractions.

Table 5.2: Results of percentage change of RMS and MPF, in each of the contraction types in both MMG and EMG, post fatigue.

		Eccentric	Isometric	Concentric	Average
MMG	RMS (%)	28	26	18	24
	MPF (%)	-3	0	0	-1
EMG	RMS (%)	11	8	5	8
	MPF (%)	8	-7	-6	-1

which fell within the 32% to 49% MVC range. MVC's up to 50% are considered low intensity, and the results in both pre/post-fatigue, and sustained fatigue, correspond with the findings in equivalent low intensity MVC fatigue literature.

5.3.4.1 Sustained Fatigue Analysis of Results

Changes during a fatigue action (stage two) produced results which agree with past literature, with a very strong ($0.8 < r < 1.0$) and strong ($0.6 < r < 0.79$) positive linear correlation against time for MMG and EMG amplitude (RMS), respectively (top row; Fig. 5.13). The large percentage incline for both MMG and EMG was found to be significant ($P < 0.01$), as well as a steep gradient for each, suggests a noticeable increase in muscle fibre firing

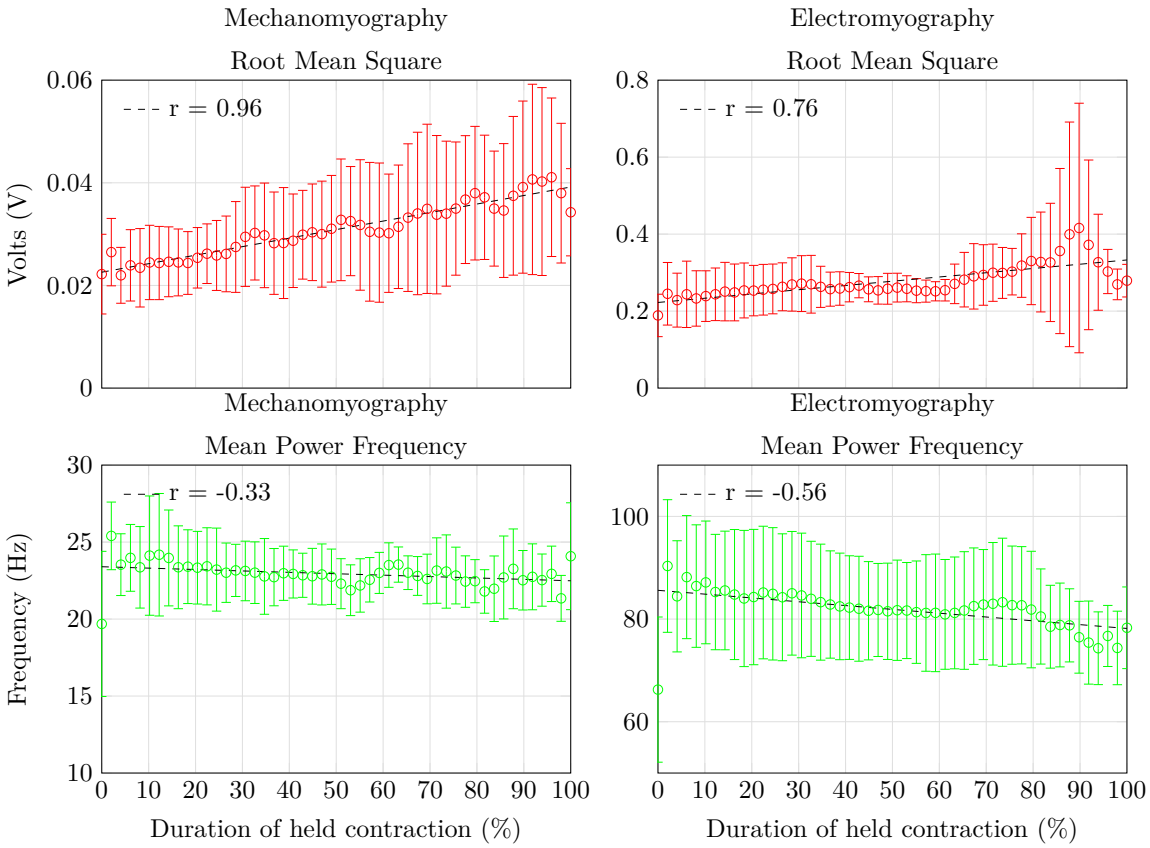


Figure 5.13: Changes in RMS (top row) and MPF (bottom row) for both MMG (left column) and EMG (right column) during the sustained fatiguing action. Standard deviation error bars are plotted, as well as linear lines of best fit and the calculated Pearson's correlation coefficients.

rates when the muscle becomes fatigued. Despite being unamplified, MMG had a greater response to amplitude change (74% incline) when compared with EMG (50% incline) which was amplified.

Frequency results (MPF), during the fatiguing action, also concur with literature, with a moderate ($0.4 < r < 0.59$) negative linear correlation against time for EMG results, and a weak ($0.2 < r < 0.39$) negative correlation against time for MMG results (bottom row; Fig. 5.13). Literature is mixed on MMG MPF observations, with some stating a decline in frequency, whereas others notice no change. This study recognised a significant decline in both MMG and EMG MPF, however, EMG ($P < 0.01$) was more significant that MMG ($P < 0.05$). The decline in frequency is suggested to be due to stable motor unit firing rate in response to the low contraction force[176]. The results seen here indicate a stronger sensitivity in amplitude changes during fatigue, as opposed to frequency components.

5.3.4.2 Pre and Post Fatigue Analysis of Results

An elevated RMS and a depressed MPF were seen post-fatigue for both EMG and MMG, when compared against fresh muscle. However, only MMG RMS saw a statistically significant increase, which suggests MMG is more sensitive to long lasting fatigue than EMG (Fig. 5.11).

MMG and EMG MPF saw a marginal decrease in frequency (-1% each) on average, with no significant difference seen (Fig. 5.12). However, where EMG MPF saw larger changes in isometric and concentric contraction periods (-7% and -6% respectively), EMG MPF eccentric data produced opposite results with an increase in frequency post-fatigue. It is believed this is due to motion artefacts and other disturbances. MMG MPF remained greatly unchanged with the exception of eccentric results which showed a small decline.

5.3.5 Conclusion

This study has shown comparable results with current literature, with inexpensive and easy to use sensors. Results seen here follow that seen in low intensity MMG fatigue literature, and it is believed that amplitude and frequency components will follow trends associated with other MVC forces, with medium intensity contractions expected to stabilise amplitude change, while high intensity contractions are expected to decrease amplitude. MMG Frequency components are expected to remain unchanged, regardless of MVC. While both EMG and MMG saw significant changes in amplitude and frequency components during a sustained fatiguing activity, only MMG saw a significant change in amplitude ten minutes after a fatiguing activity, suggesting MMG has a more sensitive response to fatigue.

This technique could be beneficial for monitoring fatigue in clinics which do not have access to equipment such as dynamometers, or in uncontrolled environments such as in the home. The amplifiers and wires associated with EMG in this study would make it infeasible for use in pervasive settings, however, the MMG and IMU technology were packaged into a single strap, with no external wires or preparation requirements. Further work intends to extend this study with additional IMU's to monitor ankle and hip flexion, as well as knee flexion.

5.4 Isotonic Fatigue Monitoring with Spinal Cord Injury Subjects

The spinal cord injury (SCI) population is at the low end of the fitness spectrum, with high risk of cardiovascular diseases, diabetes, obesity, and osteoporosis. Bone density decreases rapidly in SCI patients to approximately 60% of normal bone mass within one to three years after injury[193]. The bone loss occurs solely due to the lack of mechanical loads to the lower limbs necessary for maintaining bone strength. From the onset, SCI individuals will experience muscular atrophy due to the inactivity of their affected muscles, which will result in metabolic disorders and will greatly increase the risk of fractures in the proximal tibia and distal femur[194,195].

'Hybrid' functional electrical stimulation (FES) rowing is a novel exercise therapy that enables the SCI population to exercise their upper and lower body simultaneously, achieving significantly greater metabolic responses[196–200]. FES-rowing couples volitional arm and

electrically controlled leg exercise, mirroring the rowing exercise performed by able-bodied (AB).

The lack of sensation in the SCI population during muscle fatigue can result in reduced effectiveness in the stimulus applied, and therefore the monitoring of fatigue is of interest[201]. EMG has been commonly used in literature involving FES and other electrical stimulation techniques (see Section 5.5); however, identification of useful EMG signals from stimulation artefacts has been found to be challenging[202]. One method for counteracting fatigue is by increasing the stimulus intensity, however, incorrect timing in stimulus increases can result in inefficient negation, or even exacerbate fatigue[201].

Due to the limitations of EMG during electrical stimulation, MMG has been infrequently used in such studies, due to its robustness against electrical artefacts[203,204], with results suggesting a suitable detection of fatigue[205,206]. Correlating the decline in rowing performance through motion analysis with muscle function has potential benefits in efficient FES application and extension of exercise through the repression of fatigue. However, no studies have been found which combined muscle and motion monitoring in FES applications.

5.4.1 Research Question and Hypothesis

This study's aim was to monitor MMG and inertial changes during a short time, steady-state, submaximal rowing exercise to exhaustion. Results compare the effects of fatigue in MMG amplitude from the rectus femoris, inertial response, and force and rowing technique. This study examined both SCI and AB subjects in order to characterise and understand the differences between electrically stimulated non-innervated muscles in SCI patients and voluntary contraction in AB. It was hypothesized that the MMG/IMU sensor pair could detect difference AB and SCI subjects, as well as changes in rowing technique as individuals approach fatigue.

Five AB subjects, two male and three female, and five SCI subjects, four male and one female, were recruited for this study. Three of the AB subjects were previously professional rowers, whereas the remaining two were beginners. The SCI subjects are all involved in weekly training regimes with the ergometer, but had no rowing experience before injury. The SCI subjects were adults who have had a SCI (American Spinal Injury Association A,B) at the neurological level of C5-T12. Four of the SCI subjects had complete SCI, whereas one had incomplete SCI. This research was conducted in collaboration with Spaulding Rehabilitation Hospital (SRH) and Northeastern University, both in Boston, USA. This study was approved by the Imperial College Research Ethics Committee (ICREC) and by the institutional review board (IRB) at SRH. All SCI patients were recruited from the Exercise for Persons with Disabilities (ExPD) program that specialises in FES-rowing for SCI patients, ran by Spaulding's Cardiovascular Research Lab. Written consent was obtained from all subjects involved in agreement with the IRB approval.

5.4.2 Method

All rowing exercises were performed using an adapted Concept2 rower ergometer that was instrumented to collect data during rowing by adding separate force plates for the toe and heel for the left and right leg, a tension load cell for the handlebar, a string potentiometer that tracks the position of the chair, and two string potentiometers that characterise the compression forces in the front and back springs situated under the chair. Real-time data was collected from the load cells on the footplates, the tension load cell, and the string potentiometers using a biofeedback system developed in LabVIEW System Design Software which allows communication between a data acquisition system and the various sensors. The biofeedback received from the instrumented rower allows characterisation of rowing kinetics such as foot force, number of strokes, and stroke length. The ergometer was further adapted to accommodate SCI patients using a high backed seat with shoulder harness and a telescopic leg stabiliser which was adjusted to each patient's needs.

Subjects were asked to perform a rowing exercise at a constant workload, as given by the wattage of the ergometer. The workload chosen was subject specific and represented a moderate to high intensity exercise. The test stopped when the workload (wattage) dropped by 10% of the chosen work.

The AB subjects performed the task with no muscle stimulus, whereas the SCI subjects used a two channel Odstock 2 stimulator which activates skin surface electrodes targeting the hamstring and quadriceps muscle groups of each leg using the switch placed on the handlebar[207, 208]. The Odstock stimulator was set to 40 Hz pulses, with a pulse distance of 400 μs.

MMG and inertial data was collected using the same sensors and attachment method as seen in the previous fatigue study, which wrapped around the subject's thigh (Fig. 5.5). The subject's leg with the least spasticity, best response to stimulus, or had the greatest strength, was chosen for monitoring using the MMG and IMU devices. The strap was tightened until the MMG had a secure attachment, positioned atop the rectus femoris muscle, and was clipped in place with a flexural buckle. The subject's feet, legs, and chest were strapped to the rowing machine during the session (Fig. 5.14).

As with regular operation of a rowing machine, subjects start in the catch position (Fig. 5.15-A). For the SCI population, during the first part of a rowing stroke (the drive phase; Fig. 5.15-B) the rower activates the quadriceps muscles using the switch on the handlebar. The stimulation results in the contraction of the quadriceps muscle group, causing a knee extension. In the second part of the rowing stroke (the recovery phase; Fig. 5.15-C), the rower releases the switch on the handlebar which results in a contraction of the hamstring muscle group, causing a knee flexion and allowing the rower to return. The AB subjects



Figure 5.14: Subject mid-rowing session in a Concept2 indoors rowing machine. The IMU can be seen attached to the black strap on the subject's left leg, recognisable with a blue light. The MMG was also mounted in the black strap, situated atop of the rectus femoris (not seen). The white cables leading to hamstrings/quadriceps were attached to electrodes which produce the FES.

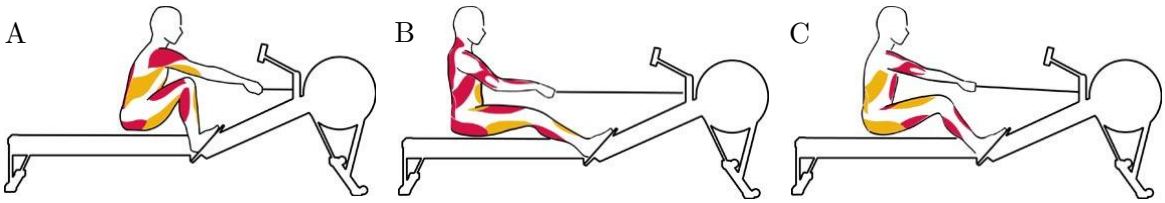


Figure 5.15: Figure showing three core stages of rowing. The catch position (A) was how the subjects begin. SCI subjects press a stimulus trigger to activate their quadriceps which pushes them back through the drive phase (B). Once releasing the stimulus button the hamstrings contract, returning the subject back to the catch position through the recovery phase (C). Muscles appear red during contraction, and yellow when relaxed. Image used with permission from Concept2[209].

performed the same rowing exercise, however, without using electrical stimulation and back support.

IMU and MMG data was transferred wirelessly via Bluetooth to a laptop, whereas instrumented data from the ergometer, including force and seat position data, were relayed through a National Instruments USB-6211 DAQ to the same laptop. All sensor types were started and stopped simultaneously using MATLAB, and was stored for offline processing.

Once all sensors and electrodes were attached, and the subject was seated and strapped into the rowing machine, an investigator started the collection of all sensors and asked the subject to start when ready. Once the subject was exhausted, as denoted by the 10% drop in rowing wattage, the investigator waited for the subject to stop moving before stopping the recording.

5.4.2.1 Data Processing

All data was processed offline in MATLAB. Each collected session included data before and after the rowing task, where the subject was stationary. In order to extract only the data during the rowing task, a threshold was determined as half the maximum gyroscope magnitude (4.1), and all data above the threshold was used as the rowing period (Fig. 5.16).

IMU data was filtered using a 1^{st} order Butterworth filter between 0.1 and 3 Hz, whereas MMG data was filtered between 10 and 100 Hz, using the same Butterworth filter. MMG and gyroscope magnitude data were resized into one minute, non-overlapping, windows. For each one minute window the MMG amplitude (RMS) and gyroscope frequency (MPF) were calculated.

Likewise, the force and position data were filtered using 1^{st} order low-pass Butterworth filter with a cut-off frequency of 10 Hz. For the monitored leg, the respective foot force was obtained by summating the heel force and toe force data. Furthermore, the data was also segmented into one minute, non-overlapping, windows. In order to compare data within or between subjects, the one minute intervals were normalised to a percent rowing cycle using a 1D spline interpolation function. This normalisation returned a one minute characteristic rowing stroke. Thus, in the case of each subject, the peak force for each minute of rowing was obtained as the maximum value of the corresponding characteristic rowing cycle. The rowing stroke and the stroke length were obtained from the chair position data, where the rowing cycles were considered from the hit of the front spring until the next hit of the front spring. In order to compare among the two groups (SCI and AB), the peak forces were normalised to body weight, and the stroke length was normalised by height.

MMG RMS, gyroscope MPF, stroke length, and foot force were averaged against AB and SCI group data, and the mean and standard deviation were calculated for analysis.

Subjects each had a unique endurance towards the task, and thus had different session durations before fatiguing, therefore, each group data is presented as percent of test duration. Linear regression analysis was performed on the MMG RMS, gyroscope MPF, stroke length, and foot force, for each group. For each, the Pearson's correlation coefficient (r) was calculated, along with significance value (P), and percentage change over test duration.

5.4.3 Results and Discussion

Both AB and SCI groups saw significant changes in all data sets during this study ($P < 0.01$). Statistical results for both AB and SCI groups are presented in Table 5.3 for foot force and MMG RMS results, and Table 5.4 for stroke length and gyroscope MPF.

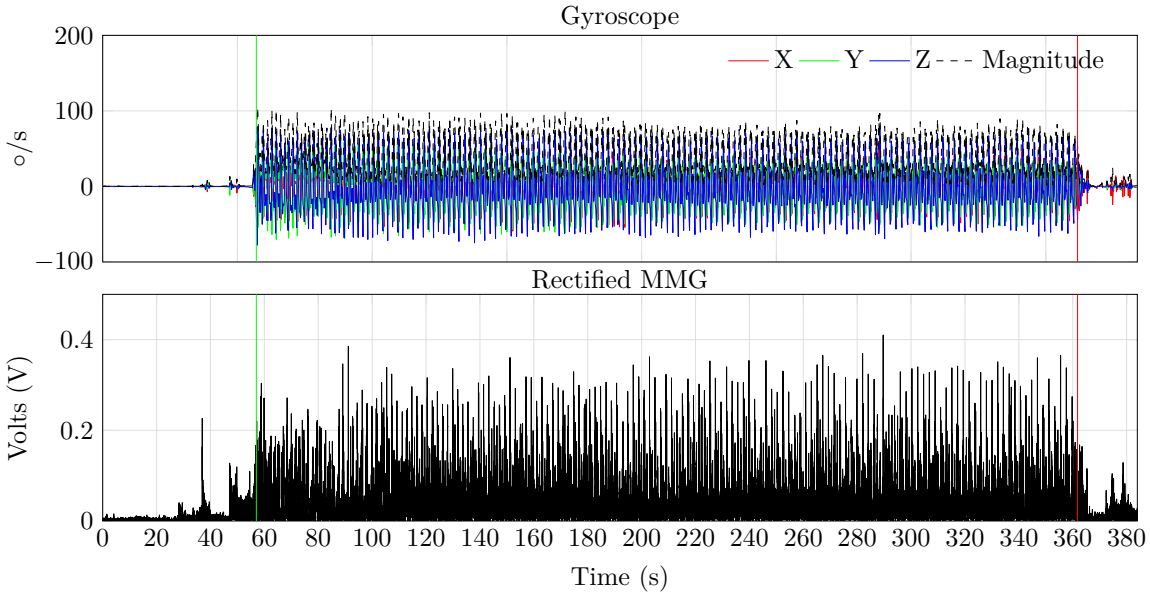


Figure 5.16: Raw data from a SCI subject. Gyroscopic data (top), with calculated magnitude (black dashed), and rectified MMG (bottom). The vertical green line indicates the starting point of data analysis, whereas the red vertical line indicates the end, as denoted by the magnitude threshold.

Fig. 5.17 and Fig. 5.18 display the data graphically. Fig. 5.17 compares peak foot force / body weight and MMG amplitude (RMS), whereas Fig. 5.18 compares stroke length / height and gyroscope frequency (MPF).

5.4.3.1 Foot Force Verses MMG Amplitude

Results of rowing foot force verses MMG amplitude were consistent with the relationship seen in the previous fatigue and force based studies of this thesis, with an increase in MMG amplitude as the observed muscle becomes fatigued, as depicted by the decline in peak force. These results are true for both the AB and SCI groups, with a significant, very strong, positive linear relationship seen in the MMG results, and a significant, very strong, negative linear relationship in the force. Both AB and SCI groups saw a close decrease in force of -10% and -11%, respectively, as well as a similar incline of 9% and 8% in MMG amplitude. While AB experience about 50% body weight force on each leg, the SCI patients applied really low forces of only about 10% body weight per leg, as seen in the foot force magnitudes.

Interestingly, both AB and SCI groups saw a very similar increase in MMG RMS activity over the course of the session, however, the SCI group saw a steeper incline in activity in the first 10% of testing, along with a steadily increasing standard deviation error. The increasing error is believed to be a result of the differing abilities of the SCI subjects involved, and an adjustment in rowing technique by increasing the use of the two springs under the seat that helps the subjects change directions during rowing. One subject had incomplete spinal cord injury and had some muscle sensation and was capable of standing on their own, another subject was well experienced in the rowing task and owned a rowing machine themselves

Table 5.3: Results comparing foot force against MMG RMS for both AB and SCI subject groups. Analysis includes Pearson's correlation coefficient (r) against test duration, significance value (P), and percentage change over test duration.

	Force			MMG RMS		
	r	P	%	r	P	%
AB	-0.97	$P < 0.01$	-10	0.84	$P < 0.01$	9
SCI	-0.89	$P < 0.01$	-11	0.81	$P < 0.01$	8

Table 5.4: Results comparing stroke length against Gyroscope MPF for both AB and SCI subject groups. Analysis includes Pearson's correlation coefficient (r) against test duration, significance value (P), and percentage change over test duration.

	Stroke Length			Gyroscope MPF		
	r	P	%	r	P	%
AB	-0.85	$P < 0.01$	-4	0.94	$P < 0.01$	7
SCI	-0.41	$P < 0.01$	-1	0.60	$P < 0.01$	2

which they used regularly, and another subject was inexperienced and new to the rowing process. All subjects, although linked with spinal injury, had very different abilities and rowing methods, which was less common or observed in the AB group. The AB also had a rising error in the MMG RMS results, while presenting a more non-linear response in their force STD error results. Expectedly, the AB group had a far greater force output than the SCI group, however, the SCI had a larger MMG RMS response. It is believed this is due to the non-voluntary nature of their stimulated contraction and the structure of their atrophied muscles, however, future work on this difference is needed to be performed.

5.4.3.2 Stroke Length Verses Gyroscope Frequency

The relationship seen in the stroke length verses gyroscope frequency were similar to that seen in the force and MMG observation. A decline in stroke length, which results in an increase in number of strokes, has been detected in the gyroscopic data with an increase seen in the gyroscope magnitude frequency. However, comparisons between the AB and SCI groups were less similar in these results. Although both groups saw a decline in stoke length and an increase in gyroscopic frequency, the change was much more prominent in the AB group, with a -4% and 7% change seen in the stroke length and gyroscope data, respectively. The SCI group, however, saw a -1% and 2% change, also in stroke and gyroscope data, respectively. Although the trend is the same between groups, the AB group saw a significant, very strong, negative linear relationship in the stroke length, and a significant, very strong, positive linear relationship in the gyroscope data. The SCI group had a weaker linear correlation, with a significant, moderate, negative, and significant, strong, positive linear relationship in stroke length and gyroscope data, respectively.

Weaker linear correlation in the SCI group data suggests a more complex relationship in rowing strategies over time. Furthermore, both gyroscope and stroke length data show a

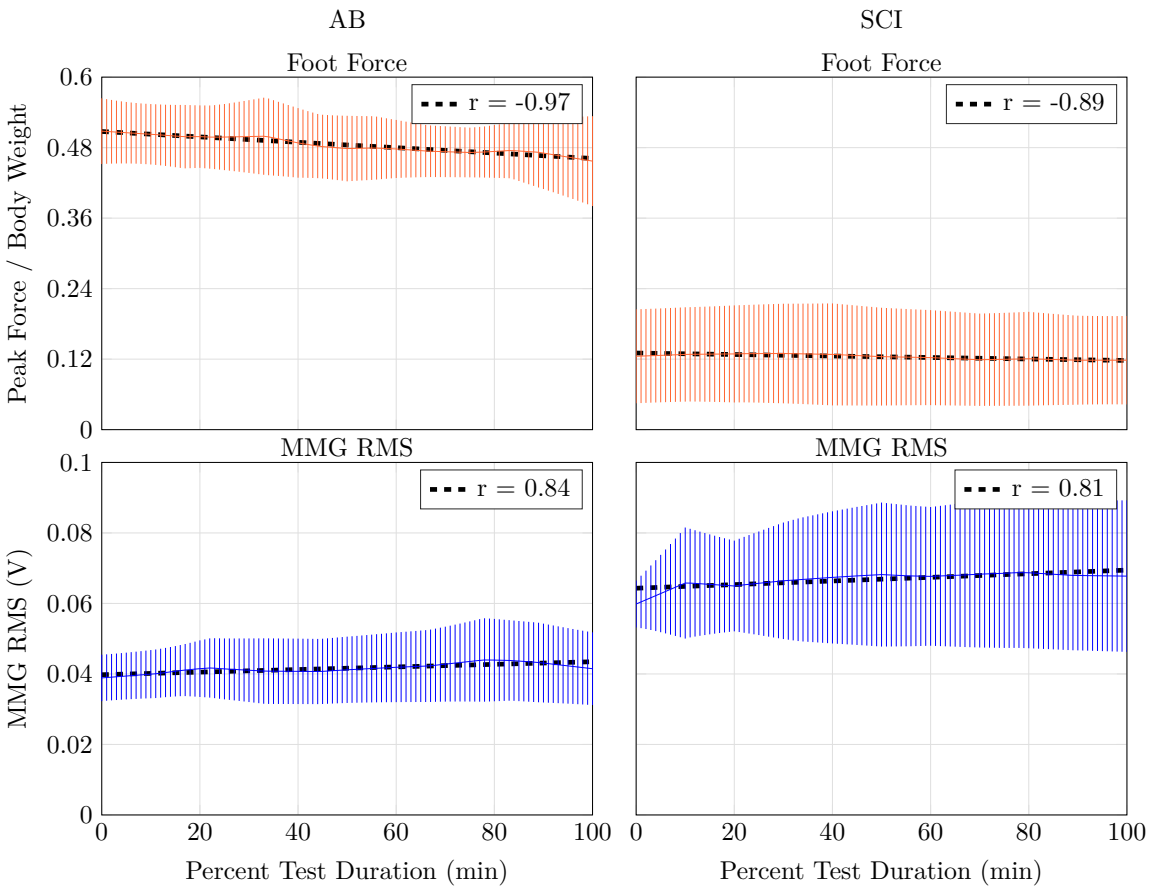


Figure 5.17: Changes in foot force (top row) and MMG RMS (bottom row) for both AB (left column) and SCI (right column) subject groups. Standard deviation error bars are plotted, as well as linear lines of best fit and the calculated Pearson's correlation coefficients.

decline in standard deviation error from 0 to 10% of test duration, however, while gyroscope errors increase from 10 to 100%, stroke length errors increased until 80% before declining once more. This complex relationship was not seen in the AB group, in which both stroke and gyro errors increase from 0 to 100%. It is believed that with muscle fatigue of the legs, the SCI subjects adjust their rowing technique in order to maintain the required workload. This adjustment results in using more of the upper body and the two springs that help them change directions during rowing, resulting in an increase of number of strokes and a decrease in stroke length.

The AB employed a more consistent rowing technique than the SCI for the entire test duration. This was supported by the smaller error seen in AB gyroscope compared to that seen in SCI. Thus, it was believed that the AB population experiences a whole body fatigue, seen in the simultaneous decrease of feet force and rowing technique (stroke length and number of strokes). In contrast, the SCI population reached leg fatigue very fast (about 10-20% of test duration as seen by force/MMG), followed by upper body fatigue in the later stages of the test. Once the lower body was fatigued, the SCI used more of the upper body to maintain the target workload, however this was seen in the increase in both stroke and gyro errors.

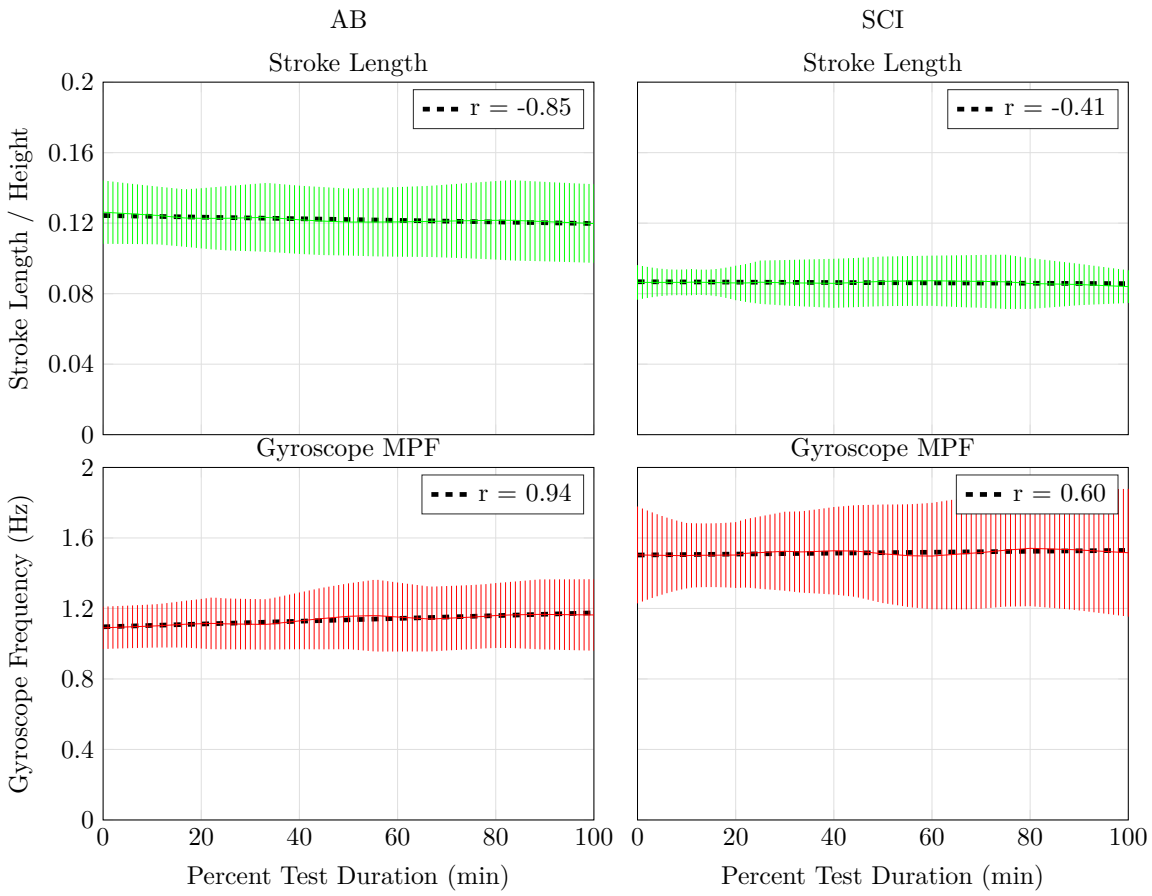


Figure 5.18: Changes in stroke length (top row) and gyroscope MPF (bottom row) for both AB (left column) and SCI (right column) subject groups. Standard deviation error bars are plotted, as well as linear lines of best fit and the calculated Pearson's correlation coefficients.

Comparative results between groups also showed a higher frequency in the gyroscope magnitude, while a shorter stroke length in the SCI group, which was expected as the short FES pulses cannot produce enough stimulation for full contraction of their muscle, and thus limited extension of their legs.

5.4.4 Conclusion

Both groups saw increases in MMG amplitude while foot force decreased, as well as an increase in gyroscope frequency as stroke length decreased. However, while force and MMG amplitude results were similar between groups, the SCI group had a more non-linear progression in stroke length and frequency throughout the session, suggesting a more complex rowing strategy. Furthermore, it was learnt that the AB and SCI groups had unknown similarities between each other, as well as expected results seen, such as a much lower force output and shorter stroke lengths in the SCI group.

This study suggests a suitable comparison between the IMU and MMG sensor pair against the Concept2 ergometer and force sensors, albeit in a cheaper, more portable package.

5.5 Clinical Application of Anaesthetic Monitoring

Applications presented so far have focused on monitoring in pervasive environments, as well as technology development for ease of use with non-trained and non-clinical personnel. This study introduces a different approach where human motion and muscle activity is monitored within a clinical environment, with trained medical professionals. Despite special attention to development of a device which is applicable outside of a controlled environment, something which current technology of a similar nature lacks, this application has demonstrated the versatility of use in a range of environments.

Through conversation with an anaesthetist it was learnt that the current technology available in peripheral nerve stimulation is not only limited, but the technology used is not designed with anaesthetists in mind. Peripheral nerve stimulation is a method used to monitor muscle reaction when a neuromuscular blocking agent (NMBA) is given to block musculoskeletal activity during surgery. This process involves an electrical stimulation which is applied to a nerve in order to determine the paralysis of the muscles associated with it. The most common location of application is the ulnar nerve, which induces a twitch in the adductor pollicis muscle in the hand when stimulated, however, the orbicularis oculi muscle is also occasionally used in research[210,211]. MMG has been a popular choice in monitoring the effects of anaesthetics and has become the gold standard in this field. Although EMG is also commonly used, it does have disadvantages over MMG including interference from diathermy and temperature[212], as well as the non-trivial rejection of the stimulation artefacts, as mentioned in the previous study.

Prior to a dose of a NMBA, of which Rocuronium, Vecuronium, or Atracurium are widely used, the anaesthetist applies an electrical stimulation of four single pulses at 2 Hz to a nerve and monitors the muscle response. These pulses, numbered T1 to T4, are known as a train of four (TOF), and usually the muscular response is monitored either visually from four corresponding twitches of the muscle, or through technological methods such as MMG or EMG. Without a paralytic, the muscle should respond to all four stimuli from the TOF. If it does not then the TOF is applied again at a higher stimulus and is repeated until four responses are received. This step is necessary to determine the baseline response of the muscle in order for successful determination when dosed, as results are unreliable without calibration[213].

Once dosed, and the necessary time has elapsed for the agent to take effect, the anaesthetist will continue to apply a TOF at regular intervals and records the muscular twitch magnitude to determine a ratio of T4:T1, which indicates the degree of neuromuscular block (5.4). Non-depolarising NMBA's will progressively decrease the magnitude of twitches from the first to the last (T1 to T4) from the onset of administration until fully dosed where all twitches are not seen. The decline in magnitude from first to last twitch is known as fade.

Depending on the length of surgery, additional doses of the agent may need to be reapplied if and when any of the twitches begin to reappear. Twitches start to reappear in reverse order, T4 to T1, until the agent has completely worn off.

$$TOF\ ratio = \frac{T4}{T1} \tag{5.4}$$

In events where no twitches are detected, the anaesthetist may opt to use another type of stimulus called tetanus. This is a 50 or 100 Hz pulse which typically lasts around five seconds. When nerves are under deep paralysis this method can overcome deep concentrations of NMBA to force a response. Furthermore, a combination of tetanus and TOF can be used in order to force a response and then apply a TOF in one process, with a recovery period in the middle (typically three to five seconds), which is called post-tetanic stimulation.

Practically, the current devices mostly monitor the adductor pollicis muscle in the hand, which requires the anaesthetist to stand beside the patient so that they have access to the arm. Application of the stimulus is only applied periodically which means the anaesthetist must move around the patient to stay clear of the operating surgeon performing the procedure. The anaesthetist had mentioned that they predominantly stand at the head of the patient during the procedure and a device which they can use while standing there would be beneficial. Secondly, they had mentioned a need for a device in which donning and doffing is more straight forward. With current devices, electrodes and wires are attached to the patient which means the device is often needed to be handheld at all times, restricting the use of their hands for other needs. Finally, the anaesthetist had mentioned a need for more advanced analysis, specifically the ability to monitor muscular fade in a more systematic way while ignoring artefacts and other disturbances which can be caused in the operating theatre.

5.5.1 Research Question and Hypothesis

This design study introduced a device developed specifically with the anaesthetist's requirements in mind, which could be used within a clinical setting, and improves on the limitations with the current technology including practicality of use. Past literature has shown a poor level of communication in the development of body worn sensors to be used in a clinical setting, due to the engineering and design teams not sufficiently asking exactly what the clinical teams wants[27]. Through strong communication the system presented here was designed for clinicians, with constant input and feedback from clinicians. The success of the device is based on three goals:

1. Development of a prototype to be used in a clinical setting, which the clinicians, engineers, and patients are happy using.
2. Successful monitoring of the baseline TOF, and determine magnitude of muscle contractions.
3. Successful monitoring of TOF while dosed, or lack thereof, and determine muscle fade.

It was hypothesized that MMG could detect TOF in dosed and non-dosed subjects. Only TOF stimulations and contractions are processed in this study, however, future work intends to apply this technology to other stimulation methods, such as tetanus. This study is performed in collaboration with Mount Sinai Hospital in Manhattan, USA. Two patients were tested over the course of a one month period with written and verbal consent obtained from all patients involved. Ethical approval was gained through Mount Sinai Hospital and the Imperial College Research Ethics Committee (ICREC).

5.5.2 Method

Due to the devices currently on the market forcing the anaesthetist to monitor muscles of the hand, this device opted to monitor the orbicularis oculi (OO) muscle surrounding the eye. Although usually reserved for use when the adductor pollicis (AP) is unavailable, the OO has been found to have a shorter latency and faster recovery than that of the AP[214]. The anaesthetist working on this project strongly recommended this muscle so that they could stay at the head of the patient and remain there throughout the procedure.

The device, as seen in Fig. 5.19, is a band that wraps around the subject's head and can be adjusted for a correct fit. The band consists to two core parts; the first is the MMG sensor located above the patients left eye to monitor the OO through stimulation of the temporal nerve, the second is the IMU situated on the side of the head to monitor motion and reject artefacts produced through movement which exceeds a threshold. The band is to be wrapped around the patients head and placed with the MMG sensor located on the OO muscle, the IMU, battery, and push button require less specific placement and therefore do not need to be specifically placed.

Once turned on, the device enters a sleep state, which can be toggled into an active state using a button located on the strap positioned over the subject's temple, which can be easily accessed by the anaesthetist. Within the sleep state, the device is in a low-power, non-collecting mode. However, once toggled into the active mode the MMG and IMU begin collecting data which is stored on the on-board SD card for offline processing. Every time the device was switched from sleep mode into active mode, a new file was created on the SD card which the data was written to. IMU data was sampled at 50 Hz, whereas MMG was sampled at 1 kHz. Current devices usually have an external processing device which samples the data from electrodes attached to the muscle of interest, which requires the device to be handheld. The technology presented here does not require any external devices which allows the anaesthetist to keep their hands free.

The anaesthetist was asked to keep a log of their activities during use of the system, including when stimulus was applied or a NMBA (re)administered. The device was toggled into an active state five seconds before each individual activity (such as application of a TOF stimulation), and toggled back into sleep five seconds after the activity, which would create

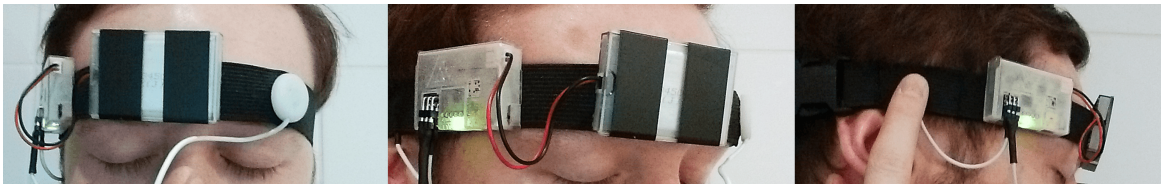


Figure 5.19: Device developed to monitor orbicularis oculi muscle surrounding the left eye during anaesthetic applications using MMG and inertial measurement. From left to right: front view showing placement of MMG sensor; 45° view of IMU placement (left) and battery (right); and side view showing push button located on the temple (under pointing finger) for easy access from anaesthetist to start and stop logging of data.

a separate file for each task performed. The log was used as a ground truth and each file created on the SD card was matched with each item within the log list.

The NMBA used was Rocuronium Bromide and the stimulator was a SunStim^{TM} Plus by Sun Medical. Following each surgical procedure where the device was used, the data files on the SD card were uploaded to a computer and were emailed back to Imperial College London where the data was analysed using MATLAB.

Gyroscope data had its magnitude (4.1) calculated, whereas MMG data was filtered between 10-100 Hz using a 1st order Butterworth filter and then rectified. Motion data was used as both a detection of movement artefacts, and as an indicator of a stimulation being applied. Inertial data was neither smoothed nor filtered.

Peak detection was applied to both the gyroscopic magnitude data and the filtered MMG data, in order to detect peaks of motion artefacts and muscle contraction information respectively.

The MMG data was processed for peaks which exceeded a threshold of five times the MMG stationary signal (typically around 0.1 V) and were saved for further analysis. Likewise, the gyroscopic data was scanned for peaks which exceeded five times the gyroscope stationary signal (typically around 5°/s) and were ruled as motion artefacts. MMG peaks which fell within one second either side of a motion artefact peak were removed from the data.

Each MMG peak had its magnitude (RMS) and frequency (MPF) calculated, and the distance between each neighbouring peak was also determined. TOF pulses were finally characterised when four peaks with a neighbouring distance of 500 ms±10% (2 Hz) were found, and FFT was applied to determine frequency of the pulses.

5.5.3 Results

TOF was monitored in both pre-NMBA muscle to obtain a baseline, and in dosed muscle post-NMBA. Results show a successful determination of all four twitches of the baseline TOF for both subjects (Fig. 5.20), as well as calculation of RMS amplitudes and MPF in

each twitch (Table 5.5). RMS magnitude information produced a TOF ratio of 1 (5.4) for both subjects, correctly estimating no fade in twitches in non-dosed muscle.

FFT analysis of the TOF twitches resulted in a frequency of 1.95Hz for both subjects, strongly suggesting the correct MMG peaks associated with a TOF stimulation (Fig. 5.21).

This study was unsuccessful in correctly determining TOF twitches during dosed muscles due to external interferences within the surgical room, as described below.

5.5.4 Discussion

This study calculated the muscle response of a TOF stimulation to the OO muscle both pre and post-NMBA in two subjects. Results were successful in the estimation of TOF stimulation in pre-NMBA muscle, however, due to electrical interference and other issues within the operating room the same could not be produced in dosed muscle.

Fig. 5.20 shows results from both subject A and B during their TOF stimulation prior to anaesthetic administration. Four peaks are noticeably prominent and peak analysis determined their magnitude and location in time which was used to determine frequency and the TOF ratio. Each twitch, T1 to T4 is assigned a colour and their magnitude marked with a symbol. Their location in time is displayed with a vertical line on each graph to show motion activity (top) during each twitch.

Despite some activity from the gyroscope, their peaks are significantly lower than the motion artefact threshold (black dashed horizontal line) and are therefore not rejected as noise. FFT analysis (Fig. 5.21) of the MMG data segment further confirms a TOF pulse by recognising a maximum peak frequency close to 2Hz. Furthermore, both subjects reported identical frequencies, which further confirms this data segment contains the TOF pulse expected.

Unknown prior to this study, a large electromagnetic interference (EMI) was present due to some of the medical equipment present in the operating room. Cauterisation, the process of burning tissue in order to close or seal during surgery, emits a significant amount of EMI which caused unexpected behaviour with the IMU, including frequently turning off and on again.

Further issues arose with the manual logging method performed by the anaesthetist. Firstly, although accurate in description, the result of unexpected toggling (on and off) of the device produced a number of short or empty ‘ghost’ files which were written to the SD card. This made matching the recorded log to the corresponding files challenging. Secondly, without any synchronisation with the applied stimulus it was found to be very difficult to determine a ground truth of when a stimulus was applied within a data set. During baseline and low occupancy of the agent the twitches were visually evident in the data, but when heavily anaesthetised the data analysis became hard to perform.

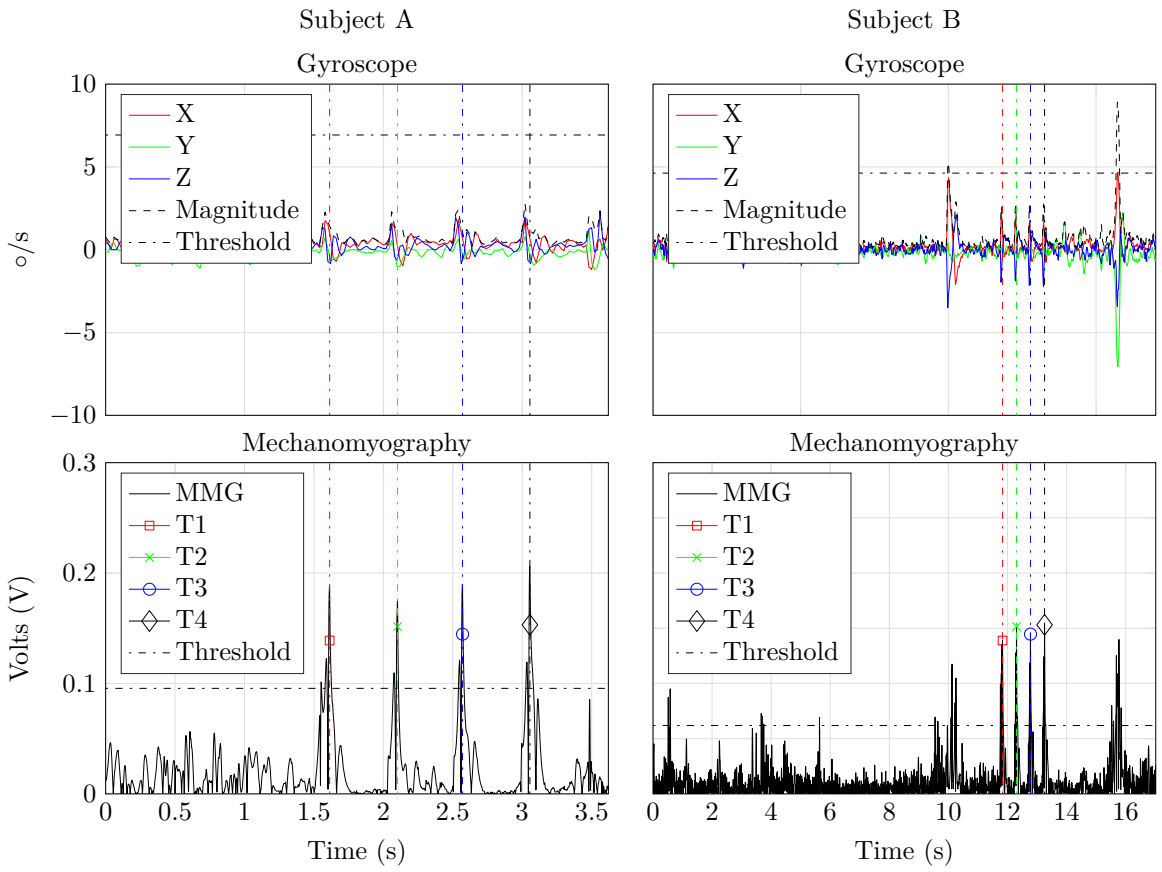


Figure 5.20: Raw results with TOF twitch estimation in pre-NMBA muscle. Twitches T1-T4 are isolated and external noise and disturbances are rejected. Column one shows the baseline results from subject A, whereas the right column shows the same for subject B.

Learning from these issues, the next iteration of this device has been designed which implements several additions for successful collection. First, the IMU will be covered in a conductive material in order to create a Faraday cage to reject EMI. Secondly, to remove the burden of the anaesthetist having to keep a detailed log of activity, additional sensors have been added to monitor the stimulus concurrently with the MMG data. Using two metal electrodes, which will be sewn into the brace much like the MMG sensor, one of the free auxiliary channels on the IMU will be used to collect the electrical stimulus produced by the stimulator, alongside the mechanical response produced by the muscle which is recorded by the MMG. This new signal collected alongside MMG will provide the ground truth needed to correlate MMG accuracy with TOF and other stimulations.

5.5.5 Conclusion

In conclusion this application was successful in achieving the first two objectives listed above; a device was developed and used successfully by an anaesthetist on patients during surgical procedures, and a baseline TOF was determined along with frequency and magnitude information of the twitches. However, due to difficulties from environmental issues and a

Table 5.5: Baseline TOF results in pre-NMBA muscle from subjects A and B.

	TOF Twitch	RMS (mV)	MPF (Hz)
Subject A	T1	39	12.74
	T2	45	12.28
	T3	45	12.77
	T4	43	12.92
Subject B	T1	37	11.71
	T2	43	11.64
	T3	43	11.45
	T4	37	11.48

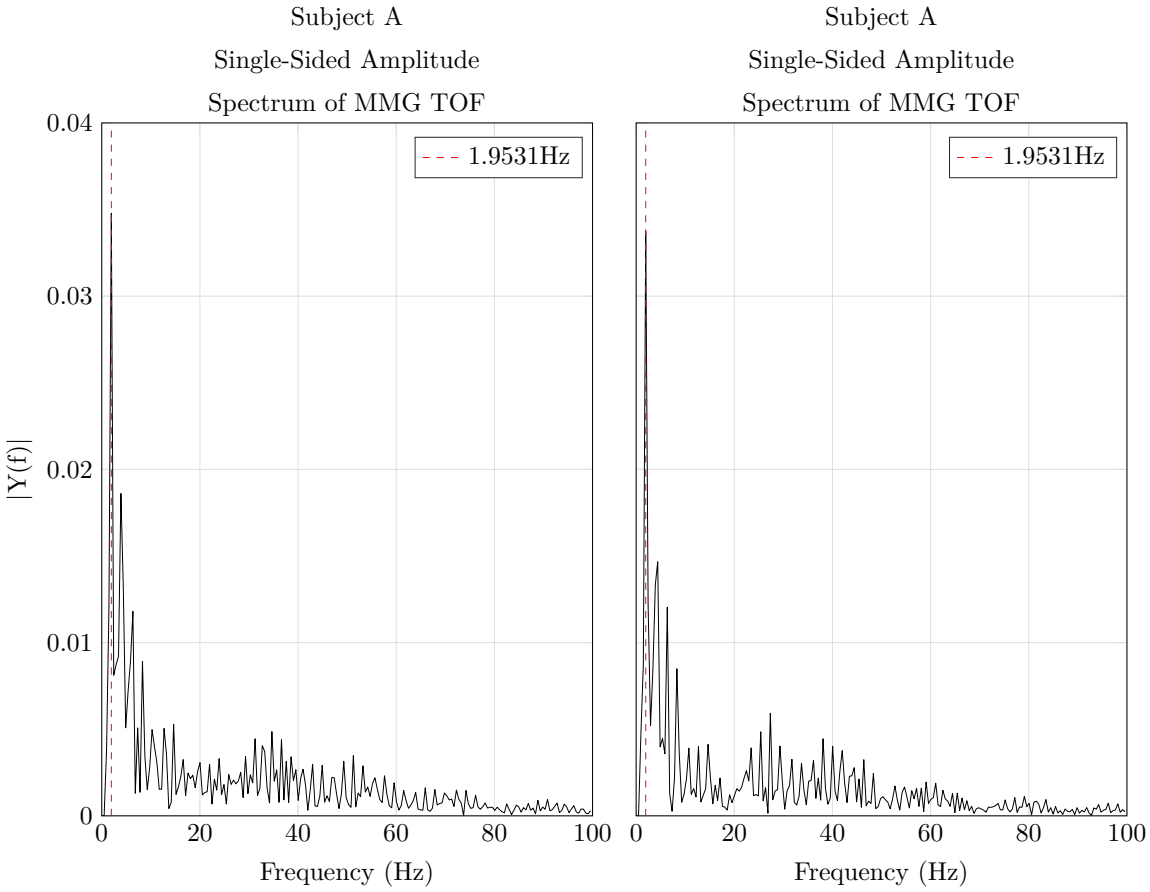


Figure 5.21: Frequency components of all peak determined during a TOF stimulation. Subject A (left) and subject B (right) have an identical maximum frequency of 1.95Hz, suggesting the peaks analysed are likely the TOF pulse stimulation.

lack of a ground truth it was infeasible to analyse stimulation information when patients were administered the anaesthetic.

Although unable to determine TOF during NMBA administration, the processing method presented here would allow the calculation of muscle fade for each twitch, using the new proposed iteration of the device. Despite the technical issues, the steps taken so far to create a device that all stakeholders of the process are happy using has been successful.

5.6 Chapter Summary

This chapter has introduced four applications in order to better understand the MMG amplitude and frequency components in response to increases in force and the introduction of muscular fatigue.

It has been confirmed that MMG has a strong linear relationship with increases to force, which agrees with present literature. MMG has also shown to be capable of monitoring changes in fatigue seen in isometric and isotonic fatiguing studies, in both voluntary and involuntary contractions, with MMG being found to have a greater sensitivity up to ten minutes post-fatigue than EMG.

This work has shown clinical level results, typically achieved with EMG and dynamometer technology for muscle and force monitoring respectively, using low-cost, portable, easy to use MMG and IMU sensors, in pervasive environments. Furthermore, although predominantly targeted at uncontrolled studies, this chapter has shown a suitable inclusion into a clinical environment, with a device developed specifically to satisfy clinicians needs.

6

Gait Analysis and Activity Monitoring

Contents

6.1 Introduction 96

6.2 Activity Classification in Typical Gait 96

6.3 Progressive Changes in the Gastrocnemius 105

6.4 Asymmetric Differences in the Rectus Femoris 113

6.5 Chapter Summary 122

6.1 Introduction

This chapter introduces three applications where human gait is analysed and processed in order to better understand activities, differences in typical and atypical conditions, and bilateral differences in individuals.

Human gait monitoring is abundant in literature, with the majority opting for optical based tracking methods within gait laboratories. A further understanding of gait is provided from muscle monitoring, concurrent to motion tracking, which can indicate abnormalities in movement through altered muscular contraction.

Although accurate, optical based tracking is only possible within a finite space, due to the subjects being monitored having to stay within the collection medium of the cameras. This limits the amount of activities that can be performed, as subjects cannot enact their normal, everyday tasks within a laboratory. Prolonged monitoring with EMG is also limited, due to sensor degradation over time and problems associated with skin impedance[155].

Through combination of IMU and MMG technologies this work presents human activity classification, the monitoring of progressive change over time, and asymmetrical differences between lower limbs. These applications will work on the limitations of optical and EMG based tracking by enabling prolonged collection outside of a clinical environment, using inexpensive and non-restricting sensors.

6.2 Activity Classification in Typical Gait

Activity classification and gait monitoring provide useful information which can be applied to many applications, including rehabilitation, health monitoring, or performance tracking. Commercially, and in recent years, fitness trackers and wearable technology have become incredibly popular with a wide choice of technology to choose from. Much like the IMU presented as part of this work, the commercial options available contain inertial components used to detect movement and classify activity through algorithms. Such technology can relay information to the user with how much they slept, how many steps they took, and how much running, walking, or cycling they did in a day, week, or month.

Academically, activity and gait tracking is also a vibrant field, with most applications targeted towards clinical problems such as monitoring patients participation in rehabilitation tasks and diagnosis of disease and disabilities[215,216]. Again, due to the advancement of technology, many researchers can perform such analysis using off-the-shelf devices, or can even use smart phones, due to a large proportion containing the inertial sensors necessary for motion analysis[71].

Motion and muscle analysis is common in gait laboratory analysis, including classification of daily activities[217,218]. However, as previously stated the limitations imposed by the confinements of a motion capture environment, as well as a lengthy sensor donning process, makes prolonged collection infeasible in gait laboratories. Furthermore, gaining a true understanding of daily activities can only be achieved through an uncontrolled process of users actually performing their daily tasks, something which is not possible in gait laboratories.

Although research exists where inertial and other motion monitoring technologies have been used outside of a laboratory[219–221], no work has been found where motion and muscle activity have been combined to obtain complementary results in activity classification in an uncontrolled, pervasive environment.

6.2.1 Research Question and Hypothesis

The work presented here introduces an unsupervised activity classification algorithm which utilises both inertial measurement information and MMG muscle activity using the technology detailed in Chapter 3. It was recognised that information from both muscle and motion can provide more accurate results in activity analysis, than that capable from either data types alone. Using a K-means algorithm and *a priori* knowledge, a total of nine commonly performed activities have been classified from real-world data, outside of a laboratory. It was hypothesized that MMG and inertial data could differentiate between daily activities, such as walking, stairs, and running.

Six subjects were recruited, one female and five male, aged between 25 and 31 (STD 2.34) and a height of 165 to 185 cm (STD 7.34), to perform a number of differing activities for a period of time during an experiment to validate the accuracy of the proposed algorithm. This research was approved by the Imperial College Research Ethics Committee (ICREC) and written consent was obtained from the subjects involved.

6.2.2 Method

Data collected over a prolonged period of time, both inertial and muscular, contains a lot of information and features specific to individual users. However, without proper analysis, these characteristics can be hard to distinguish from the noise and irrelevant data. Therefore an algorithm was developed to identify eight commonly performed activities:

Walking
Running
Ascending stairs
Descending stairs
Ascending within an elevator
Descending within an elevator
Standing
Lying down

A ninth activity was also categorized which contains noise and other unclassified activities data, which could be further analysed in future adaptations.

This model is based on previous work which used multiple IMU's and single accelerometers to determine multiple activities[81,82], however, the method presented here is unique in that the model was completely uncontrolled and unsupervised with no pre-collection data labelling for activities required, along with the concurrent collection of muscular activity.

The subjects, all with typical gait, were selected on their differing height, as opposed to sex, weight, or ability. Height influences stride length and cadence which were a key element in classifying walking from running in this algorithm.

Each subject performed two trials in which they took a pseudo-random walk lasting ten minutes involving multiple activities from the list above, while given a different set of activities to perform. Subjects were not asked to perform their tasks in a particular order, length of time per activity, nor instructed in how to perform the task, they were only asked to perform their given tasks at least once during their trials.

A very similar brace was used as seen in Fig. 4.5 for validation of this system, with the IMU situated on the lateral side of their right leg and the MMG sensor on the lateral head of the gastrocnemius. A push button was used which the subject pressed before changing to a different activity, in order to validate the data collected against a ground truth.

6.2.2.1 Signal Processing

All inertial data (accelerometer, gyroscope, magnetometer, and barometer) was smoothed using a moving average seen in (6.1), where ys_n is the smoothed value for the n^{th} data point, N is the number of neighbouring data points on either side of ys_n, and $2N+1$ is the span, which in this case is 15 data points.

$$ys_n = \frac{1}{2N+1}(y_{(n+N)} + y_{(n+N-1)} + ... + y_{(n-N)}) \tag{6.1}$$

After smoothing, data from each sensor type was windowed in order to be processed by the algorithm. Past literature has shown that windows with a 50% overlap produce suitably good results at 50 Hz for the inertial data[81,82]. For this study the inertial window size was

set to 200 samples (four seconds of data at 50 Hz) which can be easily resized to obtain the same window size for the other sensors sampled at a different rate; a four sample window for the barometer at 1 Hz, and a 4000 sample window for the MMG at 1 kHz. The data was resized into windows of four seconds with a 50% overlap and four features (mean, standard deviation, power, and covariance - (6.2)) were determined from each of the three axes of the accelerometer (X, Y, and Z) resulting in twelve parameters per window.

$$\begin{aligned} \mu &= \frac{1}{N}\sum_{n=1}^{N} y_n \\ \sigma &= \sqrt{\frac{1}{N-1}\sum_{n=1}^{N}(y_n-\mu)^2} \\ power &= \sum_{n=1}^{N}\frac{y_n^2}{N} \\ COV(a,b) &= \sum_{n=1}^{N}\frac{(a_n-\mu_a)(b_n-\mu_b)}{N} \end{aligned} \tag{6.2}$$

Where n is the current data point, N is the total number of data points in the window, i.e. 200, y is the data set of one axis, μ is the mean, σ is the standard deviation, and a and b correspond to one of the three accelerometer axes (X, Y, or Z).

Values in the diagonal of the covariance matrix where the covariance of an axis was applied against itself results in the variance of that axis, and were therefore ignored. Likewise, values below the diagonal were mirror values of that above the diagonal and were also ignored, see (6.3) where only the values in green were used.

$$COV = \begin{bmatrix} X,X & X,Y & X,Z \\ Y,X & Y,Y & Y,Z \\ Z,X & Z,Y & Z,Z \end{bmatrix} \tag{6.3}$$

A K-means clustering algorithm using a squared Euclidean distance method was used to cluster windowed data into one of three clusters based on the parameter matrix created from the four features above. As this study was uncontrolled there was no way of determining prior to collection how many of the activities the subject would be performing. It was not guaranteed they would perform all or even the majority of the activities, therefore clustering for the nine activities listed above would be unfeasible. This algorithm processes the data in two stages: a gross group clustering stage where each window was split into one of three groups; stationary activities (standing, lying, and elevator), dynamic (walking, running, and noise), and dynamic-altitude (stairs), and a second activity classification stage where windows from each cluster group were further classified into one of nine activities. The objective function of the K-means algorithm is seen in (6.4).

$$J = \sum_{n=1}^{N} \sum_{k=1}^{K} r_{nk} ||y_n - c_k||^2 \tag{6.4}$$

Where again y, n, and N are the dataset, current data point, and total number of data points, respectively. K is the number of clusters, i.e. three, k is the current cluster, c is the centroid of the cluster, and r_{nk} is the binary indicator variable (where r_{nk} is equal to one if a data point belongs to cluster k, otherwise zero).

In order to predict data points belonging to one of the three cluster groups the values of r_{nk} and c_k had to be found in order to minimise J. Initial values of c_k are randomly determined, then the two stage process of calculating r_{nk} and c_k were repeated until results converge.

1. Centroids of the clusters were initialised with random values.
2. Each data point was attributed to the closest cluster using (6.5).
3. The position of each cluster was re-evaluated so that it corresponds with the mean of all data points belonging to that cluster using (6.6).
4. Steps 2 and 3 were repeated until results converge.

$$r_{nk} = \begin{cases} 1 & \text{if } k = argmin_j ||y_n - c_j||^2 \\ 0 & \text{otherwise} \end{cases} \tag{6.5}$$

$$c_k = \frac{\Sigma_n \, r_{nk} \, y_n}{\Sigma_n \, r_{nk}} \tag{6.6}$$

As different initial cluster centroids can produce slightly differing results the algorithm was replicated five times with a new set of initial cluster centroid positions for more accurate results.

With each window now placed within one of three clusters it was still unknown what group (stationary, dynamic, or dynamic-altitude) each cluster belongs to. The average gyroscopic magnitude (4.1) and barometer gradient were determined from each window of data belonging to each of the three unknown clusters and the cluster average was used to determine which group they belong to. The stationary group was defined by detecting a gyroscopic magnitude below a threshold of 50°/s, the dynamic group determines if the same gyroscopic magnitude data exceeds the same threshold and the barometer gradient was below a threshold of 0.1 m.s, and finally the dynamic-altitude group was defined by exceeding both the gyroscopic magnitude threshold and barometer gradient threshold. See Fig. 6.1 - cluster group stage. If the subject did not perform any activities from one of the cluster groups, for example if they did not perform any of the stairs activities and thus no dynamic-altitude group was to be detected, then the other cluster groups may have multiple clusters belonging to them.

The threshold values used were determined by trial and error prior to this study and were found to sufficiently characterise activities for all subjects tested. These values were not

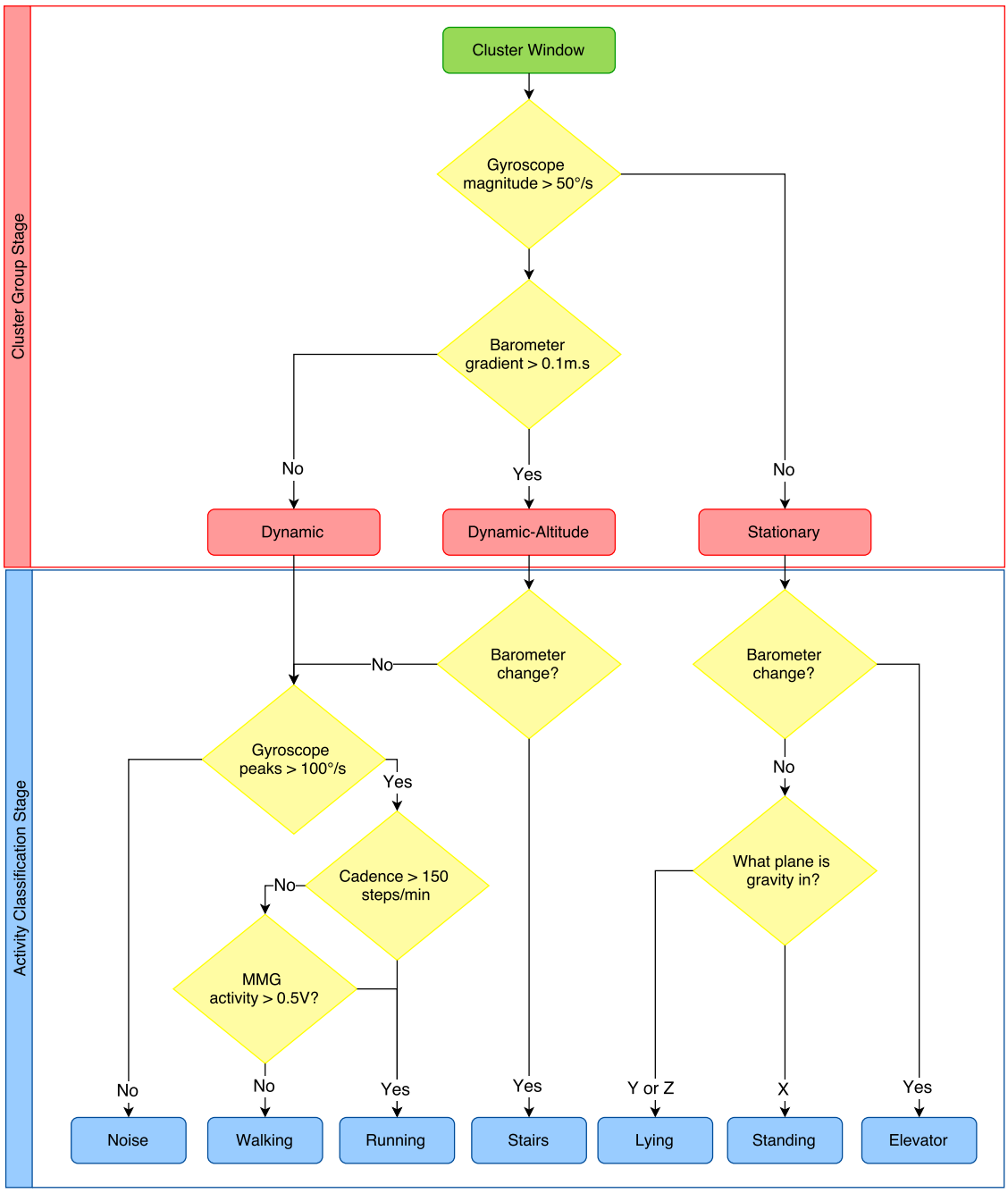


Figure 6.1: Flow chart showing the two part *a priori* process of characterising the windowed data into activities.

redetermined for each subject and therefore this algorithm still accomplishes an unsupervised methodology.

The second stage of the algorithm processes each window within a cluster group to classify the individual activities by using information from all sensors available and exploiting unique attributes from each of the nine activities. See Fig. 6.1 - activity classification stage. MMG data was denoised of vibration artefact as described in Chapter 4 Section 4.4 (see Fig. 4.6).

The elevator and stairs activities were further split into two each by determining the direction of barometer pressure change. An increase in pressure results in a decrease in altitude (going down in the lift/stairs) and a decrease in pressure results in an increase in altitude.

In order to determine the robustness of the algorithm each subject was asked to perform differing activities where some do not perform any tasks from the dynamic, stationary, or altitude based groups. Some subjects were asked to avoid tasks such as going up/down stairs, in order to remove any classification from the dynamic-altitude based group, whereas others were asked to only perform stationary tasks, to remove both dynamic and dynamic-altitude tasks.

An investigator accompanied each subject on their trials to record what activity they performed, and at what time, so that this data could be compared against the activity determined by the algorithm. Accuracy was determined by validating each window activity against its recorded actual activity. The subjects pressed a button each time they changed activities which was collected alongside inertial and MMG data. The button presses created known points of activity change, which were used to further assist in validation.

In order to validate the improvement through MMG inclusion in the algorithm, the data was processed twice. Once with the algorithm presented above, and another with the muscle data component removed. The accuracy of the algorithm with MMG was compared against that without MMG, in order to determine its importance in the classification of activities. Data processed with MMG and without MMG was passed through a paired t-test to determine significance.

6.2.3 Results

The activities each subject performed, their missing cluster group (if any), and their average accuracy over two trials is presented in Table 6.1. The overall algorithm accuracy, by taking the mean of accuracy across all subjects and trials, was found to be 98.4%.

The calculated t-test found no significant difference in subject data between the algorithms with and without MMG, except for subject five where the comparison was significantly different ($P < 0.05$).

Fig. 6.2 shows the raw gyroscope data of a trial from subject four who did not perform any ascending or descending stairs activities, and therefore no dynamic-altitude group was classified. The coloured backgrounds represent the specific activities the subject performed, which were standing (yellow), walking (blue), ascending within an elevator (dark red), and descending in an elevator (light red). The black dotted lines represent button presses to indicate a change of activity.

Table 6.1: Table showing tasks performed by each subject, any cluster group not performed, and the overall accuracy across two trials for both the algorithm with MMG data included, and without.

Subject	Activities	Missing Group	Accuracy w\o MMG (%)	Accuracy w\MMG (%)
1	S, W, SD, LU	None	99.2	99.2
2	S, W, SU, LD	None	96.3	96.3
3	S, W, SU, SD	None	97.5	97.5
4	S, W, LU, LD	Dynamic-Altitude	98.3	98.3
5	S, W, R	Dynamic-Altitude	89.2	99.3
6	S, L	Dynamic, Dynamic-Altitude	100.0	100.00
Average			96.8	98.4

S = standing, L = lying, W = walking, R = running, SD = stairs down,
SU = stairs up, LD = lift down, LU = lift up.

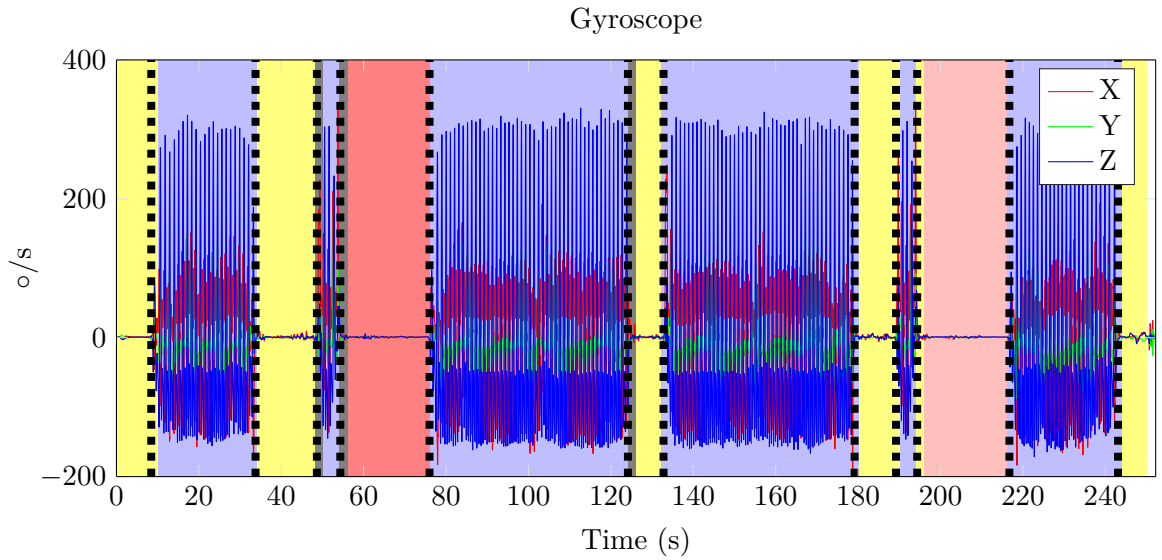


Figure 6.2: Raw gyroscope data showing the classification of numerous activities performed by subject four. Activities include standing (yellow), walking (blue), ascending in an elevator (dark red), and descending in an elevator (light red). A few incorrectly estimated windows can be seen, with three windows classified as noise (grey) throughout the trial. Black dotted lines represent button presses to indicate a change of activity.

6.2.4 Discussion and Conclusion

Through a semi-controlled process, this study suggests that a high accuracy in human activity classification can be obtain from future uncontrolled tests. Subjects who did not perform particular activities, which belonged to a certain group clusters, were also highly estimated to the correct activity when processed.

Subjects one to three performed activities from all three groups and thus each of the three clusters calculated by the K-means algorithm were assigned a unique group label each (stationary, dynamic, or dynamic-altitude). Errors from these three subjects were almost entirely due to incorrectly classification of a standing task as an elevator activity, during the transition from a standing to dynamic task (walking or running). It was believed this

was due to the sudden pressure change produced during the start of a dynamic task, which the algorithm processes as 'elevator' as it recognises both stationary and barometer change parameters in classification of those windows.

Subject four did not perform any stair based activities, and therefore the dynamic-altitude group was correctly not assigned to any of the clusters. Out of the three clusters, two were assigned to the dynamic group, due to the majority of the trial consisting of dynamic based activities, and the final cluster put in the stationary group. Errors seen during this subject's trials were windows being determined as noise, seen entirely at the start of a change of activity (see Fig. 6.2, grey backgrounds).

Subject five, also missing the dynamic-altitude group, performed standing, walking, and running activities, not performing any stair or elevator based activities. Errors seen during their trials were also the classification of windows as noise. This was believed to be because of the increase in artefacts produced from the running activities.

Subject six only performed stationary activities (standing and lying) and therefore no dynamic or dynamic-altitude groups were classified and all three clusters were assigned to the stationary group. No errors were seen in either trial of this subject. It was believed this was because of the reduction in artefacts from very limited movement.

The results between subject five's trials were significantly different ($P < 0.05$) in comparison of classification with and without MMG data components. All other subject comparisons were not significantly different. This was expected due to subject five being the only participant which performed a running task, of which the MMG data assisted in classifying (Fig. 6.1 - activity classification stage). During the start of a running task it took a number of strides before an accurate cadence could be calculated in order to classify the running activity. Without MMG the algorithm recognised multiple windows at the beginning and end of a running task, when the subject was speeding up and slowing down, as walking. The inclusion of MMG data allowed for an additional thresholding method which would recognise muscle activity high enough to be determined as running, before a running cadence value could be estimated. Although the average accuracy of subject five's trials was sufficiently high (89%) without MMG data, it was significantly lower than the calculation with MMG (99%).

It is worth noting that in regards to human activity, standing while stationary and standing within an elevator have no discernible different in physiological effort. However, in other applications, such as position tracking, understanding altitude change is useful. Furthermore, distinguishing between standing and sitting is not possible with this methodology, as the IMU mounted on the lower leg has no change in orientation based on the two activities. However, inclusion of a second IMU on the upper leg, as well as additional MMG sensors monitoring the quadriceps which are also used in ambulation, could monitor changes in these two tasks.

This method differs from that of other literature in that it is the first to combine both motion and muscle activity in an unsupervised classification algorithm. Although muscle activity was only used in the dynamic activities of this application, of which made up 50% of the total number of activities (excluding noise), it was still proven valuable in accuracy of walking and running tasks.

Bao and Ravi both produced similar high accuracy results in their classification algorithms, however, their supervised methods required additional known trials of each activity[81,82]. In applications where gait or muscle activity changes are expected over time, such as physiotherapy or gait retraining, these known trials will need to be redetermined before each session, making it infeasible for practical use. The outcome here suggests a suitably high accuracy at uncontrolled human activity classification, particularly in pervasive environments.

Further work intends to reduce the controlled aspects of the experiment presented here, as well as inclusion of more activities by analysing other motion and muscle attributes unique to other tasks. Furthermore, it is hypothesized that combining this application with the other studies presented in this report could monitor both short term changes, such as from an inactive to activate state during a day, and long term changes, such as muscular fatigue and differences in gait performance over weeks or months.

6.3 Progressive Changes in the Gastrocnemius

Differences in human gait have long been an area of interest in literature, most prominently the differences between typical and atypical movement, as well as progressive changes over time[222–224]. Atypical conditions that can affect gait are broad and can range from degenerative conditions such as Amyotrophic lateral sclerosis (ALS) and Parkinson's disease, to non-progressive conditions such as cerebral palsy (CP) or amputation. This study was interested in the latter, as through two separate conversations, one with a hemiplegic spastic cerebral palsy sufferer, and another with a single leg, below the knee (transtibial), amputee, both had mentioned how they recognised muscular and movement changes over the course of a day.

The CP subject mentioned a feeling of loosening of the muscle spasticity, specifically in the calf and thigh area, as the day progressed, and as he become more mobile. Through this loosening he noticed an improvement in gait and mobility, and a decrease in pain, typically before midday of a typical day. However, the amputee subject cited a decline in gait performance throughout the day, which he hypothesized as an overcompensation of his non-amputated leg for his amputated leg. As movement and activities are performed as the day progresses, the subject spoke of a dull, fatigue-like ache or tiredness in the calf muscles of the non-amputated leg.

Although not impossible, monitoring this type of progressive change over the course of a day is impractical for analysis within a gait laboratory, as subjects would either have to spend the entire day there, or come back at regular intervals. Marker and electrode placement for the laboratory based technology is very time consuming, so performing this multiple times a day would add to the complexity and would become a frustrating task. Furthermore, reproducibility of results by replacing the markers in the exact same place time after time would be troublesome. Of course, all of this is under the assumption that the subject would be happy spending their entire day at the laboratory, or returning multiple times throughout the day, which is undoubtedly not too desirable as their daily routine would be affected.

6.3.1 Research Question and Hypothesis

Three subjects from three gait groups have been monitored to detect a change over time in both muscle activity and gait; typical, hemiplegic cerebral palsy, and amputee. The typical subject was used as a control, as they reported no discomfort, change, or noticeable difference in their leg muscles or movement. Muscle signal amplitudes from an MMG sensor on the gastrocnemius calf muscle have been analysed and any change reported, while gait movement patterns have also be monitored for change using an IMU. This technology allowed for prolonged collection over a day, while staying concealable and unnoticeable so the subject can go about their normal daily routine.

It was hypothesized that MMG and inertial information could be used to detect differences in gastrocnemius activity over the course of a day between CP, amputee, and typical subjects. This research was approved by the Imperial College Research Ethics Committee (ICREC) and written consent was obtained from the subject involved.

6.3.2 Method

The same brace was used as in the previous activity monitoring study, with the IMU mounted on the lateral side of the right leg, and the MMG sensor situated on the lateral head of the gastrocnemius. The right leg was the amputees non-amputated leg, whereas the right leg of the cerebral palsy subject was his affected side, therefore each subject (including typical) wore the brace on their right leg. Fig. 6.3 shows the amputated subject wearing the brace.

Each subject was asked to begin collecting at the beginning of the day, pulling the sensor on and starting collection when they wake up, and to go about their usual activities and tasks, recording for approximately five hours a day. The brace required no special training other than some brief instructions on where the MMG sensor had to be placed over the gastrocnemius. As everything was sewn in place, the correct positioning of the MMG sensor meant that the IMU was also positioned correctly. Throughout this study the typical and amputee subjects were able to collect for two days, and the cerebral palsy subject collected for one.



Figure 6.3: Single leg amputee subject wearing brace containing IMU and MMG sensors on their non-amputated leg.

Data was processed separately for each day and the average change was determined across days. Data was saved to the device's SD card and all processing was performed offline. The same sampling rates and processing methods were used as presented in Section 6.2, where data was windowed, classified using a K-means algorithm, and then further analysed into one of nine tasks. The grouped data classified as 'walking' was used and analysed, while other grouped tasks remained unused for this study. Unlike the previous activity monitoring application, there was no push button attached to the brace to indicate a change of activity, as this was only used for validation of the classification technique.

Following from the K-mean classification of walking data, individual strides were identified using a thresholding method which looked for peaks in the gyroscope Z plane, which represented the swing phase of gait. As seen in Fig. 6.4, peaks which exceed a threshold of 250°/s, which was determined by trial and error prior to testing, and was applicable to all subjects tested, were used as starting points. Using an *a priori* understanding of human gait, by working backwards from the centre point the first dip was recognised as the pre-swing phase of gait (PSw), whereas working further backwards to the next dip was recognised as the initial contact phase of gait (IC). Working forward from the centre point the first dip was the initial contact (IC) of the next stride. The data between initial contact to initial contact represents one stride.

To determine change in motion over time, the gyroscopic magnitude (4.1) from each stride was determined and the amplitude (RMS) of that signal was calculated. Furthermore, the

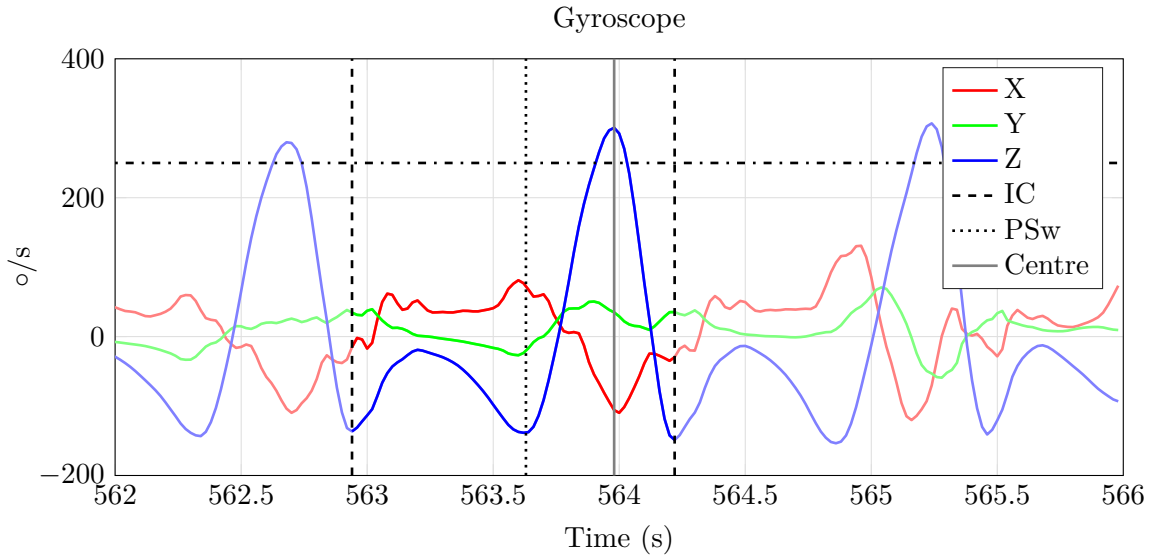


Figure 6.4: Figure displaying the process taken for individual stride segmentation from gyroscopic data of the lower leg. The black horizontal line shows the threshold in which gyroscope data from the Z plane (which represents gait swing) had to exceed. The grey vertical line represents a centre peak which exceeds this threshold. The first dip prior to the centre point was recognised as the pre-swing phase of gait (PSw), whereas the second dip was recognised as the initial contact phase of gait (IC). The first dip following the centre point was the initial contact (IC) of the next stride. Data between initial contact to initial contact represents one stride. This data was taken from the typical gait subject.

cadence of each stride was determined by taking the stride duration and calculating the step duration (6.7), and then estimating the steps per minute (6.8).

Muscle activity was denoised of vibration artefact as described in Section 4.4 (Fig. 4.6), and the RMS of the MMG signal was calculated from the flat foot stage of each stride (between IC and PSw in Fig. 6.4). As mentioned previously, the majority of muscular activity from the gastrocnemius is produced during plantar flexion of the ankle which occurs during the flat foot stage of gait.

$$Step\ Duration\ (s) = \frac{Stride\ Duration}{2} \tag{6.7}$$

$$Cadence\ (steps/min) = \frac{60}{Step\ Duration} \tag{6.8}$$

Linear regression analysis was performed on the gyroscope magnitude, cadence, and MMG RMS, against time. For each, the Pearson's correlation coefficient (r) was calculated, along with significance value (P), the linear slope gradient (b), and percentage change over time, from the start to finish of the total time sampled.

6.3.3 Results

The percentage change over time for MMG RMS, cadence, and gyroscope RMS, can be seen in Table 6.2, as well as subject information. A graphical representation of the average change for each data type for each subject can be seen in Fig. 6.5.

The typical subject saw a marginal decline of -7% in MMG RMS (r = -0.14, b = -0.1 mV.%, $P > 0.05$) with a very weak linear relationship, and an increase of 10% in cadence (r = 0.59, b = 0.22 steps/min.%, $P < 0.01$), and 19% in gyroscope RMS (r = 0.68, b = 0.61°/s.%, $P <$ 0.01) with strong linear relationships. Changes in MMG RMS were not significant, where both gyroscope RMS and cadence were.

The amputee subject saw a larger decline of -31% in MMG RMS (r = -0.55, b = -0.38 mV.%, $P < 0.01$) and a decrease of -9% in cadence (r = -0.57, b = -0.20 steps/min.%, $P < 0.01$), and -15% in gyroscope RMS (r = -0.56, b = -0.48°/s.%, $P < 0.01$), all with moderate linear relationships. Changes in MMG RMS, gyroscope RMS, and cadence were all significant.

The cerebral palsy subject saw increases of 122% in MMG RMS (r = 0.46, b = 1.15 mV.%, $P < 0.01$), 3% in cadence (r = 0.13, b = 0.06 steps/min.%, $P > 0.05$), and 8% in gyroscope RMS (r = 0.34, b = 0.18°/s.%, $P < 0.05$). MMG RMS, cadence, and gyroscope RMS had a moderate, very weak, and weak linear relationship, respectively. MMG RMS and gyroscope RMS changed significantly, whereas no significant change in cadence was seen.

6.3.4 Discussion

Collectively, a differing result was seen between all three subject groups, which are discussed in turn below.

Typical

Results show a significant increase of 10% in cadence over time, as well as a significant increase of 19% in gyroscope RMS. However, muscle change was insignificant ($P > 0.05$) with a decrease of -7%. Furthermore, MMG RMS had a very weak linear relationship, suggesting a large fluctuation over collection time and no real implication of change over time. Although both cadence and gyroscope parameters were expected to change in relation to each other, it was evident the significant increase in motion had no effect on muscle performance, with a small decrease seen in gradient. It was not believed that the increase in motion parameters was anything to do with a physiological change, and was understood to simply be a voluntary change in gait over the course of collection. The subject reported no discomfort, fatigue, or tiredness at the end of the trials, however, they were unaware of any voluntary changes in their gait over the trials either. Results seen here further suggest this technology could be used in activity monitoring

Table 6.2: Subject information and percentage change for muscle and motion parameters.

	Typical	Amputee	Cerebral Palsy
Age	26	25	33
Height (cm)	180	197	178
Average Cadence (steps/min)	108	102	107
MMG Change (%)	-7	-31	122
Cadence Change (%)	10	-9	3
Gyroscope RMS Change (%)	19	-15	8

applications, as well as presenting an expected lack of change in muscle activity, despite an increase in motion activity.

Amputee Motion changes showed a significant decrease in both cadence (-9%) and gyroscope RMS (-15%), which were very similar to that seen in the typical subject data, as well as similar gradients, albeit, a decline in performance as opposed to an increase. However, a much larger change was seen in muscle activity, with a significant decrease in amplitude of -31% and a moderate linear relationship. The subject reported a tiredness in their calf muscles following the trials, as they normally feel on active days. Gyroscope RMS and cadence also have significant moderate negative linear correlations, which implies a relationship between a decline in motion with a decline in muscle activity.

Cerebral Palsy Results seen in the CP group were much different than that of the typical and amputee groups. First, their muscle amplitude increases with a large gradient and significant change of 122% over time. Furthermore, cadence and gyroscope RMS results display a low gradient, poor linear correlation, and changes of a 3% and 8% increase, respectively. However, while cadence results were insignificant, gyroscope RMS were found to show a significant change. While the change in muscle was expected to increase, due to the subject's description of a loosening of the muscle over time and a decline in stiffness, the low linearity in both gyroscope RMS and cadence suggests a physiological change as opposed to a voluntary one, similar to that seen in the amputee results. Over the course of the trial the subject's gait strategy did not appear to change, nor did their speed as cadence results fluctuated. This would imply the muscle change was not due to a change in activity, but more in relation to the loosening of the muscle as the subject becomes more active throughout the day.

6.3.4.1 Comparison of Typical and Atypical Results

Cadences between all three groups were unexpectedly similar, with each within the normal cadence speed, estimated between 90-130 steps/minute[225,226]. The CP subject in particular was expected to have the lowest cadence, but with an average of 107 steps/minute these

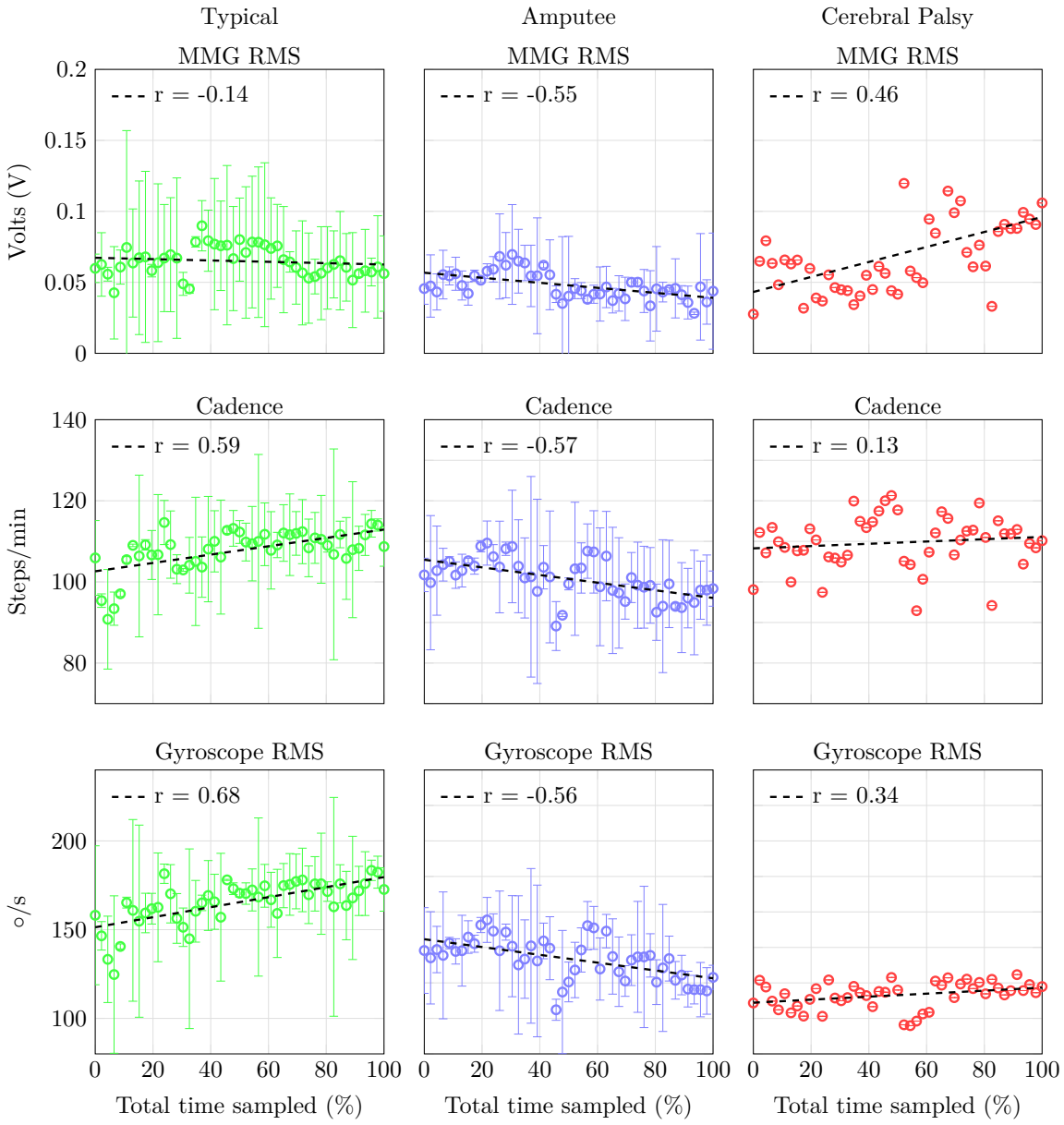


Figure 6.5: Results for progressive changes in the gastrocnemius between typical and atypical gait. Columns left to right show results from typical (green), amputee (blue), and cerebral palsy (red) subjects. Rows top to bottom show the MMG RMS, cadence, and gyroscope RMS, respectively. Each plot has linear regression line plotted as well as their corresponding Pearson's correlation coefficient values. CP results do not have standard deviation error bars due to only one trial being collected for that subject.

results suggest a typical speed. However, the CP subject showed no significant cadence change over the course of the trial, whereas the typical and amputee subjects did. Through discussion with the CP subject, it was learnt that they have recognised a much faster performance indoors, by using walls, doors, and other structures as support. As the vast majority of the collection was within the subject's home and office while they worked, this is expected to influence the faster than expected cadence. The low linear correlation ($r = 0.13$) and a fluctuation of cadence speed throughout the trial suggestion little change in gait

performance throughout the collection period.

Furthermore, although cadence in children with CP is reported as slower than typical children of the same age, these results are less apparent in adolescence years[227, 228]. The CP subject involved in this study had also reported to have participated in strength training and physiotherapy, which have also shown to improve gait[229]. However, it is worth noting that there is little uniformity across those with cerebral palsy, due to difference in type (hemiplegia, diplegia, dyskinesia), severity, and age, and therefore differing gait results are seen from person to person[230].

The amputee subject had a more expected cadence. Despite a much greater height than the other two subject, which normally corresponds with a higher cadence, they had mentioned that their prosthesis limits their speed. The typical subject was, expectedly, also in the normal range with an average cadence of 108 steps/min.

Although cadence remained consistent between groups, the gyroscope RMS results showed higher results in the typical group (average 166°/s) as opposed to amputee (average 133°/s) and cerebral palsy (average 113°/s) results. The decline in power from typical to amputee to cerebral palsy results is believe to be due to the amputees compensation of their prosthesis, and the CP hemiplegic spasticity, both of which limits their gait respectively.

MMG results were more sporadic in the CP results when compared to the other two groups, although still showed a high gradient change over time as well as a moderate linear correlation. The much higher percentage of change seen in the CP MMG results suggests their observation of muscle loosening over the course of a day occurs much faster and was much more prominent than the amputee's muscle tiring due to overcompensation. Large standard deviations and a poor linear correlation in the typical subject's MMG data implies no change in muscular activity.

6.3.5 Conclusion

The results seen here demonstrate that the technology presented can be used to monitor muscular and motion changes over time, pervasively, and for a prolonged period of time. Future work would apply the same application to a larger subject pool, longer collection times, as well as more specific filtering and analysis methods for atypical gait. However, each subject had a unique gait strategy, regardless of condition, and therefore this application would not produce suitable results for understanding conditions in a global sense, and is more suited towards gait and physiological changes in individuals. This work has demonstrated that this technology used could be suitable for applications where analysis within a gait laboratory is not feasible.

6.4 Asymmetric Differences in the Rectus Femoris

Continuing from the previous study of unilateral monitoring, it was recognised that a bilateral experiment, one where human motion and muscle activity is analysed from both sides of an individual, could show differences in one-sided conditions, such as hemiplegia or single-leg amputation.

This study has identified differences, and to what degree, unilateral lower limb conditions have on a bilateral scale for individuals. Monitoring motion, as well as muscle contraction information, from both legs of an individual can provide an understanding on how one side of the body is under performing when compared with the other. With this information, corrective measures could be applied in order to regain functionality of affected limbs, or to know at what point rehabilitation has been successful, when data on a bilateral scale match.

Using IMU's and MMG technology, the subjects collected data while performing their regular day-to-day activities in a pervasive environment. As with before, the analysis of information was achieved through extraction of user strides when walking. Those without unilateral conditions were expected to have a high level of synchronicity between both legs when walking, meaning an efficient gait. However, it was hypothesized that those with conditions such as amputation would have noticeable differences in both motion and muscle parameters.

Unlike the previous study, this application did not monitor change over time, as differences in those with unilateral conditions are apparent from the onset. This work was more focused towards quantity of strides, which will improve accuracy when determining an average step for each leg. As with previous applications it is evident that performing this study within a gait laboratory is again impractical, as the collection of hundreds of strides will take a long time, requiring the subject to walk up and down the laboratory collection space multiple times. Furthermore, continuous walking within a laboratory would likely result in perspiration, which has been found to degrade EMG results[231].

6.4.1 Research Question and Hypothesis

This application looked at two groups of differing performance; typical and amputation. Two subjects, one from each group, wore this technology for a prolonged time over two days in order to collect sufficient gait information for analysis. For consistency, the same subjects from the typical and amputee groups in the last study were again recruited for this work. The typical subject was used as the control group, with no prior gait abnormalities or noticeable difference in bilateral performance. The amputee subject, who had a unilateral transtibial amputation of the left leg, had recognised an asymmetric difference in his gait, having to noticeably compensate for their prosthesis when walking. Furthermore, the amputee subject

had described a difference in leg length due to a misfitting prosthesis socket, which they also believe to be responsible for an unbalanced gait. Due to the lack of gastrocnemius muscle with the amputee subject's left leg, this application opted for collection from the rectus femoris quadriceps muscle, with motion collection from the upper segment of the leg.

It was hypothesized that symmetrical differences would be apparent between typical and amputee subjects. This research was approved by the Imperial College Research Ethics Committee (ICREC) and written consent was obtained from the subject involved.

6.4.2 Method

Sensor attachment differs in this application. Due to the lack of a gastrocnemius muscle of the amputees left leg, comparison of bilateral muscle function was not possible using the previous sensor attachment method. Using elastic straps (Fig. 6.6) which wrap around the thigh, the MMG and IMU sensors were sewn into a band, with the MMG positioned atop of the rectus femoris, found as the point 50% between the anterior spina iliaca superior and the patella[173].

Despite sufficient tightness to the leg, the straps were found to move and drop down the leg when the wearer was in motion, therefore the straps were grouped with a pair of exercise shorts and were Velcroed in place (Fig. 6.7). The shorts have a square hole cut over the quadriceps of each leg to allow the MMG sensor to have skin contact. Velcro strips were attached to the shorts on either side of the hole, and the straps had corresponding Velcro strips on either side of the MMG sensor. The shorts and strap combination allowed for comfortable attachment which did not hinder performance, while restricting the movement of the straps when the user was in motion. Furthermore, the sensors did not protrude from the body significantly (16 mm at its highest point) and were therefore concealable underneath regular attire, without hindering performance.

The force gauge developed, as presented in Chapter 3, Section 3.5, was used in this study as a precise contact pressure was required so as not to create a bias between legs. The user was asked to use the force gauge prior to each use, and loosen/tighten the strap so that each MMG sensor had a contact pressure of 100 g. 100 g was chosen as the level as force as it adhered to the skin well, was comfortable while not too tight, and was sufficiently lower than the recommended maximum applying force of 200 g[104].

Each subject was asked to start collection at the beginning of their day, by first donning the shorts, then attaching the straps with specific placement of the MMG over the rectus femoris. Great importance was taken when positioning the straps, as any deviations of the MMG sensor away from the line between the anterior spina iliaca superior and the patella would result in an offset of the IMU 3D planes with the opposing leg, as well an increase in potential cross talk in MMG signals from neighbouring muscles. Following attachment of the straps the contact pressure of the MMG sensors was determined using the force gauge

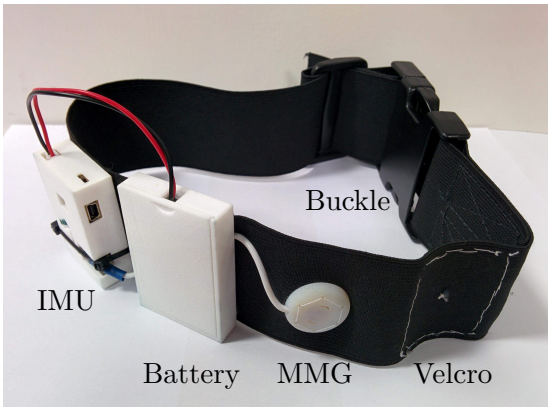


Figure 6.6: Strap used for sensor attachment. The IMU and battery were contained in 3D printed cases and were sewn to the strap. A small hole was cut into the strap and the MMG fitted in the usual way (also sewn in place). The Velcro strip, which was sewn to the opposing side of the strap, was used for attachment to the shorts, which kept the strap from slipping when worn. Another Velcro strip was attached on the other side of the MMG sensor, behind the battery case (not seen). Strap tightness can be adjusted and clipped in place using a standard flexural buckle.

provided. At this point, additional clothing can be worn over the sensors and the user can begin collection before going about their daily routine.

Both the typical and amputee subjects collected data for two hours a day, over two days. To avoid monitoring a change in performance over time, as analysed in the previous study (Section 6.3), the subjects were limited to two hours a day. Further analysis is require to determine both the symmetric differences in gait while monitoring contractional change over time, which is beyond the scope of this application.

6.4.2.1 Signal Processing

Data was collected and processed in the same way as previous studies in this chapter, with offline collection (data stored on an SD media card) and the processing method and data sampling rates presented in Section 6.2. The data was windowed, classified using a K-means algorithm, and then further analysed into one of nine tasks. Despite the algorithm being designed for lower leg analysis, it was capable of characterising activities from upper leg data due to the universal parameters used in classification; mean, standard deviation, power, and covariance of the accelerometer signal. As inertial activity, barometric pressure, and stationary periods were the same, regardless of upper or lower leg attachment, the algorithm was able to classify with no alteration to the design. The grouped data classified as 'walking' was used and analysed, while other grouped activities remained unused for this study.

After K-means classification of the data, and extraction of the walking data windows, the individual strides were determined in the same way to that of the calf analysis study (Section 6.3). Despite a difference in signal response, the gait shape is very similar regardless of upper or lower leg collection. Where lower leg gyroscope results display both a flat foot stage and a swing stage (Fig. 6.4), upper leg gyroscope results were more sinusoidal, although similarities were seen in identification of gait phases (Fig. 6.8). As before, the gyroscope Z plane corresponds to the direction of the gait swing, and was therefore used for analysis of strides. The threshold value which peaks must exceed was found to be lower than that used in the calf study, however, still high enough to reject peaks represented in motion noise. As before, the threshold was determined by trial and error prior to testing, and was applicable



Figure 6.7: Typical subject wearing sensor ensemble consisting of straps containing the MMG sensors, positioned atop the rectus femoris, and IMU's situated on the lateral side of the leg. Shorts were used to keep the straps in place through movement with Velcro attachment and holes removed for direct skin contact of the MMG sensors. Left: Shorts and straps attached for collection. Centre: Right strap removed to show hole in the shorts used for direct skin contact. Right: Photo overlay of the subject wearing the shorts/straps underneath regular attire. Sensors were slim and do not protrude much from the body, resulting in a concealable system.

to all subjects tested. These centre peaks were used as starting points, and by working forwards and backwards from that point the initial contact points of the start and end of the stride were found.

This application was looking at muscle activity in a difference phase of gait to the calf analysis study. While the gastrocnemius is contracting during plantar flexion of the ankle, which is produced during the flat foot stage of gait, the rectus femoris is involved in extension of the knee and contracts for a much shorter period, seen during the pre-swing phase of gait until early initial swing (ISw) (see Fig. 4.7)[232].

The stride extraction method was applied to data from both legs. The total number of steps per leg were averaged against each other in order to produce a 'template' step which represented movement of that leg. Motion data was analysed by comparing the RMSE of the gyroscope data, in each of the three planes (X, Y, Z), of each leg 'template'. Small percentage differences in each plane indicate a strong agreement in bilateral similarity. The RMSE calculation (4.2) used here can be seen in Chapter 4 where it was used in the validation of the IMU against optical tracking. Individual RMS values were also calculated from each

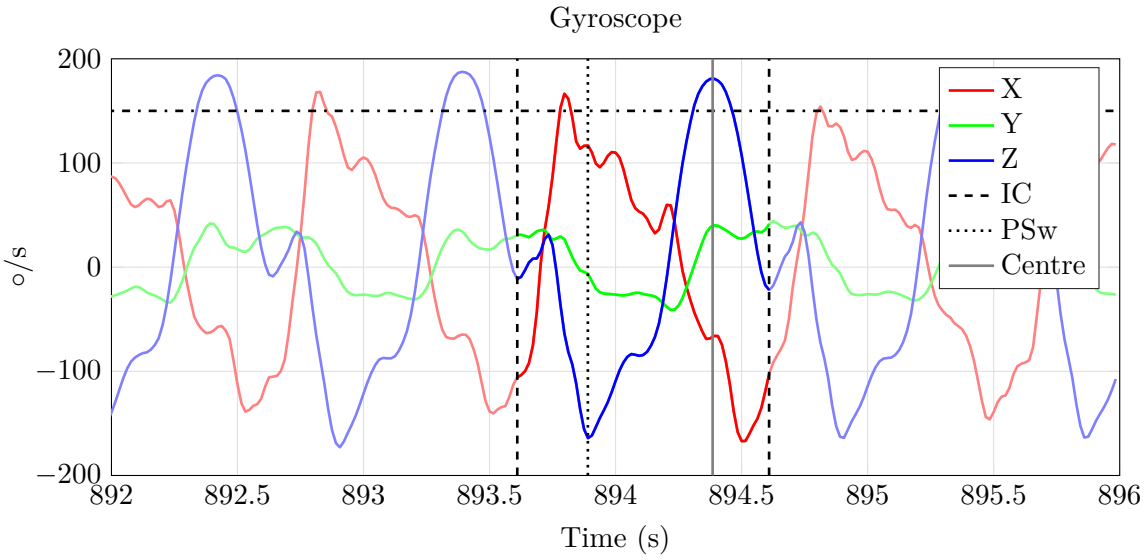


Figure 6.8: Figure displaying the process taken for individual stride segmentation from gyroscopic data of the upper leg. The black horizontal line shows the threshold in which gyroscope data from the Z plane (which represents gait swing) had to exceed. The grey vertical line represents a centre peak which exceeds this threshold. Working backwards from the centre point the first dip was recognised as the pre-swing phase of gait (PSw), whereas working further backwards to the next dip was recognised as the initial contact phase of gait (IC). Working forward from the centre point the first dip was the initial contact (IC) of the next stride. The data between initial contact to initial contact represents one stride. This data was taken from the typical gait subject.

gyroscope plane, to determine difference in amplitude between limbs.

Muscle activity was processed in the same way, with an RMSE calculated for each limb and compared against each other. Individual RMS values per limb were also determined and presented.

Differences in RMSE and RMS in all data between legs was presented as a percentage difference, for ease of analysis. Differences were further analysed with a paired t-test, which was used to determine significance between legs in both gyroscope RMS and MMG RMS data, for both typical and amputee subjects. Furthermore, a t-test was applied to motion and MMG RMS results between subjects, to determine a significant difference between typical and atypical gait.

6.4.3 Results and Discussion

Gyroscope RMSE and MMG amplitude are plotted in Fig. 6.9. Left column represented the typical subject's results, whereas the right displays the amputee's data. The leg rotations (X; red), abduction/adduction (Y; green), flexion/extension (leg swing, Z; blue), and MMG (black) are shown top to bottom, respectively. Each graph compares the right (dot-dashed) and left (solid) leg.

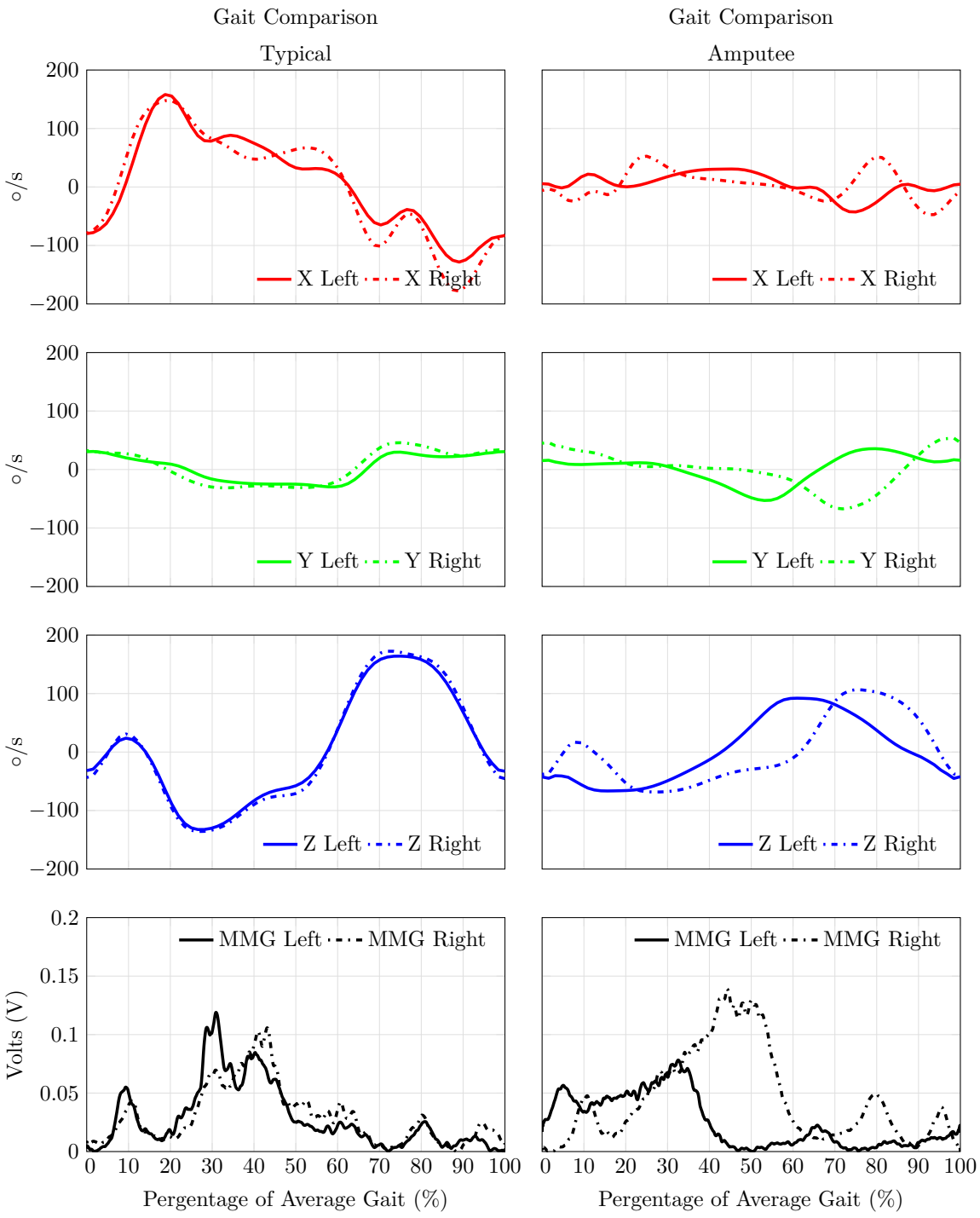


Figure 6.9: Gyroscope and MMG results for both left (solid) and right (dot-dashed) legs. Leg rotation (Gyroscope X; red), abduction/adduction (Gyroscope Y; green), and flexion/extension (Gyroscope Z; blue), as well as muscle activity (MMG RMS; black) can be seen top to bottom, respectively. The left shows typical subject results whereas the right presents the amputee subject results.

Table 6.3 shows results of RMSE errors (%) between each leg, and the equivalent RMS amplitude differences (%), for each of the three gyroscope planes, and the MMG.

The paired *t*-test reported no significant difference between left and right leg for gyroscope

RMS, nor MMG RMS, for both typical and amputee subjects individually. However, a significant difference was seen ($P < 0.05$) in motion rotation (X) and flexion extension (Z) between subjects (Table 6.4). Abduction/adduction (Y), and MMG, were not significantly different between typical and atypical gait.

6.4.3.1 Typical Analysis of Results

RMSE results (Table 6.3) for the typical subject show a close 'overlap' of data for each gyroscope plane, and MMG data. A low RMSE represents a close match between each leg, signifying a good symmetry in gait. Motion results for the typical subject show a RMSE percentage difference of only 3% for the Z plane, which represents flexion/extension motion, or the swing information, of the gait and therefore contains the highest amount of motion. Similarly with the validation chapter of this research, the plane with the most motion contains the highest accuracy of agreement. This was further confirmed by the 17% RMSE seen in the Y plane, which contains the abduction/adduction data, and had the least amount of motion. The X plane, which contains rotational information of the limb, had an average error of 9% RMSE. A very close comparison can be seen in Fig. 6.9 for the typical subject motion results between legs, as well as the MMG response which shows contraction around the pre-swing phase of gait (~30% of the average gait cycle), as expected.

While RMSE results show how well the left and right leg information 'fits' on top of each other, the RMS represents the mean magnitude of each gyroscope plane and MMG results. The typical subject produced RMS differences of 14%, 23%, and 6% for the leg rotations (X plane), abduction/adduction (Y plane), and flexion/extension (Z plane), respectively. RMS differences between MMG, however, were very close, with a 2% difference between legs. Further confirming symmetry in gait.

As expected, no significant difference was seen between limbs from the *t*-test results, in any of the motion planes or muscle data.

6.4.3.2 Atypical Analysis of Results

The amputee data, however, shows a clear time delay seen most prominently in the Y and Z planes (abduction/adduction and flexion/extension) in Fig. 6.9. Other literature studying gait asymmetry using gyroscopes found that differing weight on a single leg of typical subjects produced significant time delays[233]. It was hypothesized that the different weight in legs, prosthetic verses non-amputated, was responsible for the time delay seen here. The smaller peak seen between 0 and 20% in the right leg Z plane was not seen for the left leg. This peak was produced during the plantar flexion of the ankle at the flat foot stage of gait and it was believed it was missing on the left leg due to the passive ankle prosthesis damping the response.

Table 6.3: Subject results for motion and muscle differences between right and left leg. RMSE results represent how well right and left leg information overlay with each other, whereas the RMS represents the mean magnitude of the stride.

	Typical		Amputee	
	RMSE (%)	RMS (%)	RMSE (%)	RMS (%)
Rotation (X)	9	14	42	27
Abduction/Adduction (Y)	17	23	46	28
Flexion/Extension (Z)	3	6	35	3
MMG	11	2	64	57

Percentage represents positive difference right leg had against left leg.

The abduction/adduction (Y plane) data was similar between legs, despite the time delay seen. However, the prominent peak seen around 55% of the average gait for the left leg, and 70% for the right leg, correlate strongly with the swing peak seen in the Z plane for each leg, indicating the abduction of the leg was in response to the swing.

Leg rotations (X plane) were not similar between legs, unlike the other two planes. The right leg had shown a greater gyroscopic response when compared to the left leg, indicating more leg rotational activity in the non-amputated leg during gait. However, when comparing rotations of both legs from the amputee against the typical subject's results a clear difference in gait strategies was seen across subject groups.

This time delay was further reflected in the MMG results. It was seen that both right and left leg MMG amplitudes were most prominent at the pre-swing phase of gait, much like that seen in the typical subject data, however, these peaks also display a time delay and correspond with the point of pre-swing in the respective left and right leg extension (Z plane). The MMG RMS difference between legs showed 57% more activity in the right leg when compared to the left (Table 6.3). This difference was believed to be due to overcompensation of the amputated limb, as previously hypothesized in the previous study.

RMSE results for motion were expectedly high because of the time difference in legs (Table 6.3), however, RMS results were much lower in comparison, and were equally as comparable with the typical subject RMS results. This suggested that although a difference was seen in the time domain, both legs were producing a similar force to each other.

Despite the differences seen in both RMSE and RMS in the motion and muscle data, no significant difference was seen between limbs. This suggests that although a time delay and differences have been recognised, they do not indicate a significant asymmetry in gait.

6.4.3.3 Comparison of Typical and Atypical Results

Results presented here indicate a strong symmetry across both legs for the typical subject, whereas more visible differences were seen in the amputee data. Abduction/adduction (Y plane) showed a close similarity across typical and amputee data, whereas the left and right

Table 6.4: *t*-test results of gyroscope and MMG comparison between typical and atypical subjects for each gyroscope plane, and MMG results. Significant values ($P < 0.05$) have a yellow background, non-significant values have red backgrounds. Gyroscope X and Y planes show a significant difference between subjects (both left and right legs), whereas gyroscope Z plane and MMG do not.

	Gyro X	Gyro Y	Gyro Z	MMG
Left	P<0.05	P>0.05	P<0.05	P>0.05
Right	P<0.05	P>0.05	P<0.05	P>0.05

leg swing information (Z plane) for the typical subject only somewhat resembled the results seen in the amputees right leg information of the same plane. Despite a similar shape, the amputee right leg Z plane data was more damped and does not produce the same range of gyroscopic information as the typical subject data. Although their non-amputated leg, the right leg of the amputee data was believed to be compensating for their amputated leg, and was therefore hindered, despite being their unaffected limb. MMG amplitudes, although different between left and right leg in the amputee results, were quite similar between subjects.

A significant difference between subjects was seen in the gyroscope X and Z plane, which represent the leg rotations and flexion/extension of gait (Table 6.4). Abduction/adduction (Y plane) and MMG RMS between subjects were not found to be significant, and therefore show similarities between subject groups.

6.4.4 Conclusion

A difference was seen between limbs for the amputee subject, however, it was not been found to be significant in asymmetry. Expectedly, the typical subject results were also not significant in difference, and showed a much smaller difference in RMSE and RMS results across motion and muscle data. Right and left leg results showed very similar patterns in the typical subject gyroscope data, with a higher error seen in the planes with lower motion, as previously seen in validation of this technology. The amputee results, however, also showed a similar pattern for both the Y and Z plane results, despite a time delay difference. The rotational information seen in the X plane differed between legs, and was believed to be a result of a reduction in gait performance due to the prosthesis. Visually, the amputee subject recruited in this study had a natural gait, and a lack of significant difference between limbs is not surprising. Significant differences have been observed between subjects in leg rotational information and flexion/extension of gait. This suggests that although significant differences have not been seen on a bilateral level in atypical unilateral conditions, such as amputation, there were significant differences when compared against typical gait.

Future work intends to combine the studies of monitoring motion and muscle changes over time (Section 6.3) with the monitoring of bilateral differences in limbs presented in this study. Furthermore, recruitment of atypical subjects with more visible asymmetry is expected to show a significant difference between limbs during gait.

6.5 Chapter Summary

This chapter has shown it is possible to classify human activity into a total of nine activities, to a high accuracy of 98%, using a novel, unsupervised, K-means algorithm. Furthermore, the monitoring of progressive changes over time in subjects with abnormal gait, as well as the detection of bilateral gait differences in subjects with unilateral conditions, has also been achieved.

Performing these applications with the current standard of human motion and muscle monitoring is infeasible, as a finite collection space and duration times associated with optical tracking and EMG technologies hinder the ability to monitor conditions over prolonged periods of time. Furthermore, monitoring in an external environment allows for natural activity, which may be hidden in laboratory settings where activity is controlled.

This work has shown suitable results in monitoring motion and muscle activity in pervasive settings, with methods proposed to suppress the artefacts and noises associated with uncontrolled studies.

7

Human Machine Interfaces

Contents

7.1 Introduction 124

7.2 Prosthesis Control and Gesture Switching 124

7.3 Chapter Summary 137

7.1 Introduction

Humans interact with technology and machines daily, including computers, mobile phones, and household appliances. However, able-bodied people will often find the process of using these devices easy or second nature, whereas those with disabilities, such as upper limb amputation, may struggle with tasks that others find rudimentary.

Previous chapters have looked at offline data collection in order to better understand human performance, muscle physiology, or motion characteristics. This chapter demonstrates the real-time capabilities of the Aktiv IMU and MMG sensor pair by displaying and processing data as it happens.

A novel interface between humans and prosthesis is presented here, using the technology developed as control mechanisms. Human motion and muscle activity was fused in order to enable more easily accessible gesture switching in those with upper limb amputation.

7.2 Prosthesis Control and Gesture Switching

Prosthesis control using both EMG and MMG has been well documented in literature, with many reporting benefits of MMG over EMG including non-specific placement, no need for direct skin contact, unaffected by changes in skin impedance (such as perspiration), and requires less amplification[128,136].

Myoelectric prostheses, or 'muscle activated', introduce a significant amount of functionality over non-controllable aesthetic prostheses, and cable operated limbs. Despite 'myoelectric' coming from the words 'myo', meaning muscle, and 'electric' which suggests EMG control, the term is often associated with MMG control as well. Commercial myoelectric prostheses are largely controlled by dry electrode EMG due to their ease of application, but suffer greatly from skin impedance issues, more so than that of wet electrode EMG counterparts. Current myoelectric hands open and close grasps using the muscle based input. However, in order to change gesture, for example from a pointing action to a gripping action, a user input is required such as opposing the thumb or pressing a button on the back of the palm (BeBionic) or through a mobile phone application (i-limb). Although these prostheses usually have a great number of gestures available, for many different activities or needs, it was recognised that the additional user input required is not always practical. For example, in the case of a single arm amputee the process of pressing a button on the back of the palm, moving the orientation of the thumb, or using a mobile phone to change the gesture, is only possible if the non-amputated hand is free and available. In a situation where the non-amputated hand is currently holding an item, or in the situation where the subject has both arms amputated, the process of changing grip becomes much more difficult.

7.2.1 Research Question and Hypothesis

This application introduces a new inertial based method of gesture switching using information from an IMU. The IMU, which was situated on the subjects forearm, recognises different arm orientations and allows a change of gesture when a contraction signal was detected from muscle monitoring sensors. Furthermore, this application will compare the grip control using MMG against wet electrode EMG, including time taken to don and doff the system used. Despite dry electrode EMG being used in the majority of prosthesis applications, which would produce a much faster donning and doffing time, the signal quality from dry electrode is less than that from wet electrode EMG, due to greater skin impedance which must be kept to an absolute minimum for best results.

It was hypothesized that MMG could be used to control a prosthetic hand, while data from the IMU could be used as an automated method to change grip. Five able-bodied subjects were recruited to perform a pick and place task using a BeBionic V2 prosthetic hand which required a number of gesture switches to perform the activity. This research was approved by the Imperial College Research Ethics Committee (ICREC) and written consent was obtained from the subject involved.

7.2.2 Method

Each subject was asked to sit at the test station where they were instructed to moved and interact with a number of objects presented in front of them using the BeBionic V2 prosthetic hand. The test environment was based on that presented by Mace *et al* where they performed a similar study testing the validity of a tongue controlled interface with the same prosthetic hand[234]. This environment consists of three equal sized spaces on a desk (15x25 cm) with a bottle, tray, and tape roll, situated in each space, left to right respectively (Fig. 7.1).

Grasp control (opening and closing the grip) was achieved by monitoring the extensor carpi radialis longus (ECRL) muscle on the subjects left arm and an open/close operation was achieved by the subject extending their wrist. As only a single sensor (per EMG/MMG) was used, the extension of the wrist performed both the open and close command, whereas in practice a sensor would be used on the extensor and flexor muscles for open and close respectively. For this study, in a situation where the grip is currently open the wrist would have to be extended and returned to 0° to close the hand, likewise, the same activity of extension/return to 0° would be required to open the hand once more.

Prior to testing, the ECRL was located and the centre of the bulk of the muscle was marked as the location of the MMG sensor. 2.5 cm either side of the MMG point, following the length of the muscle, were also marked as the locations of the two EMG electrodes (Fig. 7.2). A reference electrode for the EMG was placed on the ulnar head of the left wrist. The

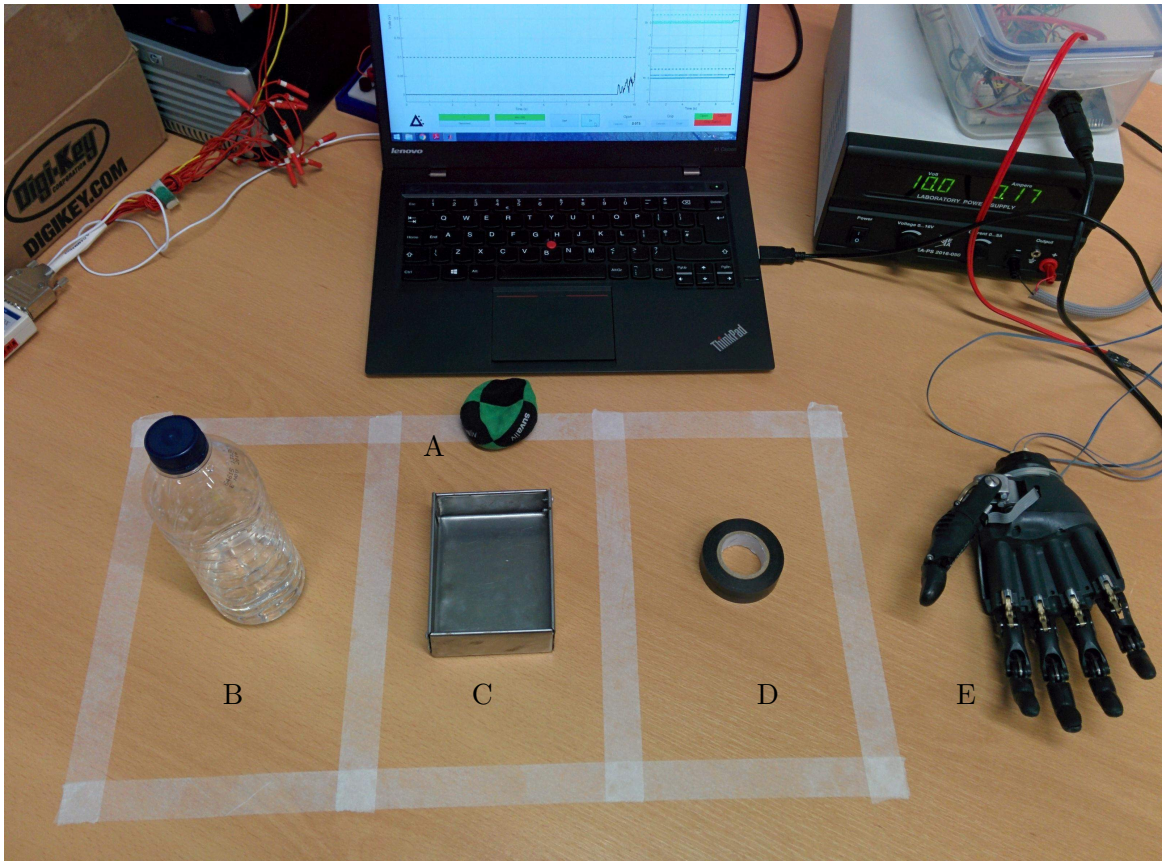


Figure 7.1: Photograph of the test environment. A: start and stop node requiring a finger point gesture; B: bottle requiring power grip gesture; C: Metal tray requiring key grip gesture; D: Tape roll requiring tripod grip gesture; E: BeBionic V2 prosthetic hand.

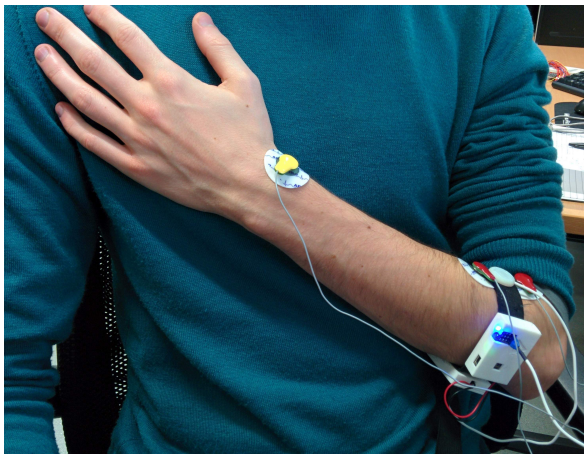


Figure 7.2: Sensor attachment and configuration. Reference electrode located on the ulnar head of the wrist for EMG (yellow) in relation to two EMG electrodes located on the extensor carpi radialis longus muscle near the elbow (red). The MMG sensor (white) was situation between the two EMG electrodes with the IMU (white box) situated on top of the arm attached to a band. Image shows the subject with their arm in the correct orientation, prior to wrist flexion which would change gesture.

subjects were timed for both donning (EMG or MMG, depending on task) and the test itself.

The BeBionic hand allows up to eight gestures to be used at any one time, however, for this study a total of four gestures have been used, to reduce complexity and improve usability. There were two user input methods in order to change gestures with the BeBionic prosthesis; abduction/adduction of the thumb, which were performed manually through physical movement of the thumb, and the toggling of a button situated on the back of the

palm, which the user must press. For this study a hardware alteration was made to the hand where the button on the back of the palm had been replaced with a wired interface to a computer, where information processed from the IMU was sent to the hand to change gesture in lieu of a button press.

The four grips used in this study are listed below, and both their open and closed states can be seen in Fig. 7.3.

Finger Point Fist closed with index finger pointing straight. Used for pointing and tapping. Thumb is adducted.

Power Grip A closed fist. Used for gripping objects. Thumb is abducted.

Tripod Grip Index and middle finger pinch at the thumb. Used for picking up small items. Thumb is abducted.

Key Grip All fingers partially closed and thumb rests on the index finger. Used for holding flat objects, such as a key. Thumb is adducted.

Some grips are only available based on the orientation of the thumb. For example, the power grip and tripod grip are only accessible when the thumb is abducted, whereas the finger point and key grip switches are only available when the thumb is adducted. On a commercial BeBionic hand the switching between the two grips per thumb orientation is achieved by pressing the button on the back of the palm, but in this study the switch was achieved using a novel IMU positioning technique. Accelerations in each of the three planes (X, Y, and Z) of the accelerometer on-board the IMU were used to recognise a specific orientation, which in this study was when the arm was placed across the chest (Fig. 7.2), and the ECRL muscle was contracted through flexion of the wrist in the same way the open/close command was achieved. The process of opening and closing the grip, as well as gesture switching, can be seen in Fig. 7.4. The method of arm placement to change gesture will be referred to as arm-across-chest (AAC) from here onwards.

Fig. 7.5 shows a flow diagram of the user input required to change between the four grips in this study. Once the hand was powered it starts in 'IMU Mode 1' which, depending on the starting orientation of the thumb (abducted/adducted), produced either a power grip or finger point gesture when a contraction signal was sent to the hand to open/close the grip. Toggling between the 'IMU Modes' was achieved through AAC, which accesses the other two grips available for this study. For example, with the thumb abducted the hand would start in the power grip gesture. Movement of the thumb into adduction would switch to the finger point gesture. Using the AAC method to switch IMU modes, and the thumb still adducted, the hand would enter key grip mode. Finally, movement of the thumb back to abduction would switch to the tripod grip.

Due to restrictions of the hand, the physical thumb movement was necessary to get the gestures of interest, including power/tripod and finger/key grips. Although this study was targeted at complete removal of physical user interaction with the hand, the application presented here can be applied to other prostheses with automated thumbs, or for just the



Figure 7.3: Figure showing the grips used in this study, as well as their open and closed states. Attention should be directed towards the finger point and key grip open gestures, where the thumb is adducted, and the power grip and tripod grip, where the thumb is abducted.

gestures available for either the abducted/adducted thumb. For this work the necessary thumb movements were performed by an investigator, who stood by the subject during testing. This resulted in no physical interaction with the hand from the subject.

The EMG system used was a g.tec g.BSamp biological amplifier with a g.tec g.GAMMAbox electrode driver. The amplified EMG signal had a maximum output of 10 V, therefore its voltage was dropped using a passive voltage divider so that it would not damage the IMU (maximum voltage input of 3.3 V), and was then sampled at 1 kHz using channel one of the IMU's auxiliary port. Likewise, the MMG sensor was attached to channel two of the IMU's auxiliary port and was also sampled at 1 kHz. MMG was not amplified. The IMU itself was sampled at 50 Hz and collected gyroscope, accelerometer, and magnetometer data. EMG, MMG, and IMU data was transmitted to a laptop via Bluetooth where the data was processed in MATLAB. MMG data was filtered between 10-100 Hz using a 1^{st} order Butterworth filter and then rectified, whereas EMG was filtered between 10-500 Hz using the same Butterworth filter and also rectified. IMU data was smoothed using a moving average but not filtered. Open/close and gesture switch signals were passed via a serial connection

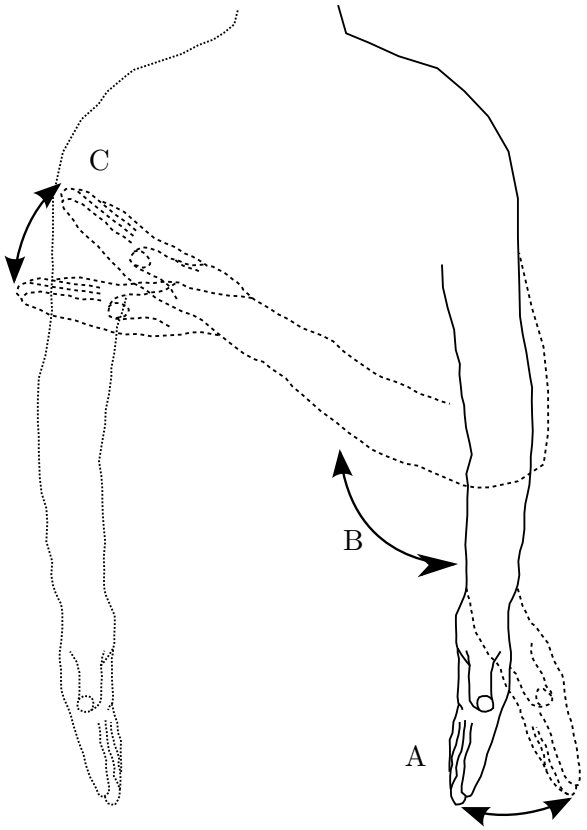


Figure 7.4: Figure showing the three stages of prosthesis grip control; A: Extension of the wrist open/closes the hand grip. The extension of the wrist opens/closes the hand grip, while the flexion back to 0° is ignored. B: Moving the arm across the chest with hand on shoulder to orientate the accelerometer into the AAC position. C: Another flexion of the wrist while in the AAC position changes the gesture of the hand.

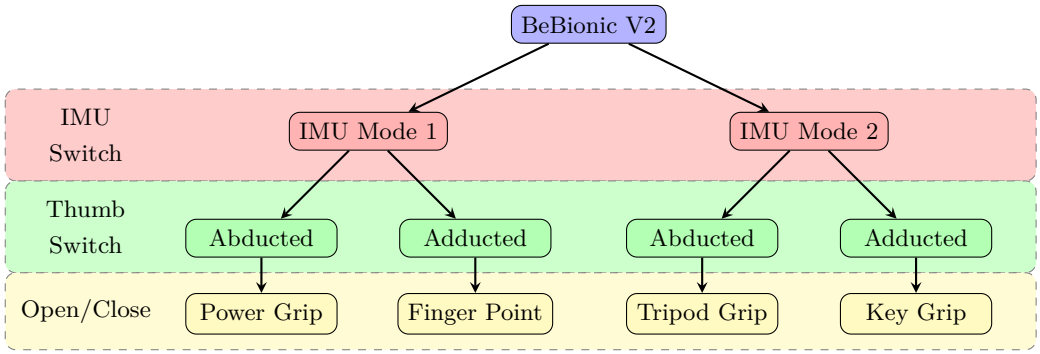


Figure 7.5: Flow chart showing the different grips and the methods required to access them. IMU switch was performed using the AAC method. Thumb switch was performed through movement of the thumb into an abducted or adducted state. Depending on the IMU switch and thumb switch state, the hand can perform one of four gestures.

from MATLAB to a control box which interfaced with the hand. A block diagram of the system configuration can be seen in Fig. 7.6.

7.2.2.1 System Calibration

Prior to collection the subject was asked to perform ten wrist extensions where the mean peak-to-peak signal was collected and used as a threshold to send open/close commands to the hand. Likewise, prior to collection the subject was asked to place their arm across their chest in a natural way while the three-dimensional orientation from the accelerometer

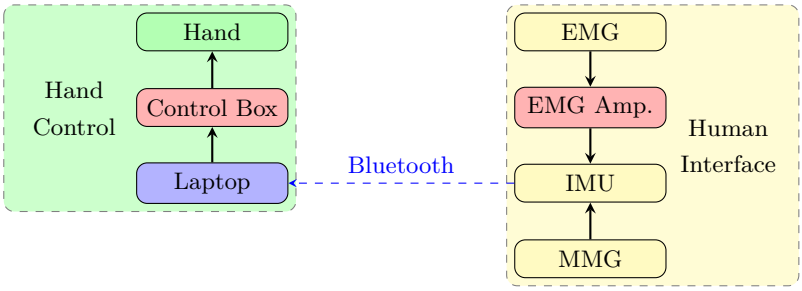


Figure 7.6: Block diagram showing HMI between a subject and the prosthetic hand. IMU, MMG, and EMG, sensors and electrodes were attached to the subjects forearm. Sensor data was transmitted to a laptop via Bluetooth where the signals were processed in MATLAB and a serial connection to the hand, via a control box, sends open and close commands, as well as gesture switching commands.

was collected and stored (Fig. 7.2). The subject would rest their arm and repeat the same orientation for a total of three times to determine an averaged threshold for the AAC switching orientation.

During testing, and in real-time with a 250 ms delay, MATLAB would process 250 ms windows of data for both IMU and muscle data (either EMG or MMG depending on the trial). Muscle data had its average peak-to-peak signal analysed, whereas accelerometer data had its accelerations determine for each plane to see if they fell within a ± 0.25 g window. If both were true the hand would switch grip, if just the muscle data exceeded the threshold but the IMU was not in the orientation position the hand would open/close, otherwise no action occurred. To further reduce motion and noise artefacts the hand would not perform any action if the magnitude of the gyroscope exceeded $10°/s$. Fig. 7.7 shows a flow diagram of this process. Before testing, the subject was allowed five minutes of getting use to the system with both MMG and EMG methods, including opening and closing the grip as well as gesture switching.

Subjects were given instructions on how to don and doff the sensors, including the IMU band, MMG sensor (attached to the band), and EMG electrodes. The donning task was as follows:

EMG

1. Shave the electrode areas.
2. Lightly abrase the area with a fine sandpaper.
3. Clean using an alcohol wipe.
4. Peal the adhesive backing off the electrodes and apply to the area.
5. Pull on the band containing the IMU into place.

MMG

1. Pull on the band containing the IMU into place.
2. Rearrange the band so that the MMG sensor is in place.

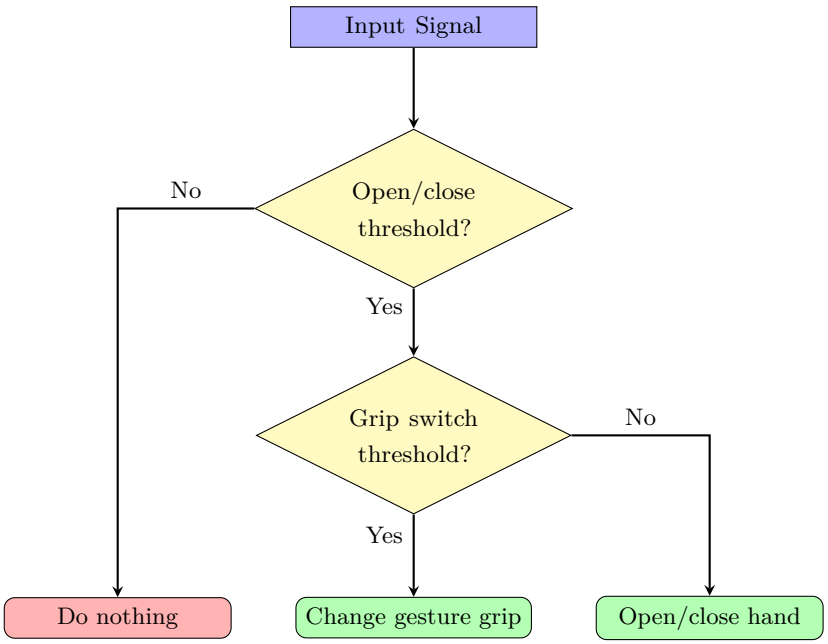


Figure 7.7: Flow diagram which shows the process taken for manipulation of the BeBionic Prosthetic hand. If the Muscle signal exceeds the predefined threshold the acceleration data was checked to see if the user has orientated their arm in the grip switch position. If both thresholds were met the gesture was changed, if just the muscle data exceeds its threshold the hand open/closes, otherwise no action was taken.

Before testing, the hand gesture was set to 'finger point' and the grip opened. The subject held the prosthesis in their right hand, while open/close/grip switch actions were performed with their left arm. The activity task, within the testing environment (Fig. 7.1), was as follows:

1. Pick up the hand and close grip to get the finger point gesture.
2. Tap the start/stop node which starts the timer.
3. Open grip. *Thumb is abducted for the user by investigator, grip is now changed to power grip.*
4. Close grip to grasp the bottle and place in metal tray.
5. Open grip to release bottle in tray.
6. Change gesture using AAC technique. *Grip is now changed to Tripod grip.*
7. Close grip to pick up tape roll and place in metal tray.
8. Open grip to release tape roll in tray. *Thumb is adducted for the user by investigator, grip is now changed to key grip.*
9. Close grip to pick up tray with bottle and tape inside. Move tray from square two to square three in the testing environment.
10. Open grip to release tray.
11. Change gesture using AAC technique. *Grip is now changed to finger point grip.*
12. Tap the start/stop node which stops the timer.

The subject performed three trials of five tests:

Natural Using their own hand, the subject was to perform the tasks listed above to set a baseline time which the other four tests were compared against.

MMG with visual With MMG control, the subject was allowed visual feedback using a graphic user interface.

EMG with visual Same as with MMG, the subject used EMG with a visual feedback to assist in control of the prosthesis.

EMG without visual EMG control of the hand, this time with the visual feedback removed.

MMG without visual MMG control, again with the visual feedback removed.

The visual feedback, seen in Fig. 7.8, provided the user with a graphical representation of the muscular contraction intensity and a threshold that had to be met for an open/close command (A), along with a window of which they had to get their arm orientated in for the gesture switch process (E, F, and G).

Each subject was subsequently timed while they donned the sensors, and duration times to complete each of the tests above were collected for each subject and trial. Furthermore, the time taken for each subject to don the sensors (EMG/IMU and MMG/IMU, respectively) were added to each respective test and trial and were separately analysed.

The mean duration time (excluding donning time) for each test from each subject was calculated, and a paired t-test was used to determine significance between each test.

7.2.3 Results

Table 7.1 presents each subjects average time (across three trials) of each of the five tests, as well as the duration time taken to don both the EMG and MMG sensors. The mean and standard deviation have been calculated for each test/donning group. Table 7.2 shows a comparison of significant difference in duration between each of the tests, with green and yellow backgrounds signifying significance ($P < 0.01$ and $P < 0.05$, respectively), whereas red backgrounds signify no significant difference ($P > 0.05$).

The duration results for each trial and test, per subject, are presented in Fig. 7.9 for duration time without donning time added, and Fig. 7.10 with the EMG donning time added to the EMG tests (with and without visual) and the same for MMG donning time added to the equivalent MMG tests.

7.2.4 Discussion and Conclusion

The duration times for each test presented in Table 7.1 show a close average between all MMG and EMG tests, with EMG performing only slightly faster, on average. However, MMG donning took substantially less time, which is reflected in the comparison data in the

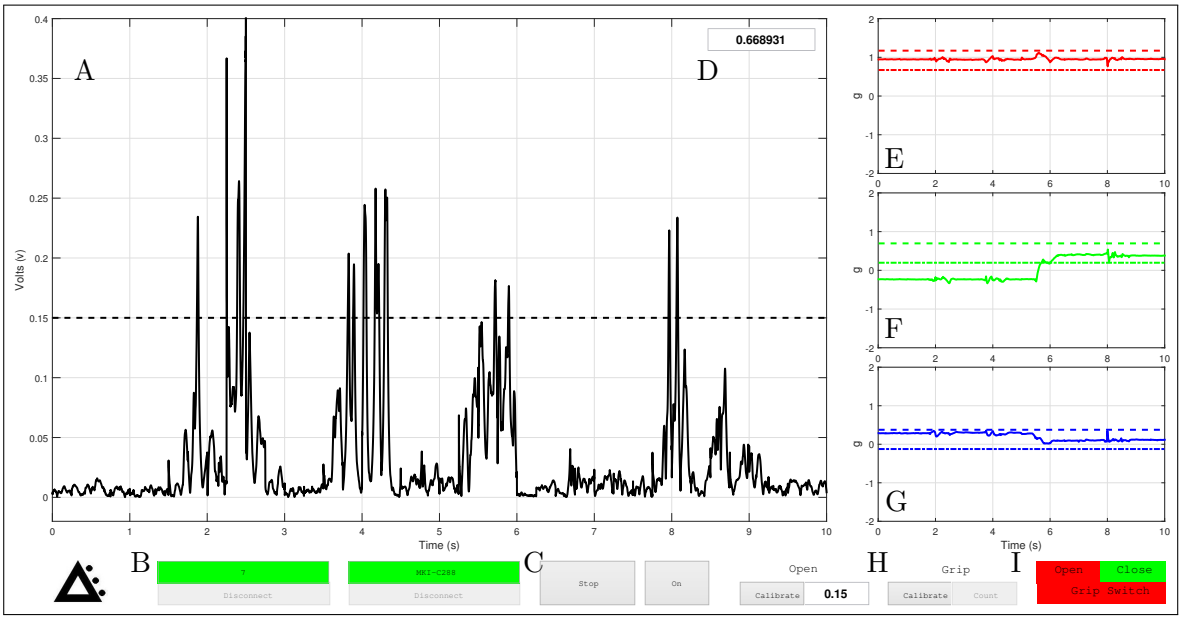


Figure 7.8: Screenshot showing the graphic user interface used as a control mechanism and visual feedback for the subject. A: Main plot showing muscle activity signal (MMG or EMG), filtered and rectified. Horizontal line at 0.15 V shows the threshold to be met to open/close the hand; B: Buttons and visual feedback indicating the connection status of the hand control box (connected on serial COM port 7), and IMU via Bluetooth. The green backgrounds indicate a successful connection; C: Stop/start button which controls the data streaming (shown as 'stop' in this graphic as data was currently streaming) and an on/off button to control the hand (shown as 'off' as the hand was currently on); D: numerical feedback indicating the averaged magnitude of the gyroscope. If movement exceeded 10°/s no hand action would be performed; E,F,G: Individual plots of the accelerometer data, X, Y, and Z planes respectively. Solid line indicates the current acceleration of that plane, dashed is the upper threshold of the orientation window, and dot-dashed is the lower threshold of the orientation window; H: Calibration buttons to change muscle contraction threshold (set at 0.15 V) and change the orientation window thresholds; I: Visual notifications to indicate the current status of the hand (open or closed) and when a grip switch signal has been received. Backgrounds turn green as an indicator.

unbiased data plots seen in Fig. 7.9 against the same data with donning times added, seen in Fig. 7.10.

The paired *t*-tests which compared average duration time for each test per subject shows a significant difference in duration seen between the natural task and all EMG and MMG tasks, which was expected. No significant difference in duration was seen between any of the EMG and MMG tests, except that of 'MMG with visual' verses 'MMG without visual'. Due to non-randomised process of performing the tests, the 'MMG with visual' test was the 2nd to be performed, following the 'natural' test, and 'MMG without visual' was the last test to be performed. Although less significant with a P value less than 0.05, the value is still statistically significant and this is believed to be due to the learning process each subject made as they progressed through the tasks and performed better after each.

Differences between 'EMG with visual' and 'EMG without visual' were not significantly different and were the 3rd and 4th test performed, suggesting no advantage in performance was gained from the visual feedback. Subjects generally learnt the force required from the

Table 7.1: Table showing the average duration for three trials, per test, per subject. Donning times for EMG and MMG are also presented. All values are in seconds (s) and are rounded to the nearest second. Overall averages and standard deviations have been calculated.

Subject	Natural	MMG w/ Visual	EMG w/ Visual	MMG w/o Visual	EMG w/o Visual	EMG Donning	MMG Donning
A	11	53	44	48	40	46	6
B	9	55	49	38	41	49	5
C	10	53	41	48	36	44	7
D	8	36	31	34	35	39	6
E	10	44	59	34	44	50	7
Mean	10	48	45	40	39	46	6
STD	1	7	9	6	3	4	1

Table 7.2: Results of paired t-test between each test duration. Significant values ($P < 0.01$ and $P < 0.05$) have green and yellow backgrounds, respectively. Non-significant vales ($P > 0.05$) have red backgrounds.

w/o Bias	Natural	MMG w/ Visual	EMG w/ Visual	MMG w/o Visual	EMG w/o Visual
Natural		P<0.01	P<0.01	P<0.01	P<0.01
MMG w/ Visual			P>0.05	P<0.05	P>0.05
EMG w/ Visual				P>0.05	P>0.05
MMG w/o Visual					P>0.05
EMG w/o Visual					

wrist extension in order to operate the hand, as well as the AAC position required to change grip, very quickly. It was observed that a level of proprioception was used much more than the visual feedback provided as subjects were able to recall the necessary orientation to position the arm with no feedback provided. However, the BeBionic hand emits an auditory sound and vibrates when a gesture switch is performed, which was believed each subject relied on more than the visual information.

The choice not to randomise the order of tests was not believed to have created a bias in EMG and MMG results, as subjects were not aware of which sensor type they were using for each test, only that they would have a visual or non-visual feedback.

False open/close commands and incorrect/failed gesture switches were minimal, with the exception of subject A in trial three for 'EMG with visual' feedback where they had a particularly bad experience. It is believed the filtering methods used, as well as the gyroscopic motion method used to restrict hand activity if movement above 10 °/s were detected, was responsible for the reduction in false commands.

The time taken to don the IMU/EMG pair and IMU/MMG pair was expectedly different. The number of steps and requirements for donning EMG electrodes vastly exceeded the time taken to don the equivalent MMG/IMU pair. Table 7.1 shows the time taken for each subject to don each sensor type, with EMG taking over seven times longer to attach than MMG. As stated in the introduction, this is not a perfect study, as prosthesis control using EMG is greatly achieved using dry electrode EMG sensors, which are expected to have a very similar

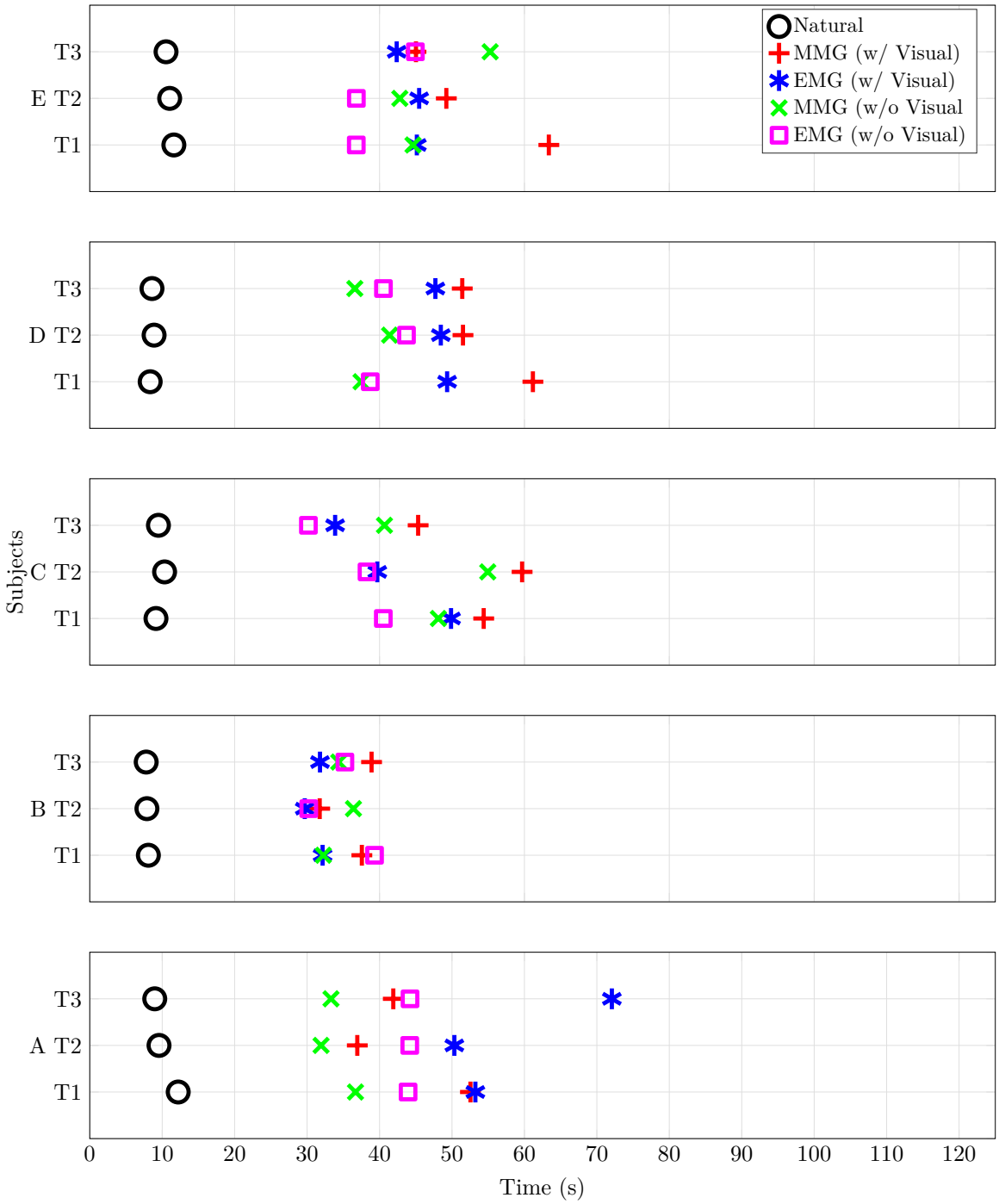


Figure 7.9: Results showing elapsed time for each subject (A-E) for natural, MMG with and without visual feedback, and EMG with and without feedback. These results only take into consideration the time taken to perform the activity task, not including the donning time. T1-T3 are trials one to three.

donning time to MMG. However, this would come with a reduction in performance from the EMG due to the higher skin impedance introduced from the dry electrodes, although it is believed this would be reflected in the difficulty in completing the task and further studies are needed.

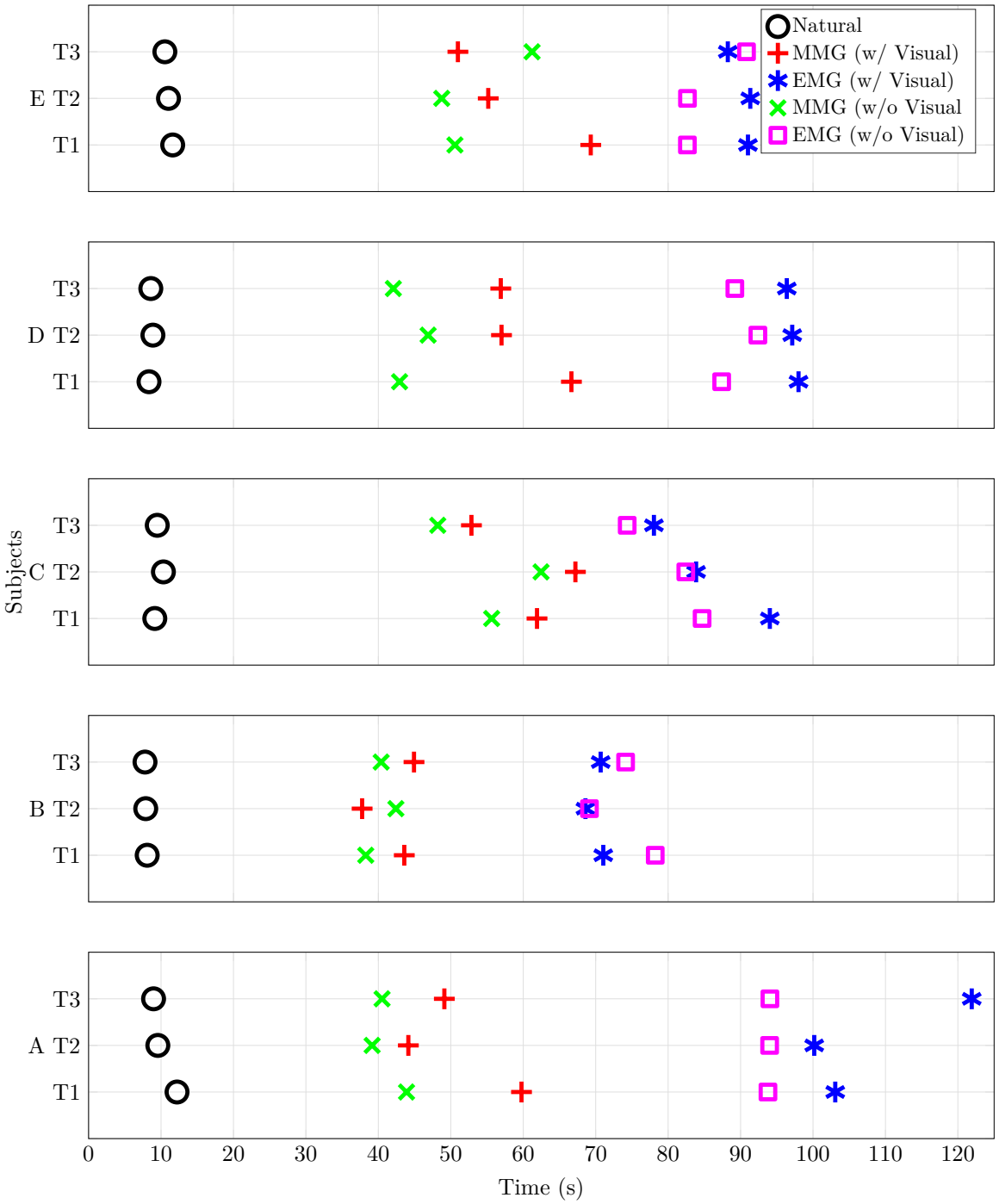


Figure 7.10: Results showing elapsed time for each subject (A-E) for natural, MMG with and without visual feedback, and EMG with and without feedback. These results show the time taken to perform the activities with time taken to don the IMU/MMG sensors added to the MMG results, and time taken to don the IMU/EMG sensors added to the EMG results. T1-T3 are trials one to three.

Future work intends to apply this method to prostheses with additional gesture orientations to switch through a range of grips. For example, the current study only implemented an orientation of the arm being placed across the chest, however other orientations such as arm across the waist could be used to switch to another gesture.

It has been shown that MMG can perform as well as EMG in prosthetic control, but without limitations such as skin impedance change through perspiration and without the amplification required from EMG. Furthermore, the gesture controlled method of grip switching has been successful with no input required from another hand. Although thumb abduction/adduction still required a manually move, in this study by an investigator, future work intends to apply this method of grip switching to prosthesis with automatic opposable thumbs. The comparison of MMG against EMG donning times also shows a large difference. Although not completely fair for this application, it does show that MMG can be worn much faster than wet electrode EMG which is very applicable to applications where time is of the essence.

7.3 Chapter Summary

Work in this chapter has presented a novel grip switching method for prosthetic hands, as well as a comparison of MMG and EMG in prosthetic hand control. Using static information from the accelerometer on-board the Aktiv IMU, a user was able to switch hand gestures by orientating their arm in a specific way. This method introduced a method in which interaction with the hand itself, in order to switch grip, was obsolete.

Comparison of MMG and EMG methods of controlling the hand have shown a close similarity in speed and performance, suggesting suitable use of MMG in future prosthetic applications. It is suggested that the technology presented here has suitable use in other rehabilitation HMI applications, as well as further work in prosthetic studies.

8

Discussion

Contents

8.1 Introduction 140
8.2 Summary of Contributions 140
8.3 Limitations 141
8.4 Future Work 142

8.1 Introduction

The goal of this thesis was to develop a system capable of collecting human motion and muscle information, for a prolonged period, in uncontrolled environments.

Suitable sensors to perform this were narrowed down and selected based on their pros and cons, followed by validation against the gold standard in order to determine their accuracy in human motion and muscle monitoring. The sensors were applied to three core areas of interest, including physiological studies, gait analysis and activity monitoring, and human machine interfaces.

8.2 Summary of Contributions

Significant findings, including reiteration of the aims and objectives listed in the introduction, are listed below, along with their location within this thesis:

- A system capable of pervasive and prolonged monitoring was developed and successfully applied to a number of applications. Validation against the gold standard in human motion tracking muscle monitoring technologies (optical tracking and EMG, respectively) produced a high comparable accuracy, which suggested suitable use in human monitoring, albeit, in uncontrolled environments, which optical and EMG systems cannot do. (Chapters 3 and 4)
- Using IMU's as a substitution to expensive and non-mobile technology, such as dynamometers, this system has been found to agree with current literature in that skeletal muscle amplitude and frequency components increases, and are highly correlated, to an increase in force. Results showed that MMG has a higher sensitivity to fatigue, both during a sustained contraction and post-fatigue, than EMG. Furthermore, through inexpensive sensors and a semi-controlled environment it has been confirmed that fatigue monitoring is possible outside of a laboratory. (Chapter 5)
- A clinical application of anaesthetic monitoring has shown that through full inclusion of the stakeholders in technology development a system has been created which successfully accommodates their needs. (Chapter 5)
- Characterising differing gait activities using an offline, unsupervised, K-means algorithm method was achieved, with nine activities correctly classified to an accurate of 98.4%. (Chapter 6)
- Progressive changes were monitored in two atypical gait groups; cerebral palsy and amputee, and significant differences were found in both motion and muscle components when compared against typical gait, where progressive changes were not expected. (Chapter 6)

- Pervasive and prolonged collection of bilateral leg data showed insignificant differences between legs in an atypical subject with a unilateral amputation. However, significant differences were seen between typical and atypical gait. (Chapter 6)
- Using an IMU to monitor arm orientation, a novel method of prosthetic hand grip switching was developed and applied. Furthermore, MMG comparison against EMG in prosthesis control showed very close similarities in speed and performance, suggesting MMG's suitability in further prosthesis applications. (Chapter 7)

8.3 Limitations

Throughout this research some limitations were identified in the use of this technology.

First, MMG data collection, especially in relation to dynamic movement (although also seen in isometric contractions to a lesser extent), can result in large motion artefacts which are challenging to remove. Unlike EMG, which is less affected by such artefacts, MMG sensors such as the one developed are vulnerable to external noise, including taps or disturbances to the sensor itself. Although filtering methods are capable of lowering the disturbance, especially when the frequencies of interest are known, complex noise frequencies are often still present post-filtering. The work presented here selected microphones as opposed to accelerometers for MMG collection, due to their better response at rejecting motion artefacts, however, artefacts are still present. Furthermore, due to MMG's wide frequency band, between 2 and 100 Hz, it is difficult to filter without potentially removing data of interest. Although this work has applied a number of techniques to minimise such disturbances, such as the accelerometer-based filter used in Chapter 6, this limitation is still prominent.

A well-known limitation of inertial based systems is their non-trivial position estimation, due to issues associated with sensor drift. As discussed in Chapter 2, the estimation of position using inertial systems, consisting of accelerometers, gyroscopes, and often magnetometers, is very limited, due to small integration errors which progressively and exponentially increase over time. Many have opted for 'ground truths' in order to zero the integration error which causes positional drift, such as through detection of stationary periods or inclusion of additional sensors, such as GPS. However, they have only reduced the issue, with no current implementation which completely removes drift. This research performed motion data analysis in a relative form, which did not require positional estimation. However, having position data in order to determine joint angle movements, or how far a subject travelled, would significantly broaden the potential for pervasive motion tracking applications.

Inclusion of stakeholders was an important aspect of this research, as previous reports have shown how often wearable devices are not designed with the user in mind[6]. Although this work has fully adopted this ideology, it was not completely successful in the anaesthetic monitoring application (Chapter 5). However, a strong relationship was formed with the clinician involved in this study, as well as constant communication in order to understand

their needs. Although the first iteration of the system had issues, they have since been corrected, with the second version expected to be reapplied to this application in the near future.

8.4 Future Work

It is envisioned that future work would further what has been achieved here in two main areas:

Expansion Through expansion of further data collection and subject numbers, the results presented here will be strengthened and the conclusions determined throughout this research will be further reinforced. In certain applications, additional subjects within each of the atypical groups presented here could expand the understanding of motion and muscle differences on a global condition scale, as opposed to individually. Furthermore, expanding the length of condition monitoring, such as in the gait analysis studies, could show greater changes in activities over the course of weeks and months, as opposed to hours and days presented here.

Intervention Many of the applications presented here identify differences, or noticeable changes in performance over time, in both typical and atypical subjects. However, this research only goes as far as to identify these changes. Future work would include communication with clinicians for medical intervention to be applied, in order to correct or alleviate declining change over time. This would be a continuation to the original goal of full stakeholder inclusion.

Algorithm and software development is also a future goal, with improvements to accuracy in classification and recognition, specifically in the activity monitoring study. Furthermore, additional activities are intended to be included into the activity classification algorithm by utilising additional unique attributes seen in activities such as walking up and down inclined planes; something sought after in the prosthesis community in order to adapt joint parameters[235].

Further hardware development, although beneficial to improve upon every couple of years, due to advances in technology as described by Moores Law[43], is not seen to be a pressing requirement, nor as a necessity for the near future. However, improvements in sensor aesthetics and further implementation into clothing and bands would greatly increase the wearability, concealability, and practicality, in wearing such a device for a prolonged period of time.

9

Conclusion

Contents

9.1 Final Comments 144

9.1 Final Comments

This work has developed a wearable device which is capable of collecting human motion and muscle activity, in pervasive and uncontrolled environments. This technology has been validated against the gold standard, confirming a high accuracy and suitability in human application, however, without the limitations associated with the current monitoring methods confined to a laboratory or clinic.

Each study presented here has demonstrated the capabilities of the Aktiv IMU and MMG sensor, and have universally shown that concurrent motion and muscle monitoring is possible. Furthermore, this research has demonstrated applications not possible in a controlled environment, including prolonged monitoring for changes in performance, and full inclusion within subject's day-to-day environment. The technology has been developed with stakeholder input, in order to create a device which accommodates their needs.

This system is not applied as a replacement for laboratory based methods, which hold the benefit of accuracy and acceptance in literature and clinical studies, but as an alternative in environments, situations, or duration requirements, where the current standards are unsuitable or inapplicable.

Bibliography

[1] R Lauer, B Smith, and R Betz. Application of a neuro-fuzzy network for gait event detection using electromyography in the child with cerebral palsy. *IEEE transactions on bio-medical engineering*, 52(9), September 2005.

[2] J Youdas and C Amundson. Surface electromyographic activation patterns and elbow joint motion during a pull-up, chin-up, or perfect-pullup rotational exercise. *The Journal of Strength and Conditioning Research*, 21(12), 2010.

[3] G Shan. Biomechanical evaluation of bike power saver. *Applied ergonomics*, 39(1), January 2008.

[4] H Zhou and H Hu. Human motion tracking for rehabilitation–A survey. *Biomedical Signal Processing and Control*, 3(1), January 2008.

[5] S Simon. Quantification of human motion: gait analysis-benefits and limitations to its application to clinical problems. *Journal of biomechanics*, 37(12), December 2004.

[6] J Bergmann and A McGregor. Body-worn sensor design: what do patients and clinicians want? *Annals of biomedical engineering*, 39(9), September 2011.

[7] M Stokes and P Dalton. Acoustic myography for investigating human skeletal muscle fatigue. *Journal of applied physiology*, 71(4), October 1991.

[8] D Barry, S Geiringer, and R Ball. Acoustic myography: a noninvasive monitor of motor unit fatigue. *Muscle & Nerve*, 8(3), 1985.

[9] M Stokes. Acoustic myography: applications and considerations in measuring muscle performance. *Isokinetics and Exercise Science*, 3(1), 1993.

[10] U Jow, M Kiani, X Huo, and M Ghovanloo. Towards a smart experimental arena for long-term electrophysiology experiments. *IEEE transactions on biomedical circuits and systems*, 6(5), October 2012.

[11] H Wi, H Sohal, A McEwan, E Woo, and T Oh. Multi-frequency electrical impedance tomography system with automatic self-calibration for long-term monitoring. *IEEE transactions on biomedical circuits and systems*, 8(1), February 2014.

[12] A Murgia, V Kerkhofs, H Savelberg, and K Meijer. A portable device for the clinical assessment of upper limb motion and muscle synergies. In *IEEE EMBS, 2010*, volume 2010, January 2010.

[13] H Ghasemzadeh, R Jafari, and B Prabhakaran. A body sensor network with electromyogram and inertial sensors: multimodal interpretation of muscular activities. *IEEE transactions on information technology in biomedicine*, 14(2), March 2010.

[14] ARD. ARD Research Lab. [Online] `http://www.analisidelmovimento.it/benvenuti.htm`.

[15] B Najafi, K Aminian, F Loew, Y Blanc, and P Robert. Measurement of stand-sit and sit-stand transitions using a miniature gyroscope and its application in fall risk evaluation in the elderly. *IEEE Transactions on Biomedical Engineering*, 49(8), August 2002.

[16] U Ugbolue, E Papi, K Kaliarntas, A Kerr, L Earl, V Pomeroy, and P Rowe. The evaluation of an inexpensive, 2D, video based gait assessment system for clinical use. *Gait and Posture*, 38(3):483–489, 2013.

[17] T Dutta. Evaluation of the Kinect sensor for 3-D kinematic measurement in the workplace. *Applied Ergonomics*, 43(4):645–649, 2012.

[18] M Windolf, N Götzen, and M Morlock. Systematic accuracy and precision analysis of video motion capturing systems–exemplified on the Vicon-460 system. *Journal of biomechanics*, 41(12), August 2008.

[19] B Carse, B Meadows, R Bowers, and P Rowe. Affordable clinical gait analysis: an assessment of the marker tracking accuracy of a new low-cost optical 3D motion analysis system. *Physiotherapy*, 99(4), December 2013.

[20] A Cutti, G Paolini, M Troncossi, A Cappello, and A Davalli. Soft tissue artefact assessment in humeral axial rotation. *Gait and Posture*, 21(3):341–349, 2005.

[21] A Cutti, A Cappello, and A Davalli. In vivo validation of a new technique that compensates for soft tissue artefact in the upper-arm: Preliminary results. *Clinical Biomechanics*, 21(SUPPL. 1):13–19, 2006.

[22] M Kuo, T Tsai, C Lin, T Lu, H Hsu, and W Shen. Influence of soft tissue artifacts on the calculated kinematics and kinetics of total knee replacements during sit-to-stand. *Gait and Posture*, 33(3):379–384, 2011.

[23] M Akbarshahi, A Schache, J Fernandez, R Baker, S Banks, and M Pandy. Non-invasive assessment of soft-tissue artifact and its effect on knee joint kinematics during functional activity. *Journal of Biomechanics*, 43(7):1292–1301, 2010.

[24] A Peters, B Galna, M Sangeux, M Morris, and R Baker. Quantification of soft tissue artifact in lower limb human motion analysis: a systematic review. *Gait & posture*, 31(1), January 2010.

[25] R Baker, L Finney, and J Orr. A new approach to determine the hip rotation profile from clinical gait analysis data. *Human movement science*, 18, 1999.

[26] T Cloete and C Scheffer. Benchmarking of a full-body inertial motion capture system for clinical gait analysis. In *IEEE EMBS, 2008*, volume 7. IEEE, 2008.

[27] J Bergmann, R Mayagoitia, and I Smith. A portable system for collecting anatomical joint angles during stair ascent: a comparison with an optical tracking device. *Dynamic medicine : DM*, 8(3), January 2009.

[28] D Vickers, C Palk, A McIntosh, and K Beatty. Elderly unilateral transtibial amputee gait on an inclined walkway: a biomechanical analysis. *Gait & posture*, 27(3), April 2008.

[29] Q Cai and J Aggarwal. Tracking human motion in structured environments using a distributed-camera system. In *IEEE Transactions on Pattern Analysis and Machine Intelligence*, volume 21, 1999.

[30] A Sundaresan and R Chellappa. Multicamera tracking of articulated human motion using shape and motion cues. *IEEE transactions on image processing : a publication of the IEEE Signal Processing Society*, 18(9), September 2009.

[31] A Yilmaz, O Javed, and M Shah. Object tracking: A survey. *Acm computing surveys (CSUR)*, 38(4), December 2006.

[32] A Pfister, A West, S Bronner, and J Noah. Comparative abilities of Microsoft Kinect and Vicon 3D motion capture for gait analysis. *Journal of medical engineering & technology*, 38(5), July 2014.

[33] MetaMotion. Gypsy 7 Torso Motion Capture System. [Online] `http://www.metamotion.com/gypsy/Gypsy-6-torso.html`.

[34] G Welch and E Foxlin. Motion tracking: No silver bullet, but a respectable arsenal. *IEEE Computer Graphics and Applications*, 22(6), 2002.

[35] J Lenz. A review of magnetic sensors. In *Proceedings of the IEEE*, 1990.

[36] O Suess, S Suess, S Mularski, B Kühn, T Picht, S Hammersen, R Stendel, M Brock, and T Kombos. Study on the clinical application of pulsed DC magnetic technology for tracking of intraoperative head motion during frameless stereotaxy. *Head & face medicine*, 2, January 2006.

[37] M Boonstra, R van der Slikke, N Keijsers, R van Lummel, M de Waal Malefijt, and N Verdonschot. The accuracy of measuring the kinematics of rising from a chair with accelerometers and gyroscopes. *Journal of Biomechanics*, 39(2), January 2006.

[38] G Cooper, I Sheret, L McMillan, K Siliverdis, N Sha, D Hodgins, L Kenney, and D Howard. Inertial sensor-based knee flexion/extension angle estimation. *Journal of biomechanics*, 42(16), December 2009.

[39] R Mayagoitia, A Nene, and P Veltink. Accelerometer and rate gyroscope measurement of kinematics: an inexpensive alternative to optical motion analysis systems. *Journal of Biomechanics*, 35(4), April 2002.

[40] H Zhou, H Hu, and N Harris. Wearable inertial sensors for arm motion tracking in home-based rehabilitation. In *Proceedings of the 9th International Conference on Intelligent Autonomous Systems*. Citeseer, 2006.

[41] H Zhou and H Hu. Inertial motion tracking of human arm movements in stroke rehabilitation. In *Mechatronics and Automation, 2005 IEEE International Conference*, volume 3. IEEE, 2005.

[42] H Zhou and H Hu. Kinematic model aided inertial motion tracking of human upper limb. In *Information Acquisition, 2005 IEEE International Conference on*. IEEE, 2005.

[43] G Moore. Cramming more components onto integrated circuits. *Proceedings of the IEEE*, 86(1), 1998.

[44] D Won, J Ahn, S Sung, M Heo, S Im, and Y Lee. Performance Improvement of Inertial Navigation System by Using Magnetometer with Vehicle Dynamic Constraints. *Journal of Sensors*, 2015:11, 2015.

[45] X Yun and E Bachmann. Design, implementation, and experimental results of a quaternion-based Kalman filter for human body motion tracking. *IEEE Transactions on Robotics*, 22(6), 2006.

[46] A Kim and M Golnaraghi. A quaternion-based orientation estimation algorithm using an inertial measurement unit. In *Position Location and Navigation Symposium, 2004*, pages 268–272, 2004.

[47] R Zhu and Z Zhou. A real-time articulated human motion tracking using tri-axis inertial/magnetic sensors package. *IEEE Transactions on Neural Systems and Rehabilitation Engineering*, 12(2), June 2004.

[48] X Yun, C Aparicio, E Bachmann, and R Mcghee. Implementation and Experimental Results of a Quaternion-Based Kalman Filter for Human Body Motion Tracking. In *IEEE Conference on Robotics and Automation*, 2005.

[49] J Marins, X Yun, and E Bachmann. An extended Kalman filter for quaternion-based orientation estimation using MARG sensors. In *International Conference on Intelligent Robots and Systems, 2001.*, 2001.

[50] S Madgwick, A Harrison, and R Vaidyanathan. Estimation of IMU and MARG orientation using a gradient descent algorithm. In *IEEE International Conference on Rehabilitation Robotics*, volume 2011, 2011.

[51] E Bachmann, R McGhee, and X Yun. Inertial and magnetic posture tracking for inserting humans into networked virtual environments. In *ACM Symposium on Virtual Reality Software and Technology (VRST)*, 2001.

[52] H Tan, A Wilson, and J Lowe. Measurement of stride parameters using a wearable GPS and inertial measurement unit. *Journal of biomechanics*, 41(7), January 2008.

[53] J Chen, C Yang, J Hofschulte, W Jiang, and C Zhang. A robust optical/inertial data fusion system for motion tracking of the robot manipulator. *Journal of Zhejiang University SCIENCE C*, 15(7), July 2014.

[54] P Corke, J Lobo, and J Dias. An introduction to inertial and visual sensing. *The International Journal of Robotics Research*, 26(6), June 2007.

[55] K Tsukada and M Yasumura. Activebelt: Belt-type wearable tactile display for directional navigation. In *UbiComp 2004: Ubiquitous Computing*, volume 3205. Springer, 2004.

[56] P Veltink and D De Rossi. Wearable technology for biomechanics: e-textile or micromechanical sensors?[Conversations in BME]. *IEEE Engineering in Medicine and Biology Magazine*, 29(3), 2010.

[57] H Zhou, T Stone, H Hu, and N Harris. Use of multiple wearable inertial sensors in upper limb motion tracking. *Medical Engineering & Physics*, 30(1), January 2008.

[58] E Papi, D Osei-Kuffour, Y Chen, and A McGregor. Use of wearable technology for performance assessment: A validation study. *Medical Engineering & Physics*, [In press], 2015.

[59] U Varshney. Pervasive healthcare and wireless health monitoring. *Mobile Networks and Applications*, 12(2-3):113–127, 2007.

[60] O Aziz, B Lo, R King, A Darzi, and G Yang. Pervasive body sensor network: an approach to monitoring the post-operative surgical patient. In *International Workshop on Wearable and Implantable Body Sensor Networks (BSN'06)*, pages 4–7, 2006.

[61] K Leuenberger and R Gassert. Low-power sensor module for long-term activity monitoring. In *IEEE EMBS, 2011*, January 2011.

[62] Y Kan and C Chen. A wearable inertial sensor node for body motion analysis. *IEEE Sensors Journal*, 12(3), 2012.

[63] C Ryan, P Grant, W Tigbe, and M Granat. The validity and reliability of a novel activity monitor as a measure of walking. *British journal of sports medicine*, 40(9), September 2006.

[64] V van Acht, E Bongers, N Lambert, and R Verberne. Miniature wireless inertial sensor for measuring human motions. *International Conference of the IEEE Engineering in Medicine and Biology Society*, 2007, January 2007.

[65] Y Tsai, T Tu, H Bae, and P Chou. EcoIMU: A Dual Triaxial-Accelerometer Inertial Measurement Unit for Wearable Applications. In *2010 International Conference on Body Sensor Networks*. Ieee, June 2010.

[66] E Bishop and Q Li. Walking speed estimation using shank-mounted accelerometers. In *Robotics and Automation (ICRA), 2010 IEEE International Conference on*. IEEE, May 2010.

[67] S Madgwick, A Harrison, P Sharkey, R Vaidyanathan, and W Harwin. Measuring motion with kinematically redundant accelerometer arrays: Theory, simulation and implementation. *Mechatronics*, 23(5), August 2013.

[68] M Yuwono, S Su, Y Guo, B Moulton, and H Nguyen. Unsupervised nonparametric method for gait analysis using a waist-worn inertial sensor. In *Applied Soft Computing*, volume 14. Elsevier B.V., January 2014.

[69] J van den Noort, A Ferrari, A Cutti, J Becher, and J Harlaar. Gait analysis in children with cerebral palsy via inertial and magnetic sensors. *Medical & Biological Engineering & Computing*, 51(4), April 2013.

[70] P Bours and R Shrestha. Eigensteps: A giant leap for gait recognition. In *2010 2nd International Workshop on Security and Communication Networks (IWSCN)*. Ieee, May 2010.

[71] M Hynes, H Wang, and L Kilmartin. Off-the-shelf mobile handset environments for deploying accelerometer based gait and activity analysis algorithms. In *IEEE EMBS, 2009*, volume 2009, January 2009.

[72] M Derawi. Accelerometer-Based Gait Analysis, A survey. In *Norsk informasjonssikkerhetskonferanse (NISK)*, 2010.

[73] P van Coevering, L Harnack, K Schmitz, J Fulton, D Galuska, and S Gao. Feasibility of using accelerometers to measure physical activity in young adolescents. *Medicine & Science in Sports & Exercise*, 37(5), May 2005.

[74] B Zhang, Y Zhang, and R Begg. Gait classification in children with cerebral palsy by Bayesian approach. *Pattern Recognition*, 42(4), April 2009.

[75] B Noehren, J Scholz, and I Davis. The effect of real-time gait retraining on hip kinematics, pain and function in subjects with patellofemoral pain syndrome. *British journal of sports medicine*, 45(9), July 2011.

[76] P Veltink, H Bussmann, W de Vries, W Martens, and R Van Lummel. Detection of static and dynamic activities using uniaxial accelerometers. *IEEE Transactions on Rehabilitation Engineering*, 4(4), December 1996.

[77] G Lyons, K Culhane, D Hilton, P Grace, and D Lyons. A description of an accelerometer-based mobility monitoring technique. *Medical Engineering & Physics*, 27(6), July 2005.

[78] D Gafurov and K Helkala. Biometric gait authentication using accelerometer sensor. *Journal of computers*, 1(7), 2006.

[79] H Junker, O Amft, and P Lukowicz. Gesture spotting with body-worn inertial sensors to detect user activities. *Pattern Recognition*, 41(6), 2008.

[80] R DeVaul and S Dunn. Real-time motion classification for wearable computing applications. Technical report, MIT Media Laboratory, Boston, MA, 2001.

[81] N Ravi, N Dandekar, P Mysore, and M Littman. Activity recognition from accelerometer data. In *Association for the Advancement of Artificial Intelligence*, 2005.

[82] L Bao and S Intille. Activity recognition from user-annotated acceleration data. In *Pervasive Computing*, 2004.

[83] K Van Laerhoven and O Cakmakci. What shall we teach our pants? In *Wearable Computers, The Fourth International Symposium on*. IEEE Comput. Soc, 2000.

[84] H Fourati, N Manamanni, and L Afilal. Posture and body acceleration tracking by inertial and magnetic sensing: Application in behavioral analysis of free-ranging animals. *Biomedical Signal Processing and Control*, 6(1), 2011.

[85] K Seo, S Oh, Y Park, and S Park. Human motion reconstruction based on inertial motion sensors. In *Ubiquitous Robots and Ambient Intelligence*, 2011.

[86] J Aggarwal and Q Cai. Human Motion Analysis: A Review. *Computer Vision and Image Understanding*, 73(3), March 1999.

[87] D Fong. The Use of Wearable Inertial Motion Sensors in Human Lower Limb Biomechanics Studies: A Systematic Review. *Sensors*, 10(12), December 2010.

[88] J Weir, K Ayers, J Lacefield, and K Walsh. Mechanomyographic and electromyographic responses during fatigue in humans: influence of muscle length. *European journal of applied physiology*, 81(4):352–359, 2000.

[89] E Al-Zahrani, C Gunasekaran, M Callaghan, P Gaydecki, D Benitez, and J Oldham. Within-day and between-days reliability of quadriceps isometric muscle fatigue using mechanomyography on healthy subjects. *Journal of Electromyography and Kinesiology*, 19(4):695–703, 2009.

[90] E Ryan, J Cramer, T Housh, T Beck, T Herda, and M Hartman. Inter-individual variability in the torque-related patterns of responses for mechanomyographic amplitude and mean power frequency. *Journal of Neuroscience Methods*, 161(2):212–219, 2007.

[91] J Betts, P DeSaix, E Johnson, J Johnson, O Korol, D Kruse, B Poe, J Wise, M Womble, and K Young. Muscle Tissue. In *Human Anatomy and Physiology*, chapter 10, page 404. OpenStax College, seventh edition, 2013.

[92] C Pylatiuk, M Müller-Riederer, A Kargov, S Schulz, O Schill, M Reischl, and G Bretthauer. Comparison of surface EMG monitoring electrodes for long-term use in rehabilitation device control. In *2009 IEEE International Conference on Rehabilitation Robotics*, pages 300–304, 2009.

[93] M Ahsan, M Ibrahimy, and O Khalifa. Advances in electromyogram signal classification to improve the quality of life for the disabled and aged people. *Journal of Computer Science*, 6(7):706–715, 2010.

[94] C De Luca, L Donald Gilmore, M Kuznetsov, and S Roy. Filtering the surface EMG signal: Movement artifact and baseline noise contamination. *Journal of Biomechanics*, 43(8):1573–1579, 2010.

[95] S Alty and A Georgakis. Mean Frequency Estimation of Surface Emg Signals Using. In *19th European Signal Processing Conference*, pages 1387–1390, 2011.

[96] A Merlo, D Farina, and R Merletti. A fast and reliable technique for muscle activity detection from surface EMG signals. *IEEE Transactions on Biomedical Engineering*, 50(3):316–323, 2003.

[97] A Norali and M Som. Surface Electromyography Signal Processing and Application: A Review. In *International Conference on Man-Machine Systems*, number October, pages 11–13, 2009.

[98] C De Luca. The use of surface electromyography in biomechanics. *Journal of Applied Biomechanics*, 13:135–163, 1997.

[99] E Andersson, J Nilsson, and A Thorstensson. Intramuscular EMG from the hip flexor muscles during human locomotion. *Acta physiologica Scandinavica*, 161(3):361–370, 1997.

[100] C Orizio, D Liberati, C Locatelli, D De Grandis, and A Veicsteinas. Surface mechanomyogram reflects muscle fibres twitches summation. *Journal of biomechanics*, 29(4), 1996.

[101] Y Yoshitake and T Moritani. The muscle sound properties of different muscle fiber types during voluntary and electrically induced contractions. *Journal of electromyography and kinesiology*, 9(3), June 1999.

[102] G Gordon. The sounds from single motor units in a contracting muscle. *The Journal of Physiology*, 107(4), 1948.

[103] G Oster and J Jaffe. Low frequency sounds from sustained contraction of human skeletal muscle. *Biophysical journal*, 30(1), April 1980.

[104] C Orizio. Muscle Sound: Bases for the Introduction of a Mechanmyographic Signal in Muscle Studies. *Critical reviews in biomedical engineering*, 21(3), 1993.

[105] J Silva, T Chau, and A Goldenberg. MMG-based multisensor data fusion for prosthesis control. In *Engineering in Medicine and Biology Society, 2003. Proceedings of the 25th Annual International Conference of the IEEE*, volume 3. IEEE, 2003.

[106] D Barry. Acoustic signals from frog skeletal muscle. *Biophysical journal*, 51(5), May 1987.

[107] C Orizio. Soundmyogram and EMG cross-spectrum during exhausting isometric contractions in humans. *Journal of electromyography and kinesiology*, 2(3), January 1992.

[108] C Orizio, R Perini, and A Veicsteinas. Muscular sound and force relationship during isometric contraction in man. *European journal of applied physiology and occupational physiology*, 58(5), 1989.

[109] K Ebersole, T Housh, G Johnson, T Evetovich, D Smith, and S Perry. MMG and EMG responses of the superficial quadriceps femoris muscles. *Journal of electromyography and kinesiology*, 9(3), June 1999.

[110] M Tarata. Mechanomyography versus Electromyography, in monitoring the muscular fatigue. *BioMedical Engineering OnLine*, 2(1), 2003.

[111] M Watakabe, K Mita, K Akataki, and K Ito. Reliability of the mechanomyogram detected with an accelerometer during voluntary contractions. *Medical & Biological Engineering & Computing*, 41(2), March 2003.

[112] C Orizio, M Gobbo, B Diemont, F Esposito, and A Veicsteinas. The surface mechanomyogram as a tool to describe the influence of fatigue on biceps brachii motor unit activation strategy. Historical basis and novel evidence. *European journal of applied physiology*, 90(3-4), October 2003.

[113] Y Zeng, Z Yang, W Cao, and C Xia. Hand-motion patterns recognition based on mechanomyographic signal analysis. In *BioMedical Information Engineering, 2009. FBIE 2009. International Conference on Future*. IEEE, December 2009.

[114] W Armstrong, S McGregor, J Yaggie, J Bailey, S Johnson, A Goin, and S Kelly. Reliability of mechanomyography and triaxial accelerometry in the assessment of balance. *Journal of electromyography and kinesiology*, 20(4), August 2010.

[115] S Tian, Y Liu, L Li, W Fu, and C Peng. Mechanomyography is more sensitive than EMG in detecting age-related sarcopenia. *Journal of biomechanics*, 43(3), February 2010.

[116] E Krueger, E Scheeren, G Nogueira-Neto, V da S N Button, and P Nohama. Correlation between mechanomyography features and passive movements in healthy and paraplegic subjects. In *IEEE EMBS, 2011*, January 2011.

[117] Y Geng, L Chen, L Tian, and G Li. Comparison of Electromyography and Mechanomyogram in Control of Prosthetic System in Multiple Limb Positions. In *IEEE-EMBS International Conference on Biomedical and Health Informatics*, volume 25, 2012.

[118] J Silva, T Chau, S Naumann, and W Heim. Systematic characterisation of silicon-embedded accelerometers for mechanomyography. *Medical & Biological Engineering & Computing*, 41(3), 2003.

[119] M Antonelli, P Zobel, and J Giacomin. Use of MMG signals for the control of powered orthotic devices: development of a rectus femoris measurement protocol. *Assistive technology : the official journal of RESNA*, 21(1), January 2009.

[120] K Shima and T Tsuji. An MMG-based human-assisting manipulator using acceleration sensors. In *IEEE International Conference on Systems, Man and Cybernetics*, number October, San Antonio, Texas, USA, 2009.

[121] F Mokaya, C Kuo, and P Zhang. MARS: a muscle activity recognition system using inertial sensors. In *Proceedings of the 11th international conference on Information Processing in Sensor networks*, 2012.

[122] T Suzuki, N Fukano, O Kitajima, S Saeki, and S Ogawa. Normalization of acceleromyographic train-of-four ratio by baseline value for detecting residual neuromuscular block. *British journal of anaesthesia*, 96(1), January 2006.

[123] Y Yoshitake, H Ue, M Miyazaki, and T Moritani. Assessment of lower-back muscle fatigue using electromyography, mechanomyography, and near-infrared spectroscopy. *European Journal of Applied Physiology*, 84(3), March 2001.

[124] J Marusiak, A Jaskólska, E Jarocka, W Najwer, K Kisiel-Sajewicz, and A Jaskólski. Electromyography and mechanomyography of elbow agonists and antagonists in Parkinson disease. *Muscle & Nerve*, 40(2), August 2009.

[125] A Posatskiy and T Chau. Design and evaluation of a novel microphone-based mechanomyography sensor with cylindrical and conical acoustic chambers. *Medical Engineering & Physics*, 34(8), January 2012.

[126] J Silva, T Chau, and S Naumann. Optimization of the signal-to-noise ratio of silicon-embedded microphones for mechanomyography. In *Canadian Conference on Electrical and Computer Engineering*, number Mvc, 2003.

[127] N Alves and T Chau. Uncovering patterns of forearm muscle activity using multi-channel mechanomyography. *Journal of electromyography and kinesiology*, 20(5), October 2010.

[128] D Barry, J Leonard, A Gitter, and R Ball. Acoustic myography as a control signal for an externally powered prosthesis. *Archives of physical medicine and rehabilitation*, 67(4), 1986.

[129] N Alves, T Falk, and T Chau. A novel integrated mechanomyogram-vocalization access solution. *Medical Engineering & Physics*, 32(8), October 2010.

[130] M Stokes and P Dalton. Acoustic myographic activity increases linearly up to maximal voluntary isometric force in the human quadriceps muscle. *Journal of the neurological sciences*, 101, 1991.

[131] F Esposito, C Orizio, and A Veicsteinas. Electromyogram and mechanomyogram changes in fresh and fatigued muscle during sustained contraction in men. *European journal of applied physiology and occupational physiology*, 78(6), November 1998.

[132] T Evetovich, T Housh, J Stout, G Johnson, D Smith, and K Ebersole. Mechanomyographic responses to concentric isokinetic muscle contractions. *European journal of applied physiology and occupational physiology*, 75(2), January 1997.

[133] D McAndrew, M Gorelick, and J Brown. Muscles within muscles: a mechanomyographic analysis of muscle segment contractile properties within human gluteus maximus. *Journal of Musculoskeletal Research*, 10(1), 2006.

[134] A Posatskiy. The effects of motion artifact on mechanomyography: A comparative study of microphones and accelerometers. *Journal of Electromyography and Kinesiology*, 22(2), 2012.

[135] J Silva and T Chau. Coupled microphone-accelerometer sensor pair for dynamic noise reduction in MMG signal recording. *Electronics Letters*, 39(21), 2003.

[136] J Silva, W Heim, and T Chau. A self-contained, mechanomyography-driven externally powered prosthesis. *Archives of physical medicine and rehabilitation*, 86(10), October 2005.

[137] M Cifrek, V Medved, S Tonković, and S Ostojić. Surface EMG based muscle fatigue evaluation in biomechanics. *Clinical Biomechanics*, 24(4):327–340, 2009.

[138] R Edwards, D Hill, D Jones, and P Merton. Fatigue of long duration in human skeletal muscle after exercise. *The Journal of physiology*, 272(3), November 1977.

[139] A Islam, K Sundaraj, R Ahmad, N Ahamed, and A Ali. Mechanomyography Sensor Development, Related Signal Processing, and Applications: A Systematic Review. *IEEE Sensors Journal*, 13(7), July 2013.

[140] A Islam, K Sundaraj, R Ahmad, S Sundaraj, N Ahamed, and A Ali. Analysis of Crosstalk in the Mechanomyographic Signals Generated by Forearm Muscles During Different Wrist Postures. *Muscle & Nerve*, 2014.

[141] T Beck, T Housh, J Cramer, J Weir, G Johnson, J Coburn, M Malek, and M Mielke. Mechanomyographic amplitude and frequency responses during dynamic muscle actions: a comprehensive review. *BioMedical Engineering OnLine*, 4(1), January 2005.

[142] M Malek and J Coburn. The utility of electromyography and mechanomyography for assessing neuromuscular function: a noninvasive approach. *Physical medicine and rehabilitation clinics of North America*, 23(1), February 2012.

[143] R Escamilla, N Zheng, T Macleod, W Brent Edwards, R Imamura, A Hreljac, G Fleisig, K Wilk, C Moorman, and J Andrews. Patellofemoral joint force and stress during the wall squat and one-leg squat. *Medicine and Science in Sports and Exercise*, 41(2):879–888, 2009.

[144] D Sanderson, P Martin, G Honeyman, and J Keefer. Gastrocnemius and soleus muscle length, velocity, and EMG responses to changes in pedalling cadence. *Journal of Electromyography and Kinesiology*, 16(6):642–649, 2006.

[145] M Jamal. Signal Acquisition Using Surface EMG and Circuit Design Considerations for Robotic Prosthesis. In *Computational Intelligence in Electromyography Analysis - A Perspective on Current Applications and Future Challenges*, chapter 18, pages 427–448. INTECH, 2012.

[146] J Silva, W Heim, and T Chau. MMG-based classification of muscle activity for prosthesis control. In *IEEE EMBS, 2004*, volume 2, January 2004.

[147] Y Hong-liu, Z Sheng-nan, and H Jia-hua. MMG signal and its applications in prosthesis control. In *International Convention on Rehabilitation Engineering & Assistive Technology*, 2010.

[148] N Alves and T Chau. Automatic detection of muscle activity from mechanomyogram signals: a comparison of amplitude and wavelet-based methods. *Physiological measurement*, 31(4), April 2010.

[149] N Alves and T Chau. Vision-based segmentation of continuous mechanomyographic grasping sequences for training multifunction prostheses. In *IEEE EMBS, 2006*, January 2006.

[150] A Grossman, J Silva, and T Chauz. Functional mapping of multiple mechanomyographic signals to hand kinematics. In *Canadian Conference on Electrical and Computer Engineering*, 2004.

[151] Y Suzuki, S Moromugi, T Tanaka, S Kaneko, and M Feng. Soft Sensor Suits as Man-Machine Interface for Wearable Power Amplifier. In *2005 IEEE International Conference on Systems, Man and Cybernetics*, volume 2. Ieee, 2005.

[152] S Fara, C Vikram, C Gavriel, and A Faisal. Robust, ultra low-cost MMG system with brain-machine-interface applications. In *2013 6th International IEEE/EMBS Conference on Neural Engineering (NER)*. Ieee, November 2013.

[153] T Fuchs-Buder, C Claudius, L Skovgaard, L Eriksson, R Mirakhur, and J Viby-Mogensen. Good clinical research practice in pharmacodynamic studies of neuromuscular blocking agents II: the Stockholm revision. *Acta anaesthesiologica Scandinavica*, 51(7), August 2007.

[154] A Xiong, Y Chen, X Zhao, J Han, and G Liu. A novel HCI based on EMG and IMU. In *2011 IEEE International Conference on Robotics and Biomimetics*, pages 2653–2657, 2011.

[155] C Gavriel and A Faisal. A Comparison of Day-Long Recording Stability and Muscle Force Prediction between BSN-Based Mechanomyography and Electromyography. In *2014 11th International Conference on Wearable and Implantable Body Sensor Networks*. Ieee, June 2014.

[156] Q Meng, B Li, and H Holstein. Recognition of human periodic movements from unstructured information using a motion-based frequency domain approach. *Image and Vision Computing*, 24(8):795–809, 2006.

[157] D Rodríguez-Martín, C Pérez-López, A Samà, J Cabestany, and A Català. A wearable inertial measurement unit for long-term monitoring in the dependency care area. *Sensors (Basel, Switzerland)*, 13(10):14079–14104, 2013.

[158] C Orizio, R Perini, B Diemont, M Maranzana Figini, and A Veicsteinas. Spectral analysis of muscular sound during isometric contraction of biceps brachii. *Journal of applied physiology (Bethesda, Md. : 1985)*, 68, 1990.

[159] J Perry and J Burnfield. Ankle-Foot Complex. In *Gait Analysis: Normal and Pathological Function*, chapter 4, page 59. SLACK Incorporated, second edition, 2010.

[160] J Perry and J Burnfield. *Gait Analysis: Normal and Pathological Function*. SLACK Incorporated, second edition, 2010.

[161] T Lee, J Shirr, and D Cho. Position estimation for mobile robot using in-plane 3-axis IMU and active beacon. In *IEEE International Symposium on Industrial Electronics*, pages 1956–1961, 2009.

[162] A Kim and M Golnaraghi. Initial calibration of an inertial measurement unit using an optical position tracking system. In *Position Location and Navigation ...*, pages 96–101, 2004.

[163] F Caron, E Duflos, D Pomorski, and P Vanheeghe. GPS/IMU data fusion using multisensor Kalman filtering: Introduction of contextual aspects. *Information Fusion*, 7(2):221–230, 2006.

[164] O Lammert, F Jorgensen, and N Einer-Jensen. Accelerometermyography (AMG) I: method for measuring mechanical vibrations from isometrically contracted muscles. *Biomechanics*, A:152–156, 1976.

[165] M Zwarts and M Keidel. Relationship between electrical and vibratory output of muscle during voluntary contraction and fatigue. *Muscle & nerve*, 14(8):756–761, 1991.

[166] B Maton, M Petitjean, and J Cnockaert. Phonomyogram and electromyogram relationships with isometric force reinvestigated in man. *European journal of applied physiology and occupational physiology*, 60(3):194–201, 1990.

[167] A Ashour. Relationship between isometric muscle force and surface EMG of wrist muscles at different shoulder and elbow angles. *Journal of American Science*, 10(5):26–34, 2014.

[168] K Akataki, K Mita, and M Watakabe. Electromyographic and mechanomyographic estimation of motor unit activation strategy in voluntary force production. *Electromyography and clinical neurophysiology*, 44(8):489–496, 2004.

[169] E Ryan, T Beck, T Herda, M Hartman, J Stout, T Housh, and J Cramer. Mechanomyographic amplitude and mean power frequency responses during isometric ramp vs. step muscle actions. *Journal of Neuroscience Methods*, 168(2):293–305, 2008.

[170] P Dalton and M Stokes. Acoustic myography reflects force changes during dynamic concentric and eccentric contractions of the human biceps brachii muscle. *European Journal of Applied Physiology and Occupational Physiology*, 63(6):412–416, 1991.

[171] M Petitjean, B Maton, and J Cnockaert. Evaluation of human dynamic contraction by phonomyography. *Journal of applied physiology*, 73(6):2567–2573, 1992.

[172] P Dalton and M Stokes. Frequency of acoustic myography during isometric contraction of fresh and fatigued muscle and during dynamic contractions. *Muscle & nerve*, 16(3):255–261, 1993.

[173] Seniam. Recommendations for sensor locations on individual muscles. [Online] `http://seniam.org/sensor_location.htm`.

[174] J Evans. *Straightforward Statistics for the Behavioral Sciences*. Brooks/Cole Pub Co, 1995.

[175] T Beck. Surface mechanomyographic responses to muscle fatigue. In *Applications of Mechanomyography for Examining Muscle Function*, chapter 3. 2010.

[176] C Orizio, R Perini, B Diemont, and A Veicsteinas. Muscle sound and electromyogram spectrum analysis during exhausting contractions in man. *European Journal of Applied Physiology and Occupational Physiology*, 65(1):1–7, 1992.

[177] A Blangsted, P Vedsted, G Sjø gaard, and K Sø gaard. Intramuscular pressure and tissue oxygenation during low-force static contraction do not underlie muscle fatigue. *Acta Physiologica Scandinavica*, 183(4):379–388, 2005.

[178] P Madeleine, L Jø rgensen, K Sø gaard, L Arendt-Nielsen, and G Sjø gaard. Development of muscle fatigue as assessed by electromyography and mechanomyography during continuous and intermittent low-force contractions: Effects of the feedback mode. *European Journal of Applied Physiology*, 87(1):28–37, 2002.

[179] P Madeleine, H Ge, A Jaskólska, D Farina, A Jaskölski, and L Arendt-Nielsen. Spectral moments of mechanomyographic signals recorded with accelerometer and microphone during sustained fatiguing contractions. *Medical and Biological Engineering and Computing*, 44(4):290–297, 2006.

[180] Y Itoh, K Akataki, K Mita, M Watakabe, and K Itoh. Time-Frequency Analysis of Mechanomyogram during Sustained Contractions with Muscle Fatigue. *Systems and Computers in Japan*, 35(1):26–36, 2004.

[181] C Orizio, R Perini, and a Veicsteinas. Changes of muscular sound during sustained isometric contraction up to exhaustion. *Journal of applied physiology (Bethesda, Md. : 1985)*, 66(4):1593–1598, 1989.

[182] M Goldenberg, H Yack, F Cerny, and H Burton. Acoustic myography as an indicator of force during sustained contractions of a small hand muscle. *Journal of applied physiology (Bethesda, Md. : 1985)*, 70(1):87–91, 1991.

[183] M Kouzaki, M Shinohara, and T Fukunaga. Non-uniform mechanical activity of quadriceps muscle during fatigue by repeated maximal voluntary contraction in humans. *European Journal of Applied Physiology and Occupational Physiology*, 80(1):9–15, 1999.

[184] W Herzog, Y Zhang, M Vaz, A Guimaraes, and C Janssen. Assessment of muscular fatigue using vibromyography. *Muscle & Nerve*, 17(10):1156–1161, 1994.

[185] C Orizio, F Esposito, E Alfonsi, and F Umana. Surface mechanomyogram refects the changes in the mechanical properties of muscle at fatigue. *European journal of applied physiology and occupational physiology*, 80(4):276–284, 1999.

[186] A Blangsted, G Sjø gaard, P Madeleine, H Olsen, and K Sø gaard. Voluntary low-force contraction elicits prolonged low-frequency fatigue and changes in surface electromyography and mechanomyography. *Journal of Electromyography and Kinesiology*, 15(2):138–148, 2005.

[187] M Vaz, Y Zhang, W Herzog, A Guimaraes, and B MacIntosh. The behavior of rectus femoris and vastus lateralis during fatigue and recovery: an electromyographic and vibromyographic study. *Electromyography and clinical neurophysiology*, 36(4):221–230, 1996.

[188] J Isear, J Erickson, and T Worrell. EMG analysis of lower extremity muscle recruitment patterns during an unloaded squat. *Medicine and science in sports and exercise*, 29(4):532–539, 1997.

[189] P Schaub and T Worrell. EMG activity of six muscles and VMO:VL ratio determination during a maximal squat exercise. *Journal of sport rehabilitation*, 4(Champaign):195–202, 1995.

[190] S Lynn and G Noffal. Lower Extremity Biomechanics During a Regular and Counterbalanced Squat, 2012.

[191] S Gryzlo, R Patek, M Pink, and J Perry. Electromyographic analysis of knee rehabilitation exercises. *The Journal of orthopaedic and sports physical therapy*, 20(1):36–43, 1994.

[192] C Sousa, J Jamacy, D Ferreira, A Catarina, L Medeiros, A Carvalho, R Pereira, D Guedes, and J Alencar. Electromyograhic activity in squatting at 40° , 60° and 90° knee flexion positions. *Revista Brasileira de Medicina do Esporte*, 13(5):280–286, 2007.

[193] S Jiang, L Dai, and L Jiang. Osteoporosis after spinal cord injury. *Osteoporosis international : a journal established as result of cooperation between the European Foundation for Osteoporosis and the National Osteoporosis Foundation of the USA*, 17(2):180–192, 2006.

[194] L Giangregorio and N McCartney. Bone loss and muscle atrophy in spinal cord injury: Epidemioloqy, fracture prediction, and rehabilitation strategies. *The Journal of Spinal Cord Medicine*, 29(5):489–500, 2006.

[195] M Dauty, B Perrouin Verbe, Y Maugars, C Dubois, and J Mathe. Supralesional and sublesional bone mineral density in spinal cord-injured patients. *Bone*, 27(2):305–309, 2000.

[196] A Draghici and S Shefelbine. Assessing Kinetics of FES Rowing in Spinal Cord Injury Patients. In *Bioengineering Conference (NEBEC), 2014 40th Annual Northeast*, pages 1–2, 2014.

[197] D Hettinga and B Andrews. The feasibility of functional electrical stimulation indoor rowing for high-energy training and sport. *Neuromodulation*, 10(3):291–297, 2007.

[198] D Hettinga and B Andrews. Oxygen Consumption during Functional Electrical Stimulation-Assisted Exercise in Persons with Spinal Cord Injury. *Sports Medicine*, 38(10):825–838, 2008.

[199] J Taylor, G Picard, and J Widrick. Aerobic Capacity With Hybrid FES Rowing in Spinal Cord Injury: Comparison With Arms-Only Exercise and Preliminary Findings With Regular Training. *Physical Medicine and Rehabilitation*, 3(9):817–824, 2011.

[200] T Gordon and J Mao. Muscle atrophy and procedures for training after spinal cord injury. *Physical therapy*, 74(1):50–60, 1994.

[201] J Winslow, P Jacobs, and D Tepavac. Fatigue compensation during FES using surface EMG. *Journal of Electromyography and Kinesiology*, 13(6):555–568, 2003.

[202] N Chesler and W Durfee. Surface EMG as a fatigue indicator during FES-induced isometric muscle contractions. *Journal of Electromyography and Kinesiology*, 7(1):27–37, 1997.

[203] E Scheeren, G Nogueira-Neto, E Krueger-Beck, V Button, and P Nohama. Investigation of Muscle Behavior During Different Functional Electrical Stimulation Profiles Using Mechanomyography. In *Engineering in Medicine and Biology Society (EMBC), 2010 Annual International Conference of the IEEE*, pages 3970–3973, 2010.

[204] E Krueger-Beck, E Scheeren, G Nogueira-Neto, V Button, and P Nohama. Mechanomyographic response during FES in healthy and paraplegic subjects. In *2010 Annual International Conference of the IEEE Engineering in Medicine and Biology Society, EMBC'10*, pages 626–629, 2010.

[205] M Decker, L Griffin, L Abraham, and L Brandt. Alternating stimulation of synergistic muscles during functional electrical stimulation cycling improves endurance in persons with spinal cord injury. *Journal of Electromyography and Kinesiology*, 20(6):1163–1169, 2010.

[206] M Ng, M Pourmajidian, and N Hamzaid. Mechanomyography Sensors for Detection of Muscle Activities and Fatigue during Fes-Evoked Contraction. In *Functional Electrical Stimulation Society Annual Conference (IFESS), 2014 IEEE 19th International*, pages 1–3, 2014.

[207] R Davoodi, B Andrews, G Wheeler, and R Lederer. Development of an indoor rowing machine with manual FES controller for total body exercise in paraplegia. *IEEE Transactions on Neural Systems and Rehabilitation Engineering*, 10(3):197–203, 2002.

[208] OML. Odstock 2 Channel Stimulator Kit. [Online] `http://www.odstockmedical.com/products/odstock-2-channel-stimulator-kit`.

[209] Concept2. Rowing and your Mucles. [Online] `http://www.concept2.com/indoor-rowers/training/muscles-used`.

[210] H Lee, K Kim, J Jeong, M Cheong, and J Shim. Comparison of the adductor pollicis, orbicularis oculi, and corrugator supercilii as indicators of adequacy of muscle relaxation for tracheal intubation. *British Journal of Anaesthesia*, 102(6):869–874, 2009.

[211] B Debaene, C Meistelman, M Beaussier, and A Lienhart. Visual estimation of train-of-four responses at the orbicularis oculi and posttetanic count at the adductor pollicis during intense neuromuscular block. *Anesthesia and analgesia*, 78(4):697–700, 1994.

[212] C McGrath and J Hunter. Monitoring of neuromuscular block. *Continuing Education in Anaesthesia, Critical Care & Pain*, 6(1):7–12, 2006.

[213] M Martin-Flores, R Gleed, K Basher, J Scarlett, L Campoy, and A Kopman. TOF-Watch monitor: Failure to calculate the train-of-four ratio in the absence of baseline calibration in anaesthetized dogs. *British Journal of Anaesthesia*, 108(2):240–244, 2012.

[214] P Larsen, M Gätke, B Fredensborg, H Berg, J Engbaek, and J Viby-Mogensen. Acceleromyography of the orbicularis oculi muscle II: comparing the orbicularis oculi and adductor pollicis muscles. *Acta anaesthesiologica Scandinavica*, 46(9):1131–1136, 2002.

[215] Y Higashi, M Sekimoto, F Horiuchi, T Kodama, T Yuji, T Fujimoto, M Sekine, and T Tamura. Monitoring rehabilitation training for hemiplegic patients by using a tri-axial accelerometer. In *2001 Conference Proceedings of the 23rd Annual International Conference of the IEEE Engineering in Medicine and Biology Society*, volume 2, pages 1472–1474, 2001.

[216] H Kayyali, S Weimer, C Frederick, C Martin, D Basa, J Juguilon, and F Jugilioni. Remotely attended home monitoring of sleep disorders. *Telemedicine journal and e-health : the official journal of the American Telemedicine Association*, 14(4):371–374, 2008.

[217] J Gronley, C Newsam, S Mulroy, S Rao, J Perry, and M Helm. Electromyographic and kinematic analysis of the shoulder during four activities of daily living in men with C6 tetraplegia. *Journal of rehabilitation research and development*, 37(4):423–432, 2000.

[218] H He, K Kiguchi, and E Horikawa. A Study on Lower-Limb Muscle Activities during Daily Lower-Limb Motions. *International Journal of Bioelectromagnetism*, 9(2):79–84, 2007.

[219] N Wang, E Ambikairajah, N Lovell, and B Celler. Accelerometry based classification of walking patterns using time-frequency analysis. *Conference proceedings : ... Annual International Conference of the IEEE Engineering in Medicine and Biology Society. IEEE Engineering in Medicine and Biology Society. Conference*, 2007:4899–4902, 2007.

[220] F Wang, E Stone, M Skubic, J Keller, C Abbott, and M Rantz. Toward a passive low-cost in-home gait assessment system for older adults. *IEEE Journal of Biomedical and Health Informatics*, 17(2):346–355, 2013.

[221] B Tessendorf, F Gravenhorst, B Arnrich, and G Troster. An IMU-based sensor network to continuously monitor rowing technique on the water. *Proceedings of the 2011 7th International Conference on Intelligent Sensors, Sensor Networks and Information Processing, ISSNIP 2011*, pages 253–258, 2011.

[222] H Stolze, G Petersen, J Raethjen, R Wenzelburger, and G Deuschl. The gait disorder of advanced essential tremor. *Brain : a journal of neurology*, 124(11):2278–2286, 2001.

[223] H von Schroeder, R Coutts, P Lyden, E Billings, and V Nickel. Gait parameters following stroke: a practical assessment. *Journal of rehabilitation research and development*, 32(1):25–31, 1995.

[224] M Schwartz, A Rozumalski, and J Trost. The effect of walking speed on the gait of typically developing children. *Journal of Biomechanics*, 41(8):1639–1650, 2008.

[225] C Kirtley and M W Whittle. Influence of walking speed on gait parameters. *Journal of biomedical engineering*, 7:282–288, 1985.

[226] C BenAbdelkader, R Cutler, and L Davis. Stride and cadence as a biometric in automatic person identification and verification. In *Proceedings - 5th IEEE International Conference on Automatic Face Gesture Recognition, FGR 2002*, pages 372–377, 2002.

[227] D Sutherland, R Olshen, L Cooper, and S Woo. The development of mature gait. *The Journal of Bone and Joint Surgery*, 62:336–353, 1980.

[228] C Kim and S Son. Comparison of Spatiotemporal Gait Parameters between Children with Normal Development and Children with Diplegic Cerebral Palsy. *Journal of Physical Therapy Science*, 26:1317–1319, 2014.

[229] D Damiano and M Abel. Functional outcomes of strength training in spastic cerebral palsy. *Archives of Physical Medicine and Rehabilitation*, 79(2):119–125, 1998.

[230] C Andersson and E Mattsson. Adults with cerebral palsy: a survey describing problems, needs, and resources, with special emphasis on locomotion. *Developmental medicine and child neurology*, 43(2):76–82, 2001.

[231] M Abdoli-Eramaki, C Damecour, J Christenson, and J Stevenson. The effect of perspiration on the sEMG amplitude and power spectrum. *Journal of Electromyography and Kinesiology*, 22(6):908–913, 2012.

[232] J Perry and J Burnfield. Knee. In *Gait Analysis: Normal and Pathological Function*, chapter 5, page 89. SLACK Incorporated, second edition, 2010.

[233] D Gouwanda and S Arosha Senanayake. Identifying gait asymmetry using gyroscopes-A cross-correlation and Normalized Symmetry Index approach. *Journal of Biomechanics*, 44(5):972–978, 2011.

[234] M Mace, K Abdullah-al Mamun, A Naeem, L Gupta, S Wang, and R Vaidyanathan. A heterogeneous framework for real-time decoding of bioacoustic signals: Applications to assistive interfaces and prosthesis control. *Expert Systems with Applications*, 40(13), October 2013.

[235] A Lapre and F Sup. Simulation of a slope adapting ankle prosthesis provided by semi-active damping. In *Proceedings of the Annual International Conference of the IEEE Engineering in Medicine and Biology Society, EMBS*, pages 587–590, 2011.

[236] A Harvey-cook. A Wearable Device to Measure Foetal Movements. Technical report, Imperial College London, 2013.

[237] A Olesen and J Svare. Decreased fetal movements: background, assessment, and clinical management. *Acta obstetricia et gynecologica scandinavica*, 83, 2004.

[238] J Pearson and J Weaver. Fetal activity and fetal wellbeing: an evaluation. *British medical journal*, 1(May), 1976.

[239] W Rayburn. Clinical significance of perceptible fetal motion. *American journal of obstetrics and gynecology*, 138(2), 1980.

[240] O O'Sullivan, G Stephen, E Martindale, and A Heazell. Predicting poor perinatal outcome in women who present with decreased fetal movements. *Journal of obstetrics and gynaecology : the journal of the Institute of Obstetrics and Gynaecology*, 29(8), November 2009.

[241] I Nijhuis, J ten Hof, E Mulder, J Nijhuis, H Narayan, D Taylor, and G Visser. Fetal heart rate in relation to its variation in normal and growth retarded fetuses. *European Journal of Obstetrics & Gynecology and Reproductive Biology*, 89(1), March 2000.

[242] J DiPietro, M Bornstein, K Costigan, E Pressman, C Hahn, K Painter, B Smith, and L Yi. What does fetal movement predict about behavior during the first two years of life? *Developmental psychobiology*, 40(4), May 2002.

[243] J Hall, K Aldinger, and K Tanaka. Amyoplasia revisited. *American journal of medical genetics. Part A*, 164A(3), March 2014.

[244] E Sadovsky and H Yaffe. Daily fetal movement recording and fetal prognosis. *Obstetrics & Gynecology*, 41(6), 1973.

[245] K Hertogs, A Roberts, and D Cooper. Maternal perception of fetal motor activity. *British medical journal*, 2(November), 1979.

[246] Z Hijazi, S Callan, and C East. Maternal perception of foetal movement compared with movement detected by real-time ultrasound: an exploratory study. *The Australian & New Zealand journal of obstetrics & gynaecology*, 50(2), April 2010.

[247] J Froen, A Heazell, J Tveit, E Saastad, R Fretts, and V Flenady. Fetal movement assessment. *Seminars in perinatology*, 32(4), August 2008.

[248] I Donald, J Macvicar, and T Brown. Investigation of abdominal masses by pulsed ultrasound. *The Lancet*, 271(7032), 1958.

[249] A M Flynn, J Kelly, H Mansfield, P Needham, M O'Conor, and O Viegas. A randomized controlled trial of non-stress antepartum cardiotocography. *British journal of obstetrics and gynaecology*, 89(6):427–433, 1982.

[250] E Graatsma, B Jacod, L van Egmond, E Mulder, and G Visser. Fetal electrocardiography: feasibility of long-term fetal heart rate recordings. *BJOG : an international journal of obstetrics and gynaecology*, 116(2), January 2009.

[251] J Pieri, J Crowe, and B Hayes-Gill. Compact long-term recorder for the transabdominal foetal and maternal electrocardiogram. *Medical & Biological Engineering & Computing*, 39, 2001.

[252] F Kovács, M Torok, and I Habermajer. A rule-based phonocardiographic method for long-term fetal heart rate monitoring. *IEEE Transactions on Biomedical Engineering*, 47(1), 2000.

[253] F Kovacs and C Horváth. Long-term phonocardiographic fetal home monitoring for telemedicine systems. In *Engineering in Medicine ...*, number 1, 2006.

[254] M Cesarelli, M Ruffo, M Romano, and P Bifulco. Simulation of foetal phonocardiographic recordings for testing of FHR extraction algorithms. *Computer methods and programs in biomedicine*, 107(3), September 2012.

[255] R Govindan, S Vairavan, U Ulusar, J Wilson, S McKelvey, H Preissl, and H Eswaran. A novel approach to track fetal movement using multi-sensor magnetocardiographic recordings. *Annals of biomedical engineering*, 39(3), March 2011.

[256] P Kintraia, M Zarnadze, N Kintraia, and I Kashakashvili. Development of daily rhythmicity in heart rate and locomotor activity in the human fetus. *Journal of circadian rhythms*, 3:5, 2005.

[257] C Kähler and B Grimm. The application of fetal magnetocardiography (FMCG) to investigate fetal arrhythmias and congenital heart defects (CHD). *Prenatal ...*, 21(July 2000), 2001.

[258] M Peters, J Crowe, and J Piéri. Monitoring the fetal heart non-invasively: a review of methods. *Journal of perinatal ...*, 29(5), 2001.

[259] E Ryo, K Nishihara, S Matsumoto, and H Kamata. A new method for long-term home monitoring of fetal movement by pregnant women themselves. *Medical Engineering & Physics*, 34(5), June 2012.

[260] E Ryo, H Kamata, and M Seto. Decreased fetal movements at home were recorded by a newly developed fetal movement recorder in a case of a non-reassuring fetal status. *Journal of Maternal-Fetal and Neonatal Medicine*, 27(15):1604–1606, 2014.

[261] M Khlif, B Boashash, S Layeghy, T Ben-Jabeur, M Mesbah, C East, and P Colditz. Time-frequency characterization of tri-axial accelerometer data for fetal movement detection. In *2011 IEEE International Symposium on Signal Processing and Information Technology (ISSPIT)*. Ieee, December 2011.

[262] B Boashash, M Khlif, T Ben-Jabeur, C East, and P Colditz. Passive detection of accelerometer-recorded fetal movements using a time-frequency signal processing approach. *Digital Signal Processing: A Review Journal*, 25(1):134–155, 2014.

[263] A Zuckerwar, R Pretlow, J Stoughton, and D Baker. Development of a piezopolymer pressure sensor for a portable fetal heart rate monitor. *IEEE transactions on bio-medical engineering*, 40(9), September 1993.

[264] K Nishihara, S Horiuchi, H Eto, and M Honda. A long-term monitoring of fetal movement at home using a newly developed sensor: an introduction of maternal micro-arousals evoked by fetal movement during maternal sleep. *Early human development*, 84(9), September 2008.

[265] A Jiménez-González and C James. Extracting sources from noisy abdominal phonograms: a single-channel blind source separation method. *Medical & Biological Engineering & Computing*, 47(6), June 2009.

[266] A Jiménez-González and C James. On the interpretation of the independent components underlying the abdominal phonogram: a study of their physiological relevance. *Physiological measurement*, 33(2), January 2012.

[267] M Ruffo, M Cesarelli, M Romano, P Bifulco, and A Fratini. An algorithm for FHR estimation from foetal phonocardiographic signals. *Biomedical Signal Processing and Control*, 5(2), April 2010.

[268] K Nelson and J Dambrosia. Uncertain value of electronic fetal monitoring in predicting cerebral palsy. *New England Journal ...*, 334(10), 1996.

[269] U Schneider and J Haueisen. Prenatal diagnosis of a long QT syndrome by fetal magnetocardiography in an unshielded bedside environment. *Prenatal ...*, 25(8), August 2005.

[270] M Taylor and M Smith. Non-invasive fetal electrocardiography in singleton and multiple pregnancies. *BJOG: An International Journal of Obstetrics and Gynaecology*, 110(July), 2003.

A

Appendix: Non-Muscular Acoustic Application

Contents

A.1 Introduction **164**

A.2 Foetal Activity and Pregnancy Monitoring **164**

A.3 Summary **172**

A.1 Introduction

Through development of the work presented in the previous chapters, it was recognised that the same means of collecting vibrations emitted from contracting muscle could be used to monitor other physiological activities which produce oscillations or sound. Early pilot studies have indicated that acoustic sensors can capture vibrations from foetal movement[236], which correlates with maternal perception. It was recognised that foetal activity could be monitored using the technology developed as part of this work, as both muscle contractions and foetal kicks, for example, fall within a similar low frequency (between 1 and 100 Hz).

This chapter continues the pilot study mentioned above in the development of a wearable device to monitor foetal activity. Using acoustic sensors and inertial measurement units, foetal movement has been monitored and tracked through non-invasive techniques.

A.2 Foetal Activity and Pregnancy Monitoring

Foetal monitoring has become an increasing field of research due to links correlating foetal movement, or lack thereof, with prenatal development[237–239]. Problems identified include stillbirth and in-utero growth restriction[240,241], behaviour and temperament issues[242], and skeletal disorders such as amyoplasia and hip dysplasia[243].

While cessation of a foetal heart rate is an obvious sign of issues, a decrease in foetal movement has been found to be a good indication of early distress which may not be presented with a change in heartbeats[244]. Expecting mothers are often asked to count perceivable foetal activity in order to reduce mortality brought on through lack of movement. Accuracy in mother perception is questionable, with some literature stating a high tolerance to detecting movements[245], whereas others showing a low tolerance[246]. Furthermore, research has yet to determine a quantitative alarm limit and therefore it has been suggested that counting be discouraged[247].

Non-invasive foetal monitoring by means of obstetric ultrasonography has been in use since the late 1950's where it first became used for monitoring foetal health and gender[248]. Two dimensional ultrasound, and in later years three-dimensional, is able to display images of the foetus in real-time, allowing clinicians to see the unborn child. With the addition of the Doppler Effect, ultrasonography can monitor blood vessels, such as the carotid artery, which can determine heart rate of the foetus.

Although accurate, ultrasound is predominantly a short term monitoring device due to its use of handheld linear transducers, water-based gels to form a close impedance match between the transducer and skin, and large scanning systems (Fig. A.1). Other, more



Figure A.1: Image of a Samsung UGEO WS80A medical ultrasound scanner. Although semi-portable the device can only be used by trained professionals and cannot be used in a home environment. Image taken at the Queen Charlotte's & Chelsea Hospital with permission.

portable options, include Electrocardiography (ECG) which monitors the electrical activity from contracting cardiac muscle to determine Foetal Heart Rate (FHR), magnetocardiogram which calculates heart rate from the magnetic field also produced from the electrical activity of the heart, and phonocardiography which listens for heart sounds produced by the heart valves opening and closing. However, cardiotocography (CTG), a method which monitors both foetal heart rate and uterine contractions, remains the most clinically used method outside of ultrasound[237,249]

In situations where prolonged or pervasive collection is necessary, these technologies have been further developed in order to monitor differing aspects of foetal health for long periods of time. ECG has been used in some instances to achieve recording times of up to 24 hours[250,251], whereas others have opted to use phonocardiograms[252–254], and magnetocardiogram to achieve the same results[255]. Each technology has their own pros and cons, although each have differing gestation times in which they can be used. ECG can be used to monitor the foetus from the second trimester (14 weeks) onwards, whereas magnetocardiogram can produce results from the 20$^{\text{th}}$ week onwards[256–258]. Accelerometers have become to be used in foetal monitoring due to their small size, light weight, and cost, with results exceeding maternal perception[259–262], whereas piezopolymer pressure sensors have also been used[263]. Literature has noted the importance of user operated technology, which does not require calibration or clinician/engineer involvement, for truly long-term applications[253,259,264].

Pervasive applications introduce new issues which are perhaps not evident in static recording situations. Noise and motion artefacts can contaminate and interfere with results, with some

that look similar to physiological activity which could produce false positives. Filtering and rejection of certain data can reduce noise, however, some have opted for more technical algorithms such as independent component analysis (ICA)[265,266] or match filtering[267].

While most applications attempt to determine heart rate or baseline physiological responses like breathing, others attempt further data analysis to predict conditions such as cerebral palsy[268], or diagnose anomalies like long QT syndrome[269]. Other applications have monitored foetal movement during maternal sleep in order to reduce sleep disturbances[264], and the detection of multiple foetuses in the case of twins or triplets[270].

While work that monitors both mother and foetal activity for prolonged periods is minimal, some literature does exist. Pieri *et al* monitored both mother and foetal ECG over 24 hours and reported accuracies of 65%[251], whereas Ryo *et al* have collected data for a similar length of time, although over night while the mothers sleep[259,260]. Ryo's results showed a high accuracy of foetal detection against ultrasound validation, however, they concluded their recorder had a higher sensitivity than maternal perception, but less so than ultrasound techniques. Despite high accuracies, both Ryo and Pieri's devices have relied on adhesive sensors which must be placed on the skin by the expecting mother, which limits the pervasive nature of their use.

A.2.1 Research Question and Hypothesis

The work presented here introduces a new device which uses acoustic sensors and an IMU to monitor both mother and foetal activity over a prolonged period of time in a home-based setting. While the acoustic sensors were used to monitor the foetal activity, motion artefacts produced by movement of the mother were removed using information from the IMU. Additionally, a push button was implemented which the mother was to press every time a sensation of foetal activity was detected. Furthermore, the device was designed to be concealable, non-restrictive, and easy to don/doff and use.

It was hypothesized that MMG and inertial data could be used to detect foetal activity. One subject was recruited in this study who was in late stage gestation between 30 and 38 weeks. She was asked to wear the device while at home and for as long as she felt comfortable over the course of three weeks. This research was approved by the Imperial College Research Ethics Committee (ICREC) and written consent was obtained from the subject involved.

A.2.2 Method

The acoustic sensor used in this study was the same as that developed for MMG monitoring. Previous pilot work confirmed that foetal movement had a similarly low frequency to MMG contractions, and that the acoustic sensors developed as part of this work were suitable for foetal monitoring[236]. This study started prior to the design and manufacturing of the Aktiv IMU, therefore an x-IMU, developed by x-IO, was used in lieu of the IMU used in the

other applications of this thesis. The x-IMU contains the same inertial components as the Aktiv, including an accelerometer, gyroscope, and magnetometer, however, no barometer. Bluetooth and on-board (SD card) recording capabilities were available, and measures closely to the Aktiv in size and weight.

The IMU was used to monitor both the mothers movement, using the on-board inertial sensors, while four acoustic sensors monitored the foetal movement and were sampled using the on-board auxiliary port. Fig. A.2 shows the device used, consisting of a Velcro band which wrapped around the mothers waist, the x-IMU, and the acoustic sensors positioned across the abdomen. A push button was implemented which the mother was asked to press whenever she felt a kick. This data was used as a ground truth in data analysis.

The subject was asked to wear the device while relaxing at home. All data collection in this study was while the subject was awake, although future studies intend to monitor during sleep as well.

The band was easy to don and doff, as well as operate which was controlled by a single button which would start and stop data collection. The IMU was sampled at 64 Hz, whereas the acoustic data was sampled at 512 Hz. Despite no literature detailing dangers associated with Bluetooth transmissions, the Bluetooth module was disabled for all use of this study and all data was collected offline onto the SD card provided. All data was collected offline and was processed within MATLAB.

A.2.2.1 Data Pre-Processing

Acoustic sensor data was band-passed using a 1st order Butterworth filter between 2 and 50 Hz and was rectified. The magnitude (4.1) of accelerometer data was calculated and the mean was removed to discard gravity. The magnitude of the acoustic data was calculated using (A.1), where n is the current sample, N is the total number of samples collected, and $AS1$ through $AS4$ are acoustic sensors one to four. Data from the accelerometer, each of the four acoustic sensors, acoustic magnitude, and push button, were windowed into two second, 50% overlapping windows

$$Magnitude = \sum_{n=1}^{N} (AS1_n{}^2 + AS2_n{}^2 + AS3_n{}^2 + AS4_n{}^2)^{0.5} \tag{A.1}$$

To remove motion artefacts produced by mother movement (MM), any windows which contain accelerations that exceed 0.1 g were ignored. Unlike the activity monitoring classification, this application uses the microphone data for classification as opposed to inertial information.

The algorithm process was similar to that used for the activity monitoring classification (Section 6.2). Each of the four microphones had their mean, standard deviation, and power calculated (6.2) resulting in twelve parameters per window. These parameters were processed through a K-means algorithm, sorting data into two clusters: foetal activity and 'other'. The

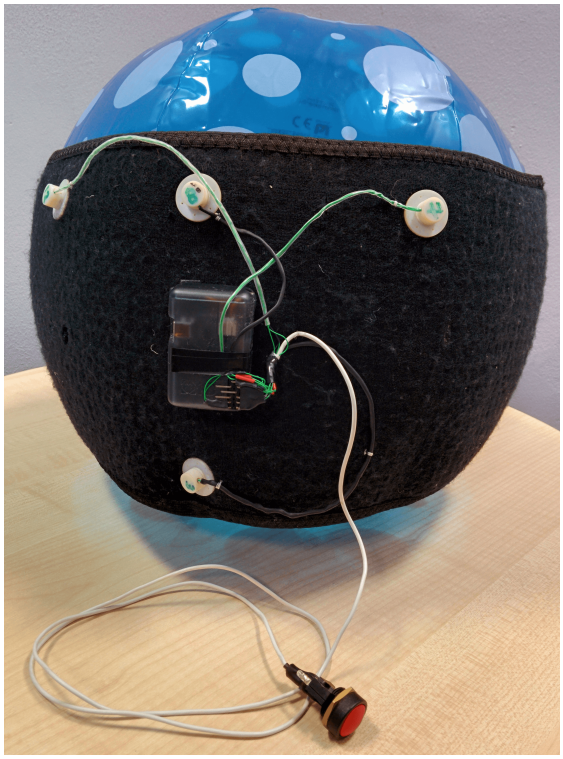


Figure A.2: The prototype pregnancy monitor band consists of a Velcro belt which wraps around the mothers abdomen, an inertial measurement unit (x-IMU), and four acoustic sensors positioned across the mothers abdomen. A push button was used so that the mother could log each kick or movement she detected from the foetus, which was used as validation data for the analysis.

'other' cluster includes stationary data and noise. The cluster with the highest signal power was considered to contain foetal activity, whereas the other cluster was considered to be stationary/foetal noise.

Each window belonged to one of three groups: Foetal activity, stationary/foetal noise, and MM. The former two groups were classified using the K-means method, whereas the latter group was determined using the thresholding accelerometer method mentioned above.

A.2.2.2 Foetal Peaks and Push Button Detection

Looping through each window belonging to the 'foetal activity' group the peaks from the acoustic magnitude data were detected which exceed a threshold of 0.1 V. Due to the 50% overlapping windows, duplicate peaks were detected and removed. Any windows which do not have peaks which satisfy the threshold were reclassified as 'stationary/foetal noise'.

A.2.2.3 Validation

Button press data was processed and the start of each press was used in validation. As with the acoustic data, duplicate presses detected due to the 50% windows were removed. A window of five seconds prior to each button press logged was analysed for any acoustic peak activity, as foetal kicks happen before the mother perception and button press, respectively.

Results were analysed as:

True Positive A button press and a peak were detected within the same five second window. The mother had perceived a kick and the algorithm had recognised one.

True Negative A peak was not detected within the five second period prior to a button press. The mother had perceived a kick but one had not been recognised.

False Positive A peak was recognised but the mother did not perceive one.

A.2.2.4 Algorithm

False negatives were where neither a button nor peak was detected, however, this information was not calculated nor processed in this study. Accuracy of the algorithm was calculated by taking the total number of true positives and dividing it by the total number of button presses. This was represented as a percentage using (A.2).

$$Accuracy\ (\%) = \frac{True\ Positive}{Total\ Button\ Presses} * 100 \tag{A.2}$$

A.2.3 Results and Discussion

During this session the subject collected over a 24 hours worth of data. Results are presented in Table A.1, and an overall accuracy of 85% true positive was achieved. Over 47 separate session, 5159 foetal kicks were detected, whereas the mother perceived 2905 kicks which she recorded with a button press, resulting in 3.4x more activity monitored than perceived.

Fig. A.3 shows the raw results seen from one of the collected trials. The accelerations from mother movement, acoustic data from foetal activity, and button presses denoting the mothers perceptions of foetal activity, can be seen top to bottom respectively. Red shaded backgrounds indicate windows of mother movement, and green shaded backgrounds show windows of detected foetal activity.

This study has recognised foetal movement to a high accuracy, while rejecting movement produced from mother activity. Using low cost and wearable technology, the results suggest this technology could be used in both commercial and clinical monitoring of foetuses to a higher degree than mother perception.

Despite a high accuracy in true positive analysis, this processing method produced a large amount of false positives with 3.4x more foetal kicks detected by the system than the mother. It was believed this was due to:

1. A stronger sensitivity from the sensor when compared to mother perception.
2. The mother missing, forgetting, or pressing the button too late for a correct true positive analysis using this algorithm.

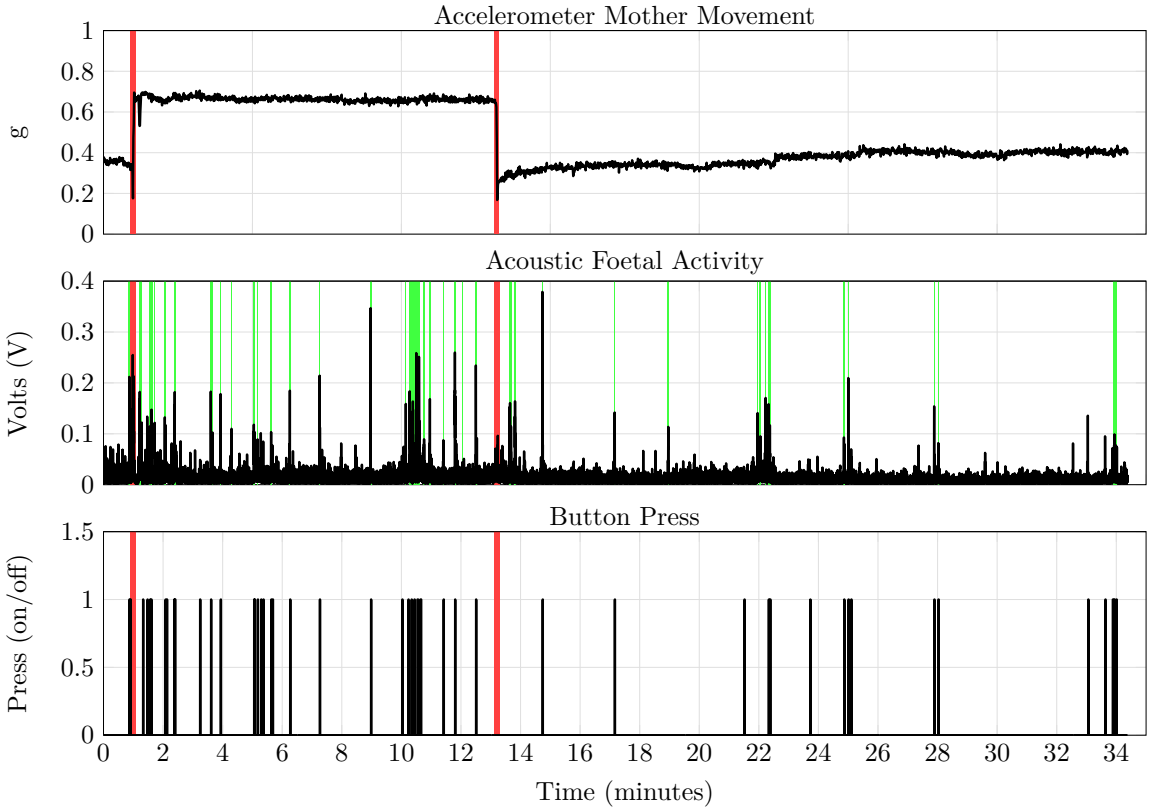


Figure A.3: Figure shows data from the accelerometer, acoustic sensors, and button presses from a subject in their third trimester of pregnancy. Red shaded backgrounds indicate a detected mother movement, whereas green shaded backgrounds contain foetal activity.

Table A.1: Subject results and information on collection parameters.

Number of Sessions	Collection Time (HH:MM;SS)	Number of Foetal Peaks	Number of Button Presses	Mean Difference[a]	Accuracy (%)
47	24:39;51	5159	2905	3.4	85

[a] Mean difference was calculated as the number of foetal kicks divided by the number of button presses per session. The average difference across each session is presented here.

3. Other foetal activity. Aside from foetal movement other activities are likely to have been monitored, such as foetal heart rate, breathing, and hiccups.
4. Mother physiological activity, such as mother heart rate, breathing, or digestive activity.
5. Noise and external disturbances are of course also assumed to have contributed to the higher false positives.

A.2.4 Conclusion

This work has presented a novel and easy to use device for monitoring foetal activity. Results suggest a high accuracy when compared against mother perception and the non-invasive design allows for a prolonged, pervasive collection which does not require clinical assistance or training.

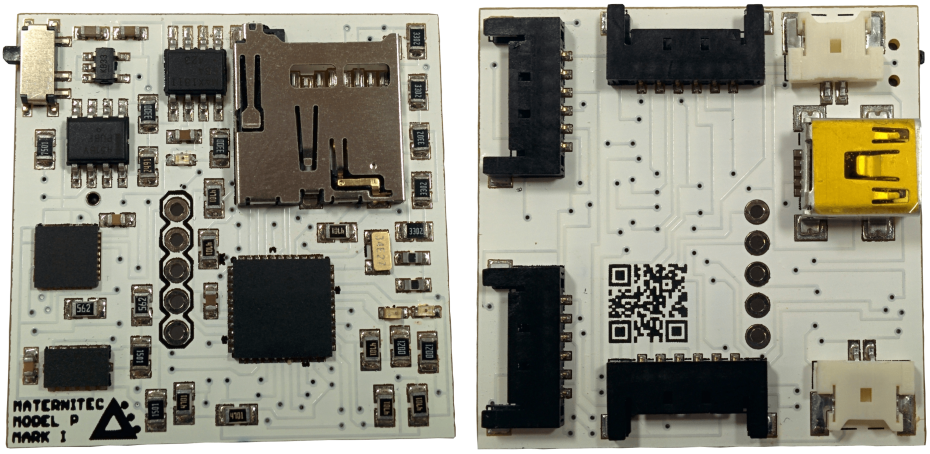


Figure A.4: The Aktiv-P IMU without battery - front (left) and back (right).

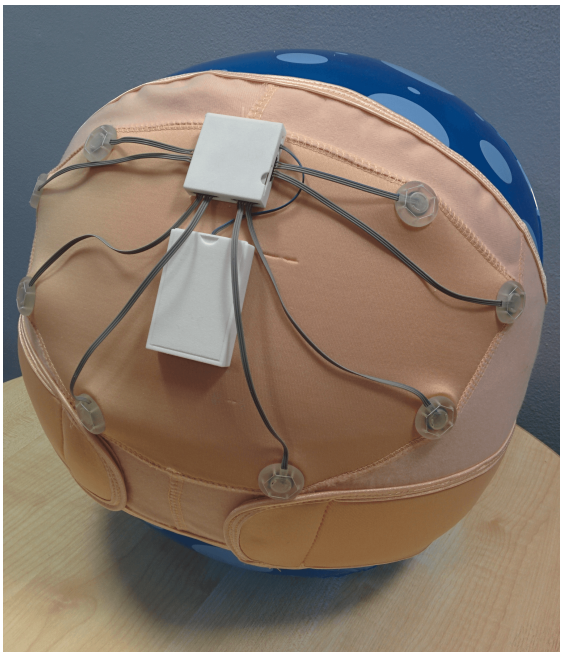


Figure A.5: The redesigned pregnancy monitor uses a specially dedicated pregnancy brace along with a custom made Aktiv-P IMU and a lower profile acoustic sensor.

Future development of this device has already begun, with a custom IMU having already been developed (Fig. A.4), as well as a new prototype design (Fig. A.5). The new IMU (36x36x7 mm (LxWxH)) has just an accelerometer which significantly increases battery life. No Bluetooth module is present, and all data collection is achieved using the SD card port, or transmission via USB. The new prototype also has double the acoustic sensors for additional information on foetal positioning. Future developments in signal processing intend to analyse foetal orientation in the womb, based on kick location estimated through varying acoustic signal magnitudes in the sensor array, as well as more accurate results and fewer false positives.

A.3 Summary

This appendix has shown an alternative use to the technology developed for human motion and muscle monitoring. Through pilot work in foetal monitoring it was recognised that the acoustic sensors used for MMG monitoring were also capable of tracking foetal activity. The study presented here has continued this work and has achieved a wearable device capable of collection in the home environment with an accuracy of 85%.

B

Appendix: Mechanomyography Muscles of Interest

Contents

B.1 MMG use in Literature 175

Table B.1: Use of MMG in literature and muscles of interest.

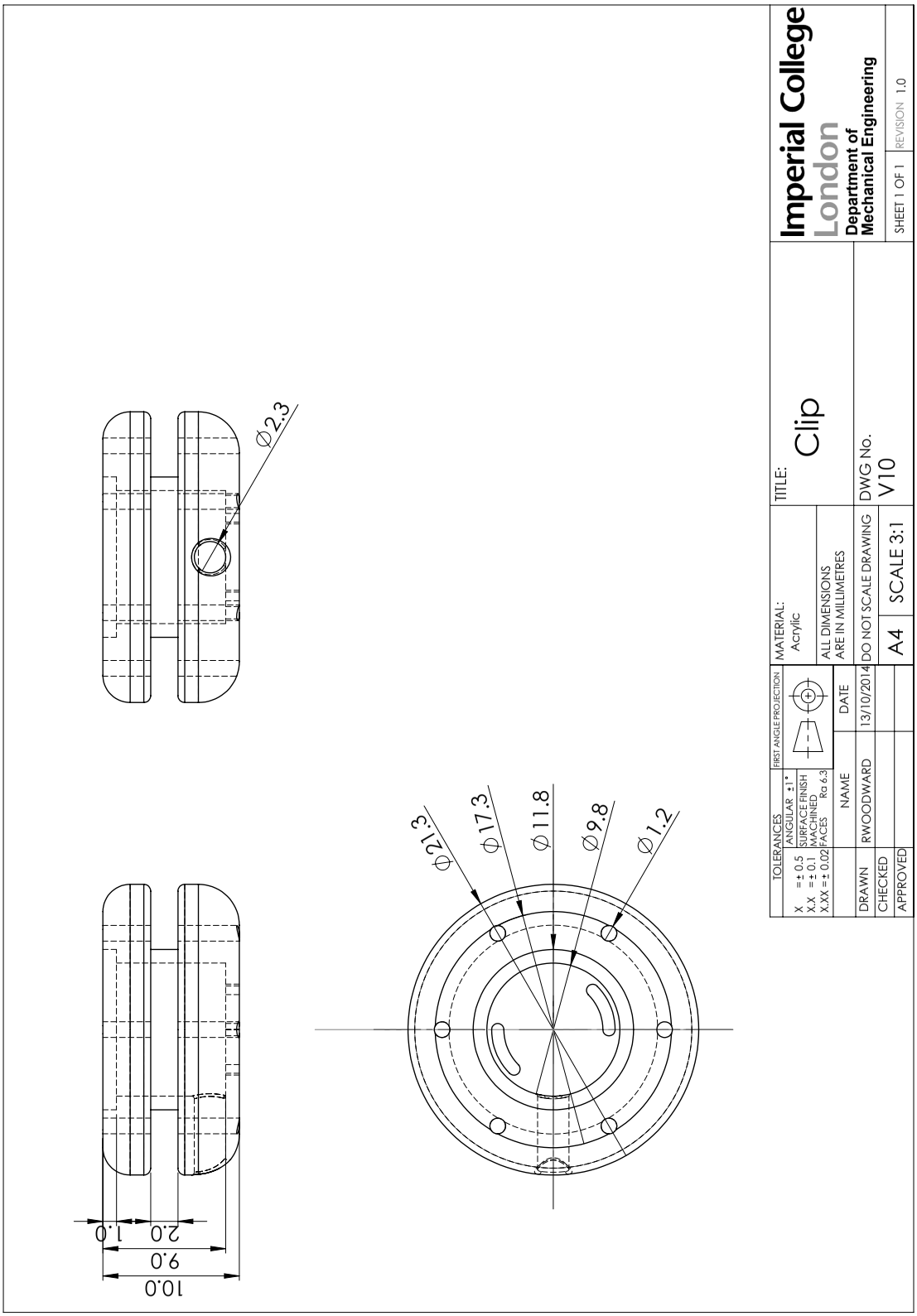
Head	Occipitofrontalis	Alves, 2010[129]
	Orbicularis Oculi	Gordon, 1948[102]
	Laryngeal Adductor	Fuchs-Buder, 2007[153]
Body	Erector spinae	Yoshitake, 2001[101]
Arm	Biceps Brachii	Orizio, 1989[108]; Orizio, 1992[107]; Esposito, 1998[131]; Orizio, 2003[112]; Barry, 1985[8]; Tarata, 2003[110]; Marusiak, 2009[124]
	Triceps Brachii	Marusiak, 2009[124]
	Brachioradialis	Tarata, 2003[110]
	Pronator Teres	Alves, 2010[127]
	Flexor Carpi Radialis	Alves, 2010[127]; Alves, 2010[148]
	Palmaris Longus	Alves, 2010[127]
	Flexor Carpi Ulnaris	Alves, 2010[127]
	Extensor Digitorum Communis	Alves, 2010[127]; Orizio, 1996[100]; Alves, 2006[149]
	Extensor Carpi Radialis Longus	Alves, 2010[127]
	Extensor Carpi Ulnaris	Alves, 2010[127]; Posatskiy, 2011[134]; Zeng, 2009[113]
	Flexor Digitorum Profundus	Alves, 2006[149]
	Flexor Pollicis longus	Alves, 2006[149]
Hand	Adductor Pollicis	Edwards, 1977[138]; Fuchs-Buder, 2007[153]
	Ipsilateral Adductor Pollicis	Suzuki, 2006[122]
Leg	Rectus Femoris	Stokes, 1991[7]; Watakabe, 2003[111]; Antonelli, 2009[119]; Stokes, 1991[130]; Ebersole, 1998[109]; Krueger, 2011[116]
	Vastus lateralis	Tian, 2010[115]; Evetovich, 1997[132]; Ebersole, 1998[131]; Krueger, 2011[116]; Armstrong, 2010[114]
	Vastus Medialis	Ebersole, 1998[131]; Armstrong, 2010[114]
	Gastrocnemius	Yoshitake, 1999[101]; Barry, 1987[106]
	Soleus	Yoshitake, 1999[101]
Foot	Flexor Hallucis Brevis	Fuchs-Buder, 2007[153]

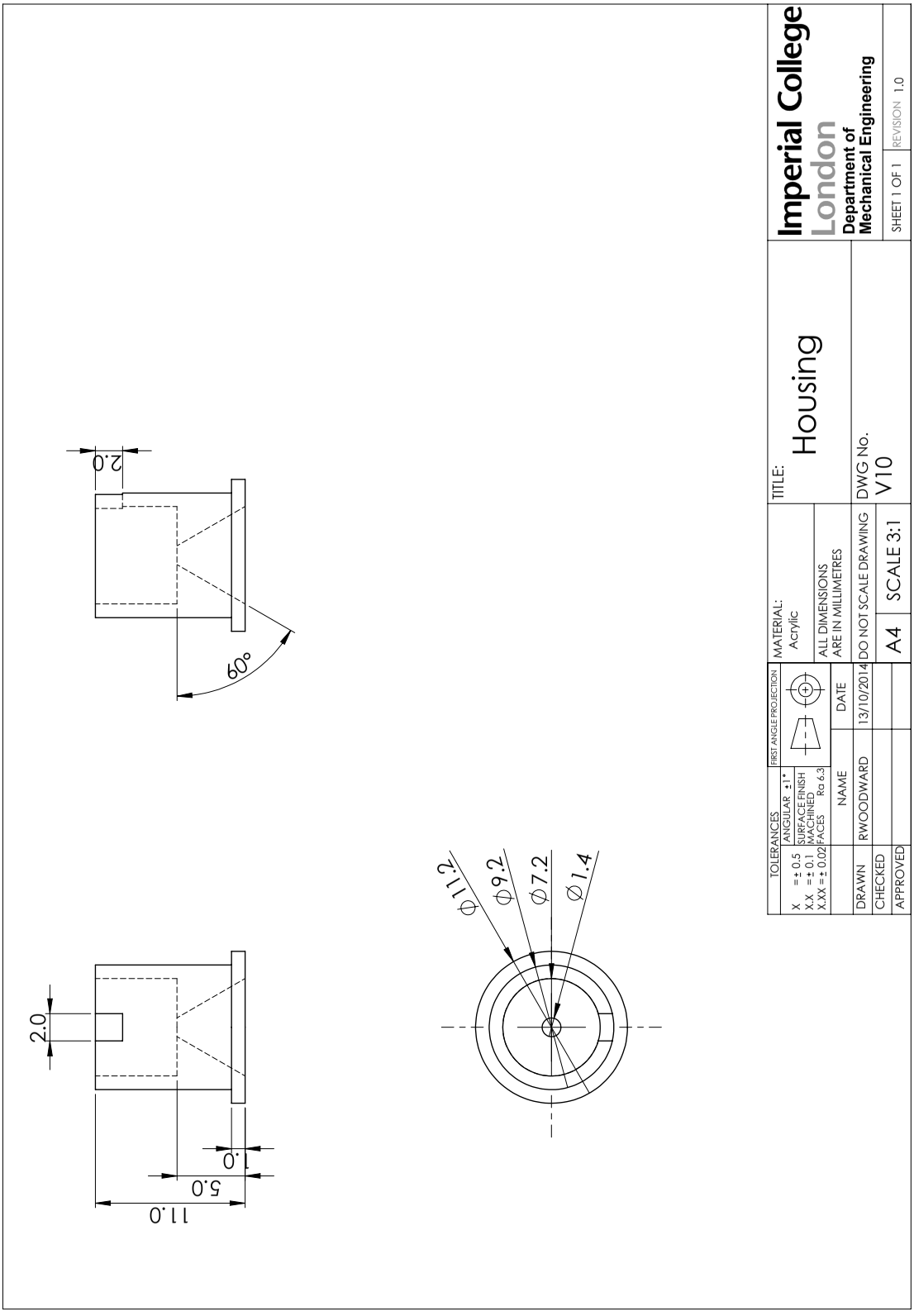
C

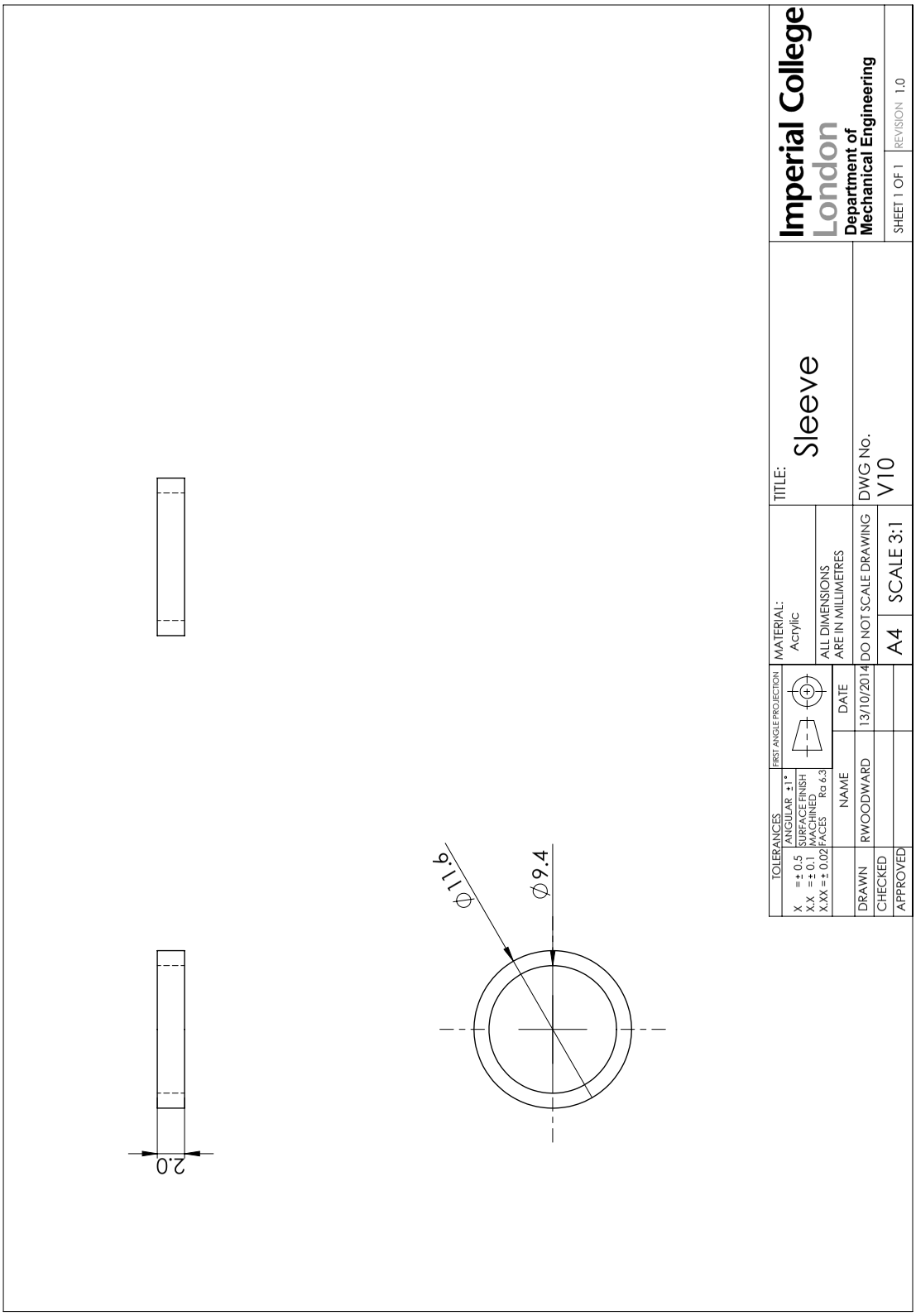
Appendix: Technical Design and Drawings

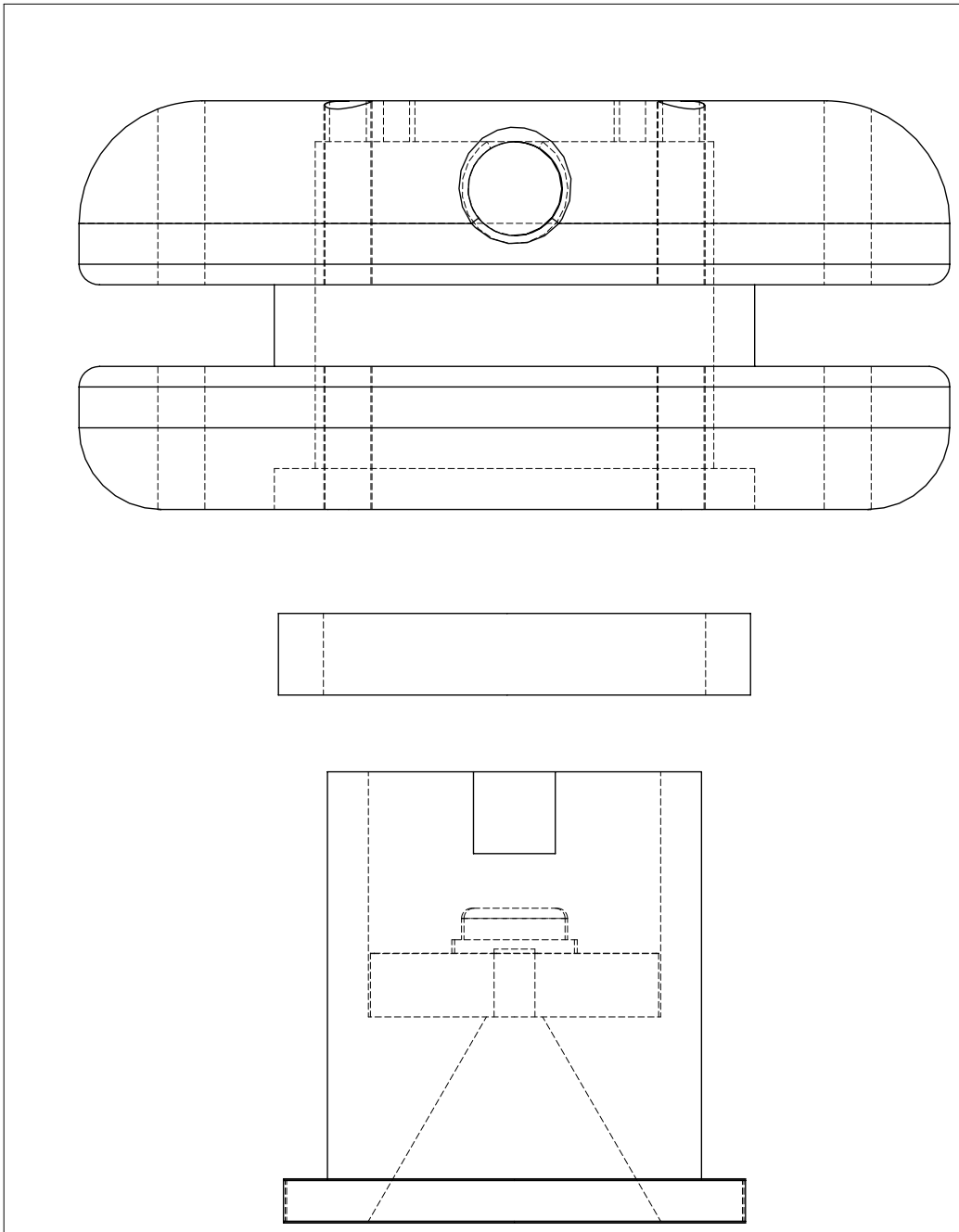
Contents

C.1 MMG Technical Drawings 176
C.2 Aktiv Case Technical Drawings 180
C.3 Battery Case Technical Drawings 183
C.4 MMG Circuit Diagrams 186
C.5 Aktiv Circuit Diagrams 187
C.6 Aktiv BOM List 191
C.7 Aktiv-P Circuit Diagrams 191
C.8 Aktiv-P BOM List 195
C.9 Force Gauge Circuit Diagrams 195

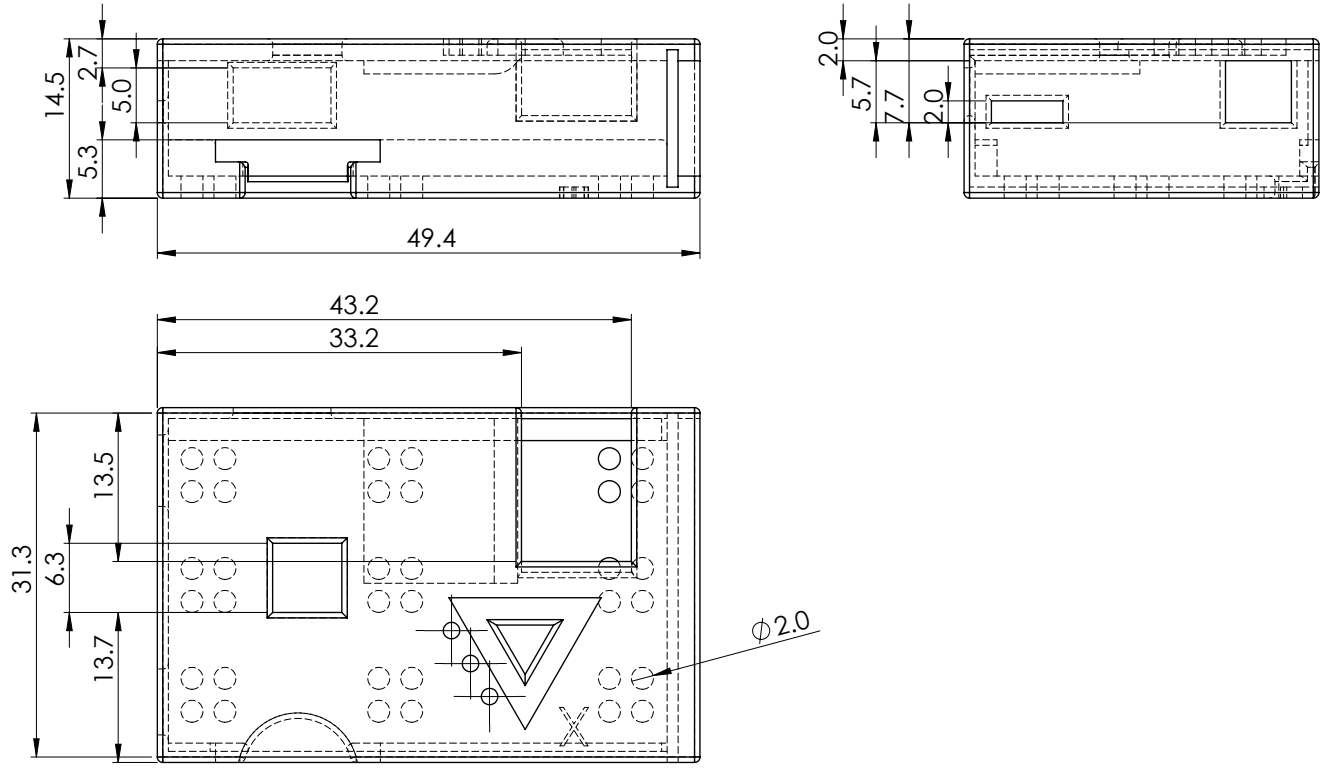

Ø2.3
10.0
9.0
2.0
1.0
Ø21.3
Ø17.3
Ø11.8
Ø9.8
Ø1.2
TOLERANCES
ANGULAR ±1°
X =± 0.5
X.X =± 0.1
X.XX =± 0.02
SURFACE FINISH
MACHINED FACES Ra 6.3
FIRST ANGLE PROJECTION
NAME
DATE
DRAWN RWOODWARD 13/10/2014
CHECKED
APPROVED
MATERIAL:
Acrylic
ALL DIMENSIONS ARE IN MILLIMETRES
TITLE:
Clip
DO NOT SCALE DRAWING
DWG No.
V10
A4
SCALE 3:1
Imperial College London
Department of Mechanical Engineering
SHEET 1 OF 1
REVISION 1.0


2.0
60°
2.0
11.0
5.0
1.0
ϕ11.2
ϕ9.2
ϕ7.2
ϕ1.4
TOLERANCES
ANGULAR ±1°
X =± 0.5
X.X =± 0.1
X.XX =± 0.02
SURFACE FINISH
MACHINED Ra 6.3
FACES
FIRST ANGLE PROJECTION
NAME
DATE
DRAWN
RWOODWARD
13/10/2014
CHECKED
APPROVED
MATERIAL:
Acrylic
ALL DIMENSIONS
ARE IN MILLIMETRES
DO NOT SCALE DRAWING
A4
SCALE 3:1
TITLE:
Housing
DWG No.
V10
Imperial College
London
Department of
Mechanical Engineering
SHEET 1 OF 1
REVISION 1.0

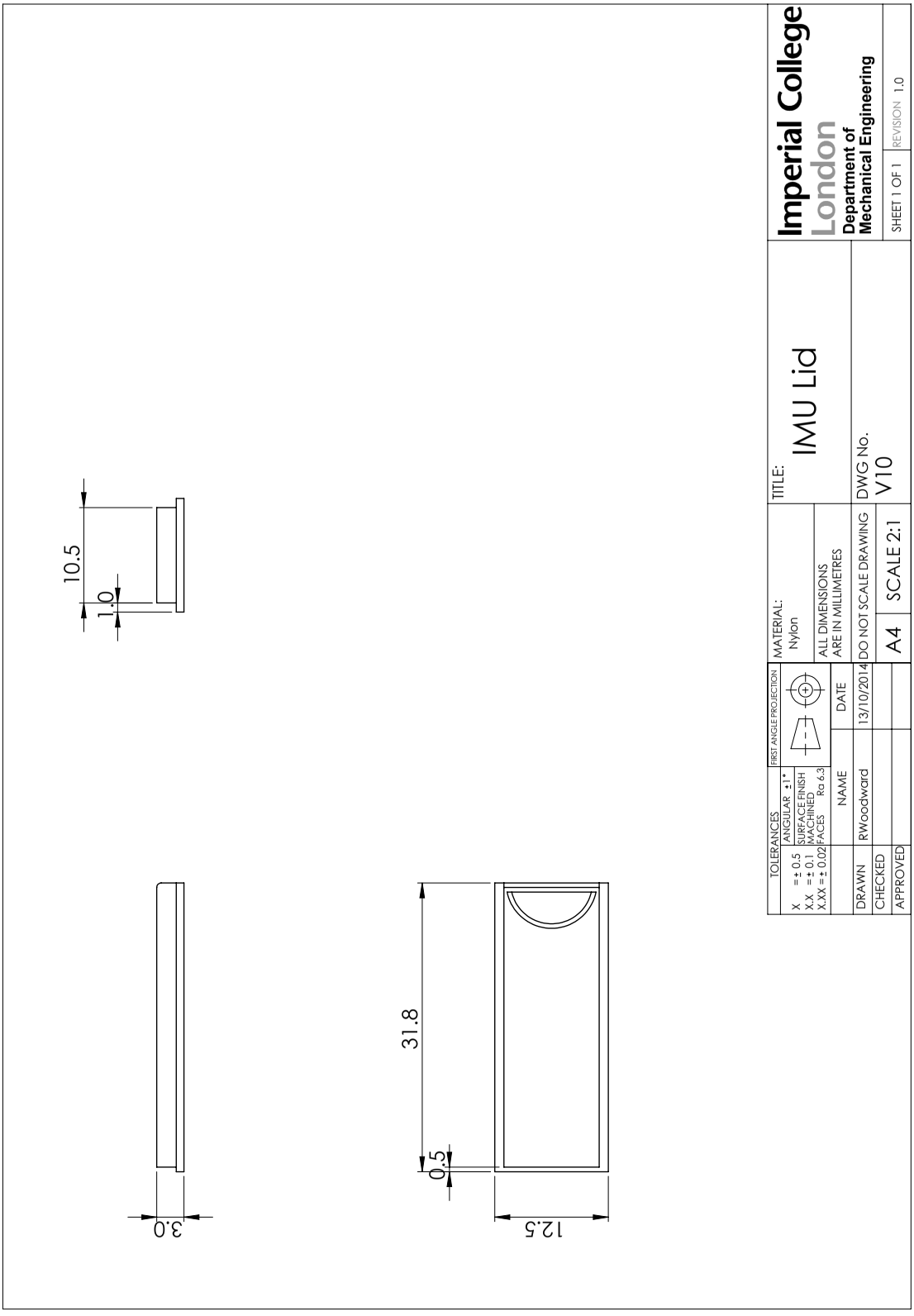

2.0
ϕ11.6
ϕ9.4
TOLERANCES
ANGULAR ±1°
X =± 0.5
X.X =± 0.1
X.XX =± 0.02
SURFACE FINISH
MACHINED FACES Ra 6.3
FIRST ANGLE PROJECTION
NAME
DATE
DRAWN RWOODWARD 13/10/2014
CHECKED
APPROVED
MATERIAL:
Acrylic
ALL DIMENSIONS ARE IN MILLIMETRES
TITLE:
Sleeve
DO NOT SCALE DRAWING
DWG No.
V10
A4
SCALE 3:1
Imperial College London
Department of Mechanical Engineering
SHEET 1 OF 1
REVISION 1.0

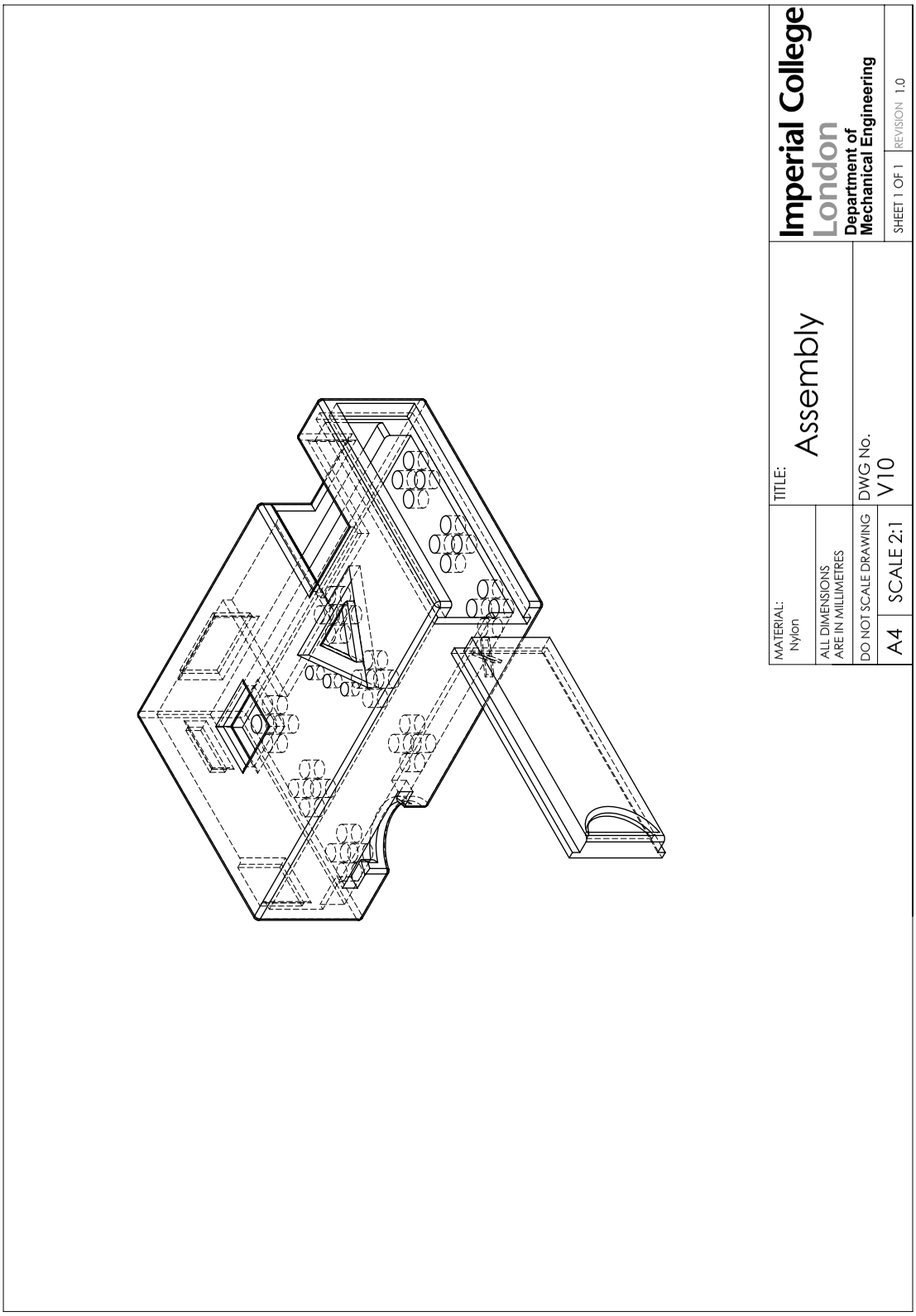


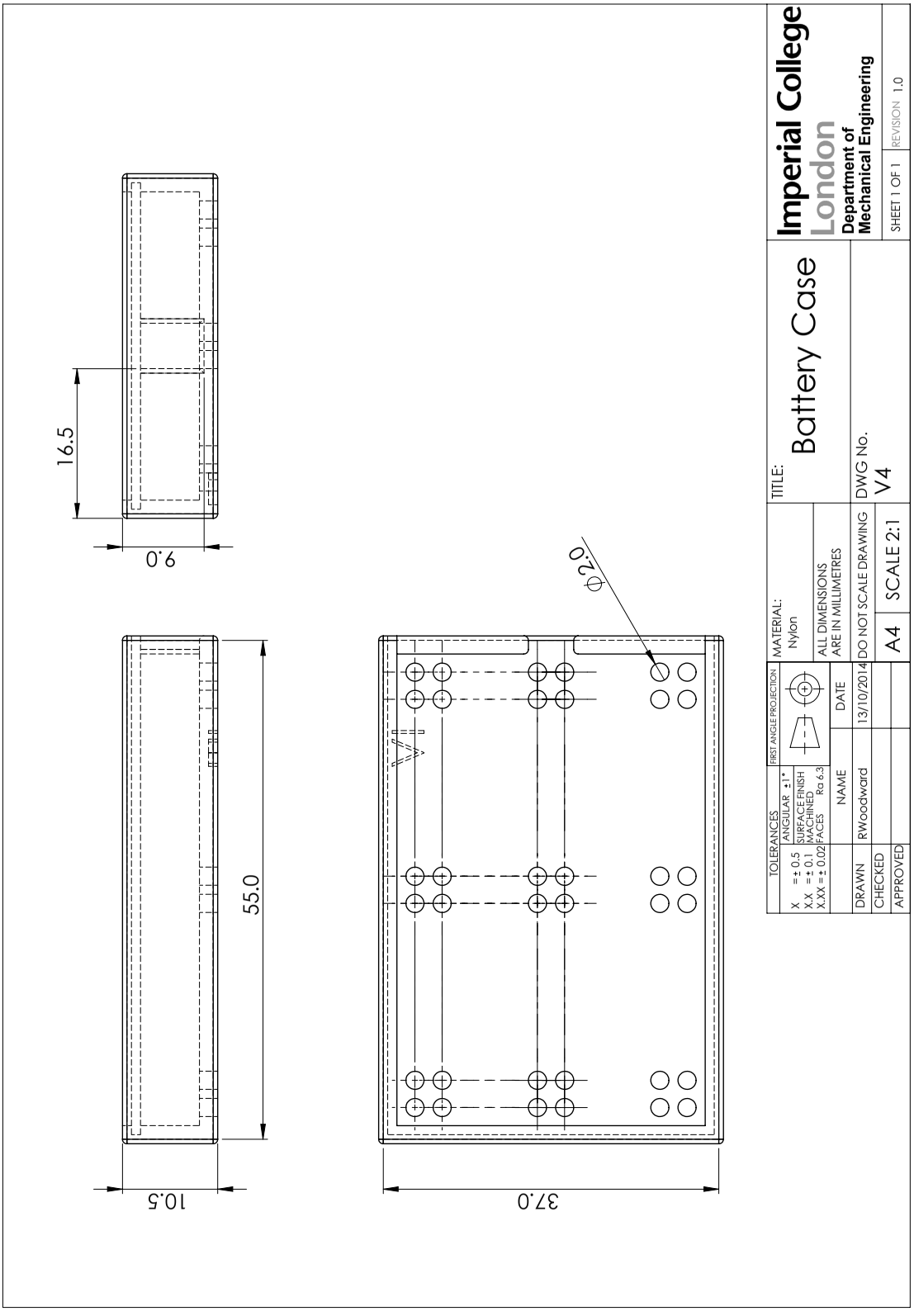
MATERIAL: Acrylic		TITLE: Assembly	Imperial College London Department of Mechanical Engineering
ALL DIMENSIONS ARE IN MILLIMETRES			
DO NOT SCALE DRAWING		DWG No. V10	
A4	SCALE 8:1		SHEET 1 OF 1 REVISION 1.0

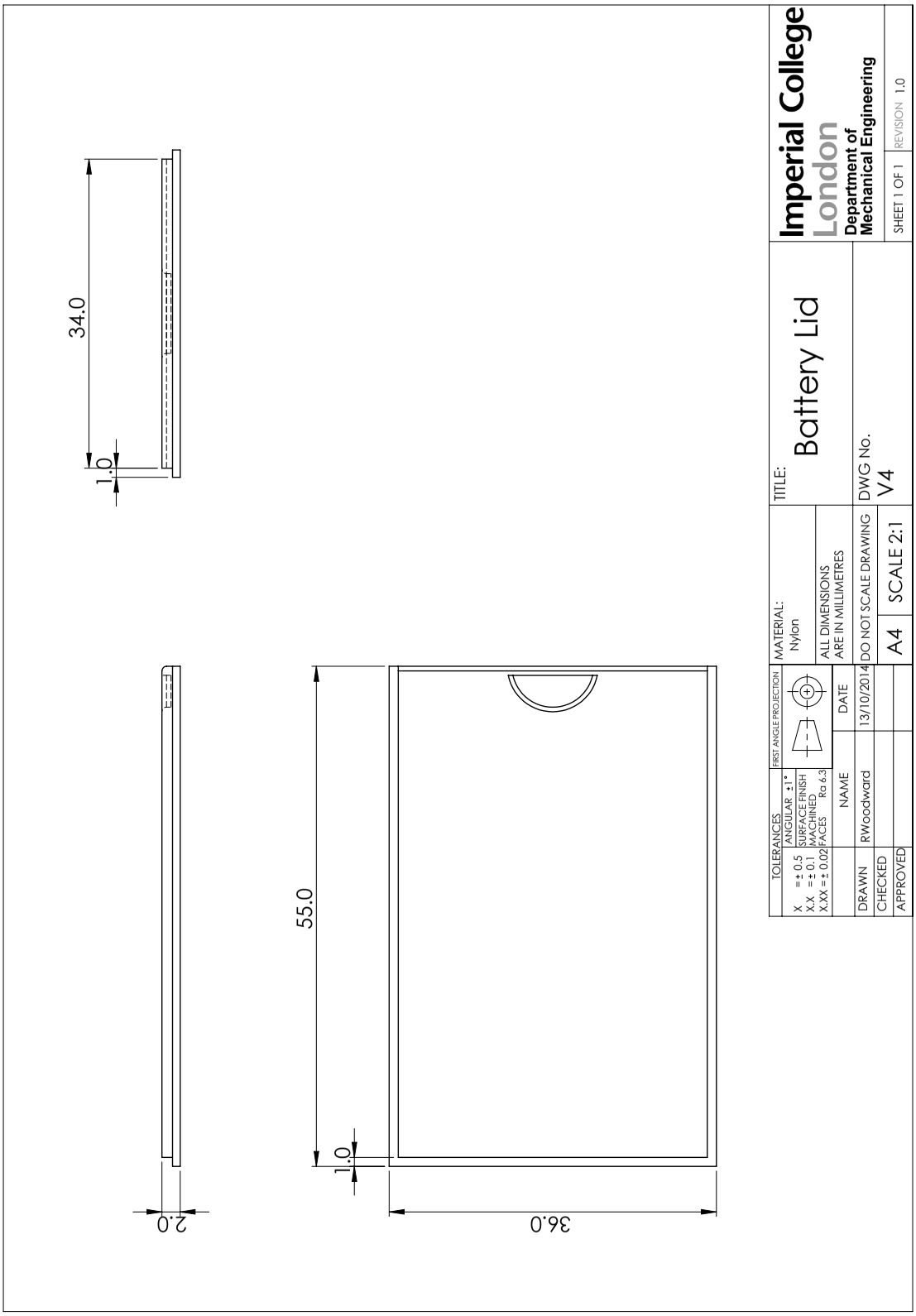


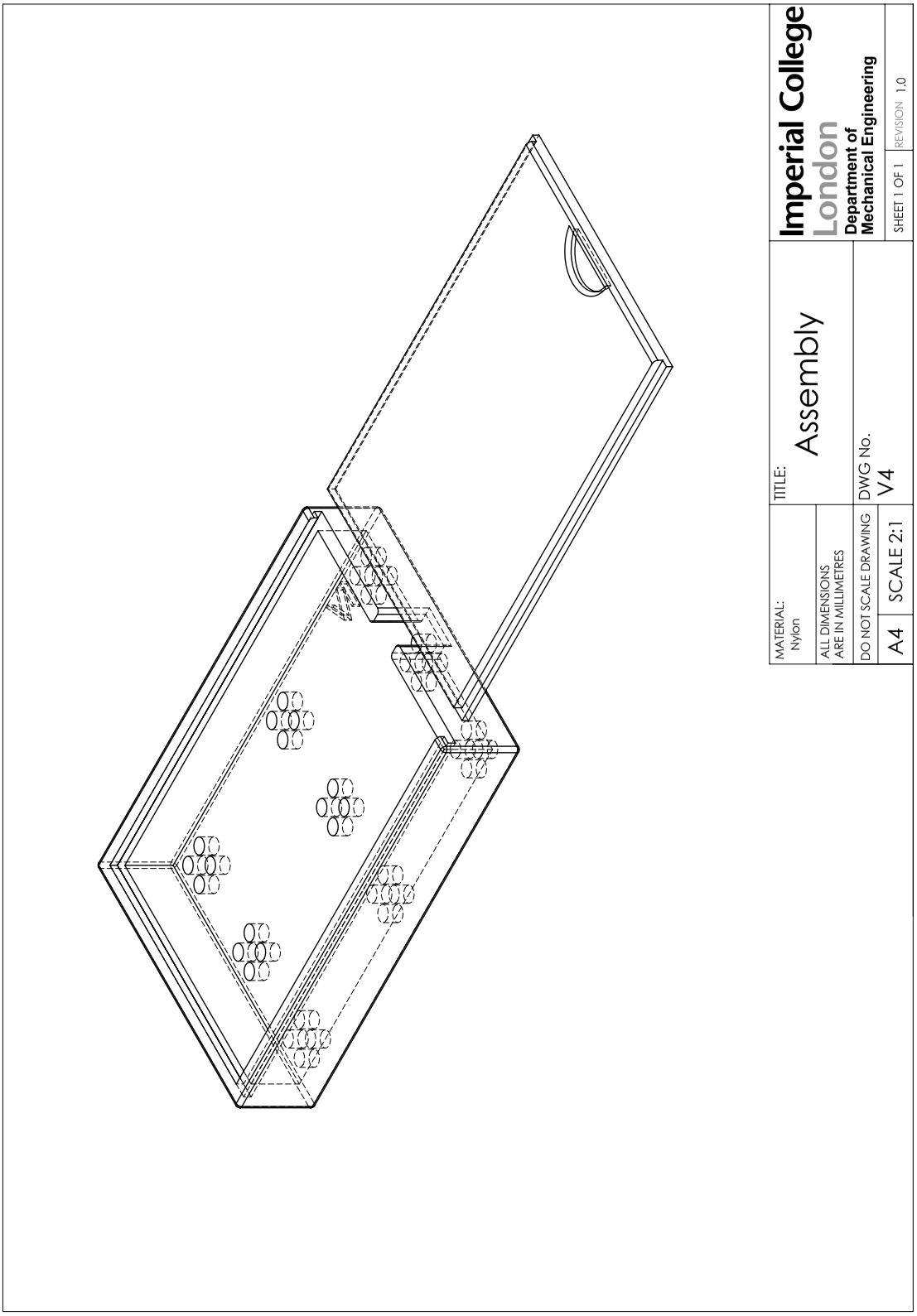
TOLERANCES		FIRST ANGLE PROJECTION	MATERIAL:	TITLE:	Imperial College London
X =± 0.5 X.X =± 0.1 X.XX =± 0.02	ANGULAR ±1° SURFACE FINISH MACHINED FACES Ra 6.3		Nylon	IMU Case	Department of Mechanical Engineering
	NAME	DATE	ALL DIMENSIONS ARE IN MILLIMETRES		
DRAWN	RWoodward	13/10/2014	DO NOT SCALE DRAWING	DWG No.	
CHECKED					
APPROVED			A4 SCALE 2:1	V10	SHEET 1 OF 1 REVISION 1.0


10.5
1.0
3.0
31.8
0.5
12.5
TOLERANCES
ANGULAR ±1°
X =± 0.5
X.X =± 0.1
X.XX =± 0.02
SURFACE FINISH
MACHINED Ra 6.3
FACES
FIRST ANGLE PROJECTION
NAME
DATE
DRAWN
RWoodward
13/10/2014
CHECKED
APPROVED
MATERIAL:
Nylon
ALL DIMENSIONS
ARE IN MILLIMETRES
TITLE:
IMU Lid
DO NOT SCALE DRAWING
DWG No.
V10
A4
SCALE 2:1
Imperial College
London
Department of
Mechanical Engineering
SHEET 1 OF 1
REVISION 1.0


Imperial College London
Department of Mechanical Engineering
TITLE:
Assembly
DWG No.
V10
MATERIAL:
Nylon
ALL DIMENSIONS ARE IN MILLIMETRES
DO NOT SCALE DRAWING
A4
SCALE 2:1
SHEET 1 OF 1
REVISION 1.0


16.5
9.0
10.5
55.0
37.0
Ø2.0
Imperial College London
Department of Mechanical Engineering
TITLE:
Battery Case
DWG No.
V4
MATERIAL:
Nylon
ALL DIMENSIONS ARE IN MILLIMETRES
TOLERANCES
ANGULAR ±1°
X =± 0.5
X.X =± 0.1
X.XX =± 0.02
SURFACE FINISH
MACHINED FACES Ra 6.3
FIRST ANGLE PROJECTION
NAME
DATE
DRAWN
RWoodward
13/10/2014
CHECKED
APPROVED
DO NOT SCALE DRAWING
A4
SCALE 2:1
SHEET 1 OF 1
REVISION 1.0


34.0
1.0
2.0
55.0
1.0
36.0
TOLERANCES
ANGULAR ±1°
X =± 0.5
X.X =± 0.1
X.XX =± 0.02
SURFACE FINISH
MACHINED FACES Ra 6.3
FIRST ANGLE PROJECTION
NAME
DATE
DRAWN
RWoodward
13/10/2014
CHECKED
APPROVED
MATERIAL:
Nylon
ALL DIMENSIONS ARE IN MILLIMETRES
DO NOT SCALE DRAWING
A4
SCALE 2:1
TITLE:
Battery Lid
DWG No.
V4
Imperial College London
Department of Mechanical Engineering
SHEET 1 OF 1
REVISION 1.0


Imperial College
London
Department of
Mechanical Engineering
TITLE:
Assembly
DWG No.
V4
SHEET 1 OF 1
REVISION 1.0
MATERIAL:
Nylon
ALL DIMENSIONS
ARE IN MILLIMETRES
DO NOT SCALE DRAWING
A4
SCALE 2:1

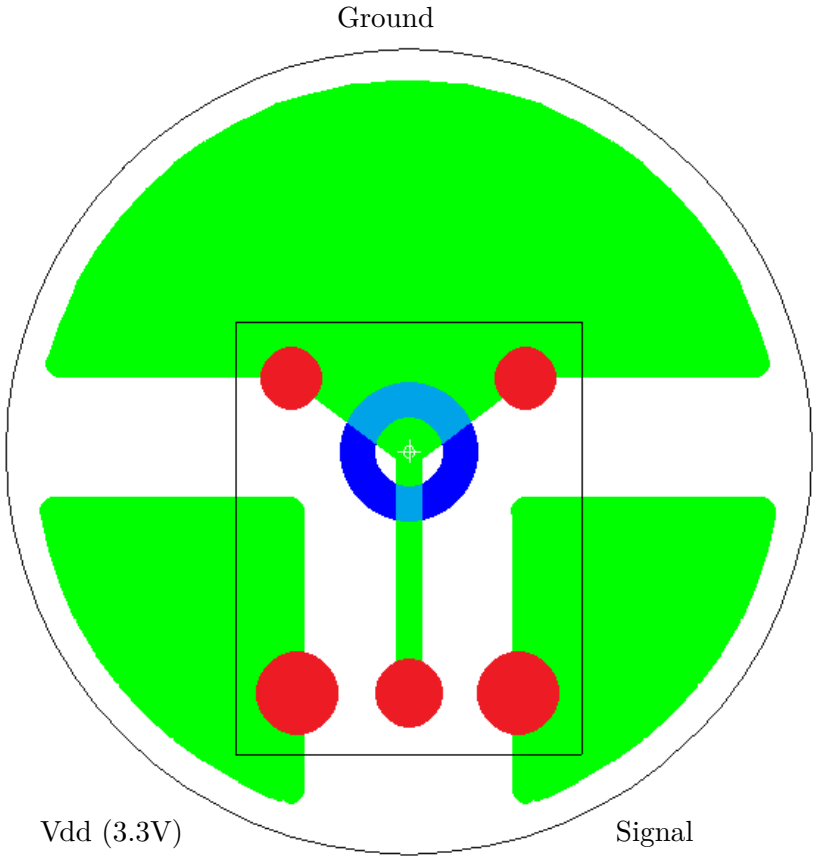
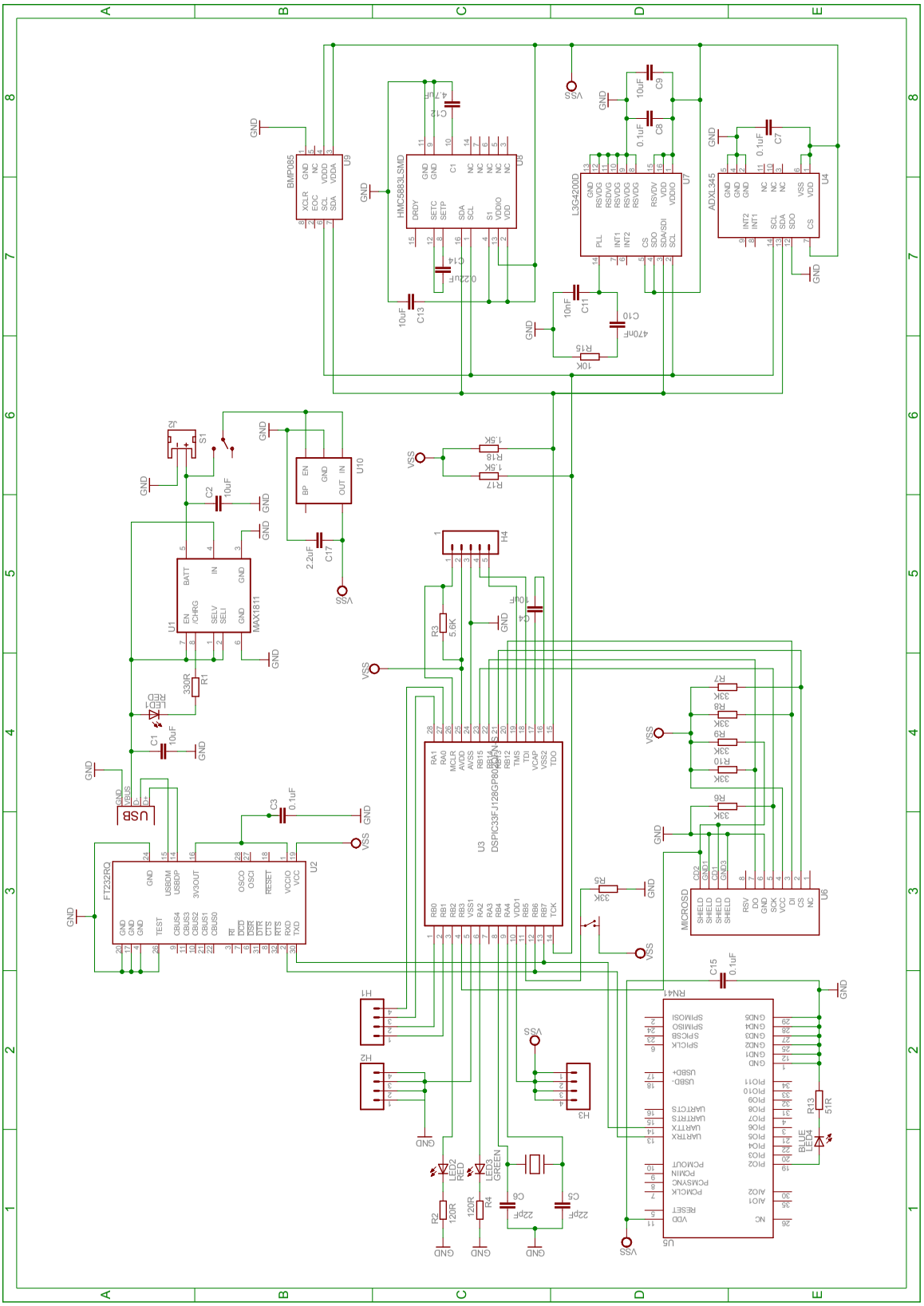
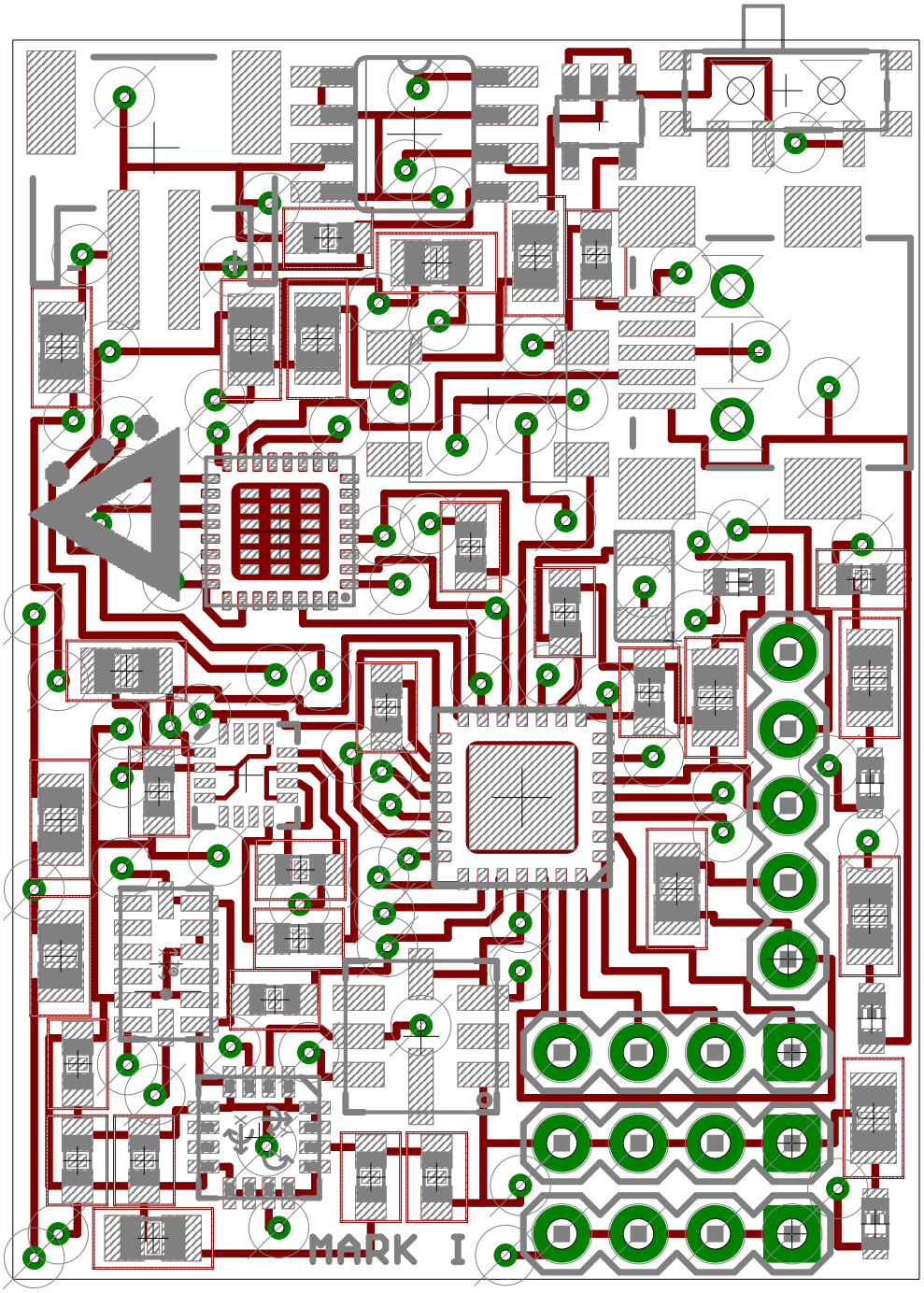


Figure C.1: MMG microphone schematic, displaying Knowles SPU1410LR5H microphone footprints (red and blue) and copper plans which the connecting wires are soldered to.

Table C.1: Bill of materials (BOM) for the developed MMG sensor.

Qty	Device	Package	Part
1	SPU1410LR5H-QB	Custom	M1


A
B
C
D
E
1
2
3
4
5
6
7
8
BMP085
HMC5883L-SMD
L3G4200D
ADXL345
MAX1811
FT232RQ
USB
DSPIC33FJ128GP802
MICROSD
RN41
LED1
LED2
LED3
LED4
BLUE
GREEN
VSS
GND
10uF
0.1uF
4.7uF
0.22uF
10nF
47nF
2.2uF
0.1uF
10K
1.5K
5.6K
330R
120R
22pF
51R
33K


MARK I

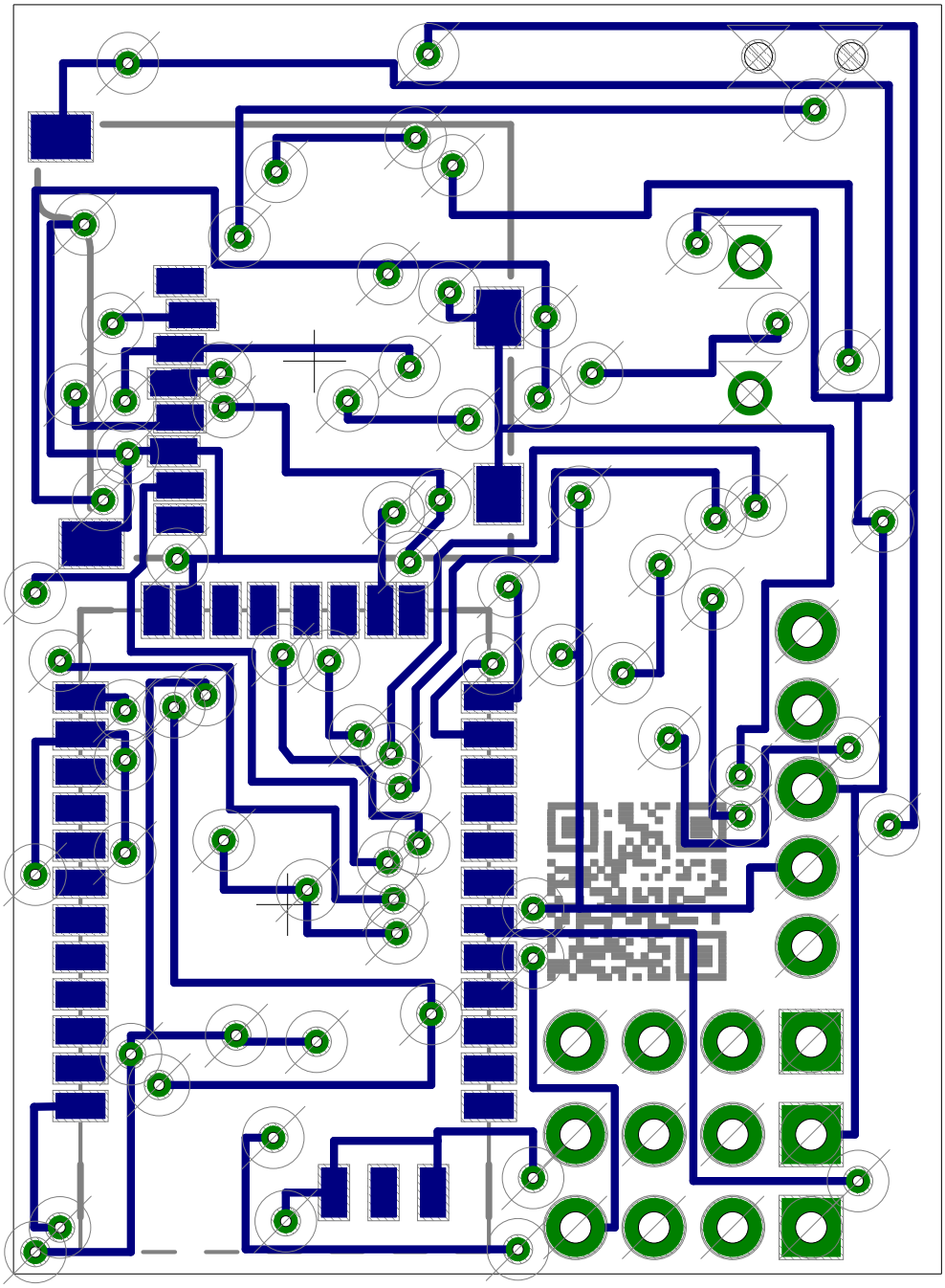
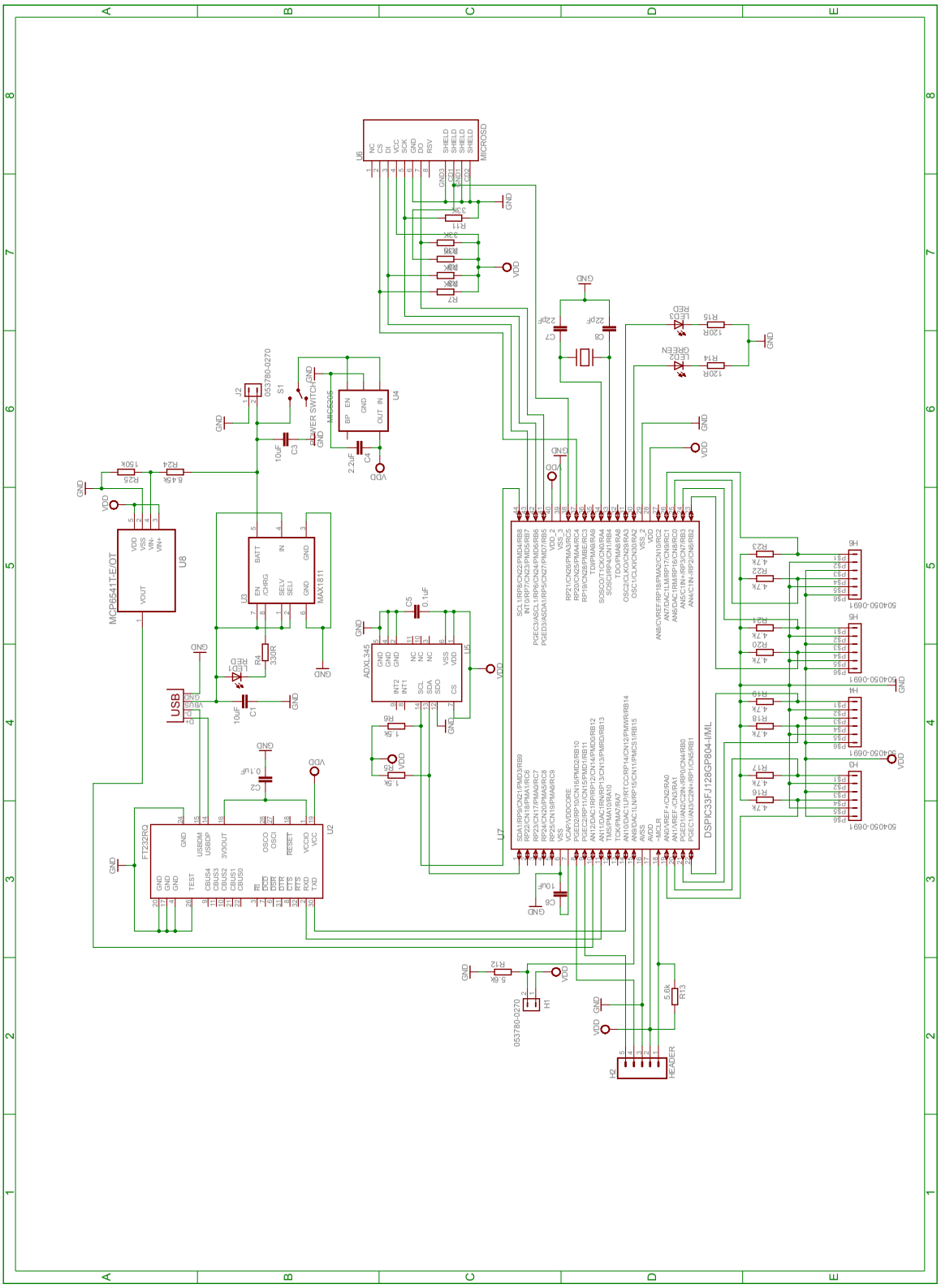
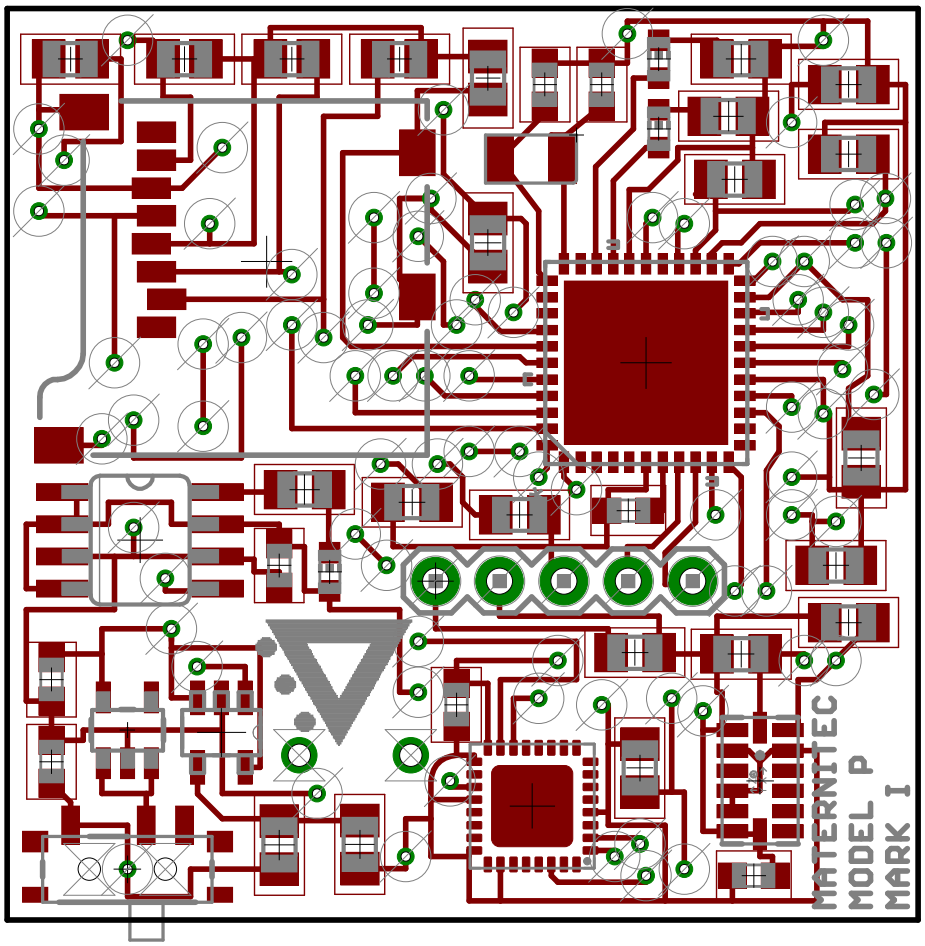


Table C.2: Bill of materials (BOM) for the Aktiv (Mark I) inertial measurement unit.

Qty	Value	Device	Package	Parts
3		M04PTH	1X04	H1, H2, H3
1		MIC52053.3V	SOT23-5	U10
1		SWITCH-SPDT-SMD-A	SWITCH-SPST-SMD-A	S1
1		JST_2MM_MALE	JST-2-SMD	J2
1		M05PTH	1X05	H4
4	0.1uF	C-EUC0603	C0603	C3, C7, C8, C15
1	0.22uF	C-EUC0603	C0603	C14
2	1.5K	R-EU_R0805	R0805	R17, R18
1	10K	R-EU_R0805	R0805	R15
1	10nF	C-EUC0603	C0603	C11
5	10uF	C-EUC0603	C0603	C1, C2, C4, C9, C13
2	120R	R-EU_R0805	R0805	R2, R4
1	2.2uF	C-EUC0603	C0603	C17
2	22pF	C-EUC0603	C0603	C5, C6
1	330R	R-EU_R0805	R0805	R1
6	33K	R-EU_R0805	R0805	R5, R6, R7, R8, R9, R10
1	4.7uF	C-EUC0603	C0603	C12
1	470nF	C-EUC0603	C0603	C10
1	5.6K	R-EU_R0805	R0805	R3
1	51R	R-EU_R0805	R0805	R13
1	ADXL345	ADXL345	LGA14	U4
1	BLUE	LEDCHIP-LED0603	CHIP-LED0603	LED4
1	BMP085	BMP085	BMP085	U9
1	COM-08720	COM-08720	COM-08720	S2
1	DSPIC33FJ128GP802QFN-S	DSPIC33FJ128GP802QFN-S	DSPIC33FJ128GP802	U3
1	ECX_31B	ECX_31B	ECX-31B	O1
1	FT232RQ	FT232RQ	QFN32	U2
1	GREEN	LEDCHIP-LED0603	CHIP-LED0603	LED3
1	HMC5883LSMD	HMC5883LSMD	16LPCC	U8
1	L3G4200D	L3G4200D	LGA16-4X4	U7
1	MAX1811	MAX1811	SO08	U1
1	MICROSD	MICROSD	MICROSD	U6
2	RED	LEDCHIP-LED0603	CHIP-LED0603	LED1, LED2
1	RN41	RN41	RN41	U5
1	USB-SMD-NS	USB-SMD-NS	USB-MINIB-NOSTOP	J1


MICROSD
MICRO SWITCH
MICRO5
MAX1811
MCP65411T-E/OT
ADXL345
F7232RQ
DSPIC33FJ128GP804-I/ML
HEADER
USB
LED1
LED2
LED3
S1
J2
U2
U3
U4
U5
U6
U7
U8
H1
H2
H3
H4
H5
H6
C1
C2
C3
C4
C5
C6
C7
C8
R4
R5
R6
R7
R8
R9
R10
R11
R12
R13
R14
R15
R16
R17
R18
R19
R20
R21
R22
R23
R24
R25
GND
VDD


MATERNITEC
MODEL P
MARK I

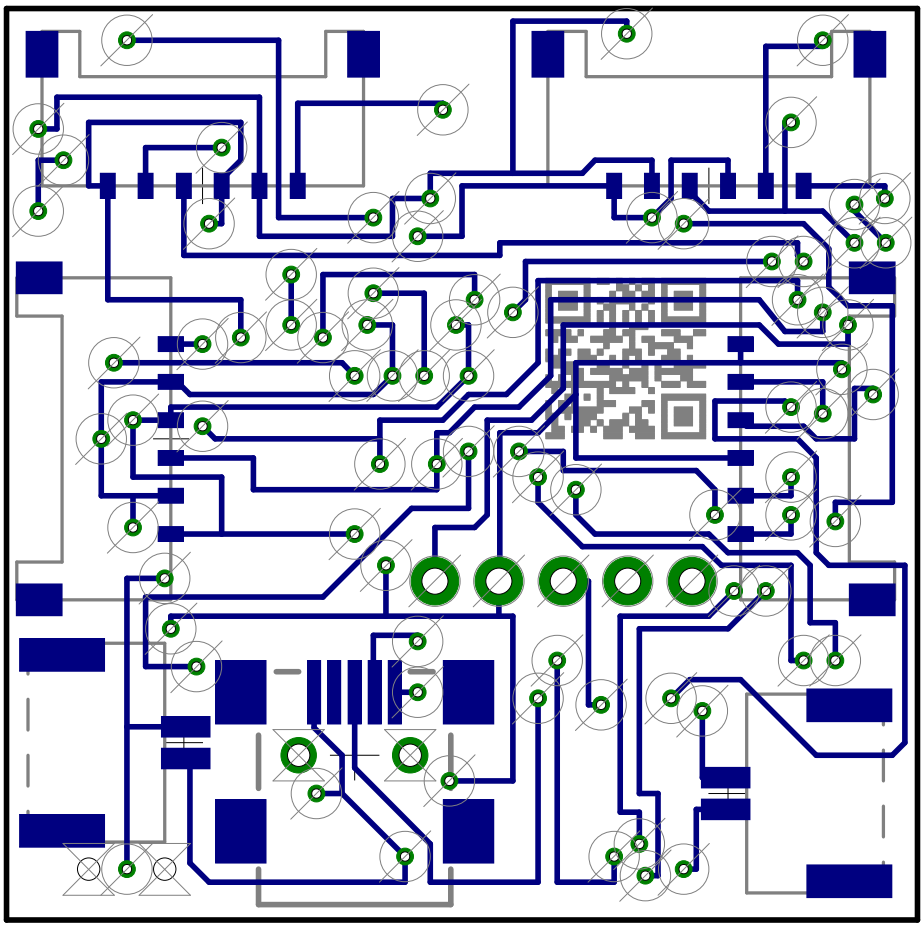


Table C.3: Bill of materials (BOM) for the Aktiv-P (Mark I) inertial measurement unit.

Qty	Value	Device	Package	Parts
2		053780-0270	053780-0270	H1, J2
4		504050-0691	504050-0691	H3, H4, H5, H6
1		MIC52053.3V	SOT23-5	U4
1		SWITCH-SPDT-SMD-A	SWITCH-SPST-SMD-A	S1
1		M05PTH	1X05	H2
2	0.1uF	C-EUC0603	C0603	C2, C5
2	1.5k	R-EU_R0805	R0805	R5, R6
3	10uF	C-EUC0603	C0603	C1, C3, C6
2	120R	R-EU_R0805	R0805	R14, R15
1	150k	R-EU_R0805	R0805	R25
1	2.2uF	C-EUC0603	C0603	C4
2	22pF	C-EUC0603	C0603	C7, C8
1	330R	R-EU_R0805	R0805	R4
5	33K	R-EU_R0805	R0805@1	R7, R8, R9, R10, R11
8	4.7k	R-EU_R0805	R0805	R16, R17, R18, R19, R20, R21, R22, R23
2	5.6k	R-EU_R0805	R0805	R12, R13
1	8.45k	R-EU_R0805	R0805	R24
1	ADXL345	ADXL345	LGA14	U5
1	DSPIC33FJ128GP804-I/ML	DSPIC33FJ128GP804-I/ML	QFN65P800X800X100-44N	U7
1	ECX_31B	ECX_31B	ECX-31B	O1
1	FT232RQ	FT232RQ	QFN32	U2
1	GREEN	LEDCHIP-LED0603	CHIP-LED0603	LED2
1	MAX1811	MAX1811	SO08	U3
1	MCP6541T-E/OT	MCP6541T-E/OT	SOT95P320X145-5N	U8
1	MICROSD	MICROSD	MICROSD	U6
2	RED	LEDCHIP-LED0603	CHIP-LED0603	LED1, LED3
1	USB-SMD-NS	USB-SMD-NS	USB-MINIB-NOSTOP	J1

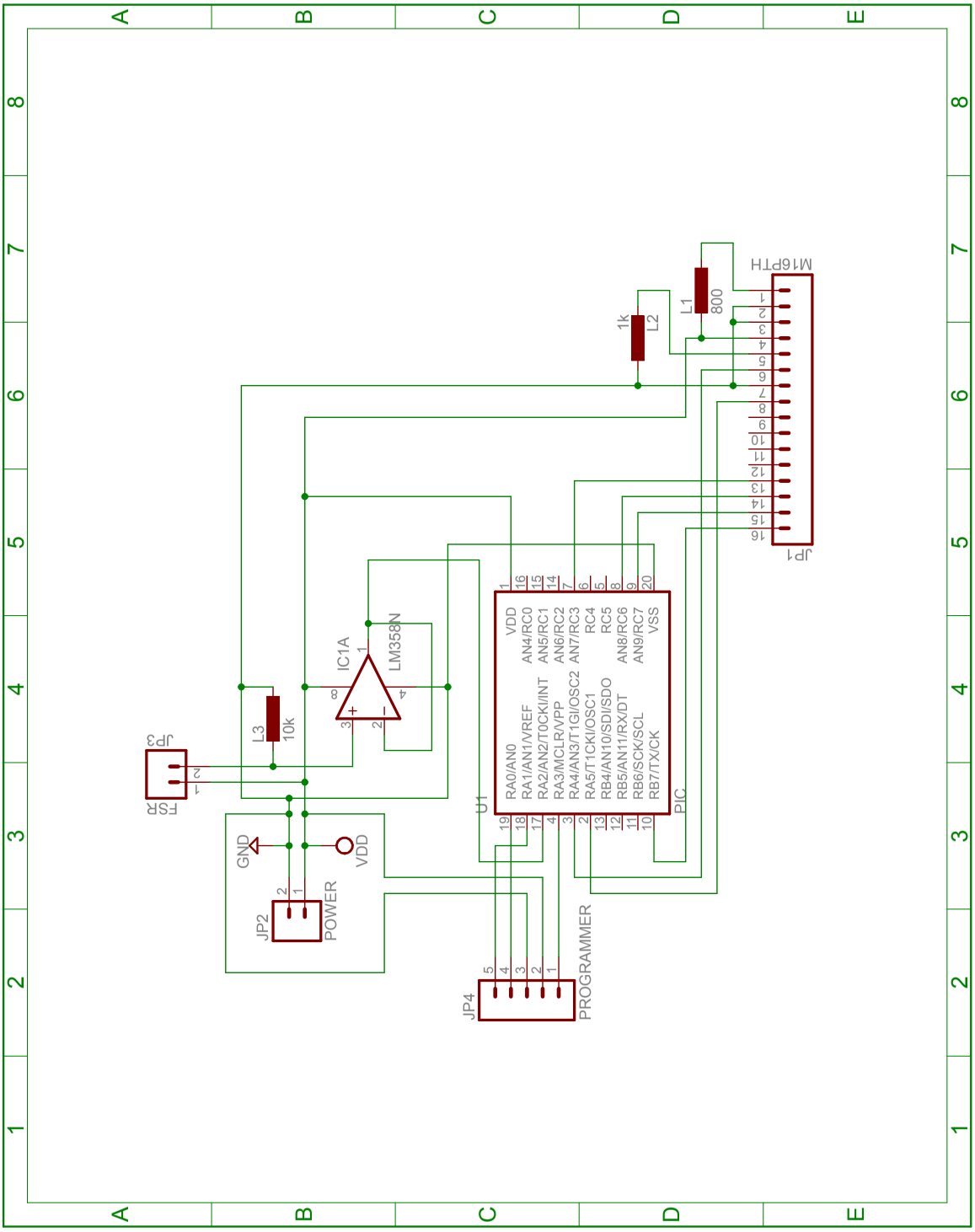

A
B
C
D
E
1
2
3
4
5
6
7
8
M16PTH
JP1
L1
800
L2
1k
L3
10k
IC1A
LM358N
JP3
FSR
U1
PIC
VDD
VSS
RA0/AN0
RA1/AN1/VREF
RA2/AN2/T0CKI/INT
RA3/MCLR/VPP
RA4/AN3/T1GI/OSC2
RA5/T1CKI/OSC1
RB4/AN10/SDI/SDO
RB5/AN11/RX/DT
RB6/SCK/SCL
RB7/TX/CK
AN4/RC0
AN5/RC1
AN6/RC2
AN7/RC3
RC4
RC5
AN8/RC6
AN9/RC7
GND
VDD
JP2
POWER
JP4
PROGRAMMER

Table C.4: Bill of materials (BOM) for the force gauge.

Qty	Value	Device	Package	Parts
1	10k	L-EU0207/10	0207/10	L3
1	1k	L-EU0207/10	0207/10	L2
1	800	L-EU0207/10	0207/10	L1
1	FSR	M02PTH	1X02	JP3
1	LM358N	LM358N	DIL08	IC1
1	M16PTH	M16PTH	1X16	JP1
1	PIC	PIC16F6XX	DIL20	U1
1	POWER	M02PTH	1X02	JP2
1	PROGRAMMER	M05PTH	1X05	JP4